eman ta zabal zazu

Universidad   Euskal Herriko
del País Vasco   Unibertsitatea

Department of Analytical Chemistry

Understanding Mars through the Earth:

Geochemical characterization of submarine volcano scenarios to be used as Martian analogues

Dissertation presented for the international PhD degree

Patricia Ruiz Galende

July 2020

Supervised by:

Kepa Castro Ortiz de Pinedo

Gorka Arana Momoitio

ACKNOWLEDGEMENTS

Tras los agradecimientos oficiales (los fáciles) a continuación aparecen los personales, que espero no me ocupen más de lo necesario. Antes de nada, aclaremos, NO van en orden de importancia, que nadie se ofenda ☺

A mis directores por estar siempre ahí y ser parte muy importante de este trabajo. Kepa, desde que fuiste mi profesor en primero de carrera tenía la sensación de que nuestra relación iría para largo. Has sido mi tutor/director de TFG, TFM y Tesis Doctoral y 10 años han pasado desde las clases de Metodología donde aprendíamos a hacer calibrados con Excel a fuerza de repetición. De verdad, gracias por todo, por confiar siempre en mí incluso en las recuperaciones… Nunca te/me perdonaré (ni olvidaré) la recuperación de Química Analítica II que tuve que hacer tras un examen perfecto y haberme olvidado dividir entre σ en Unescrumbler…

Gorka, aunque no sean tantos años como con Kepa, también te agradezco mucho la confianza. El siempre tener un comentario positivo o gracioso para alegrar hasta los

momentos más tensos y ser siempre tan rápido con las correcciones. Teniendo en cuenta lo nerviosa e impaciente que soy, esto ha sido una gran ayuda para mí. Gracias de verdad.

Por último, en el apartado de las altas esferas, Juanma, el jefe jefe que creo que ha aportado más ilusión que nadie a este trabajo y al proyecto en general. Sé que es repetitivo, pero creo que la confianza es lo más importante en cualquier tipo de relación, así que muchísimas gracias por eso. También van 10 años desde que nos diste clase por primera vez sobre procedimientos de muestreo en Química Analítica I y tampoco olvidaré nunca el ejercicio del terreno dividido en cuadraditos… vaya desastre, pero al final lo entendí jajajaja. Gracias por arrojar luz en los momentos en los que más negro veía todo y por hacerme ver la calidad de mi trabajo cuando no era capaz de hacerlo por mi misma.

A mi familia, en general. Ver su orgullo en cada paso que he dado ha sido siempre el empujón necesario para continuar. Mis padres son los que han aguantado todo, todo, todo. Mis locuras, mi mala leche, me han mantenido durante este tiempo aunque yo siempre les digo que a ver si se independizan ;) En definitiva, por hacer lo que hacen los padres sin quejas y sin esperar nada a cambio. Os quiero mucho. A Lydia, Pepi y Elena por demostrarme que la familia no es solo la que comparte sangre,

Aunque en la portada de esta tesis está escrito mi nombre, creo que nada de lo que hay puesto en ella hubiera sido posible sin la ayuda de mi compi de batalla. Gracias Imanol por darme el punto de calma que muchas veces me ha hecho falta. Creo que nadie como tú sabe cómo ha sido el proceso de esta tesis y que ha sabido cuando hablar y cuando era mejor dejarme en mi burbuja. Sabes que todo lo que hay aquí escrito también es tuyo y que espero un párrafo al menos igual de bonito que este en los agradecimientos de tu tesis… jajajaja Aunque no me sorprendería que no los escribieses y pusieses algo así como:

A mis padres.

Y nos dejarías a todos con las ganas de saber que pasa por esa cabecita jajaja Lo dicho, muchas gracias.

La otra parte del trío con el que empezamos esta tesis y que últimamente ha estado más desaparecida porque es una curranta nata, no podía faltar. Fani, gracias por los momentos de risas en Zamu, por tu mala leche que muchas veces nos daba la vida a Imanol y a mí ;) y porque al final siempre has tenido un comentario de ánimo para el resto. Gracias.

Dos personas muy importantes sin las que, no solo esta tesis, si no mi estancia en Zamudio o cualquier sitio donde nos mandasen estar, no hubiese sido ni la mitad de divertida, productiva y memorable, son Julene y Leti. Nos aceptasteis como iguales desde el primer día y nos ayudasteis siempre en todo lo que pudisteis sin poner ninguna pega. Creo que hablo en nombre de más de uno cuando os doy las gracias por todo esto. Muestreos, viajes a Madrid, días de trabajo y de no tan trabajo, charlas sobre la

vida y filosóficas, consejos, reuniones interminables, experimentación conjunta para darnos apoyo moral…. Muchísimos momentos que están escondidos detrás de los tecnicismos de esta tesis y que se quedarán en mi memoria para siempre. Gracias rubias ☺.

Ilaria, Cris y Jenni, porque sobre todo en la última fase de esta tesis habéis formado parte muy importante de mi día a día animándome y confiando en que iba a poder con todo lo que me venía y más. Ilaria, te seguiré mandando videos de Carlos Ríos y de La Resistencia para que nos sigamos riendo de las bobadas que ponen. Cris, gracias por amenizarnos los días con tus canticos y tus reflexiones, permíteme decirlo, de bombera jubilada jajajaja, siempre tendrás aquí a alguien que te descubrirá algo nuevo en cuanto a edición de imágenes. Jenni, última incorporación que ha llenado de ilusión el laboratorio… gracias y muchísima suerte en esta andadura que acabas de comenzar. No seré yo quién te diga que es algo fácil, pero estoy segura de que podrás con ello y conseguirás todo lo que te propongas. De verdad chicas, muchas gracias.

A la amistad más duradera que tengo, nos conocimos antes de nacer a través de las barrigas de nuestras madres… Ana, que nos llevamos aguantando 28 años (que se dice pronto) y espero que nos queden muchos más. ¡Gracias por darme dosis de realidad siempre! Que aunque a veces te diga que hay que soñar más, tener los pies en la tierra es muy necesario.

Nene, Sarra, Drew, mis PJ people, los cuartos que me completan… La verdad que no sé qué deciros que no sepáis, pero por si acaso, GRACIAS. Habéis estado presentes en todos los momentos, buenos y malos, de esta tesis. Para apoyarme, darme vuestra opinión, echarme la bronca… en fin, para todo, como siempre. Porque la mayoría de momentos divertidos e inolvidables durante estos años, han sido gracias a vosotras… En este tiempo hemos crecido juntas y espero que sigamos haciéndolo. Porque nunca me hubiera imaginado que la carrera me iba a dar algo tan indispensable como vuestra amistad… Muchísimas gracias, os quiero infinito. ¡No me olvido de vuestros maridos por supuesto! Qué familia bonita hemos creado ☺.

Bodegueros míos… muchos de vosotros, por no decir la mayoría no sabréis lo importantes que habéis sido en todos estos años… Pensar en pasar momentos con vosotros que me hicieran evadirme por completo, cada fiesta, cada ida de olla, cada cerveza (que no han sido pocas), todo. Que penséis que trabajo para la NASA y ver el orgullo en vuestros ojos… De verdad que, solo con que escuchaseis la explicación de lo que era mi trabajo aún sin entender nada, para mí ha valido más que el oro. Espero que lo que nos une desde que tenemos uso de razón no se acabe y nos mantenga unidos aunque sea para vernos una vez al año y alegrarnos por el simple hecho de estar juntos. Gracias de verdad!

¡Muchísimas gracias a todos!

"We are, all of us, growing volcanoes that approach the hour of their eruption, but how near or distant that is, nobody knows."

Friedrich Nietzsche

CHAPTER 1:

INTRODUCTION

Scientific interest in the solar system bodies together with their study and exploration have been the main topic of several research works. The study of the composition, structure and distribution of planets and other objects that are orbiting the Sun, can help in the understanding of the conditions in the early solar nebula and the processes that controlled the formation of the planets [1]. The planetary science addresses three fundamental issues: the origin and chemical evolution of matter, the origin and evolution processes of the universe and the understanding of the origin and development of life [2].

The planets of the Solar System are Mercury, Venus, Earth, Mars, Jupiter, Saturn, Uranus and Neptune (Figure 1.1). In this Figure, Pluto also appears as the most prominent member of a new class of objects [3]. The first four are called terrestrial planets and the others are the Jovian planets being between them the asteroids belt [4]. The terrestrial ones differ from the main belt asteroids in being much more massive, and from Jovian planets in being much less massive and without extensive mantles of hydrogen and helium as the outer planets [5].
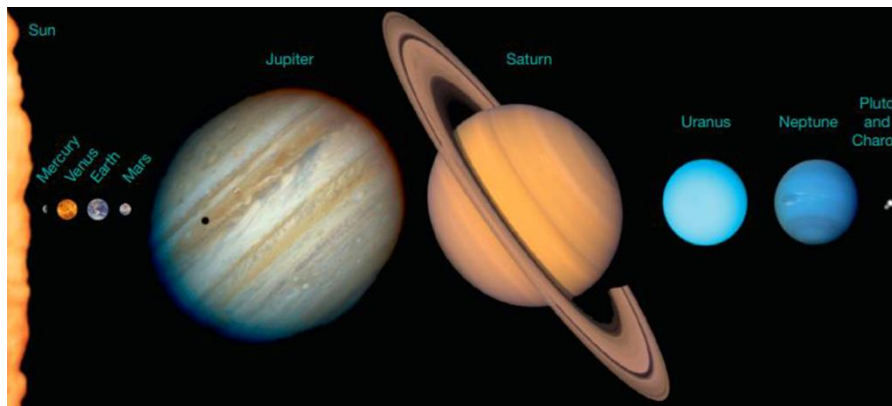
Figure 1.1. The Solar System [3]

The terrestrial planets are characterized by small masses and radii, and large densities. The rotations and magnetic fields indicate that the interior of these bodies are layered and divided into iron-rich cores, silicate mantles, and rocky crusts, which arise from the partial melting of the mantles. The chemical composition of these planets is difficult to determine since it is affected by many factors that cannot be controlled nor surely established. The knowledge of their composition is based on a combination of data from, chemistry of chondrites (stony meteorites with ultramafic compositions predominantly of Mg, Si and Fe elements, which are in the form of olivine and pyroxene as major minerals [6]) and the remote data coming from the spatial missions [7]. Saxena et al. [7] developed a method in which they checked all possible pressures and temperatures conditions of the nebula cloud and searched those where the mentioned solids would be stable. According to that, they concluded that Venus, Earth and Mars should have simple chemistry forming between 600 and 700 K at various pressures from 1^{-12} to 1^{-3} bars.

1.1.   Understanding Mars

The red planet was named after the Roman god of war. Mars is the fourth planet in the Solar System and it was formed during planet accretion 4.6 billion years (Giga-annum, Ga) ago. With a mean radius of 2289.5 km, it is intermediate in size between the Earth (6378 km) and the Moon (1738 km). The Mars day is 24 h and 40 min and the year is 687 Earth days or 669 sols (Martian days). The orbit of Mars is eccentric, between 1.381 and 1.666 AU (Astronomical Units), in contrast to the near-circular orbit of the Earth, and this affects the length and the intensity of its four seasons. They are due to the rotation axis of Mars, which is tilted 25º with respect to the orbit plane. Finally, Mars has two small moons with irregular surfaces, Phobos and Deimos [8, 9].

1.1.1.   Geology of Mars

Hartman and Neukum [10] suggested a Noachian period from 4.5 to 3.7 Ga, the Hesperian one from 3.7 to 3.0 Ga and the Amazonian era from 3.0 Ga to the present. As can be seen in Figure 1.2, other authors (such as Bibring et al. [11], Carr et al. [12] and Westall et al. [13]) proposed other geological time-scale based on the surface mineralogy [9].
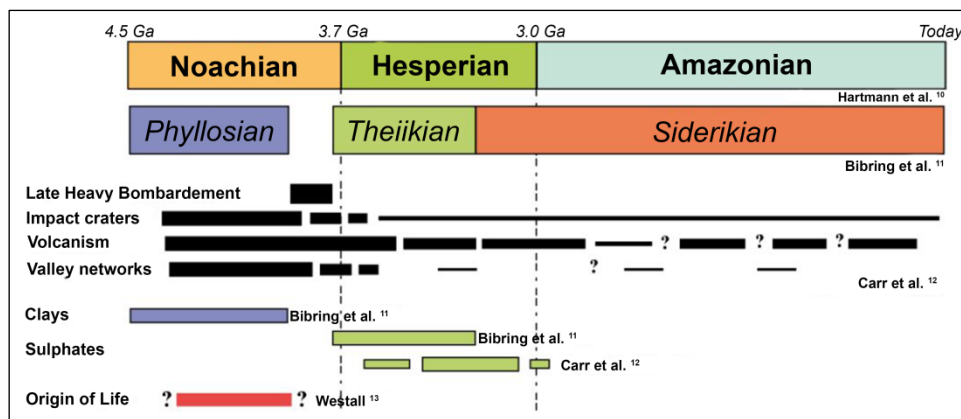
Figure 1.2. Time scale of Mars (Image adapted from Bost [9])

Noachian is characterized by the higher amount of craters, erosion and valley formation. During this period, the major part of the volcanism in the Tharsis region took place. Surface runoff patterns and lakes suggest episodic rainfall and warm conditions during this period. In the Hesperian period, the volcanism promoted lava broad plains, canyons were formed and, in the occidental hemisphere, sulfate deposits were accumulated. The Mount Olympus, which is the highest volcano in the Solar System, probably began to form during this last period. In the late Hesperian, the liquid water on Mars would be equivalent to the content of a 1 km deep ocean. Finally, the Amazonian era covers 2/3 parts of the time scale of the planet. Surface processes related with the ice and the wind, are more evident than in the previous periods.

Like the Earth, Mars can be differentiated into a crust, mantle and core. However, as there is not seismic data, the size of the core is poorly defined. Knowing that nowadays Mars has no magnetic field, the core is probably solid, but remnant crustal magnetic anomalies indicate that the core was molten early in the planet's history. The crust is estimated to range in thickness from 5 to 100 km, with a thicker crust in the southern hemisphere than in the north [8].

The Martian surface is characterized by a global dichotomy with two different features observed by the Thermal Emission Spectrometer (TES). A 5 km difference in surface elevation and 26 km difference in crustal thickness between the northern and southern hemispheres are observed [14]. The rocks from the Noachian takes up 45% of the surface, the Hesperian ones cover 31% and the rocks of Amazonian are in 24% of the surface [15]. In the southern highlands there are many craters whereas in the north a smoother surface is observed. At the low latitudes (southern hemisphere), there is not dust and, therefore, the surface shows a TES spectrum characteristic of basalts. In contrast, in the higher latitudes (northern hemisphere), a different spectrum is observed. It is interpreted as weathered basalt, since weathering processes occur preferentially in high latitudes. Mars seems to be essentially composed of volcanic rocks associated with sediments derived from basaltic alteration and weathering [8, 9].

Regarding the mineralogy, it is considered a record of the evolution of Mars, as minerals are the fingerprint of the processes that may have happened on the surface. Many

minerals have been discovered, in association with particular geological units, and used to understand geological processes. The mineralogy of Mars could be grouped into a few major distinctive types of igneous terrains that have variable spectral properties given by different proportions of some minerals, which are the most ubiquitous along the surface of the red planet. High-silica phases are present in high abundance in the northern plains (Amazonian-aged regions) and plagioclases and clinopyroxenes are the dominant minerals in the southern latitudes (Noachian or Hesperian-ages regions). The oldest area of Mars (Noachian crust) shows low-calcium pyroxene and olivine relative to the Hesperian lava provinces [16, 17].

All families of minerals that are going to be described below have been identified on the Martian surface and, except for olivine, pyroxenes and plagioclases, have arisen due to alteration processes such as hydric alteration, related to the sediments, hydrothermalism, associated to the volcanic activity, and atmospheric weathering due to which the regolith has been formed [18].

1.1.1.1. Primary silicates

Primary silicates on Mars have a basaltic-andesitic composition being olivine, pyroxenes and plagioclases the most common observed minerals.

Olivine ($(Mg,Fe)_2SiO_4$) on Mars shows a wide variability in composition [19], ranging from Fo_{91} (91% of fosterite, Mg-rich olivine) to Fo_5. It has been detected, for example, where Noachican-aged materials are exposed, in early Hesperian Crater floors and inter-crater plains in the southern highlands. Nevertheless, it has been found in almost all the Martian surface. Pyroxenes ($(Ca,Mg,Fe)_2Si_2O_6$) are also a dominant component of the igneous Martian crust. The Low-Calcium Pyroxenes (LCP) have been identified only in Noachian-aged terrains, suggesting that early Mars mantle was formed of aluminium and calcium rich minerals. The High-Calcium Pyroxenes (HCP), for their part, have been found throughout all the stratigraphy, usually in combination with LCP and olivine in Hesperian-aged volcanic flows [19, 20]. Finally, plagioclases ($(Na,Ca)(Si,Al)_4O_8$) are the most abundant minerals on the surface of Mars and they provide information about the magmatic evolution of the crust. The variability in their composition ranges from An_{50} (50% of anorthite, Ca-rich plagioclase) to An_{90}. They have been found in several areas, such as northern Hellas region or Nili Patera caldera in Syrtus Major, and are often associated with hydrated minerals.

1.1.1.2. Phyllosilicates

Phyllosilicates have been predominantly identified in ancient Noachian-aged terrains. These minerals are interpreted to be alteration products of mafic materials due to interaction between water and rock in both hydrothermal and near-surface open systems under neutral to alkaline conditions [21]. The OMEGA (Observatoire pour la Minéralogie l'Eau les Glaces et l'Activité) and CRISM (Compact Reconnaissance Imaging Spectrometer) Mars mappings showed that phyllosilicates are widespread distributed,

but the most extensive region of these minerals are located in Mawrth Vallis and Nili Fossae, and are associated with a range of geomorphic features that are restricted to ancient terrains [22]. This fact supports the hypothesis that Mars was once warm and wet. The majority of phyllosilicates described in Mars are Fe/Mg- and Al-smectites (nontronite $((CaO_{0.5},Na)_{0.3}Fe^{3+}_2(Si,Al)_4O_{10}(OH)_2 \cdot nH_2O)$ and montmorillonite $(Na,Ca)_{0.3}(Al,Mg)_2Si_4O_{10}(OH)_2 \cdot nH_2O))$, and in minor abundance kaolinites, chlorites, serpentines and micas [23].

1.1.1.3. Sulfides and sulfates

Sulfur is an important alloying element in metallic cores of Earth, Mars and Mercury due to its direct influence on the physical states, density, dynamical and thermal evolution cores. The sulfur cycle on Mars is of particular interest because it is a ubiquitous element in various Martian reservoirs. Moreover, it is thought to be a key element to maintain a liquid outer core of Mars [24].

Oxidized sulfur is one of the major components of the regolith. Sulfates arose from magmatic SO_2, but also, in a minor contribution, they could be formed from acid weathering of Fe-sulfides present on Mars. Studies of shergottites provide much information on sulfides in the interior of Mars, being pyrrhotite (Fe_7O_8) the predominant Fe-sulfide together with pentlandite (($Ni,Fe)_9S_8$) and chalcopyrite ($CuFeS_2$) [25]. Martian sulfate deposits are considered to be young, between late Noachian to Hesperian periods. The broad distribution of sulfate minerals seen by OMEGA likely points to widespread acidic surface waters and the dominant role of evaporate processes leading to sulfate precipitation. One of the largest sulfate deposits is in Valles Marineris [26].

1.1.1.4. Carbonates

The study of carbonates can serve as a powerful tool to understand the relationship between the existence of life, and the presence of water and carbon. The nature and distribution of these minerals on Mars are still unclear but it seems that carbonates do not exist as extensive bedrock (as happens on the Earth), but local deposits have been discovered [27].

Spirit Mars rover identified carbonates in the Comanche outcrops of the Columbia Hills in Gusev Crater [28]. It is composed of erosional remnants where the surrounding rocks are olivine-bearing basaltic rocks of Hesperian age. Phoenix lander also identified calcite ($CaCO_3$) in the Martian polar soil [28]. In the Phoenix landing site the surface is frost in winter. When unfrozen, the CO_2 diffused through this formed water, reacts with basaltic soil material and, therefore, the carbonates precipitate between the soil particles. Besides, in Gale Crater, Fe-rich carbonates have been determined in samples of eolian deposits probably having formed from the interaction of Fe^{2+}-rich olivine with the CO_2 atmosphere and transient water [28].

1.1.1.5. *Oxides*

The most common oxides on the Martian surface are those of iron. Ferric oxides dominate the mineralogy of Late Hesperian through Late Amazonian materials, indicating that liquid water has been rare in recent times on Mars [29]. It is thought long ago that the reddish colour of the Martian surface is given by the iron oxides, which form part of its composition. Even though iron oxides are not the main minerals, either in the bright or dark regions, their small percentage is enough to give the reddish colour [30].

1.1.2. Life on Mars

One of the most interesting topics related to the study of Mars is the detection of evidences of life on its surface. Space missions can employ two approaches to the challenge, in situ analysis on Mars and the return of samples for analysis on Earth [31]. Since life requires energy for its existence, possible energy sources found on Mars could be the direct and indirect employment of solar radiation, lightning, ionizing radiation, geothermal heat, and redox reactions involving carbon or inorganic compounds. On the other hand, nutrients are also necessary for building structures and, therefore, the availability of those nutrients could be a limitation to life. Martian life, if it ever existed, would be based as on Earth, in carbon, hydrogen, nitrogen, oxygen, phosphorus and sulfur. However, the amount of nitrogen (2.6% in volume [32]) is a potential problem and for example, nitrates, which are important nutrients for life on Earth, have not been detected yet on the surface of Mars. Access to organic carbon is another problem, even though the CO_2 (95% in volume [32]) is the dominant specie in the atmosphere of this planet. Nevertheless, reduced carbon compounds are rare on the surface. It is not possible to determine which the environmental requirements for the existence of life on Mars are. However, one environmental factor that is universally accepted as necessary for life is access to liquid water [33]. Those conditions favourable for the emergence of life, and which are similar to those on Earth, must have been present on Mars during the first hundred million years after its formation [34]. Outgassing associated with impact crater formation and volcanism are the primary sources of Martian water found in the atmosphere, polar caps and subsurface. This fact, together with the Martian dry mantle, which is known by the analyses of non-chondrite meteorites, indicates that water was incorporated into the crust and interior of Mars in very small concentrations. Images of the previous missions (Mariner 9 and Viking, described in the 1.1.4. *Previous exploration* section) revealed valley networks and outflow channel systems, leading to the conclusion that there had been liquid water circulating on the surface of Mars [29].

1.1.3. Study of Martian meteorites

The study of meteorites has provided a wide source of knowledge about the Martian mineralogy and to understand the history of Mars. In the literature there are many studies about meteorites from Mars regarding different types of meteorites and different minerals and processes. In the first example, Papike et al. [35] studied 19 Martian

meteorites that are representative of the six types of Martian rocks and made a review about the knowledge of meteorites. Torre-Fdez et al. [36] have studied a nakhlite (NWA 6148) and could estimate the metal proportion of the augite and olivine minerals present in the matrix of the meteorite. Moreover, they detected Co_3O_4 for the first time in a meteorite. Finally, Golden et al. [37] showed formation mechanisms for carbonates, magnetite and sulfides in ALH84001 Martian meteorite.

All this knowledge about Mars comes from the investigations made during the last 50 years. Apart from the study of meteorites, the orbiter, lander and rover missions carried out by different organizations described below have helped to describe and to establish the evolution of the neighbouring planet.

1.1.4. Previous exploration

The Martian missions can be classified in two groups, orbital and surface missions. In this section there is a brief description of the most important ones in relation to this PhD work and in Table 1.1 there is a summary of the different missions. Figure 1.3 shows the Mars Orbiter Laser Altimeter (MOLA) topographic map of Mars with different locations, the previous missions (in blue) and the upcoming ones (in red).
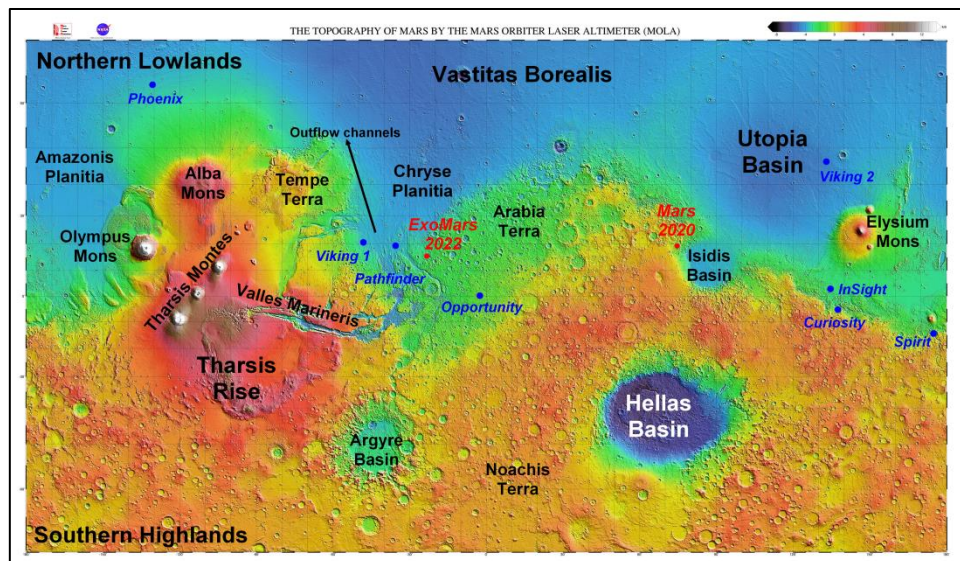
Figure 1.3. Martian map by the Mars Orbiter Laser Altimeter (MOLA) with de landing sites of the lander/rover missions (Image adapted from MOLA images [38])

After some unsuccessful missions, which, however, provided important new information to better adjust the orbital parameters, the first successful orbiter mission was Mariner 9 (NASA) in 1972. The primary objectives of this mission were to map Mars and observe its dynamic characteristics for a period of 90 days. It provided a full coverage of the Martian surface at a resolution of 50-500 m/pixel and, therefore, allowed the identification of the major surface features of Mars including the dichotomy boundary [39].

In 1975, NASA launched the Viking missions (1 and 2). It was one of the most ambitious planetary missions that consisted of two spacecraft formed each by an orbiter and a lander. The role of the orbiter was to transport the lander, to carry reconnaissance instruments for establishing the landing sites, to act as a reception station for the lander data and to perform its own measurements. Since the main scientific goal of this mission was the search for life, the landers, apart from panoramic cameras and instruments to characterize the physical properties and composition of the Martian soils and atmosphere, included experiments to search for organic matter, but non was detected. The landing sites were selected after the spacecrafts were in orbit; for Viking 1, landing site was Chryse (22ºN, 48ºW) and for Viking 2 the landing site was Utopia (44ºN, 226ºW). These missions generated more data about Mars than all the previous observations together [39, 40].

In 1996, the first probe after Viking to be launched to Mars was Mars Global Surveyor (MGS) by NASA. The programme to which it belonged (Mars Surveyor Program) focused on understanding the climates, whether or not life started and evolved, and the geological and geophysical evolution of the Red Planet. The formal science objectives for these missions were; to characterize surface morphology at high spatial resolution, to determine the composition and map the distribution of surface minerals, to determine the topography and gravitational field, to monitor global weather and thermal structure of the atmosphere, and to study surface-atmosphere interaction by monitoring surface features. It carried the Mars Orbiter Camera (MOC), the Mars Orbiter Laser Altimeter (MOLA) and the Thermal Emission Spectrometer (TES) [9, 41].

The Mars Pathfinder mission (also developed by NASA) landed on Mars in 1997 and consisted of a stationary lander (named Sagan Memorial Station) and a small rover called Sojourner. Pathfinder explored Ares Vallis, studied rocks using cameras, and analysed their elemental composition using an aAlpha Proton X-Ray Spectrometer (APXS). Sojourner examined the composition of ten rock samples, which had an andesitic to basaltic composition indicating a certain degree of differentiation from mantle-derived magmas [39, 42].

In 2003 another orbiter mission, named Mars Express (MES) was launched by ESA and is still operational. It consisted of an orbiter and a lander called Beagle-2. This lander was focused on the geochemistry and exobiology of the Martian surface. This mission contained a stereoscopic camera (High Resolution Stereo Camera, HRSC), an infrared spectrometer (Planetary Fourier Spectrometer, PFS), IR-spectro-imager OMEGA (Observatoire pour la Minéralogie l'Eau les Glaces et l'Activité), an ultraviolet spectrometer (Spectrosopic Investigation of the Characteristics of the Atmosphere of Mars, SPICAM-UV), the Mars Advanced Radar for Subsurface and Ionospheric Sounding (MARSIS), an imager of energetic neutral atoms with an analyser of space plasmas (Analyser of Space Plasmas and EneRgetic Atoms, ASPERA) and the Mars Radio Science experiment (MaRS) [43].

The Mars Exploration Rover mission (MER, NASA) was launched in two phases in 2003. The mission consisted of two identical rovers (Spirit and Opportunity), whose payload was, on the one hand, a panoramic camera (PanCam) and a thermal emission spectrometer (Mini-TES) on a mast, and, on the other hand, a Mössbauer spectrometer (MIMOS), an Alpha Particle X-Ray spectrometer (APXS) and a microscopic imager on a robotic arm. The difference between the rovers was the landing site, Gusev Crater for Spirit (focused on the aqueous alteration within Columbia Hills) and Meridiani Planum for Opportunity (looking for evidence that the deposits of this location were formed due to the evaporation of water and rising ground water) [39, 44].

The last orbital mission was the Mars Reconnaissance Orbiter (MRO) launched in 2005 by NASA and is still operational. This orbiter has a High Resolution Imaging Science Experiment (HIRISE), a Mars Color Imager (MARCI) for imaging the surface, and a Compact Reconnaissance Imaging Spectrometer to Mars (CRISM) [39]. The MRO have helped to the identification and characterization of the landing sites for next landing missions in terms of safety, but also in terms of the scientific potential for discoveries. Moreover, the data obtained from MRO has advanced the understanding of how Mars has evolved and by which processes those changes have occurred, identifying the presence, extent and role of water in shaping the planet's climate over time [45].

In 2008, Phoenix Mission by NASA landed in Vastitas Borealis at the North Pole. There, the lander detected traces of water ice and carbonates. It had four primary objectives; to determine the polar climate and weather, to characterize the geomorphology and active processes, to determine aqueous mineralogy and chemistry as well as the adsorbed gases as organic content of the regolith, and to characterize the history of water and polar climate [46]. It was equipped with a stereo imager (SSI), a combination of miniature heating ovens and a mass spectrometer (Thermal Evolved Gas Analyser, TEGA) and a wet chemistry suite (Mars Environmental Compatibility Assessment, MECA). The mission confirmed the presence of ice water about 5 cm below the surface [39].

Mars Science Laboratory (MLS, NASA) with the rover Curiosity was launched in 2011 and landed in 2012 and it is still working on the Martian surface. The selected landing site of this mission was Gale Crater. Curiosity rover was designed and built to explore the surface materials of Mars and to characterize its modern environment. Its principal objective was to search for ancient habitable environments [47]. It is equipped with different cameras; MastCam on the mast and MAHLI (Mars Hand Lens Imager) on the arm, and various mineralogical and geological instruments, such as Laser Induced Breakdown Spectroscopy (LIBS, on ChemCam), X-Ray diffraction and fluorescence (CheMin), an Alpha Particle X-Ray Spectrometer (APXS) and, a Sample Analysis at Mars (SAM) suite including a gas chromatograph, mass spectrometer and tuneable laser spectrometer, for analysing organic molecules [9].

The last mission landed on Mars by NASA was InSight, which was launched in 2018. InSight is a lander that has performed the first comprehensive surface-based geophysical investigation of Mars. The scientific goals of this mission were to understand

the formation and evolution of terrestrial planets through investigation of the interior structure and processes of Mars, and to determine its present level of tectonic activity and impact flux. It carries two scientific instruments; SEIS, a six-component seismometer, and a self-hammering mole system (Heat Flow and Physical Properties Package) [48].

Table 1.1. Previous exploration on Mars
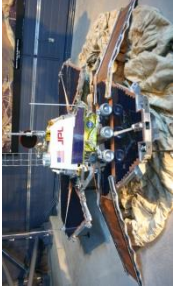
Mission	Year	Organization	Planetary finding	Photo
Mariner 4 (Flyby)	1972	NASA	- Craters on Mars - Negligible magnetic field - Thin atmosphere	
Mariner 9 (Orbiter)	1972	NASA	- Identification of dichotomy boundary - Pictures from Phobos and Deimos	
Viking 1/2 (Orbiter/Lander)	1975	NASA	- The first lander returning data - Polar cap made of water ice - 2.5 % of N_2 in the atmosphere - Inorganic composition: iron-rich clay, oxides of silica and iron	
Mars Global Surveyor (Orbiter)	1996	NASA	- There is no magnetic field - Thickest crust in south pole - Great northern ocean - Basaltic rocks and aqueous minerals	
Mars Pathfinder (Lander)	1996	NASA	- Rocks high in silica - Evidences of fluvial processes - Moment of inertia → metallic core - Airborne dust particles magnetized	

Table 1.1. (Cont.) Previous exploration on Mars
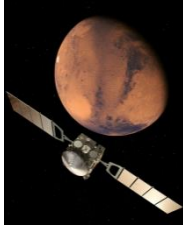
Mission	Year	Organization	Planetary finding	Photo
Mars Odyssey (Orbiter)	2001	NASA	- Hydrogen-rich layer in Southern hemisphere - First in-situ evidence of winter polar warming	
Mars Express (Orbiter)	2003	ESA	- Subsurface layers of water ice - Fleeting layer of clouds at altitudes of 100 km - Possible presence of methane - Recent and episodic volcanism	
Spirit/Opportunity (Rover)	2003	NASA	- Evidences of wetter and warmer surface - Soils with high content in silica related with hot springs	
Mars Reconnaissance Orbiter	2005	NASA	- Landing sites for Phoenix and Curiosity - Ice exposed in new craters - Chloride deposits	
Phoenix (Lander)	2007	NASA	- First chemistry tests with the wet lab - Alkaline and low saline soils - Calcium carbonate and perchlorates	

Table 1.1. (Cont.) Previous exploration on Mars

Mission	Year	Organization	Planetary finding	Photo
Curiosity (Rover)	2011	NASA	- Evidence of persistent liquid water in the past - Right chemistry for ancient life - Organic carbon and active methane	
MAVEN (Orbiter)	2013	NASA	- Mars atmosphere has been stripped by the Sun - Seasonal variation of atmospheric hydrogen - New types of aurorae	
Trace Gas Orbiter	2016	ESA Roscosmos	- No evidence of methane - Water-rich ice or minerals - Vertical distribution of dust and water	
InSight (Lander)	2018	NASA	- Odd magnetic pulsations - Electrically conductive layer	

1.1.5. Upcoming planetary missions to Mars

In the near future, ESA and NASA are going to launch two missions to Mars, ExoMars 2022 and Mars 2020, respectively. The exact date for the launch of the ESA's mission is still uncertain and in the case of the NASA's mission, the launch was scheduled between the 17th of July and the 5th of August of 2020, being the date of the arrival Mars on the 18th of February 2021. In addition, China National Space Administration (CNSA) has successfully launched Tianwen-1 mission to Mars from the Wenchang Spacecraft Launch Site on July 23 (2020). In the same way, United Arab Emirates Space Agency (UAE Space Agency) has launched the mission to Mars called Hope on July 19 (2020). Besides, even though it is still in an early state, Japan Aerospace eXploration Agency (JAXA) has planned the launch of their mission to Mars in 2024.

1.1.5.1. ExoMars 2022 (ESA)

The ExoMars 2022 mission will consists of a European rover (named Rosalind Franklin) and a Russian surface platform. A Proton rocket will be used to launch the mission, and after a nine-month journey, the rover will go through the Martian surface searching signs of life and collecting samples with a drill. Some of the instruments will operate in situ and some others in the analytical laboratory drawer with the samples collected by the drill. ExoMars 2022 will be the first mission that combines the capability to move across the surface and the ability to study Mars at depth [49].

This mission consists of 9 instruments; PanCam, ISEM, CLUPI, WISDOM, ADRON-RM, Ma-MISS, MicrOmega, RLS and MOMA (Figure 1.4).

The PanCam (Panoramic Camera) will provide images from which observations of landscape morphology, geology and atmospheric science may be derived. It will be crucial for geological target selection and characterization [50].

The ISEM (Infrared Spectrometer for ExoMars) is a pencil-bean infrared spectrometer that will measure the reflected solar radiation in the near infrared range. It will study the mineralogical and petrographic composition of the Martian surface (the water-bearing minerals being of particular interest) and will help in the selection of potential targets for close-up measurement [51].

The CLUPI (CLose-UP Imager) is a camera system, which acquires high-resolution colour close-up images of outcrops rocks, soils, etc. Its science objective is the geological characterization in terms of texture, structure and colour, searching for potential morphological biosignatures [52].

The WISDOM (Water Ice and Subsurface Deposit Observation On Mars) instrument is a ground-penetrating radar designed to provide information about the nature of the subsurface over a deep range (3-10 m). It will address information about the landing site, such as the depositional and erosional history, structural development and the role and distribution of liquid water and ice. Briefly, it will help in the selection of the scientific interest locations and choose the best sites and depths to collect samples [53].

The ADRON-RM (Autonomous Detector of Radiation of Neutrons ON board rover at Mars) is a compact passive neutron spectrometer, which will measure the spatial variability of the neutron flux emitted from the Martian surface. It is designed to study the abundance and distribution of water and neutron absorption elements [54].

Ma-MISS (Mars Multispectral Imager for Subsurface Studies) is a spectrometer designed to provide imaging and spectra by reflectance in the near-infrared region and it will produce hyperspectral images of the drill's borehole. It is the only instrument with the capability to analyse subsurface material before extracting the samples [55].

MicrOmega is a visible near-infrared hyperspectral microscope designed to characterize the texture and the composition of the Martian samples inside the rover's analytical laboratory drawer. Its prime objective is to characterize, at microscope scale, the structure and mineralogical composition of the samples collected by the drill [56].

The RLS (Raman Laser Spectrometer) is accommodated, together with MicrOmega and MOMA, in the analytical laboratory drawer. This Raman spectrometer (532 nm laser wavelength, CCD detector) gives precise identification of the mineral phases and organic matter working on the powdered samples (grain size between 200 and 250 µm) inside the analytical laboratory drawer (ALD) [57]. It is the first Raman Spectrometer qualified to flight (FM) to Mars.

MOMA (Mars Organic Molecule Analyser) instrument's objective is to search for signs of past life on Mars. It analyses the volatile organic compounds using a mass spectrometer (MS). The volatilization is achieved by one of the operational modes implemented: on the one hand, pyrolysis and liberation of species in the gas phase (being the organic compounds separated by gas chromatography and then carried to the MS). This process can also be preceded by a chemical derivatization to help in the transition to the gas phase. On the other hand, the volatilization can be produced by intense ultraviolet laser pulses inducing desorption in the gas phase and being the laser-desorbed species sent directly to the MS [58].
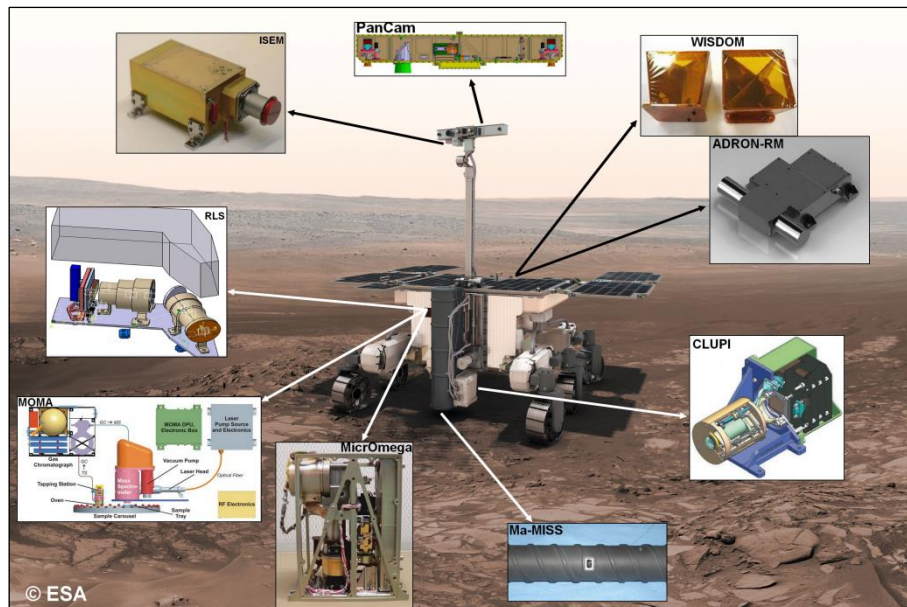
Figure 1.4. The ExoMars rover (Rosalind Franklin) with the location of each instrument (Image adapted from ExoMars 2022 mission page [49])

Regarding to the landing site, the selected area is Oxia Planum (18.14 ºN, 335.76 ºE, Figure 1.5). It is situated at the eastern margin of the Chryse basin at the outlet of the Coogoon Valles system. It is at the Martian dichotomy, in the transition between Arabia terra (eroded area in the highlands) and the northern Amazonian lowlands. Here, the diversity in geological features indicates active geological processes being one of the most studied areas on Mars. Many output channels dissect the zone, converge to Chryse Planitia, and fluvio-deltaic sediments are found on top of the clay-rich formation. Spectroscopic observations by OMEGA and CRISM indicate that the region is covered by clay deposit rich in Fe/Mg phyllosilicates [59].
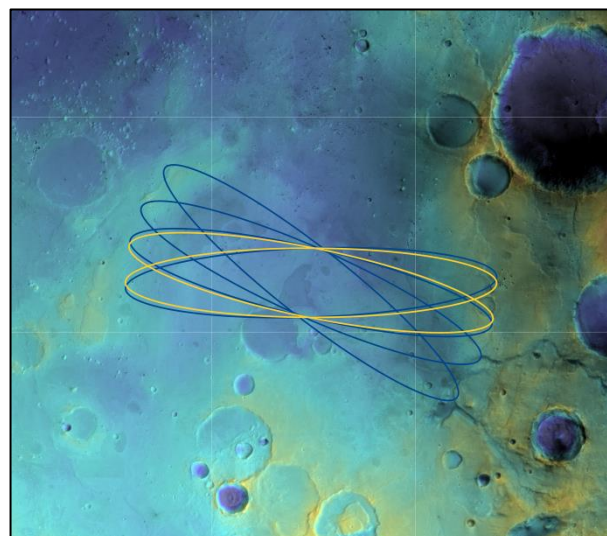
Figure 1.5. Map of Oxia Planum. HRSC images and MOLA topography together with the landing ellipses evaluated for site selection. © ESA/DLR/FU Berlin & NASA MGS MOLA Science Team [60]

The landing ellipse is placed over mostly flat and smooth-textured terrains, dominantly covered in clays. Regions where there are not alteration signatures are the Amazonian remnants [61]. Smectite clays or smectite/mica are the dominant minerals and hydrated silica and Al-rich phyllosilicates may be present to the east of the ellipse. The delta waterline suggests the presence of a standing body of water after the formation of the clay-rich unit over the entire landing ellipse area [62].

1.1.5.2. Mars 2020 (NASA)

The Mars 2020 rover (named Perseverance) mission is part of NASA's Mars Exploration Program, being one of its high-priority goals to answer key questions about the potential for life on Mars. The mission not only will search for signs of habitable conditions on ancient Mars, but will also look for signs of past microbial life itself. The rover introduces a drill that can collect samples, which could return to Earth in a future mission [63, 64]. Moreover, the mission will demonstrate technologies that address the challenges for future human expeditions, including testing a method for producing oxygen from the Martian atmosphere [65].

This rover has 7 instruments; Mastcam-Z, MEDA, MOXIE, PIXL, RIMFAX, SHERLOC and SuperCam (Figure 1.6).

The Mastcam-Z consists of two identical area-array digital cameras, which have 3:1 zoom telephoto lenses to permit images at focal lengths from 34 to 100 mm. This capability will enhance the stereoscopic imaging performance for both science and operations support [66].

MEDA (Mars Environmental Dynamics Analysed) is a suite of environmental sensors that can monitor dust and surface meteorology autonomously and will be capable of sampling environmental conditions. Its sensors will characterize the climate near the Martian surface [67].

The MOXIE (Mars Oxygen In-Situ Resource Utilization Experiment) unit is a model of an oxygen processing plant that might support a human expedition sometime in the 2030s. It will produce 22 g/h of O_2 on Mars with 99.6% purity during 50 sols. The goal is to understand the parameters, risks, challenges, margins and threats and requirements of a full-scale Mars In Situ Resource Utilization (ISRU) facility [68].

PIXL (Planetary Instrument for X-Ray Lithochemistry) is a micro-focus X-Ray fluorescence instrument located in the rover arm. It will be able to measure the abundance and distribution of elements with high spatial resolution, sensitivity and accuracy. These measurements will be correlated to visible textures through an optical system [69].

The RIMFAX (Radar Imager for Mars' subsurface eXperiment) ground penetrating radar (GPR) has the capability to image the shallow subsurface beneath the rover, at sufficient depth, resolution and timing to be of operational value, and will also provide geologic context [70].

SHERLOC (Scanning Habitable Environments with Raman and Luminiscence for Organics and Chemicals) combines imaging with UV resonance Raman and native deep UV fluorescence spectroscopy in order to identify potential biosignatures and understand the aqueous history of a site on Mars [71].

Finally, SuperCam is multi-functional spectroscopy instrument that remotely will provide observations about the mineralogy and elemental chemistry of the Martian surface and the search of organic materials. The mentioned instruments can perform Laser Induced Breakdown Spectroscopy (LIBS), Raman spectroscopy, time-resolved luminescence spectroscopy (TRLS), visible and near-infrared spectroscopy (VISIR) and high resolution colour remote micro-imaging (RMI) [72].
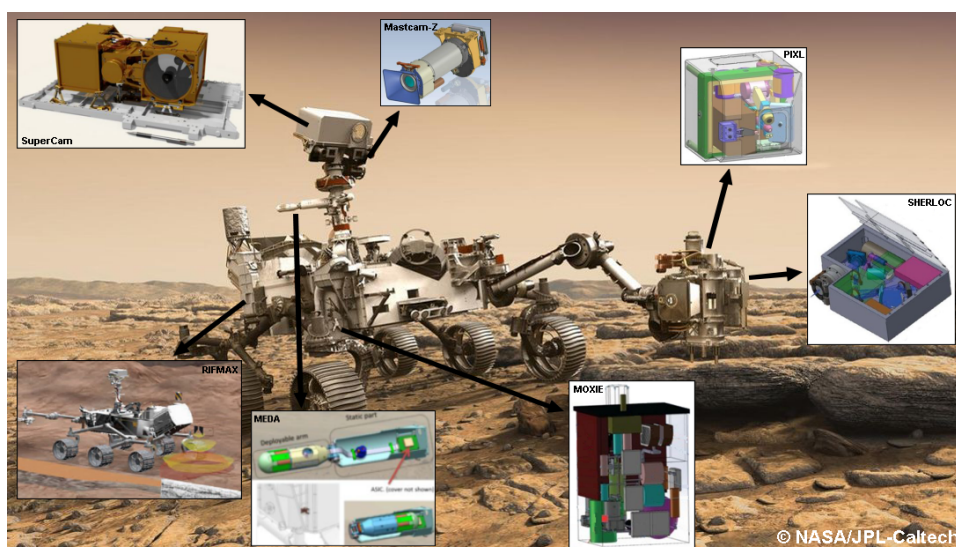
Figure 1.6. The NASA's rover (Perseverance) with the location of each instrument (Image adapted from Mars 2020 mission page [65])

The landing site of this mission will be Jezero Crater (18.4ºN, 77.7ºE, Figure 1.7). It is a Noachian crater (~45 km diameter) located on the southeast of the Nilli Fossae and immediately west to the rim of the Isidis basin. It has two inlet channels with eroded deltaic remnants, and associated outlet channel. Thanks to the CRISM data, the composition of the area has been characterized. The stratigraphically lowest units exhibit spectral evidence for Fe/Mg smectites. Above these units, strong signals of olivine and carbonates in the watershed and within Jezero Crater are observed (Briony et al. [73] stated that Jezero Crater is located in one of the largest carbonate-bearing units). The known as pitted capping unit appears to be of volcanic or impact melt origin (olivine and pyroxene signatures) and lacks alteration phases. Within the Jezero Crater there is light-toned floor unit, which is similar to the unit with the carbonate signal but is overlain by a Hesperian-aged volcanic unit with spectral evidence of pyroxene and olivine. Finally, the crater floor material distributed along the watershed represents a combination of basement terrain uplifted by the crater, volcanic material and accumulated eolian sediments [74].
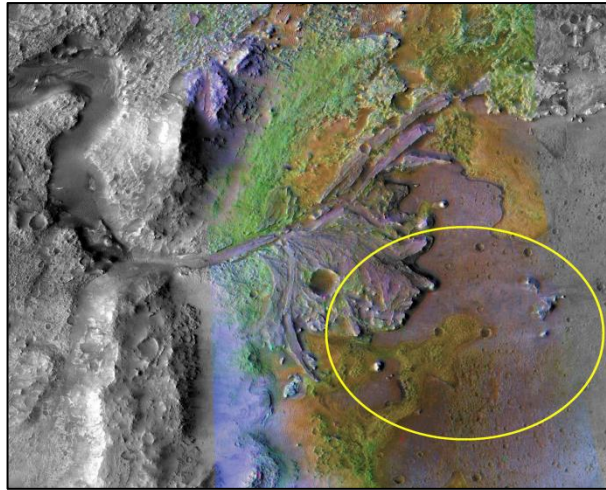
Figure 1.7. Map of Jezero Crater obtained by MRO combining information from CRISM and CTX with the landing ellipse. © NASA/JPL-Caltech/MSSS/JHU-APL [75]

The defined landing ellipse is located inside the crater (capping unit) covering the east of the phyllosilicate bearing areas, late-Noachian delta deposits and the northwest walls. The regions of interest are located in the western part of the ellipse, where the organics and biosignatures could be accessible [76].

1.1.5.3. Tianwen-1 (China National Space Administration)

The Tianwen-1 mission, carried out by CNSA, is made up of an orbiter, a lander and a six-wheeled rover that carries 12 instruments. The mission will perform global and general exploration of Mars using rover exploration. The main objectives of this mission are: to study the morphology and geological structure of Mars, to study the characteristics of the Martian soil and water-ice distribution, to study the Martian surface composition, to study the atmosphere, ionosphere, surface climate and environmental characteristics of Mars and to study Martian physical fields and internal structure.

The orbiter includes: Medium- and High- resolution Cameras, Mars Subsurface Exploration Radar, Mars Mineralogy Spectrometer, Mars Magnetometer, Mars Ions and Neutral Particle Analyzer and Mars Magnetic Particles Analyzer. The rover includes: Multispectral Camera, Subsurface Detection Radar, Mars Surface Composition Detection Package, Mars Magnetic Field Observation Station and Mars Climate Station.

During the mission, the ground application system will receive science data and perform data analysis and scientific research [77].

1.1.5.4. Martian Moons eXploration (MMX, JAXA)

The MMX (Martian Moons eXploration) carried out by JAXA, has as science objectives: to clarify the origin of the Martian moons and the process formation of the planet formation in the Solar System and to clarify the evolution process of the Martian-sphere. On the other hand, there are also engineering objectives such as; to establish the technology required for the return trip, to establish advanced sampling techniques on

celestial bodies and to establish optimal communication technologies using a newly developed ground station.

The probe has 7 science instruments: the Telescopic Nadir imager for GeOmOrphology (TENGOO) is a telescopic camera for observing the detailed terrain on the surface of the moons, Optical RadiOmeter composed of Chromatic Imagers (OROCHI) is a wide angle camera to observe the topography and material compositions in the Martian moon surface, LIDAR (Light Detection And Ranging) which is a ranging instrument to gather information on the shape of Phobos surface using a laser to reflect the light from the moon, MacrOMEGA (Macroscopique Observatoire pour la Minéralogie, l'Eau, le Glaces et l'Activité) is a near-infrared observation instrument to clarify the characteristics of minerals, Mars-moon Exploration with Gamma Rays and Neutrons (MEGANE) is a gamma Ray and neutron observation instrument to clarify the characteristics of chemical elements from the Martian moon, CMDM (Circum-Martian Dust Monitor) is a device for clarifying the dust environment around Phobos. Finally, MSA (Mass Spectrum Analyzer) is an instrument to establish the ion environment around the moon [78].

1.1.5.5. *Emirates Mars Mission (EMM, UAE Space Agency)*

The Emirates Mars Mission (whose probe is called Hope) is the first mission to Mars carried out by the United Arab Emirates. This mission is designed to orbit Mars studying the dynamics of the Martian atmosphere on both diurnal and seasonal time scales. The main objectives of EEM are; to understand climate dynamics and the global weather map, to explain how the weather changes the escape of hydrogen and oxygen and to understand the structure and variability of these two elements in the upper atmosphere and identify why Mars is losing them into space.

The orbiter include three instruments; Emirates Mars Infrared Spectrometer (EMIRS) is an interferometric thermal infrared spectrometer which will help in the understanding of the energy balance in the Martian climate and therefore how the lower atmosphere responds to solar forcing, the Emirates Exploration Imager (EXI) is a multi-wavelength radiation tolerant camera capable of taking 12-megapixeles images while maintaining the radiometric calibration needed, and finally the Emirates Mars Ultraviolet Spectrometer (EMUS) is a far ultraviolet spectrometer designed to determine the abundance and variability of carbon monoxide and oxygen in the thermosphere (100-200 km altitude), as well as the three-dimensional structure and the variability of oxygen and hydrogen in the exosphere (>200 km altitude) [79].

1.2.   Terrestrial Martian analogues

As described in the *Previous missions* section, in the different planetary missions, many minerals, important for the knowledge about the Martian history, have been identified. In this sense, it is necessary to understand the processes that could have happened during the geological history of Mars and, also, to understand those that can occur nowadays. However, without returned samples, Martian meteorites and terrestrial analogues have

been used as a reference for the interpretation of data from Mars and the characterization of its geological evolution. In this section, a number of studies of different emplacements established as key Martian analogues are described.

1.2.1. Analogues around the Earth

The exploration of Mars is largely based on comparisons with Earth analogue environments and processes [80]. There are several reasons to consider a terrestrial environment as a Martian analogue. As noted during the description of the following analogues, the volcanic origin, the presence of sediments, the processes that are happening or the geological features that are observed in the different areas, are some of the aspects to take into account to establish a Terrestrial Martian analogue.

1.2.1.1. Atacama Desert (Chile)

The Atacama Desert (Figure 1.8) is one of the driest deserts on Earth and receives very little precipitation. It lies in the northern Chile. The age of the Atacama Desert coupled with the hyper-arid (rains of a cm can occur a few times a century) environment has allowed sulfate, chloride and nitrate to accumulate. Current knowledge indicates that Mars has been arid with short episodes of aqueous activity and, therefore, the chemistry and mineralogy may be similar to Atacama [81]. Moreover, this emplacement is a relevant site for testing the robustness of the instruments developed for space flight and its autonomous operation procedures for the future planetary missions [82].

Figure 1.8. Atacama Desert (Chile). Images obtained from internet: top [83] and bottom [84]

The sediments of the hyper-arid core of the Atacama Desert are considered as an analogue of the Mars regolith. Besides, the several microbial communities discovered here make of this emplacement one of the most interesting places due to the existence of those organisms in a habitat with almost no water available and undetectable organic

carbon sources. Therefore, understanding the distribution and the microbial life in those sediments could give important information about how biosignatures may be on the Martian surface [85, 86]. Warren-Rhodes et al. [85] carried out geochemical analyses that revealed a mineralogy influenced by water bio-availability in deep sediments.

1.2.1.2.   Dry Valleys (Antarctica)

As reported by several authors, such as Gibson et al. [87], Cannon et al. [88] or Dickinson et al. [89] one of the most studied analogues are the Dry Valleys (Antarctica, Figure 1.9). This emplacement has been used as a Martian analogue for a long time (due to the environment and the weathering) even before the Viking mission to Mars. The conditions of the Dry Valleys were those expected to be present on Mars. The data returned by Viking supported the hypothesis that many geological processes that were happening on Mars were similar to those active in the Dry Valleys [87]. Antarctica has been frozen for the past 15 mega-annun (Ma) and this ice represents a major problem because it occurs not only in glacial old sediments but also in an environment thought to be free of running water, which makes this feature one of the most attractive for the proposal of this emplacement as a Martian analogue [89].
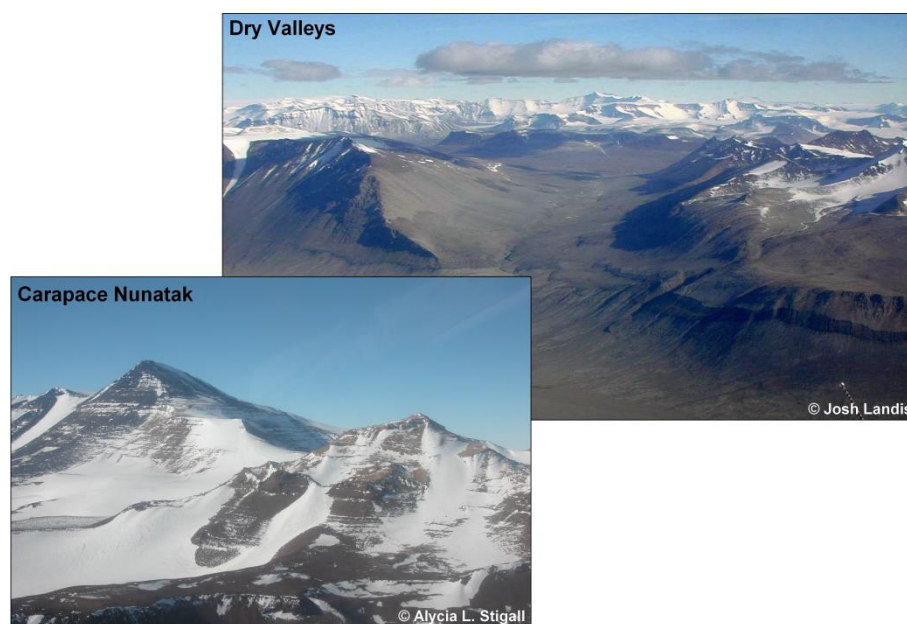
Figure 1.9. Dry Valleys (Antarctica). Images obtained from internet: top [90] and bottom [91]

On the other hand, how Martian sedimentary rocks are altered under different environmental conditions is poorly understood. It is for that reason that Cannon et al. [88] based their study on Carapace Sandstone from Carapace Nunatak (north of the Dry Valleys). They determined the alteration history of this area and the implications for the alteration of Martian sedimentary rocks. It is important for Martian studies because the sedimentary rocks are partially sourced from basaltic protolith and because of its original mineralogical and chemical immaturity. The extremely cold and dry climate provides the

only terrestrial environment similar to Martian conditions during the current Amazonian era.

1.2.1.3. *Mojave Desert (USA)*

Another desert emplacement proposed as a Martian analogue site is Mojave Desert in California (Figure 1.10). This region has received a great deal of attention due to its accessibility and the variety of landforms and processes observed relevant to Martian studies [92]. It exhibits a history of volcanism and tectonic activity, which subsequent weathering has produced physical conditions and chemical compositions similar to those on Mars. However, this region is used principally as the mechanical analogue for testing the Mars landing systems and rovers (due to its proximity to the Jet Propulsion Laboratory in California) [93].

Bishop et al. [94] stablished that carbonate rocks observed in Mojave Desert serve as potential analogues to the carbonates on Mars. This region contained pedogenic soil rich in iron oxides, clays and carbonate and much of these were eroded away. Remnants of the former aqueous environment are still found there, including an area of soil preserved under a basaltic lava flow. High concentrations of magnetite and hematite in the dust from Mojave Desert were detected apparently being the result from the alteration and erosion of other phases in the Cima volcanic ash (a volcanic field in San Bernardino County, California). The presence of magnetite and hematite on Mars could be due to a similar process. A possible environment for microbes on Mars, if present, could have been carbonate-rich waters. After its disappearance, such microbes could have survived living in the carbonate rocks, which together with iron oxide coatings could have provided a UV-protected niche [94]. Carbonate bearing regions on Mars would be suitable sites to search for biosignatures [94].

Figure 1.10. Mojave Desert (EEUU). Images obtained from internet: top[95] and bottom[94]

1.2.1.4. *Río Tinto (Spain)*

Amils et al. [96] describe Río Tinto (Spain, Figure 1.11) as a Martian analogue since in some locations on Mars, such as Meridiani planum, Noachian sulfate minerals have

been discovered, which suggests a past aqueous, acidic and sulfate-rich environment and it might be originated from the weathering of sulfide-rich minerals.

The discovery of sulfate deposits and the predominance of iron minerals on Mars reinforce the idea of the importance of the iron and sulfur geochemistry, which may have played a role in modifying surface and subsurface environments in the red planet. Due to the absence of atmosphere, the most probable region to search possible habitats is the subsurface, where aquifers of acidic waters would have provided the better conditions for the existence of organisms [97].

The finding of jarosite ($KFe_3^{3+}(SO_4)_2(OH)_6$) on Mars, thanks to the Mössbauer spectroscopy, restricted the interpretations of the Meridiani outcrop since that mineral precipitates under acidic conditions. These types of compounds in Rio Tinto, together with iron oxides, could be formed because of microbial activity. Amils et al. [96] give two reasons to demonstrate the interesting perspective for the interpretation of Martian data provided by Río Tinto as a Mars analogue site. The first one is that the iron oxides and sulfates generated in Río Tinto are under physico-chemical and biological conditions, which are well-characterized. The second one is the modern drainage where depositional processes can be observed. It is complemented by historical record of deposition preserved as sedimentary rocks in terraces at different levels above the river. This combination of deposits from different ages facilitates the comparison with Meridiani Planum among others [96].

Figure 1.11. Río Tinto (Huelva, Spain). Images obtained from internet: top [98] and bottom [99]

1.2.1.5. Námafjall (Iceland)

The land surface of Iceland consists of poor soils, bare rock and little vegetation. Extrusive basaltic lava flows have been taking place during the last 16 Ma (Mega-annum). Waters originated from precipitation (rather than from seawater) form most of the hydrologic systems. A variety of geothermal systems with different characteristics (low temperature and low sulfur content, low temperature and high sulfur content, high temperature and high sulfur content) and different physico-chemical properties give rise to diverse formation pathways of secondary minerals [100].

In the northeast of Iceland, the Námafjall volcanic system (Figure 1.12) is in an active rifting zone, characterized by basaltic subaerial lava flows and subglacialy-erupted volcanoclastic deposits and pillow basalts. These have been subjected to hydrothermal alteration producing localized areas of alteration mineral assemblages among the unaltered primary basalts [101]. These hydrothermal systems provide good analogues for Mars because of the similar Fe-rich lavas, as well as the fumarolic settings and acidic conditions. The mineral assemblages described avobe have been suggested as analogues for Meridiani Planum and Gusev Crater on Mars [102].
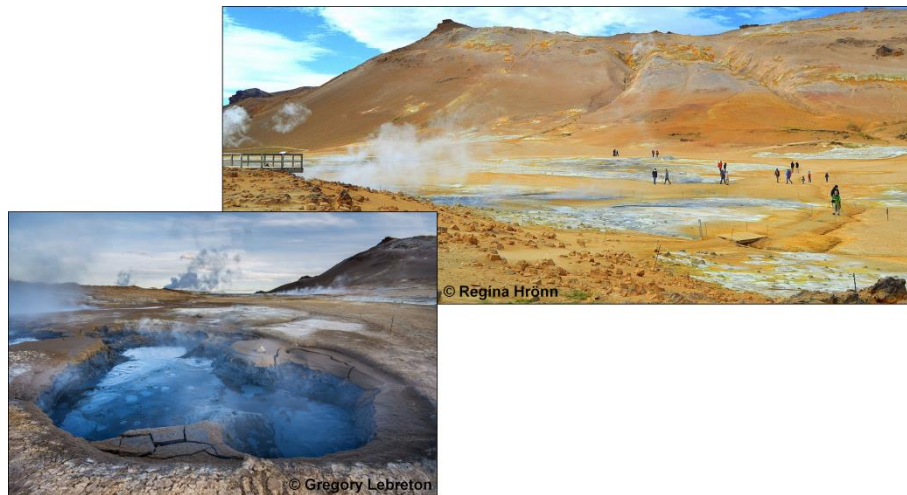
Figure 1.12. Námafjall (Iceland). Images obtained from internet: top [103] and bottom [104]

1.2.1.6.   *Skouriotissa mine (Cyprus)*

In the Skouriotissa mine (Figure 1.13), in North West Cyprus, there is an outcrop of ophiolitic basalts, which have suffered various types of chemical alterations due to the acidic water from this mine. This emplacement is proposed as a Martian analogue site due to the similarities with the Noachian era, the period when the appearance of life was more probable. In Mars, an ophiolite formation displays a dome-like structure centred on Mount Olympus, whose stratigraphy includes mantle sequence and in the north slope of the ophiolite, extrusive lavas (pillow lavas) and oceanic sediments overlap that sequence [9].

Figure 1.13. Skouriotissa mine (Cyprus). Images obtained from internet: top [105] and bottom [106]

The Skouriotissa mine exhibits a large variety of basaltic weathering products similar to the minerals observed on the Martian surface. Initially the basalt was altered by seawater and hydrothermal processes of the seafloor and then subaerially by acidic waters. Hydrothermal alteration resulted in a quartz-chlorite alteration facies, sea water processes in a smectitic facies and the acidic alteration favoured the formation of clays. The mine consists of an ellipse of massive sulfides capped by sedimentary deposits, which is a typical volcanogenic massive deposit associated with mafic volcanism [107]. Therefore, the massive sulfide ore deposit associated with basaltic volcanism makes the Skouriotissa mine into a very good analogue for understanding alteration that has taken place on the Noachian Martian surface. The rocks of this mine exhibit alteration due to both human activity and natural processes. The last one is a pseudo-deuteric alteration that resulted in the quartz facies, followed by a second weathering process that is associated with alteration by acidic waters and results in the formation of zeolites and sulfates [9].

1.2.1.7.   *The Haughton impact structure (Canada, Arctic)*

The Haughton impact structure in Devon Island (Figure 1.14) inside the Canadian High Arctic is a ~39 Ma old terrestrial impact crater with ~23 km of diameter and it has been proposed as a Martian analogue for geological features. This impact occurred into a target of dolomitic rocks, which already contained liquid hydrocarbons within fluid inclusions before the impact [108].

At Haughton, the existence of well preserved sedimentary deposits inside the crater (from Miocene age) is of particular interest since it provides a unique record of post-impact activity. Glacial and fluvial processes have modified the landscape but the amount of erosion and sedimentary record is not well established. This is a problem associated with this type of emplacements and has not been considered as an important process. Therefore, few studies of the intra-crater sedimentary deposits have focused on

understanding that record. However, these sedimentary deposits hold valuable clues for the recovery of the environment and the biological succession after large impact events. Besides, due to the requirement of water for life, intra-crater sedimentary deposits have been suggested as targets in the search of past life on Mars [109].
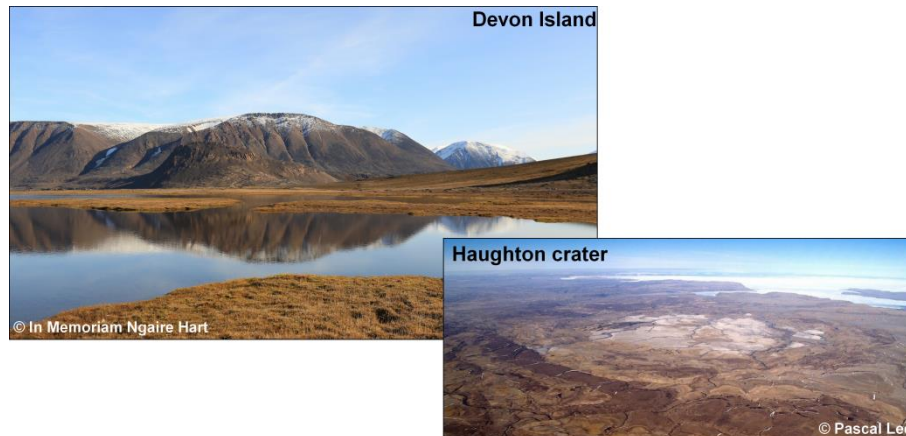
Figure 1.14. Haughton impact crater (Canada). Images obtained from internet: top [110] and bottom [111]

Lee et al. [112] proposed this emplacement as a Martian analogue since a variety of periglacial, fluvial, paleolacustrine and regolithic features and processes were observed at and near Haughton, and could be compared with those observed on Mars. They also reported the existence of lithophytic organisms there, the first time of these communities in association with impact-processes materials.

1.2.1.8.   *Kilauea volcano (Hawaii, USA)*

Kilauea volcano is one of the closest subaerial volcanos to the active hot spot of the Hawaiian Islands (Figure 1.15). It is accepted that these islands evolve in stage of volcanic eruptions, which are; the submarine eruptions (preshield), the theoleiitic basalt (shield), the chemically evolved alkali lavas (postshield), and finally, the rejuvenated stages. As the youngest subaerial volcano and probably the most active one on Earth, Kilauea is the best example of the shield stage of the Hawaiian eruptions, this stage being comparable to the Hesperian period on Mars [113]. Their very recent flows, which exhibit the last evidence of weathering alteration, show the primary mineralogical composition of the basalts, and therefore, they could help in understanding the primary composition of Martian surface, and hence, establish the geochemical processes that could have happened [114].

Figure 1.15. Kilauea Volcano (Hawaii, USA, thanks to Julene Aramendia)

All these examples show the variety of emplacements that can be considered Martian analogues. In this section, deserts, volcanic emplacements or sedimentary areas have been described and established as Martian analogues and scenarios, which help for the future interpretation of upcoming Martian data.

1.3.   Bibliography

1. Levy E. H., Solomon S. C. The science of planetary exploration. *The National Academies Press,* Washington, DC. **1979**.

2. Lewis J. S. Chapter 1: Introduction. In: *Physics and chemistry of the Solar System.* Ed. Lewis J. S. *Academic Press,* London. **1995,** pp. 1-4.

3. Spohn T. 10.01 - Physics of terrestrial planets and moons: an introduction and overview. In: *Treatise on geophysics (Second Edition).* Ed. Schubert G. *Elsevier,* Oxford. **2015,** pp. 1-22.

4. Lewis J. S. Chapter 3: General description of the Solar System. In: *Physics and chemistry of the Solar System.* Ed. Lewis J. S. *Academic Press,* London. **1995,** pp. 44-65.

5. Milone E. F., Wilson W. J. F. Solar system astrophysics. Vol. 1, Background science and the inner solar system. *Springer,* New York. **2008**.

6. Wood J. A. Chondritic meteorites and the solar nebula. *Annu. Rev. Earth Planet. Sci.,* **1988,** 16, 53-72.

7. Saxena S. K., Hrubiak R. Mapping the nebular condensates and the chemical composition of the terrestrial planets. *Earth Planet. Sci. Lett.,* **2014,** 393, 113-119.

8. Carr M. H. The surface of Mars. *Cambridge University Press,* Cambridge. **2007**.

9. Bost N. PhD thesis. *Geochemical and mineralogical analysis of Mars analogue materials and the creation of the International Space Analogue Rock Store (ISAR).*Université d'Orléans, France, **2012.**

10. Hartmann W. K., Neukum G. Cratering chronology and the evolution of Mars. *Space Sci. Rev.,* **2001,** 96, 165-194.

11. Bibring J. P., Langevin Y., Mustard J. F., Poulet F., Arvidson R., Gendrin A., Gondet B., Mangold N., Pinet P., Forget F., OMEGA team. Global mineralogical and aqueous mars history derived from OMEGA/Mars express data. *Science,* **2006,** 312, 400-404.

12. Carr M., Head J. Geologic history of Mars. *Earth Planet. Sci. Lett.,* **2010,** 294, 185-203.

13. Westall F. Early life on Earth and analogies to Mars. In: *Water on Mars and Life.* Ed. Tokano T. *Springer,* Berlin. **2005,** pp. 45-64.

14. Citron R. I., Manga M., Tan E. A hybrid origin of the Martian crustal dichotomy: Degree-1 convection antipodal to a giant impact. *Earth Planet. Sci. Lett.* **2018,** 491, 58-66.

15. Reyes K. I. PhD thesis. *Análisis geológico de la región Oxia Planum en Marte, sitio principal de aterrizaje de la Misión ExoMars 2020.* Universidad Nacional Autónima de México, México, **2016.**

16. Ehlmann B. L., Edwards C. S. Mineralogy of the Martian surface. *Annu. Rev. Earth Planet. Sci.,* **2014,** 42, 291-315.

17. Bandfield J. L., Hamilton V., Christensen P. A global view of Martian surface composition from MGS-TES. *Science,* **2000,** 287, 1626-1630.

18. Lalla E. A. PhD thesis. *Tenerife as Martian analogue: Multianalytic characterization (Raman, DRX, ATR-FTIR, SEM and MössBauer) of samples with planetary and artrobiological interest.* University of Valladolid, Valladolid, **2014.**

19. Mustard J., Poulet F., Gendrin A., Bibring J. P, Langevin Y., Gondet B., Mangold N., Bellucci G., Altieri F. Olivine and pyroxene, diversity in the crust of Mars. *Science,* **2005,** 307, 1594-1597.

20. Viviano-Beck C. E., Seelos F. P., Murchie S. L., Kahn E. G., Seelos K. D., Taylor H. W., Taylor K., Ehlmann B. L., Wisemann S. M., Mustard J. F., Morgan M. F. Revised CRISM spectral parameters and summary products based on the currently detected mineral diversity on Mars. *J. Geophys. Res. Planet.,* **2014,** 119, 1403-1431.

21. Liu Y., Catalano J. G. Implications for the aqueous history of southwest Melas Chasma, Mars as revealed by interbedded hydrated sulfate and Fe/Mg-smectite deposits. *Icarus,* **2016,** 271, 283-291.

22. Poulet F., Mangold N., Loizeau D., Bibring J. P., Langevin Y., Michalski J., Gondet B. Abundance of minerals in the phyllosilicate-rich units on Mars. *Astron. Astrophys.,* **2008,** 487, L41-L44.

23. Gavin P. PhD thesis. *Stability of phyllosilicates on Mars.* University of Arkansas, EEUU, **2012.**

24. Ding S., Dasgupta R., Tsuno K. Sulfur concentration of Martian basalts at sulfide saturation at high pressures and temperatures - Implications for deep sulfur cycle on Mars. *Geochim. Cosmochim. Acta,* **2014,** 131, 227-246.

25. Lorand J., Pont S., Chevrier V., Luguet A., Zanda B., Hewins R. Petrogenesis of Martian sulfides in the Chassigny meteorite. *Am. Mineral.,* **2018,** 103, 872-885.

26. Baldridge A. M., Hook S. J., Crowley J. K., Marion G. M., Kargel J. S., Michalski J. L., Thomson B. J., de Souza Filho C. R., Bridges N. T., Brown A. J. Contemporaneous deposition of phyllosilicates and sulfates: Using Australian acidic saline lake deposits to describe geochemical variability on Mars. *Geophys. Res. Lett.,* **2009,** 36, L19201, 1-6.

27. Niles P. B., Catling D. C., Berger G., Chassefiere E., Ehlmann B. L., Michalski J. R., Morris R., Ruff S. W., Sutter B. Geochemistry of carbonates on Mars: implications for climate history and nature of aqueous environments. *Space Sci. Rev.,* **2013,** 174, 301-328.

28. Bridges J. C., Hicks L. J., Treiman A. H. Chapter 5: Carbonates on Mars. In: *Volatiles in the Martian crust.* Ed. Filiberto J. and Schwenzer S.P. *Elsevier,* **2018,** pp. 89-118.

29. Barlow N. Mars: An introduction to its interior, surface and atmosphere. *Cambridge University Press,* UK. **2008**.

30. Sinton W. M. On the composition of Martian surface materials. *Icarus,* **1967,** 6, 222-228.

31. Sephton M. A., Carter J. N. The chances of detecting life on Mars. *Planet. Space Sci.,* **2015,** 112, 15-22.

32. Shekhtman L. *With Mars methane mystery unsolved, Curiosity serves scientists a new one: oxygen.* https://www.nasa.gov/feature/goddard/2019/with-mars-methane-mystery-unsolved-curiosity-serves-scientists-a-new-one-oxygen (last update 2020/03/24).

33. Board S. S., National Research Council An astrobiology strategy for the exploration of Mars. *National Academies Press,* **2007**.

34. Stalport F., Coll P., Cabane M., Person A., González R. N., Raulin F., Vaulay M. J., Ausset P., McKay C. P., Szopa C., Zarnecki J. Search for past life on Mars: Physical and chemical characterization of minerals of biotic and abiotic origin: part 1 - Calcite. *Geophys. Res. Lett.,* **2005,** 32, L23205, 1-5.

35. Papike J. J., Karner J. M., Shearer C. K., Burger P. V. Silicate mineralogy of martian meteorites. *Geochim. Cosmochim. Acta.* **2009,** 73, 7443-7485.

36. Torre-Fdez I., Aramendia J., Gómez-Nubla L., Castro K., Madariaga J. M. Geochemical study of the Northwest Africa 6148 Martian meteorite and its terrestrial weathering processes. *J. Raman Spectrosc.,* **2017,** 48, 1536-1543.

37. Golden D. C., Ming D., Schwandt C., Lauer H., Socki R., Morris R., Lofgren G., McKay G. A simple inorganic process for formation of carbonates, magnetite, and sulfides in Martian meteorite ALH84001. *Am. Mineral.,* **2001,** 86, 370-375.

38. National Aeronautics and Space Administration. *The Mars Orbiter Laser Altimeter.* https://attic.gsfc.nasa.gov/mola/images.html (last update 2020/04/27).

39. Wendt L. PhD thesis. *Phyllosilicates and sulfates on Mars. Case studies from Terra Cimmeria and Valles Marineris.* Freien Universität Berlin, Berlin, **2012.**

40. Soffen G. A. The Viking project. *J. Geophys. Res.,* **1977,** 82, 3959-3970.

41. Albee A., Arvidson R., Palluconi F., Thorpe T. Overview of the Mars Global Surveyor mission. *J. Geophys. Res. Planet.,* **2001,** 106, 23291-23316.

42. Golombek M., Cook R., Economou T., Folkner W., Haldemann A., Kallemeyn P., Knudsen J., Manning R., Moore H., Parker T., Rieder R., Schofield J., Smith P., Vaughan R. Overview of the Mars Pathfinder Mission and assessment of landing site predictions. *Science,* **1997,** 278, 1743-1748.

43. Schmidt R., Credland J. D., Chicarro A., Moulinier P. ESA's Mars Express mission - Europe on its way to Mars. *Esa Bulletin-European Space Agency,* **1999,** 56-66.

44. Arvidson R. E. Introduction to special section on results from the Mars Exploration Rover Spirit and Opportunity missions. *J. Geophys. Res. Planet.,* **2008,** 113, E06S01.

45. Zurek R. W., Smrekar S. E. An overview of the Mars Reconnaissance Orbiter (MRO) science mission. *J. Geophys. Res. Planet.,* **2007,** 112, E05S01, 1-22.

46. Shotwell R. Phoenix—the first Mars Scout mission. *Acta Atronaut.* **2005,** 57, 121-134.

47. Grotzinger J. P., Crisp J. A., Vasavada A. R., MSL Sci Team. Curiosity's mission of exploration at Gale Crater, Mars. *Elements,* **2015,** 11, 19-26.

48. Banerdt W., Smrekar S., Lognonné P., Spohn T., Asmar S., Banfield D., Boschi L., Christensen U., Dehant V., Folkner W., Giardini D., Goetze W., Golombek M., Grott M., Hudson T., Johnson C., Kargl G., Kobayashi N., Maki J. , Hurst K. InSight: a discovery mission to explore the interior of Mars. *LPSC 44.* **2013,** abst. 1915.

49. European Space Agency. *ExoMars Mission 2022.* https://exploration.esa.int/web/mars/-/48088-mission-overview (last update 2020/04/27).

50. Coates A. J., Jaumann R., Griffiths A. D., Leff C. E., Schmitz N., Josset J. L., Paar G., Gunn M., Hauber E., Cousins C. R., Cross R. E., Grindrod P., Bridges J. C., Balme M., Gupta S., Crawford I. A., Irwin P., Stabbins R., Tirsch D., Vago J. L., Theodorou T., Caballo-Perucha M., Osinski G. R., PanCam Team. The PanCam instrument for the ExoMars rover. *Astrobiology,* **2017,** 17 (5, 6), 511-541.

51. Korablev O. I., Dobrolensky Y., Evdokimova N., Fedorova A. A., Kuzmin R. O., Mantsevich S. N., Cloutis E. A., Carter J., Poulet F., Flahaut J., Griffiths A., Gunn M., Schmitz N., Martín-Torres J., Zorzano M., Rodionov D. S., Vago J. L., Stepanov A. V., Titov A. Y., Vyazovetsky N. A., Trokhimovskiy A. Y., Sapgir A. G., Kalinnikov Y. K.,

Ivanov Y. S., Shapkin A. A., Ivanov A. Y. Infrared spectrometer for ExoMars: a mast-mounted instrument for the rover. *Astrobiology,* **2017,** 17 (6, 7), 542-564.

52. Josset J. L., Westall F., Hofmann B. A., Spray J., Cockell C., Kempe S., Griffiths A. D., De Sanctis M. C., Colangeli L., Koschny D., Follmi K., Verrecchia E., Diamond L., Josset M., Javaux E. J., Esposito F., Gunn M., Souchon-Leitner A. L., Bontognali T. R. R., Korablev O., Erkman S., Paar G., Ulamec S., Foucher F., Martin P., Verhaeghe A., Tanevski M., Vago J. L. The Close-Up Imager onboard the ESA ExoMars rover: objectives, description, operations, and science validation activities. *Astrobiology,* **2017,** 17 (6, 7), 595-611.

53. Ciarletti V., Clifford S., Plettemeier D., Le Gall A., Herve Y., Dorizon S., Quantin-Nataf C., Benedix W., Schwenzer S., Pettinelli E., Heggy E., Herique A., Berthelier J., Kofman W., Vago J. L., Hamran S., Wisdom Team. The WISDOM Radar: Unveiling the Subsurface Beneath the ExoMars Rover and Identifying the Best Locations for Drilling. *Astrobiology,* **2017,** 17 (6, 7), 565-584.

54. Mitrofanov I. G., Litvak M. L., Nikiforov S. Y., Jun I., Bobrovnitsky Y. I., Golovin D. V., Grebennikov A. S., Fedosov F. S., Kozyrev A. S., Lisov D. I., Malakhov A. V., Mokrousov M. I., Sanin A. B., Shvetsov V. N., Timoshenko G. N., Tomilina T. M., Tret'yakov V. I., Vostrukhin A. A. The ADRON-RM instrument onboard the ExoMars rover. *Astrobiology,* **2017,** 17 (6, 7), 585-594.

55. de Sanctis M. C., Altieri F., Ammannito E., Biondi D., De Angelis S., Meini M., Mondello G., Novi S., Paolinetti R., Soldani M., Mugnuolo R., Pirrotta S., Vago J. L., Ma Miss Team. Ma-MISS on ExoMars: mineralogical characterization of the Martian subsurface. *Astrobiology,* **2017,** 17 (6, 7), 612-620.

56. Bibring J. P, Hamm V., Pilorget C., Vago J. L., MicrOmega Team. The MicrOmega investigation onboard ExoMars. *Astrobiology,* **2017,** 17 (6, 7), 621-626.

57. Rull F., Maurice S., Hutchinson I., Moral A., Pérez C., Díaz C., Colombo M., Belenguer T., López-Reyes G., Sansano A., Forni O., Parot Y., Striebig N., Woodward S., Howe C., Tarcea N., Rodríguez P., Seoane L., Santiago A., Rodríguez-Prieto J. A., Medina J., Gallego P., Canchal R., Santamaría P., Ramos G., Vago J. L., RLS Team. The Raman Laser Spectrometer for the ExoMars rover mission to Mars. *Astrobiology,* **2017,** 17 (6, 7), 627-654.

58. Goesmann F., Brinckerhoff W. B., Raulin F., Goetz W., Danell R. M., Getty S. A., Siljeström S., Missbach H., Steininger H., Arevalo R. D.,Jr., Buch A., Freissinet C., Grubisic A., Meierhenrich U. J., Pinnick V. T., Stalport F., Szopa C., Vago J. L., Lindner R., Schulte M. D., Brucato J. R., Glavin D. P., Grand N., Li X., van Amerom F. H. W., Moma Science Team. The Mars Organic Molecule Analyzer (MOMA) instrument: characterization of organic material in Martian sediments. *Astrobiology,* **2017,** 17 (6, 7), 655-685.

59. Egea-González I., Jiménez-Díaz A., Parro L. M., Mansilla F., Holmes J. A., Lewis S. R., Patel M. R., Ruiz J. Regional heat flow and subsurface temperature patterns at Elysium Planitia and Oxia Planum areas, Mars. *Icarus,* **2019,** 113379.

60. European Space Agency. *Robotic exploration of Mars - Oxia Planum.* https://exploration.esa.int/web/mars/-/54724-oxia-planum (last update 2020/04/27).

61. Carter J., Quantin C., Thollot P., Loizeau D., Ody A., Lozach L. Oxia Planum, a clay-laden landing site proposed for the ExoMars rover mission: aqueous mineralogy and alteration scenarios. *LPSC 47.* **2016,** abst. 2064.

62. Vago J. L., Westall F., Coates A. J., Jaumann R., Korablev O., Ciarletti V., Mitrofanov I., Josset J. L., De Sanctis M. C., Bibring J. P., Rull F., Goesmann F., Steininger H., Goetz W., Brinckerhoff W., Szopa C., Raulin F., Westall F., Edwards H. G. M., Whyte L. G., Fairen A. G., Bridges J., Hauber E., Ori G. G., Werner S., Loizeau D., Kuzmin R. O., Williams R. M. E., Flahaut J., Forget F., Rodionov D., Svedhem H., Sefton-Nash E., Kminek G., Lorenzoni L., Joudrier L., Mikhailov V., Zashchirinskiy A., Alexashkin S., Calantropio F., Merlo A., Poulakis P., Witasse O., Bayle O., Bayon S., Meierhenrich U., Carter J., García-Ruiz J. M., Baglioni P., Haldemann A., Ball A. J., Debus A., Lindner R., Haessig F., Monteiro D., Trautner R., Voland C., Rebeyre P., Goulty D., Didot F., Durrant S., Zekri E., Koschny D., Toni A., Visentin G., Zwick M., van Winnendael M., Azkarate M., Carreau C., Pasteur Instrument Teams, Landing Site Selection Working, ExoMars Project Team. Habitability on early Mars and the search for biosignatures with the ExoMars rover. *Astrobiology,* **2017,** 17, 471-510.

63. National Aeronautics and Space Administration. *Mars sample return.* https://www.jpl.nasa.gov/missions/mars-sample-return-msr/ (last update 2020/04/27).

64. European Space Agency. *Mars sample return.* https://www.esa.int/Science_Exploration/Human_and_Robotic_Exploration/Exploration/Mars_sample_return (last update 2020/04/27).

65. National Aeronautics and Space Administration. *Mars 2020 mission. Overview.* https://mars.nasa.gov/mars2020/mission/overview/ (last update 2020/01/07).

66. Mehall L. K., Cisneros E., Bell III J.F., Paris K. N., Wellington D., Jenson E.H., Maki J.N., Hayes A.G., Kinch K., and the Mastcam-Z Team. Mars 2020 Mastcam-Z PDS4 data archive. *4th Planetary Data Workshop.* **2019,** abst. 2151.

67. Rodríguez-Manfredi J. A., de la Torre M., Boland J. S., Bridges N. T., Conrad P., Ferri F., Genzer M., Gómez-Gómez F., Gómez-Elvira J., Harri A-M., Kemppinnen O., Lemmon M., Martínez G., Navarro S., Newman C., Pérez-Hoyos S., Prieto O., Ramos M., Saiz-López A., Sánchez-Lavega A., Schofield J. T., Sebastian E., Smith M., Tamppari L. K. and the MEDA team. MEDA, the Environmental Dynamics Analyzer for Mars 2020. *3rd International Workshop on Instrumentation for Planetary Missions.* **2016,** abst. 4114.

68. Michael H. H, Jeffrey A. H. for the MOXIE Team. The Mars Oxygen ISRU Experiment (MOXIE) on the Mars 2020 Rover. *LPSC 46.* **2015,** abst. 2774.

69. Allwood A. C., Wade L.A., Hurowitz J.A. PIXL investigation on the Mars 2020 rover: spatially-resolved fine scale elemental chemistry and the challenging search for ancient biosignatures. *AbSciCon.* **2015,** abst. 7609.

70. Hamran S., Amundsen H. E. F., Asak L., Berger T., Brovoll S., Buskenes J. I., Carter L., Damsgård L., Diaz C., Ghent R., Helleren Ø., Kohler J., Mellon M., Nunes D., Paige D., Plettemeier D., Rowe K., Russell P., Sagsveen B., Ødegaard N., Øyan M. J. The RIMFAX GPR instrument development for the Mars 2020 rover mission. *3rd International Workshop on Instrumentation for Planetary Missions.* **2016,** abst. 4031.

71. Beegle L. W., Bhartia R., Carrier B., DeFlores L., Abbey W., Asher S., Burton A., Fries M., Conrad P., Clegg S., Edgett K. S., Ehlmann B., Hug W., Reid R., Kah L., Nealson K., Nelson T., Minitti M., Popp J., Langenhorst F., Sobron P., Steele A., Tarcea N., Wiens R., Williford K., Yingst R. A. The SHERLOC investigation for Mars 2020. *LPSC 48.* **2017,** abst. 2839.

72. Ollila A. M., Wiens R. C., Maurice S., Cousin A., Anderson R., Beyssac O., Bonal L., Beck P., Clegg S., Chide B., DeFlores L., Dromart G., Fischer W., Forni O., Fouchet T., Gasnault O., Grotzinger J., Johnson J., Lasue J., Laserna J., Madariaga J. M., Madsen M., Mangold N., Nelson T., Newell R., Martínez-Frías J., McLennan S., Montmessin F., Robinson S., Sharma S., Misra A., Rull F., Venhaus D., Bernardi P., Reess J. M., Reyes-Newell A., Poulet F., Lanza N., Torre I., Aramendia J., Pérez R., Cloutis E., Angel S., Mimoun D., Lorenz R., Rapin W., Meslin P. Y., Frydenvang J., McConnochie T. , Bernard S. Preparing SuperCam for Jezero Crater, Mars: LIBS, Raman, VISIR, luminescence, imaging, and acoustic analyses. *Ninth International Conference on Mars.* **2019,** abst. 6352.

73. Horgan B. H. N., Anderson R. B., Dromart G., Amador E. S., Rice M. S. The mineral diversity of Jezero crater: Evidence for possible lacustrine carbonates on Mars. *Icarus.* **2020,** 339, 113526.

74. Salvatore M. R., Goudge T. A., Bramble M. S., Edwards C. S., Bandfield J. L., Amador E. S., Mustard J. F., Christensen P. R. Bulk mineralogy of the NE Syrtis and Jezero crater regions of Mars derived through thermal infrared spectral analyses. *Icarus,* **2018,** 301, 76-96.

75. National Aeronautics and Space Administration. *Jezero Crater, Mars 2020's landing site.* https://mars.nasa.gov/resources/22475/jezero-crater-mars-2020s-landing-site/ (last update 2020/04/27).

76. Grant J. A., Golombek M. P., Wilson S. A., Farley K. A., Williford K. H., Chen A. The science process for selecting the landing site for the 2020 Mars rover. *Planet. Space Sci.,* **2018,** 164, 106-126.

77. Yingzhuo J., Yu F., Yongliao Z. Scientific objectives and payloads of Chinese first Mars exploration. *Chinese Journal of Space Science,* **2018,** 38 (5), 650-655.

78. Japan Aerospace Exploration Agency *Martian Moons eXploration (MMX) mission.* http://mmx.isas.jaxa.jp/en/ (last update 2020/04/27).

79. UAE Space Agency *Emirates Mars Mission "Hope probe".* https://www.emiratesmarsmission.ae/ (last update 2020/07/23).

80. Ivarsson M., Sallstedt T., Carlsson D. Morphological biosignatures in volcanic rocks - Applications for life detection on Mars. *Front. Earth Sci.,* **2019,** 7, 91-114.

81. Sutter B., Dalton J. B., Ewing S. A., Amundson R., Mckay C. P. Terrestrial analogs for interpretation of infrared spectra from the Martian surface and subsurface: Sulfate, nitrate, carbonate, and phyllosilicate-bearing Atacama Desert soils. *J. Geophys. Res. Biogeo.,* **2007,** 112, G04S10, 1-19.

82. Wei J., Wang A., Lambert J. L., Wettergreen D., Cabrol N., Warren-Rhodes K., Zacny K. Autonomous soil analysis by the Mars Micro-beam Raman Spectrometer

(MMRS) on-board a rover in the Atacama Desert: a terrestrial test for planetary exploration. *J. Raman Spectrosc.,* **2015,** 46, 810-821.

83. Leman J. *What's So Special About the Atacama Desert? - LIVE SCIENCE.* https://www.livescience.com/64752-atacama-desert.html (last update 2020/05/26).

84. European Space Agency. *ESA tests self-steering rover in 'Mars' desert.* http://www.esa.int/Enabling_Support/Space_Engineering_Technology/ESA_tests_self-steering_rover_in_Mars_desert (last update 2020/05/26).

85. Warren-Rhodes K. A., Lee K. C., Archer S. D. J., Cabrol N., Ng-Boyle L., Wettergreen D., Zacny K., Pointing S. B., , The NASA Life in the Atacama Project Team. Subsurface microbial habitats in an extreme desert Mars-analog environment. *Front-Microbiol.,* **2019,** 10, 69, 1-11.

86. Azúa-Bustos A., González-Silva C., Corsini G. The hyperarid core of the Atacama Desert, an extremely dry and carbon deprived habitat of potential interest for the field of carbon science. *Front. Microbiol.,* **2017,** 8, 993, 1-6.

87. Gibson E. K., Wentworth S. J., McKay D. S. Chemical weathering and diagenesis of a cold desert soil from Wright Valley, Antarctica: An analog of Martian weathering processes. *J. Geophys. Res. Sol. Ea.,* **1983,** 88, A912-A928.

88. Cannon K. M., Mustard J. F., Salvatore M. R. Alteration of immature sedimentary rocks on Earth and Mars: Recording aqueous and surface-atmosphere processes. *Earth Planet. Sci. Lett.,* **2015,** 417, 78-86.

89. Dickinson W. W., Rosen M. R. Antarctic permafrost: An analogue for water and diagenetic minerals on Mars. *Geology,* **2003,** 31, 199-202.

90. United States Antarctic Program-National Science Foundation *USAP Photo Library.* https://photolibrary.usap.gov/PhotoDetails.aspx?filename=Bullpa1.jpg (last update 2020/05/26).

91. Stigall A. L. *Stigall Lab - Paleobiogeography, Paleoecology, Macroevolution.* https://www.alyciastigall.org/photos/dscn1113-2/ (last update 2020/05/26).

92. Salas E., Abbey W., Bhartia R., Beegle L. W. The Mojave Desert: a Martian analog site for future astrobiology themed missions. *Analogue Sites for Mars Missions: MSL and Beyond.* **2011,** abst. 161.

93. Beegle L. W., Peters G. H., Mungas G. S., Bearman G. H., Smith J. A., Anderson R. C. Mojave Martian simulant: a new Martian soil simulant. *LPSC 38.* **2007,** abst. 2005.

94. Bishop J. L., Schelble R. T., McKay C. P., Brown A. J., Perry K. A. Carbonate rocks in the Mojave Desert as an analogue for Martian carbonates. *Int. J. Astrobiol.,* **2011,** 10, 349-358.

95. Francis J. *10 Adventurous Things To Do In Mojave Desert, CA - TOURIST SECRETS.* https://www.touristsecrets.com/destinations/10-adventurous-things-to-do-in-mojave-desert-ca/ (last update 2020/05/26).

96. Amils R., Fernández-Remolar, D. and the Ipbsl Team. Río Tinto: a geochemical and mineralogical terrestrial analogue of Mars. *Life,* **2014,** 4, 511-34.

97. Fernández-Remolar D., Prieto-Ballesteros O., Rodríguez N., Gómez F., Amils R., Gómez-Elvira J., Stoker C. Underground habitats in the Río Tinto basin: a model for subsurface life habitats on Mars. *Astrobiology,* **2008,** 8 (5), 1023-1047.

98. Ahechu I. - Flickr https://www.flickr.com/photos/128718836@N03/ (last update 2020/05/26).

99. Martínez Ron A. *Expediente Río Tinto: la verdad sobre el río "extraterrestre" - VOZ PÓPULI.* https://www.vozpopuli.com/altavoz/next/Exobiologia-Astronomia-Biologia-Rio_Tinto-CAB_0_683331720.html (last update 2020/05/26).

100. Ehlmann B. L., Bish D. L., Ruff S. W., Mustard J. F. Mineralogy and chemistry of altered Icelandic basalts: Application to clay mineral detection and understanding aqueous environments on Mars. *J. Geophys. Res. Planet.,* **2012,** 117, E00J16, 1-27.

101. Harris J. K., Cousins C. R., Gunn M., Grindrod P. M., Barnes D., Crawford I. A., Cross R. E., Coates A. J. Remote detection of past habitability at Mars-analogue hydrothermal alteration terrains using an ExoMars Panoramic Camera emulator. *Icarus,* **2015,** 252, 284-300.

102. El-Maarry M., Black S., Hynek B., Mchenry L. Mineralogy of fumarolic deposits from Iceland as analogs for ancient hydrothermal systems on Mars: role of temperature. *LPSC 48.* **2017,** abst. 2870.

103. Hrön R. *Mývatn in North-Iceland - Part IV - Mt. Námafjall, Krafla & Leirhnjúkur Geothermal Areas - GUIDE TO ICELAND.* https://guidetoiceland.is/connect-with-locals/regina/the-amazing-myvatn-area---part-iv (last update 2020/05/26).

104. Lebreton G. - Locationscout *Námafjall Hverir - Iceland.* https://www.locationscout.net/iceland/1881-namafjall-hverir (last update 2020/05/26).

105. PMS Lab, University of Cyprus *PVROSION.* http://psm.ucy.ac.cy/pvrosion/experiments/technical-meeting-at-hellenic-copper-mines-ltd/attachment/hellinccopper5/ (last update 2020/05/26).

106. Kalli I. - Wordpress *Cyprus - Copper - Site.* https://ikallioutoforder.wordpress.com/2016/11/08/copper-cyprus-site/ (last update 2020/05/26).

107. Bost N., Ramboz C., Foucher F., Westall F. The Skouriotissa mine: a new terrestrial analogue for hydrated minerals formation on early Mars. *Analog Sites for Mars Missions II.* **2013,** abst. 4006.

108. Parnell J., Bowden S. A., Osinski G. R., Lee P., Green P., Taylor C., Baron M. Organic geochemistry of impactites from the Haughton impact structure, Devon Island, Nunavut, Canada. *Geochim. Cosmochim. Acta,* **2007,** 71, 1800-1819.

109. Osinski G. R., Lee P. Intra-crater sedimentary deposits at the Haughton impact structure, Devon Island, Canadian High Arctic. *Meteorit. Planet. Sci.,* **2005,** 40, 1887-1899.

110. In Memorian Ngaire Hart - Flickr https://www.flickr.com/photos/eriagn/28731154224/ (last update 2020/05/26).

111. Fong T., Bualat M., Deans M., Adams B., Allan M., Altobelli M., Bouyssounouse X., Cohen T., Flueckiger L., Garber J. Robotic follow-up for human exploration. **2010,** 25.

112. Lee P., Bunch T. E., Cabrol N., Cockell C. S., Grieve R. A. F., McKay C. P., Rice J. W. Jr., Schutt J. W., Zent A. P. Haughton-Mars 97 - I: Overview of observations at the Haughton impact crater, a unique Mars analog site in the Canadian High Arctic. *LPSC 29.* **1998,** abst. 1973.

113. Hughes S. S., Haberle C. W., Nawotniak S. E. K., Sehlke A., Garry W. B., Elphic R. C., Payler S. J., Stevens A. H., Cockell C. S., Brady A. L., Heldmann J. L., Lim D. S. S. Basaltic terrains in Idaho and Hawaii as planetary analogues for Mars geology and astrobiology. *Astrobiology,* **2019,** 19, 260-283.

114. Seelos K. D., Arvidson R. E., Jolliff B. L., Chemtob S. M., Morris R. V., Ming D. W., Swayze G. A. Silica in a Mars analog environment: Ka'u Desert, Kilauea Volcano, Hawaii. *J. Geophys. Res. Planet.,* **2010,** 115, E00D15, 1-18.

CHAPTER 2:

OBJECTIVES

The main objective of this PhD thesis was to perform a geochemical characterization of several submarine volcanic outcrops, which belong to the Basque-Cantabrian Basin (BCB, Biscay, Spain) and establish them as Terrestrial Martian analogues. This characterization provides the knowledge about some of the geochemical processes that have happened or that are happening in the Earth.

Due to the similarities between the studied emplacements and parts of the Martian surface, it could be possible to extrapolate the Earth mechanisms to Mars and, therefore, the interpretation of the data obtained in the next planetary missions would be easier, and the understanding of Mars more complete. Furthermore, the relative lack of studies about antique submarine volcanos (which are those studied in this PhD thesis) as Martian analogues, makes the BCB and its volcanic outcrops a very interesting location for this study.

Moreover, since one of the main objectives of the next planetary missions (ExoMars 2022 and Mars 2020) is searching for evidence of previous life to demonstrate the potential habitability of the red planet, some analyses were performed in order to identify possible organic molecules that could be present in the upcoming results from Mars.

In order to accomplish the main objective, some operational objectives had to be fulfilled:

- To develop a spectral database (Raman and VNIR) of minerals found on Earth and therefore to increase the knowledge in the interpretation of the studied analogues and in the future results from Mars.

- To use Raman and visible near infrared spectroscopies, among others, for the geochemical characterization since they are two of the techniques included on board the rovers of the aforementioned missions.

- To establish possible differences in the different studied locations due to the environmental conditions of each location and, therefore, the different weathering processes that could have taken place.

- To use other techniques such as ToF-SIMS or GC-MS in order to better identify the presence of organic matter.

CHAPTER 3:

EMPLACEMENTS: BASQUE–

CANTABRIAN BASIN

Located in northern Spain, the Basque-Cantabrian Basin (BCB) constitutes the western extension of the Pyrenean folded belt along extensive onshore and offshore areas of the Bay of Biscay. It is a large Cretaceous sedimentary succession developed by latest Jurassic rifting of the Iberian and European plates (creating the Bay of Biscay). This rifting resulted in the break-up of the Jurassic carbonate ramps and the emergence and erosion of former marine areas. The boundary between the Iberian and European plates probably lies in the faulted area of the Biscay synclinorium and it is associated with submarine volcanism from the late Albian [1].

The BCB has undergone a long evolution process since Permian-Triassic times to the present. During these 250 Ma, deposits were accumulated in different sectors from the Lower Cretaceous to the Middle Eocene, with thickness ranging from 2000 m to more than 10000 m. The Aptian–Albian successions widely attain a thickness of more than 5000 m. The thickness differences have been attributed to the geodynamic process of extension, differences in subsidence and sedimentation rates related to the opening of the Bay of Biscay within the overall evolution of the Atlantic Ocean [2, 3]. Therefore, it is

commonly accepted that the BCB is the result of a complex evolution process including different basin types that registered different changes related to the dominating tectonic conditions [4].

This evolution process is also explained as a succession of geological events that occurred since the Early Paleozoic era. During the Post-Paleozoic era, lateral drift of the Iberian plate and its collision with the European plate took place and, in the Mesozoic, the Pyrenean domain suffered volcanism, and sedimentary basins were developed. Through the Cretaceous, the Basque-Cantabrian chain suffered intense subsidence that generated a high amount of sediments, which were accumulating until Albian times. Since then to the Santonian, marine sedimentation and submarine volcanism took place at the same time [5]. This submarine volcanic activity of alkaline character, developed during the upper Cretaceous along the western sector of the Pyrenean chain, was related to a rift and/or transform fault in the continental crust associated to the opening of the North Atlantic Ocean. Between the sediments that form the basin, some alkaline cretaceous lavas appear in the form of pillow lavas and volcanoclastic deposits. These effusive materials, interbedded in the Cretaceous marine sediments, are those that form the Biscay synclinorium. The lavas are compositionally different, varying from basalts to trachytes [6].

Taking into account volcanic activity happened on Mars, and the existence of water in some periods of its history, it could be possible that some episode of submarine volcanism took place. Therefore, the study of this type of scenario is of high importance since such examples are not widely studied, and considered them as Martian analogues (as can be seen in the *Introduction* chapter). Many examples of this submarine volcanism can be observed along the Basque-Cantabrian basin (Figure 3.1) and some of them are described below.
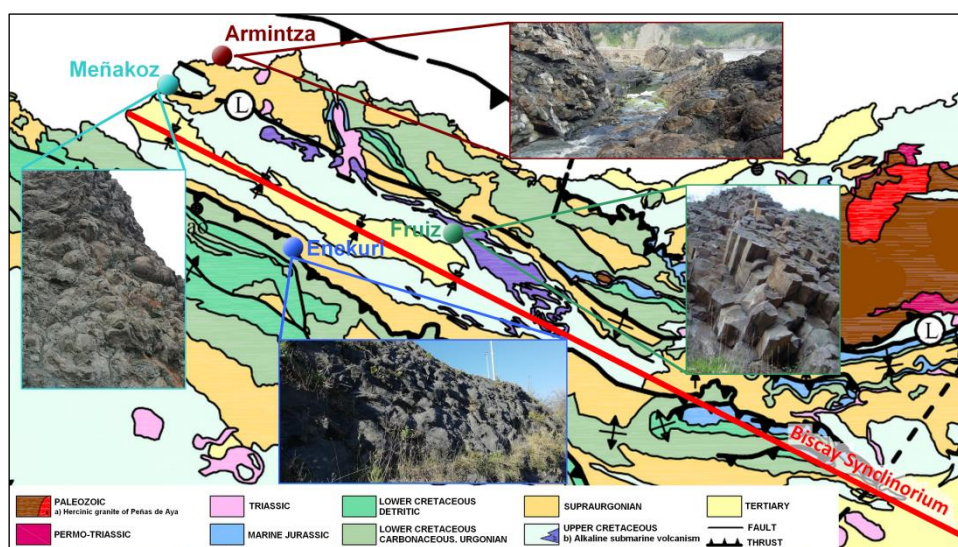

Figure 3.1. Submarine volcanic locations in the Basque-Cantabrian Basin (Image adapted from Carracedo et al. [7])

3.1. Meñakoz (Barrika, Basque Country, Spain))

The Meñakoz outcrop (43º 23' 42.14'' N, 2º 59' 23.43'' W, Figure 3.2), which appears from sea level to a height of 20 m, is located in the south-western area of the Meñakoz beach. In the Gernika-Elgoibar fault, it represents an old submarine volcanic scenario formed in the Santonian times (83.5 Ma, upper Cretaceous period) due to the Alpine orogeny (700-900 m in depth), cutting the marine Turonian sediments. This volcanic area shows typical characteristics of this type of eruptions under submarine conditions, such as pillow lavas (including a pile of cylindrical lava tubes that presents rough or smooth surfaces), megapillows and a wide range of pyroclastic and autoclastic deposits, which have been suffering several weathering processes [5].

In this type of formations, a high number of vesicles can be observed. This fact is due to the CO_2 produced by the lava flow at high temperature, which transforms chalks into lime. The existence of these vesicles and pyroclastic materials is due to the depth of volcanic formation, which corresponds to the depth at which alkaline magma causes explosive eruptions. While emerged, the volcanic rocks suffered hydrothermal transformations at 200°C and P < 1 kbar, transforming the primary minerals (plagioclase, olivine, pyroxenes, alkali feldspars, amphiboles, etc) into secondary ones (albite, calcite, chlorite, prehnite, etc) [5].
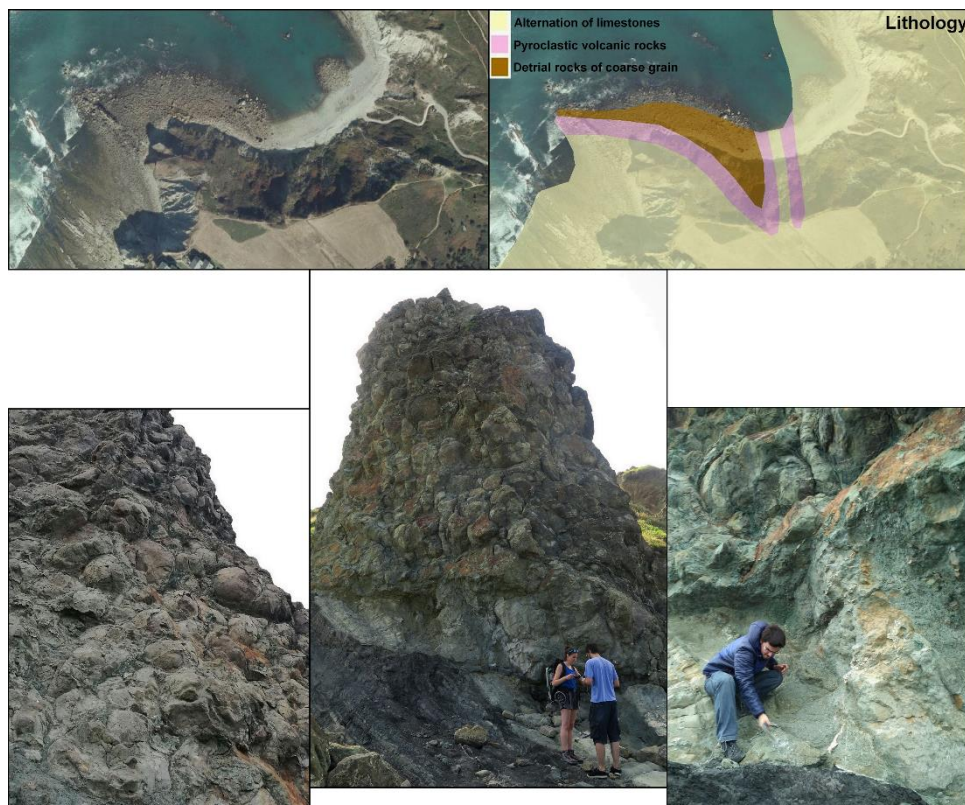

Figure 3.2. Meñakoz outcrop (Barrika). Location, geology and pillow lavas from the outcrop. Top images were obtained from geoEuskadi Visor [8]

The volcanic minerals alternated with marine sediments of this emplacement show a similar sequence to that expected to be found on some locations of Mars. Therefore, the

mineral phases found in Meñakoz should be geochemically similar to such regions on Mars.

Basaltic rocks and basic volcanoclastic deposits interbedded in marine sediments of the cliff characterize the Meñakoz outcrops. On the one hand, green areas with different hues and white areas forming veins and vesicles are the most common ones in the samples, and they are characteristic of kinds of rocks. On the other hand, some orange, brownish and grey areas are also observed. These samples will be described below.

3.2.   Armintza (Lemoiz, Basque Country, Spain)

The black flysch of Armintza (43º 25' 59.10'' N, 2º 54' 6.39'' W, Figure 3.3) is located in the occidental part of the Basque Cantabrian Basin (Armintza-Plentzia subbasin) [9] and it consists of black mudstones, sandstones, conglomerates and extrusive igneous rocks (lavas and pyroclastics). It has been demonstrated that the vertical arrangement of facies can be related to synsedimentary faulting leading to deepening and widening of the basin floor and, ultimately, to submarine volcanic activity [10]. Meschede [11] defines the Bay of Armintza as an excellent outcrop of turbiditic sediments. Here exists an Albian-Cenomanian sequence of a deep sea fan, which belongs to a large delta system developed on the region of Machichaco Cape. In the upper part of this turbiditic sequence Cretaceous alkali basalts occur. In the literature, Armintza is known as "Supra-Urgonian Complex" [12]. The massive influx of clastics in the Upper Albian produced first a reduction and later a complete disappearance of the earlier platform (Urgonian) carbonate sedimentation [12].

In the black flysch, there are volcanic sequences from the upper Albian period formed by pillow lavas, pillow brechias and volcanoclastites [10]. The flysch sediments show an overall fining sequence, indicating the progressive deepening of the deep-water marine sedimentary succession. The depositional environment progressed from upper slope with turbiditic channels, to lower slope with turbiditic lobes and channel-lobe transitions, and then, to mainly marly slope with sheet turbidites, a basalt interval and intercalated volcaniclastic horizons [12].

Figure 3.316. Armintza outcrop (Lemoiz). Location, lithology and geological features (pillow lavas and black flysch). Top images were obtained from geoEuskadi Visor [8]

3.3.   Enekuri (Erandio, Basque Country, Spain)

The volcanic rocks of Enekuri (43º29'67.07''N, 2º95'16.17''W, Figure 3.4) are in the Iberian margin and were formed in the late Albian. They appeared controlled by the NW-SE set of faults that constitute the Bilbao fault zone [13].

The outcrops located in this area are from the Upper Cretaceous and are situated in the north part of the Bilbao anticlinorium. Here, materials from volcanic origin are interbedded with fine sediments, lutites and marls. Among the volcanic materials, the presence of a basaltic flow and pillow lavas is highlighted. The presence of sandstones and shales before the volcanic sequence evidences the instability associated with the volcanic processes [14].
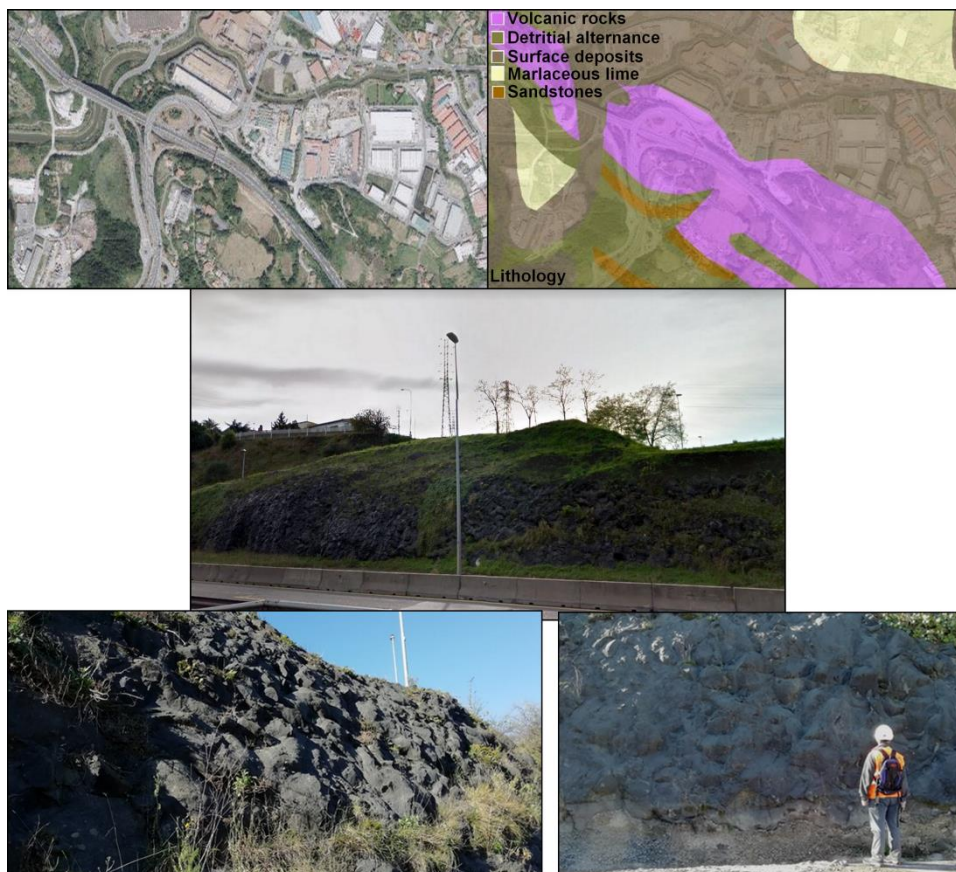
Figure 3.4. Enekuri outcrop (Erandio). Location, lithology and pillow lavas from outcrop. Top images were obtained from geoEuskadi Visor [8]

3.4.   Fruiz (Uribe-Butroe, Basque Country, Spain)

The Fruiz (43º19'53.68''N, 2º47'28.90''W, Figure 3.5) outcrop belongs to the Gernika-Elgoibar fault in the European margin to the northeast of Bilbao. The Gernika-Elgoibar fault is separated from the Bilbao fault by the late Cretaceous-Tertiary Biscay synclinorium. The volcanic rocks of Gernika-Elgoibar fault zone were dated as late Albian-Santonian (as Meñakoz) and therefore, the outcrops from this fault coincided with the youngest eruptions of the Bilbao fault [13]. This episode is the most important one due to its extension, facies diversity and internal volcanic sequences [9].

The Elgoibar fault is considered the western expression of the North Pyrenean fault. Stratigraphic and sedimentologic data suggest that the Elgoibar fault was left lateral and it controlled the development of the depositional system during the Aptian-Albian and the Late Cretaceous [15].

Fruiz is the best example of the columnar disjunction feature. At this point, several outcrops of this type appear, being two of them superposed. The prisms exhibit a pentagonal basement of up to 60 cm of side. A succession of sedimentary, volcanic and pyroclastic events can be observed [16].
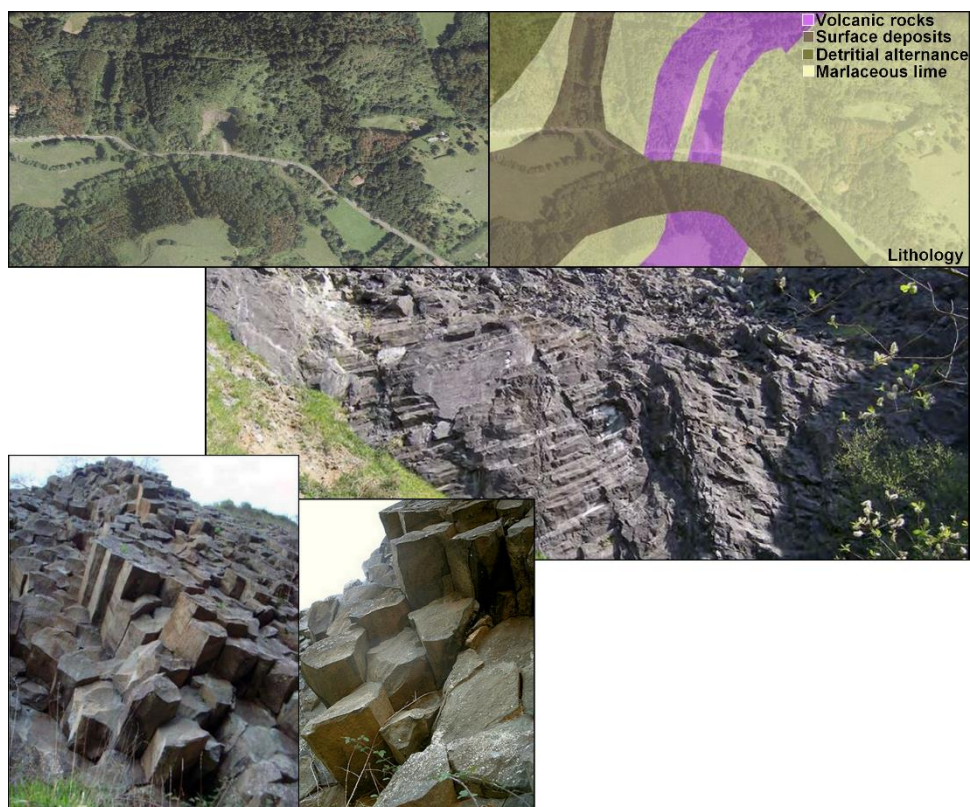
Figure 3.17. Fruiz quarry (Uribe-Butroe). Location, lithology and the columnar disjunt feature. Top images were obtained from geoEuskadi Visor [8]

3.5.   Bibliography

1. Martín-Chivelet J., Berástegui X., Rosales I., Vilas L., Vera J. A., Caus E., Gräfe K-U., Mas R., Puig C., Segura M., Robles S., Floquet M., Quesada S., Ruiz-Ortiz P. A., Fregenal-Martínez M. A., Salas R., Arias C., García A., Martín-Algarra A., Meléndez M. N., Chacón B., Molina J. M., Sanz J. L., Castro J. M., García-Hernández M., Carenas B., García-Hidalgo J., Gil J., Ortega F. Cretaceous. In: *The Geology of Spain.* Ed. Gibbons W. and Moreno T. *The Geological Society,* UK. **2002,** pp. 255.

2. García-Mondéjar J., Agirrezabala L., Aranburu A., Fernández-Mendiola P. A., Gómez-Pérez I., López-Horgue M. A., Rosales I. The Aptian-Albian tectonic pattern of the Basque Cantabrian Basin (Northern Spain). *Geol. J.,* **1996,** 31, 13-45.

3. Aróstegui J., Zuluaga M. C., Velasco F., Ortega-Huertas M., Nieto F. Diagenesis of the central Basque-Cantabrian Basin (Iberian Peninsula) based on illite-smectite distribution. *Clay Miner.,* **1991,** 26, 535-548.

4. Robles S. Evolución geológica de la Cuenca Vasco Cantábrica. In: *Geología de la Cuenca Vasco-Cantábrica.* Eds. Bodego Aldasoro A., Mendia Aranguren M., Aranburu Artano A., Apraiz Atutxa A. *Universidad del País Vasco/Euskal Herriko Unibertsitatea,* Leioa. **2014,** pp. 9-51.

5. Carracedo-Sánchez M., Sarrionandia F., Juteau T., Gil-Ibarguchi J. I. Structure and organization of submarine basaltic flows: sheet flow transformation into pillow lavas in shallow submarine environments. *Int. J. Earth Sci.,* **2012,** 101, 2201-2214.

6. Carracedo-Sánchez M., Larrea F., Alonso A. Estructura y organización de las coladas submarinas: características de las lavas almohadilladas de edad cretácica que afloran en la Cordillera Vasco-Cantábrica. *Estudios Geológicos,* **1999,** 55, 209-222.

7. Carracedo-Sánchez M., Sarrionandia F., Juteau T. El vulcanismo submarino de edad cretácica de la Cuenca Vasco-Cantábrica. *Macla,* **2012,** 16, 260-267.

8. Eusko Jaularitza/Gobierno Vasco *geoEuskadi, Infraestructura de Datos Espaciales de Euskadi.* https://www.geo.euskadi.eus/s69-bisorea/es/x72aGeoeuskadiWAR/index.jsp (last update 2020/07/23).

9. Castañares L. M., Robles S., Vicente J. C. Distribución estratigráfica de los episodios volcánicos submarinos del Albiente-Santoniense en la Cuenca Vasca (sector Gernika-Plentzia, Bizkaia). *Geogaceta,* **1997,** 22, 43-46.

10. García-Mondéjar J., Pujalte V. The black flysch (Upper Albian-Lower Cenomanian) in the Bay of Arminza, Vizcaya. *6th Eur. Meet. IAS,* **1985,** 307-392.

11. Meschede M. The tectonic and sedimentary development of the Biscay synclinorium in Northern Spain. *Geol. Rundsch.,* **1987,** 76, 567-577.

12. López-Horgue M. A., Owen H. G., Aranburu A., Fernández-Mendiola P. A., García-Mondéjar J. Early late Albian (Cretaceous) of the central region of the Basque-Cantabrian Basin, northern Spain: biostratigraphy based on ammonites and orbitolinids. *Cretaceous Res.,* **2009,** 30, 385-400.

13. García-Mondéjar J., Carracedo-Sánchez M., Owen H. G., Fernández-Mendiola P. A. The Early Aptian volcanic episode of Gutiolo (N Spain): Expression of the Bilbao Rift Fault Zone. *Geol. J.,* **2019,** 54, 3509-3526.

14. Badillo J. M., Orue-Etxebarria X., Rodríguez-Lázaro J. Las facies Supraurgonianas entre La Avanzada y el Puente de Rontegui (Bizkaia) son de esas Albiense Superior. *Estudios del Instituto Alavés de la Naturaleza,* **1987,** 2, 171-177.

15. Agirrezabala L. Kinematic indicators and mineralization on the Elgoibar fault (Basque-Cantabrian Basin). *Geogaceta,* **2001,** 30, 7-10.

16. Cuevas J., Garrote A., Tubía J. M. Análisis y significado de diferentes tipos de estructuras en el magmatismo del cretácico superior de la cuenca Vasco-Cantábrica (1ª Parte). *Munibe. Sociedad de Ciencias ARANZADI,* **1981,** 1-2, 1-20.

CHAPTER 4:

EXPERIMENTAL PROCEDURE

4.1. Sampling

The sampling procedure was different for the different emplacements; i.e. those in contact with the sea water (Meñakoz and Armintza) and those located inland (Enekuri and Fruiz). Moreover, inside each casuistry, the sampling had tiny differences.

In Meñakoz and Armintza, as they are in contact with the sea water, tides had to be taken into account. In order to gain better access to the areas of interest at the emplacements, it was necessary to assure that the tide was low.

In Meñakoz, the samples were collected from different locations with the aim of detecting differences between the areas and layers that were observed. There were two groups of samples; (a) those taken from the zones close to the sea and affected by the water and the wave's impacts, and (b) those extracted from the cliff and pillow lavas, which in some cases were affected by the water runoff showing highly weathered materials.

In Armintza, the analysed samples belong to two different groups of collected samples; (a) from the pillow lavas and (b) from the sedimentary stratification, with the aim of studying the geochemistry of both types of samples and establishing their differences and their possible relations.

For sampling Enekuri and Fruiz outcrops, it was necessary to get permissions since they are close to highways (Enekuri) and/or belong to a private company (a quarry in Fruiz). Due to their location, the samples had to be taken from the most inner and sheltered part of the outcrop in order to avoid the possible contamination from the traffic.

4.2. Pre-treatment of the samples

Depending on the analysis different sample pre-treatments were carried out.

On the one hand, for the analyses that required sample consumption (destructive techniques), such as XRD, ICP-MS or GS-MS, some samples or fragments of samples were ground mechanically by using a ball mill Fristch Pulverisette 6 (Indar-Orbestein, Germany) with agate container and balls (Figure 4.1) for 10 min., with 1 cycle for the most weathered samples (since they were softer) and 3 cycles for the hardest samples (those less weathered), at 400 rpm.

Figure 4.1. Agate container and balls and the Fristch Pulverisette 6 ball mill

On the other hand, some of the samples, analysed by non-destructive techniques such as EDXRF, Raman and visible-near infrared spectroscopies, were sliced and polished. For this purpose, a Forcipol 1 ® polishing machine (Metkon, Turkey, Figure 4.2) with automatic mover fixed speed of 300 rpm, and 1/2HP motor with overload protection was used. In the first step the fragments were ground with finer and finer sandpapers (P320-2000). Afterwards, the roughed samples were polished with a diamond suspension on a synthetic polishing cloth to produce a scratch-free surface.

Figure 4.18. Forcipol 1 ® polishing machine

4.3. Elemental analyses

4.3.1. Energy Dispersive X-Ray Fluorescence (EDXRF)

A M4 TORNADO EDXRF spectrometer (Bruker Nano GmbH, Germany, Figure 4.3.a) was used to map the analysed samples and obtain their elemental composition and distribution. The instrument is equipped with a micro-focus side window, Rh X-Ray tube powered by a low-power HV generator and is cooled by air. The spectral acquisitions were performed at the maximum voltage (50 kV) and at the maximum current (600 µA) that the X-Ray source allows. This equipment can work using policapillary lenses, which allow to perform single point measurements down to a spot size of 25 µm (spatial/lateral resolution) and to obtain Hyper Maps to determine the distribution of each detected element. A XFlash ® silicon drift detector with 30 mm^2 sensitive area and energy resolution of 145 eV for Mn Kα was used for fluorescence radiation detection. In order to improve the detection of the lightest elements (Z > 11), filters were not used and measurements were acquired under vacuum (20 mbar). The vacuum was achieved with a diaphragm pump MV 10 N VARIO-B. Two video-microscopes were used to focus the area under study, one at low magnification (1 cm^2 areas) for the exploration of the sample, and one at higher magnification (1 mm^2 areas) for the final focusing. In order to obtain the Hyper Maps, the Kα line of each element was used (at most of the cases) after a previous elemental assignation and deconvolution of the spectral information using the M4 TORNADO software (Bruker Nano GmbH, Berlin, Germany).

For the analyses carried out for the construction of the home-made mineral database that is described in *Chapter 5*, a handheld EDXRF XMET5100 (Oxford Instruments, UK, Figure 4.3.b) spectrometer equipped with a Rh tube as X-Ray source was used. This device can work at a maximum voltage and current of 45 kV and 50 mA respectively, and the size of the emitted X-Ray beam is 9 mm. The analyser includes a silicon drift detector (SDD) of high resolution that is able to provide an energetic resolution of 150 eV. The instrument contains a PDA to control the spectrometer, and also to save the obtained spectra and the quantitative information. The collected spectra were transferred

from the PDA to a computer in ASCII format. The raw files were transformed into binary files (x-axis; Energy in keV and y-axis; Intensity in Counts) using a home-made macro implemented in Excel. This spectrometer contains different Fundamental Parameters (FP) based methods (Oxford Instruments, UK) to obtain quantitative information. García-Florentino et al. [1] described more characteristics about this device. Considering that all the FP-based methods included in the device were developed for matrices different from the ones considered in this work (minerals), the concentration values presented in this work can only be considered as semi-quantitative.

Figure 4.19. EDXRF spectrometers: **a)** M4 TORNADO and **b)** XMET5100

4.4.   **Molecular analyses**

4.4.1.   **X-Ray diffraction (XRD)**

XRD analyses of the rock substrate were carried out in the SGIker analytical service of the UPV/EHU. The measurements were performed with a powder diffractometer PANalytical Xpert PRO (Figure 4.4), equipped with a copper tube ($\lambda CuK_{\alpha media}$ = 1.5418 Å, $\lambda CuK_{\alpha 1}$ = 1.54060 Å, $\lambda CuK_{\alpha 2}$ = 1.54439 Å), vertical goniometer (Bragg-Brentano geometry), programmable divergence aperture, automatic interchange of samples, secondary monochromator and PixCel detector. The measurement conditions were 40 kV and 40 mA, with an angular range (2θ) scanned between 5 and 70°. For the data treatment of the diffractograms and the identification of the mineral phases, the specific software Xpert HighScore (PANalytical) in combination with the specific powder diffraction file database (International Centre for Diffraction Data - ICDD, Pennsylvania, USA) was used.

Figure 4.20. PANalytical Xpert PRO Powder X-Ray diffractometer

4.4.2. Raman spectroscopy

A Renishaw inVia (Figure 4.5.a) High Resolution micro-Raman spectrometer (Renishaw, UK) was used for the molecular characterization, with 532 and 785 nm excitation diode lasers and a Charge Couple Device (CCD) detector (Peltier cooled). The device was coupled to a microscope and objectives of 5x (N.A. of 0.12), 20x (N.A. of 0.4) and 50x (N.A. of 0.75) were used to perform microscopic Raman measurements. Both, point by point and Raman image analyses, were carried out. Acquisition times and number of scans were set to optimize the signal to noise ratio. In both cases, the laser power was modulated to avoid thermal decomposition and chemical or mineralogical transformations (never above 10% of the nominal laser power). The calibration of equipment was performed daily with the 520.5 cm^{-1} silicon band. For data analysis and interpretation WiRE 4.2 software (Renishaw's Windows-based Raman Environment) was used. All collected spectra were compared with pure standard spectra contained in our own spectra database [2], the RRUFF[TM] online database [3] and the literature.

For the study of the minerals analysed for the construction of the spectra database (see *Chapter 5*), a Portable InnoRam spectrometer by BWTEC[INC] (Newark, USA, Figure 4.6.b) was used, with 785 nm excitation laser and with a Charge Couple Device (CCD) detector (Peltier cooled). The device was coupled to a microscope when needed, and objectives of 20x (N.A. of 0.25) and 50x (N.A. of 0.75) were used. The laser power was modulated depending on the spot and mineral under study in order to avoid thermodecomposition and chemical or mineralogical changes. Acquisition times as well as the number of scans were set to optimum values in order to obtain a good signal to noise ratio. The calibration of the equipment was performed daily using a silicon chip and its 520.5 cm^{-1} band as reference. The spectroscopic data were acquired with the BWSpec[TM] software version 3.26 (BWTEC[INC]), and for data analysis and interpretation the Wire 4.2 software (Renishaw Windows © based Raman Environment) was used.
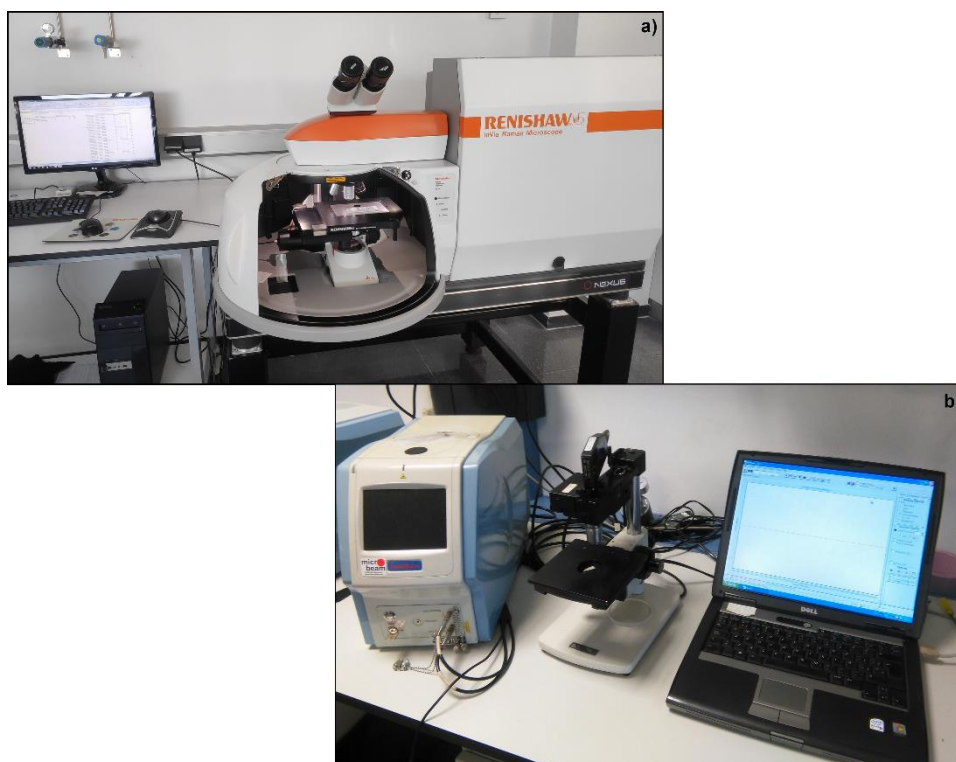
Figure 4.21. Raman spectrometers: **a)** Renishaw InVia and **b)** InnoRam

4.4.3. Visible Near InfraRed spectroscopy (VNIR)

Reflectance measurements of all samples were carried out using the ASD High Resolution FieldSpec4 spectroradiometer (Analytical Spectral Devices Inc., Boulder, USA, Figure 4.6) equipped with the ASD probe for remote mode operations either in the course of field campaigns or in the laboratory. For laboratory work, there also exist accessories for contact mode, which are explained below. A spectroradiometer is an instrument designed to measure the wavelength distribution of radiation in a wavelength interval [4]. This device works in the 350-2500 nm wavelength range, the sampling rate is 0.2 seconds per spectrum and uses three detectors for the different spectroscopic ranges: 350-1000 nm (silicon photo-diode array for VNIR), 1001-1800 nm (Te-cooled InGaAs photo-diode for SWIR1) and 1801-2500 nm (Te-cooled InGaAs photo-diode for SWIR2). The spectral resolution is 3 nm in the visible region and 8 nm in the near infrared region. Sensor optimization and calibration was set with a Spectralon® (Labsphere) white reference scanned once before each sample, and each spectrum is the result of the average of 10 scans. The Spectralon is a thermoplastic resin and provides the highest diffuse reflectance of any known material or coating over the UV-VNIR region of the spectrum. It is characterized by offer the 100% of reflectance in the measurement range (350-2500 nm) dispersing uniformly the light in all directions [5].
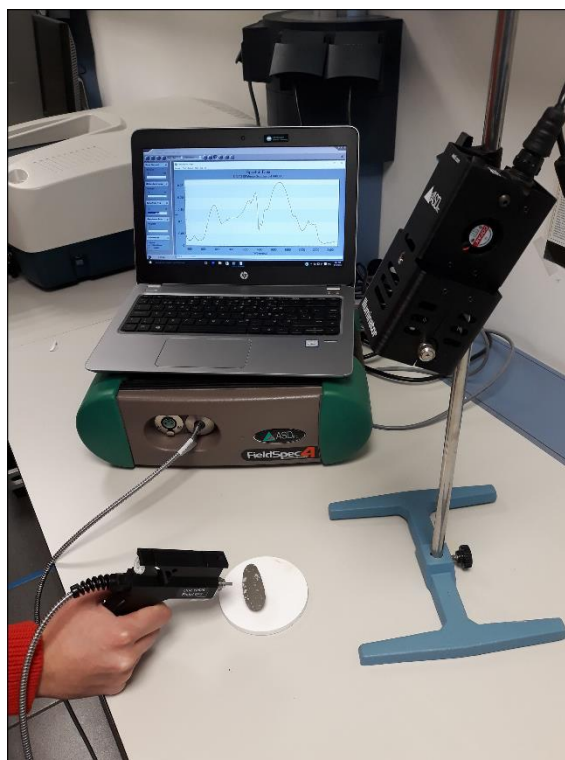
Figure 4.22. ASD High Resolution FieldSpec4 spectroradiometer

For the remote measurements, a light source is necessary. When the analyses are made on field campaigns, the sunlight acts as the source, however, in laboratory a light equivalent to that from the sun is needed. For that purpose a halogen lamp (ASD Illuminator) was used and placed at a proper distance to provide relatively even illumination in the area viewed by the fibre optic cable. This distance should be at least 30 cm (the one selected for the measurements in this PhD work) since a position closer than that may result in an unacceptable level of heating. In Table 4.1 the light spot and the distance at which the fibre should be placed are shown in relation with the position of the light source.

Table 4.1. Light source and fibre optic positioning

Height of light source (A, cm)	Light spot diameter (B, cm)	Distance of fibre (C, cm)
30	6.3	6.3
40	8.4	8.3
50	10.5	10.4

These calculations assume that the centreline of the field of view (FOV) is at the centre of the light source's beam and viewing the 80% of the illuminated diameter. A diagram with these positions can be seen in Figure 4.7.a.

The field of view (FOV) of the bare fibre is 25°, which geometrically results in a measured area that depends on the distance between the cable-end and the target. That distance was minimised, in order to reduce as much as possible the measured area, since the analysed samples were not homogeneous, and it had to be in a position that

avoided possible shadows formed between the light and the fibre. In this sense, calculations can be performed using Equation 1 and 2 (see Figure 4.7.b) to establish the optimum distance, depending on the characteristics of the measurements or the samples, to obtain the desired measured surface [6]. Moreover, it would be possible to install some accessory lenses that reduce the angle of the FOV to 10⁰ and 1⁰ leading to a potential increase in the distance between the fibre and the sample or to a decrease in the size of the sampling area.

$y = x \cdot \tan \alpha$ **Equation 1**

$measured\ area = 2 \cdot y$ **Equation 2**

As was mentioned above, measurements in contact mode can also be performed. The difference is that the configuration of the measurements is fixed. The contact accessories have their own halogen lamp to irradiate the sample, and the fibre is positioned in the proper angle to fix the measured area given by the configuration of the accessory. This type of accessories is more convenient when the samples are powdered or they are big and homogeneous, since the spot is too large to enable analyses of small surfaces.
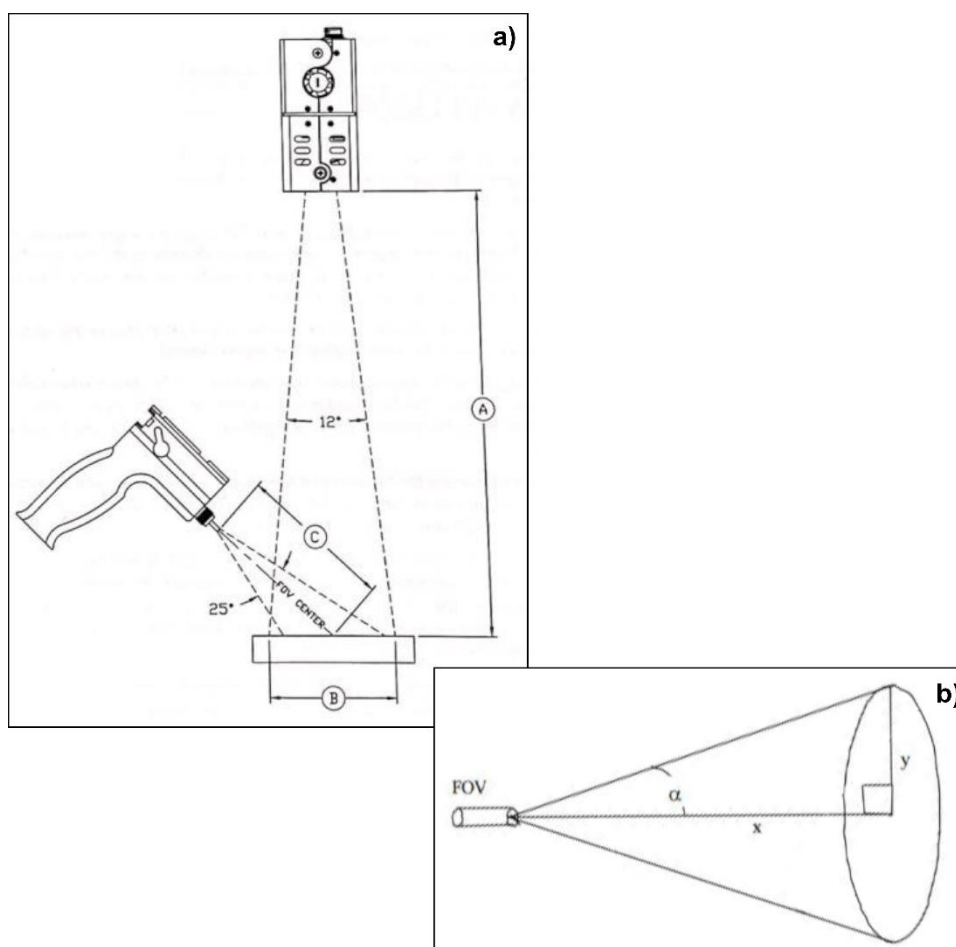

Figure 4.23. a) Light source and fibre optic cable positioning, **b)** Field of view calculation

Spectra were collected with RS3 software (ASD Inc.), analysed with ViewSpecPro software (ASD Inc.) and compared with pure standard spectra contained in our own spectral database [2], the database created by Kokaly et al. [7] and the literature.

4.5. Analysis of organics

4.5.1. Time-of-Flight-Secondary Ion Mass Spectrometry (ToF-SIMS)

The measurements with this technique were performed during a predoctoral stay in the Research Institute of Sweden (RISE) in Borås (Sweden) under the supervision of Dr. Sandra Siljeström.

The ToF-SIMS images and spectra of positive and negative ions were recorded using a ToF-SIMS IV instrument (ION-TOF GmbH, Münster, Germany, Figure 4.8) equipped with a liquid bismuth cluster ion source. Samples were analysed by rastering a 25 keV Bi^{3+} beam over a 200x200 µm² area for 200 seconds. The analyses were performed at high resolution (bunched mode: m/Δm ≥ 7000 at m/z 30, Δl ~ 5 µm) with a pulsed current of 0.1 pA. In addition, some of the spectra were collected over the same area at high spatial resolution (burst alignment mode: m/Δm ~ 100-300, Δl < 1 µm) with a pulsed current of 0.04 pA. The sample surfaces flooded with electrons for charge compensation. The positive and negative spectra were calibrated using small hydrocarbon fragments found in respective spectra. The deviation between the calculated theoretical mass of the assignments and that of the observed peaks were always less than 100 µg/g. The assignment of the peaks with the fragments was carried out using reference data found in the literature [8, 9].

Figure 4.24. ION-TOF GmbH, ToF-SIMS IV instrument

4.5.2. High performance linear ion trap mass spectrometry

These measurements were performed by Dr. Xiang Li from the Planetary Environments Laboratory in NASA Goddard Space Flight Centre (Maryland, USA). The Mars Organic

Molecule Analyzer (MOMA) on-board the ExoMars 2022 rover contains a miniaturized version of the Thermo Scientific company's design [10] which is described below. As Goesmann et al. [11] described, MOMA is a double instrument containing LDI (Laser Desorption and Ionization) and GCMS (Gass Chromatography-Mass Spectrometry). With these analyses, only the LDI part of MOMA is reflected.

The Thermo MALDI LTQ XL (Thermo Scientific, Bremen, Germany, Figure 4.9) is a high performance linear ion trap mass spectrometer that supports a laser desorption–based ion source. Samples were introduced to the instrument on a stainless-steel plate, with powdered samples being affixed to the plate with double-sided tape. The laser-based ion source on the LTQ XL is based on a sample load-lock setup where the sample plate is held at a pressure of ~75 mtorr (He) during operation. The source is equipped with a nitrogen laser (337 nm, 3 ns pulse) focused to an elliptical spot with approximate dimensions of 0.1 x 0.2 mm. For the samples tested in this study, the laser was operated with an energy of 60 μJ per pulse. Spectra were obtained in both positive and negative ion modes, collecting data from 50 to 2000 Da mass range.

Figure 4.25. Thermo MALDI LTQ XL mass spectrometer

4.5.3. Gas chromatography-mass spectrometry (GC-MS)

These measurements were carried out by Manuel Reinhardt, from the Department of Geobiology from the University of Göttingen (Germany), in order to characterize the organic matter and complete the information obtained by the previous techniques (ToF-SIMS, LTQ and Raman) regarding to the characterization of organics. These analyses were performed only with the samples from Enekuri and Fruiz.

The crushed rock samples were powdered in an acetone-cleaned pebble mill (Retsch MM 301, grain size ≥0.45μm). The powders were then used for carbon analysis (total organic carbon, TOC, and total inorganic carbon, TIC) in a Leco RC612 carbon analyzer, as well as molecular analysis of the extractable organics via gas chromatography–mass spectrometry (GC-MS).

All materials used for organic-geochemical lab work were cleaned with acetone and/or heated to 500°C (3h). Pre-combusted sea sand was used as a laboratory blank. To

obtain a total organic extract (TOE), three extraction cycles were conducted; the first with DCM (dichloromethane)/MeOH (methanol) (3/1, v/v; 10 min ultrasonication; 10 min centrifugation), the second with DCM (10 min ultrasonication; 10 min centrifugation), and the third with n-hexane (10 min ultrasonication; 10 min centrifugation). The TOEs of each sample were then concentrated to near dryness using a rotary evaporator and a N_2 concentrator. After re-dissolution in n-hexane, the TOEs were desulfurized with active copper and analyzed via GC-MS.

The TOEs were injected into a Thermo Trace 1310 gas cromatograph (GC) coupled to a Thermo TSQ Quantum Ultra triple quadrupole mass spectrometer (MS) (injector transfer T = 300 °C, He flow rate = 1.5 mL/min, Figure 4.10). For compound separation, a silica fused capillary column (Phenomenex Zebron ZB-5MS, 30 m length, 250 µm internal diameter, 0.25 µm film thickness) was used, and the GC was heated from 80 °C (held for 1 min) to 310 °C with 5 °C/min (held for 20 min). The mass spectrometer operated in electron impact mode (source T = 240 °C) at 70 eV. Mass spectra were generated in full-scan mode with a scan range from 50 to 600 Da.

Figure 4.10. Thermo Trace 1310 gas cromatograph and Thermo TSQ Quantum Ultra triple quadrupole

4.6.   Bibliography

1. García-Florentino C., Maguregui M., Morillas H., Marcaida I., Madariaga J. M. A fast in situ non-invasive approach to classify mortars from a construction of high historical value. *Microchem. J.* **2017,** 133, 104-113.

2. Ruiz-Galende P., Torre-Fdez I., Aramendia J., Gómez-Nubla L., Castro K., Arana G., Fdez-Ortiz de Vallejuelo S., Maguregui M., Medina J., Baonza V. G., Rull F., Madariaga J. M. New Raman-visible near-infrared database of inorganic and mineralogical planetary and terrestrial compounds and its implications for Mars: Phyllosilicates. *J. Raman Spectrosc.,* **2019,** 1-11.

3. Lafuente B., Downs R. T., Yang H., Stone N. The power of databases: the RRUFF project. In: *Highlights in mineralogical crystallography.* Ed. T. Armbruster, R. M. Danisi. *W. De Gruyter,* Berlin. **2015,** pp. 1-30.

4. Ellert M. PhD thesis. *Calibration and characterization of a nin-imagin field spectroradiometer supporting imagin spectrometer validation and hyperspectral sensor modelling.* Universität Zürich, Zürich, **1998.**

5. Labsphere (R) Technical guide. Reflectance materials and coatings. *www. labsphere. com.*

6. Hatchell D. C. Analytical Spectral Devices, Inc. (ASD) Technical Guide. 3rd Ed. **1999,**.

7. Kokaly R. F., Clark R. N., Swayze G. A., Livo K. E., Hoefen T. M., Pearson N. C., Wise R. A., Benzel W. M., Lowers H. A., Driscoll R. L., Klein A. J. USGS spectral library version 7. *Data Series.* **2017,** 68.

8. Siljeström S., Parenteau M. N., Jahnke L. L., Cady S. L. A comparative ToF-SIMS and GC–MS analysis of phototrophic communities collected from an alkaline silica-depositing hot spring. *Org. Geochem.* **2017,** 109, 14-30.

9. Bruuning C., Hellweg S., Dambach S., Lipinsky D., Arlinghaus H. F. Improving the interpretation of ToF-SIMS measurements on adsorbed proteins using PCA. *Surf. Interface Anal.,* **2006,** 38, 191-193.

10. Li X., Danell R. M., Brinckerhoff W. B., Pinnick V. T., van Amerom F., Arevalo R. D.,Jr., Getty S. A., Mahaffy P. R., Steininger H., Goesmann F. Detection of trace organics in Mars analog samples containing perchlorate by laser desorption/ionization mass spectrometry. *Astrobiology,* **2015,** 15, 104-110.

11. Goesmann F., Brinckerhoff W. B., Raulin F., Goetz W., Danell R. M., Getty S. A., Siljeström S., Missbach H., Steininger H., Arevalo R. D.,Jr., Buch A., Freissinet C., Grubisic A., Meierhenrich U. J., Pinnick V. T., Stalport F., Szopa C., Vago J. L., Lindner R., Schulte M. D., Brucato J. R., Glavin D. P., Grand N., Li X., van Amerom F. H. W., Moma Science Team. The Mars Organic Molecule Analyzer (MOMA) instrument: characterization of organic material in Martian sediments. Astrobiology, **2017,** 17 (6, 7), 655-685.

CHAPTER 5:

IMPAT-DATABASE

For the reliable interpretation of the spectral information obtained from present and future planetary missions and from the measurements carried out on analogues and meteorites, the mineralogical database IMPAT-Database (Inorganic and Mineralogical Planetary And Terrestrial compounds Database) was developed in the present work. The IBeA research group from the University of the Basque Country, where this work has been carried out, participates in the science groups of the next missions to Mars (ExoMars 2022 and Mars 2020) and the development of this database with spectra of pure compounds/minerals has been, among others, one of its tasks.

This database was made employing Raman and VNIR spectroscopies as they will be on-board the rovers of the two mentioned planetary missions. Moreover, these techniques are easy to use, the data that they report is very reliable and portable devices can be used, and the latter characteristic is one of the most interesting for the planetary missions because they enable in-situ measurements. Furthermore, in some cases, X-Ray fluorescence was used in order to ensure the correct identification of the analysed minerals and pure substances.

Currently, there are already databases regarding the spectroscopic techniques employed for the construction of the IMPAT-Database. In the case of Raman spectroscopy, the RRUFF™ [1] is the most used free database, and it is freely available. Even though it is a

large database, not all the minerals related to this work are available. Other databases can be found in the literature [2], but they are not available and the spectra cannot be handled with spectroscopic software. In the case of VNIR spectroscopy, Cloutis et al. [3] characterized planetary analogue materials, which are terrestrial rocks and minerals that are similar to those known or suspected to occur on the Martian surface with different origins and formation mechanisms, covering ultraviolet, visible, near-infrared, and mid-infrared regions. The spectral files are available to be downloaded, but the number of analysed compounds is only about 50. On the other hand, Clark et al. [4] published a library of minerals and other compounds (such as organic compounds, artificial materials, or soils and mixtures), which can be readily accessed and downloaded. The latter database is wider than the former one; however, the most unusual minerals are not present.

That lack of information is the reason for the creation of this database, and it was developed in collaboration with the Geominery Museum of the Spanish Geological and Miner Institute (IGME) [5]. Most of the minerals that form part of this database belong to the collection of the museum, and almost all of those are part of the permanent exhibition. They were analysed in a non-destructive way, in situ, inside the museum. Other mineral samples are part of the private collection of the IBeA research group and they were analysed in the laboratory with benchtop instruments.

Several groups of minerals (442 specimens) were analysed, focusing on those of special interest for Martian exploration (since some minerals have been already identified on the Martian surface) and on those that are uncommon, both in nature and in the bibliography. In the following figures, the spectra of some of the most interesting and relevant minerals from the IMPAT-Database are shown. The main information obtained by Raman, VNIR and EDXRF analysis is discussed below. In all cases, there was acceptable agreement between the expected chemical composition and the EDXRF semi-quantitative values obtained through in-situ measurements. Only in a few cases, that will be specifically commented on, some impurities were detected in minor areas of the samples. Therefore, those areas were not used to obtain the Raman and VNIR spectra that are reported for each mineral.

As has been described in the *Introduction* chapter (except Zeolites), the main groups of minerals found on Mars are; primary silicates (olivine, pyroxenes and plagioclases), phyllosilicates, sulfides and sulfates, carbonates and oxides. Examples of specific minerals that have been already described in references listed in the bibliography and some others that are not reported in the literature are going to be shown throughout this chapter.

5.1. Primary silicates

These minerals have been described in the *Introduction* and they are thought to be some of the most common minerals of the basaltic rocks that compose Mars.

In Figure 5.1, spectra of some primary silicates can be seen. Olivine is characterized by its Raman bands (Figure 5.1.a) at 225 (very weak, vw), 304 (weak, w), 437 (w), 543 (vw), 586 (w), 607 (w), 824 (strong, s), 856 (very strong, vs), 882 (medium, m) and 963 (m) cm^{-1}, and to the VNIR bands (Figure 5.1.b) at 639 and 1041 nm. In this case, bands related to the presence of water (1391 nm OH overtone and 1926 nm H_2O combination band) and a band related with the vibration of carbonate group (2315 nm) can be seen.

Cromodiopside is the example selected for the pyroxenes group. It has Raman bands (Figure 5.1.c) at 142 (s), 183 (vw), 196(vw), 232 (w) 256 (vw), 325 (s), 359 (m), 392 (s), 464 (vw), 509 (w), 561 (w), 667 (vs), 855 (w), 1013 (vs) and 1049 (w) cm^{-1}, and VNIR bands (Figure 5.1.d) at 449, 788, 1051, 1919 (H_2O combination band) and 2240 nm.

Finally, in the plagioclase group, we can find labradorite, which presents Raman bands (Figure 5.1.e) at 482 (w) and 511 (m) cm^{-1}, and albite, which exhibits VNIR bands (Figure 5.1.f), at 893, 1162, 1409 (OH overtone), 1917 (H_2O combination band), 2197, 2347 and 2440 nm. All these minerals have been widely studied and characterized since they are the main components of Martian meteorites and have been the object of study for many years [6-11].
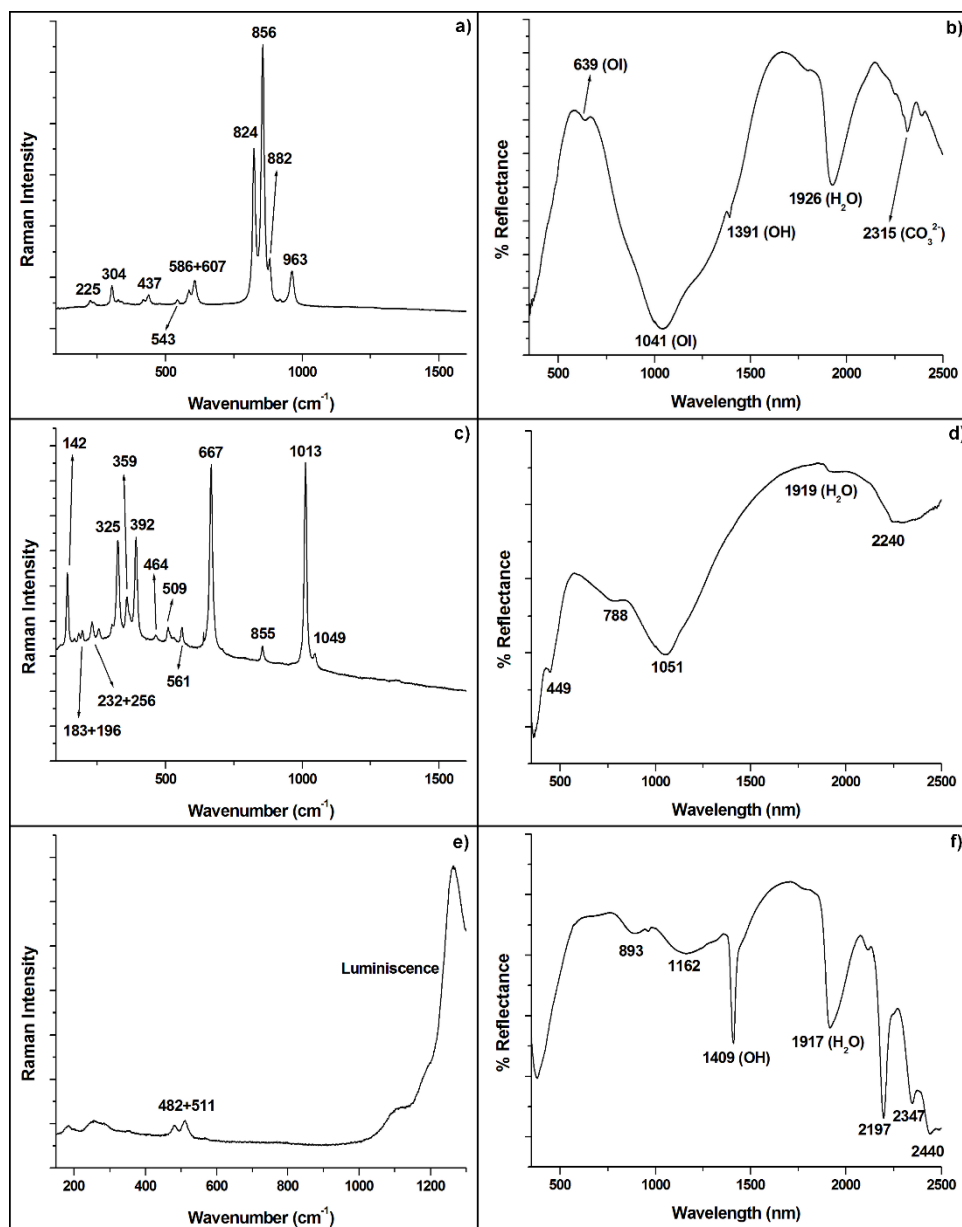
Figure 5.26. Spectra of some primary silicates. **a)** Raman spectrum of olivine, **b)** VNIR spectrum of olivine (Ol), **c)** Raman spectrum of chromodiopside, **d)** VNIR spectrum of diopside, **e)** Raman spectrum of labradorite and **f)** VNIR spectrum of albite

5.2. Phyllosilicates

As has been mentioned above, these minerals are some of the most abundant silicates on the Martian surface and, therefore, they are the most studied ones. However, due to the wide number of members that belong to this group, many of these minerals have not been reported in the literature yet.

This type of silicates need the presence of water for its formation, thus, its study is very meaningful for the understanding of past processes related to water on Mars, and would be an important factor in assessing the potential habitability of the planet. The detection of phyllosilicates on Mars has revealed a complex aqueous history, which suggests different geochemical environments separated both temporally and spatially [12]. Most of

them are thought to have been formed during the planet's earliest Noachian era [13], leading to name this period the "phyllosian" era, characterized by weakly acidic to alkaline aqueous alteration. This alteration is due to long-lasting wet periods, the subsurface water mobilization by hydrothermal activity, cratering with the supply of subsurface water to the impacted minerals or during the cooling of the mantle [14, 15].

The most abundant phyllosilicate formed during this period in the surface is the Fe-rich smectite [16]. In addition, a large variety of phyllosilicates has been observed, such as chamosite, kaolinite and illite in minor abundance. Regarding the ones formed in subsurface, they tend to be more Mg-rich and include mixtures of smectites with chlorites [16]. However, their exact origin is not clear since different theories have been reported in the literature [17, 18]. The clay bearing outcrops present on Mars might help answering questions such as how long was liquid water present on the surface of Mars or which characteristics or processes it had [19].

In Figure 5.2, spectra of clintonite $(Ca(Mg,Al)_3(Al_3SiO_{10})(OH)_2)$, pyrosmalite $(Fe^{2+}_8Si_6O_{15}(OH,Cl)_{10})$, fluoroapophyllite-(K) $(KCa_4(Si_8O_{20})F\cdot8H_2O)$ and raite $(Na_4Mn^{2+}_3Ti_{0.25}Si_8O_{20}(OH)_2\cdot10H_2O)$ are shown.

Clintonite (Figure 5.2.a and b), also named xanthophyllite, is a member of the known brittle micas, which are those that contain divalent cations in the phyllosilicate interlayer. It is one of the common brittle micas containing Ca^{2+} or Ba^{2+} as major cations (Ca^{2+} of the specific case of clintonite) [20]. Clintonite has Raman bands at 155 (w), 192 (w), 234 (m), 296 (w), 342 (m), 400 (m), 513 (m), 655 (s), 791 (w), 893 (m) and 963 (w) cm^{-1}. As the only reference of the Raman spectrum of this mineral is the RRUFF database [1], we can contribute with another Raman reference spectrum for it. Moreover, the characterization could be confirmed by means of its VNIR spectrum (Figure 5.2.b) with bands at 952, 1393, 2263 and 2323 nm, in agreement with spectra reported in the literature [4].

Pyrosmalite (Figure 5.2.c and d) is the iron-rich end-member of the pyrosmalite series. Generally, minerals of these series are related to metamorphism and are associated with Fe- and Mn-rich silicate and oxide minerals. Pyrosmalite has been reported as a retrograde hydrothermal phase [21] and its presence has been taken as evidence of the ability of high temperature hydrothermal fluids to transport iron and silica. The Raman spectrum of pyrosmalite is characterized by the following bands; 125 (vw), 149 (w), 188 (m), 282 (w), 306 (w), 326 (s), 416 (m), 481 (m), 615 (vs), 815 (vw) and 1031 (m) cm^{-1}, and the only found reference was that from the RRUFF database [1]. The VNIR spectrum has bands at 917, a doublet at 1411 and 1425 (due to the OH overtone), another doublet at 1952 and 1989 (due to the H_2O vibration), 2119, 2177, 2341 and 2453 nm. In this case, there is no VNIR spectrum available in the literature.

Fluoroapophyllite-(K) (Figure 5.2.e and f) is one of the end members of the apophyllite series, which are layered phyllosilicates with many properties similar to zeolites. Any mineral related to zeolites, or with properties similar to them, is of high interest for the

upcoming Mars missions, as they would be an exceptional finding in order to study past water processes. Apophyllite minerals occur as secondary minerals in basalts and in cavities in granites [22]. Frost et al. [22] described the Raman spectra of different apophyllites, being these compounds widely studied. However, their VNIR spectra have not been described, thus, they have a special interest for the creation of this database. In Figure 5.2.f the VNIR spectra of fluoroapophyllite-(K) can be observed with bands at 475, 571, 624, 757, 850, 984, 1096, 1165, 1216, 1327, 1440 and 2253 nm.

Finally, raite is an agpaitic mineral that is found in unusual igneous intrusive rocks that contain alkali metals. Raite is the late hydrothermal mineral, formed together with minerals such as fibrous aegirine [23]. The observed Raman bands (Figure 5.2.g) appear at 150 (m), 210 (w), 224 (w), 280 (m), 302 (m), 349 (w), 398 (w), 442 (w), 536 (w), 575 (s), 667 (s), 707 (m), 854 (w), 931 (vs) and 973 (w) cm^{-1}. In the case of the VNIR spectroscopy (Figure 5.2.h) the bands observed are located at 1917 (associated to the combination band of water), 2096, 2168, 2324 (which could be associated to the Si-O bond of silicate), 2393 and 2457 nm. In the EDXRF analyses it was observed that raite was not the only mineral present in the sample, due to the presence of Fe and Ca in the semi-quantitative analyses. The Raman analysis in those spots where Fe and Ca were detected showed the presence of iron oxy-hydroxides and calcite.
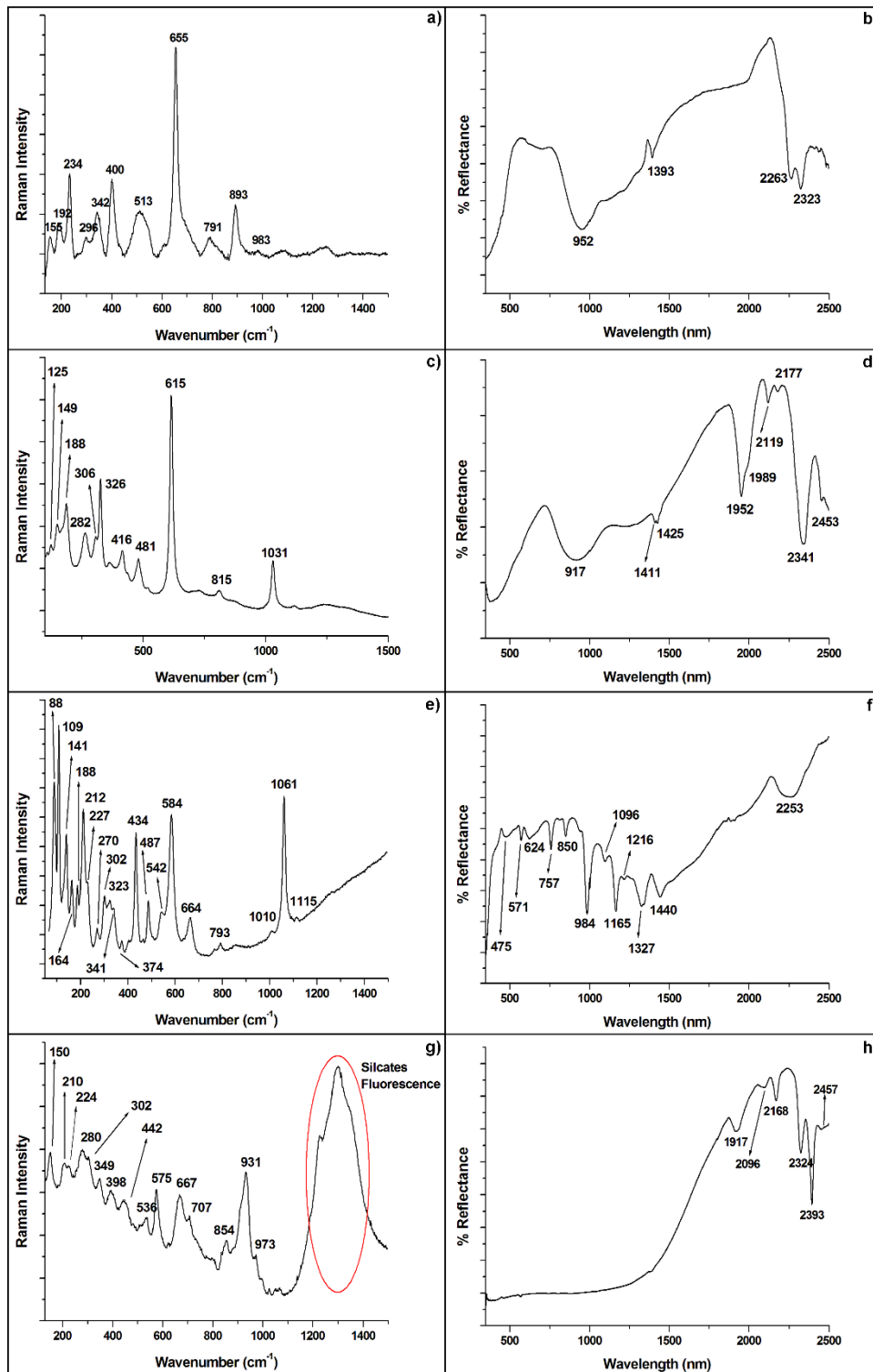
More examples of phyllosilicates can be found elsewhere [24].

Figure 5.27. Spectra of phyllosilicates. **a)** Raman spectrum of clintonite, **b)** VNIR spectrum of clintonite, **c)** Raman spectrum of pyrosmalite, **d)** VNIR spectrum of pyrosmalite, **e)** Raman spectrum of fluoroapophyllite, **f)** VNIR spectrum of fluoroapophyllite, **g)** Raman spectrum of raite and **h)** VNIR spectrum of raite

5.3.   Zeolites

Even though this group of minerals is not one of the main groups observed on Mars (and for that reason has not been mentioned in the *Introduction* chapter), their presence on its surface could play an important role in the abundance of atmospheric water [25]. Tokano et

al. [25] suggested that they have a structure with large open cavities and sites which contain exchangeable water molecules.

Zeolites generally crystalize from natural glasses during diagenesis and are petrogenetically important because many of them are formed under restricted ranges of temperature and pressure, and therefore, they are very useful indicators of petrogenesis. They can be formed in wide variety of geological environments or hydrological systems by alteration of volcanic material under various geochemical conditions being present in terrestrial basaltic and volcanic regions. Zeolites also form in cold polar desert environments and in terrestrial cold desert soils. They may also form through low temperature alteration of volcanic ash, and such material is assumed to be present on Martian surface. They are intimately associated with hydrothermal environments and in the appropriate conditions they can form very quickly [26, 27]. On Mars, these minerals have been detected thanks to Thermal Emission Spectrometer (TES) on Mars Global Surveyor (MGS) and they are associated to the bright regions of Mars that are known to be dust covered [28].

In Figure 5.3, the spectra of stilbite ($NaCa_4(Si_{27}Al_9)O_{72} \cdot 28H_2O$), analcime ($Na(Si_2Al)O_6 \cdot H_2O$), mesolite ($Na_2Ca_2Si_9Al_6O_{30} \cdot 8H_2O$) and phillipsite (($Ca,Na_2,K_2)_3Al_6Si_{10}O_{32} \cdot 12H_2O$) are shown. The first two are commonly described in the literature by both Raman and VNIR. In the case of phillipsite and mesolite, their Raman spectra are present in the literature, however, the VNIR spectra have not been described yet.

Stilbite occurs commonly in veins in volcanic units and volcanogenic sediments. It is often associated with other zeolites and is the first calcium zeolite formed in the progressive sequence of diagenesis and zeolite facies metamorphism [29]. It has Raman bands at 125 (m), 286 (w), 410 (s), 460 (w), 500 (m), 619 (vw) and 792 (vw) cm^{-1} (Figure 5.3.a). Moreover, the VNIR spectrum of stilbite (Figure 5.3.b) shows bands at 969, 1161, a doublet at 1432 and 1463, 1758 and 1916 nm.

Analcime crystallises from solid aluminosilicates and sodium rich solutions such as volcanic glass in pyroclastic sediments and saline solutions, which is its most reported formation mechanism [30]. In Figure 5.3.c its Raman spectrum is shown with its bands at 300 (w), 391 (w), 485 (s), 579 (vw) and 1105 (w) cm^{-1}. In Figure 5.3.d an analcime VNIR spectrum is displayed with bands at 982, 1162, 1348, 1444, 1517, 1799, 1914 and 2144 nm.

Mesolite has only been measured by means of VNIR exhibiting bands at 983, 1182, 1210, 1247, 1356, 1455, 1488, a doublet at 1562 and 1599, 1769, 1818, 1939, 2009, 2084, 2197, 2277 and 2433 nm (Figure 5.3.e). It forms fibrous radiating clusters and it occurs together with other zeolites such as analcime or laumontite [31]. Finally, phillipsite is a mineral that occurs in the deep sea areas of very slow sedimentation and as the final alteration product of basalt, suggesting that it is thermodynamically stable [32]. In Figure

5.3.f its VNIR spectrum is shown which exhibits bands at 968, 1162, 1425, 1466, 1796, 1922, a doublet at 2163 and 2208 and 2344 nm.
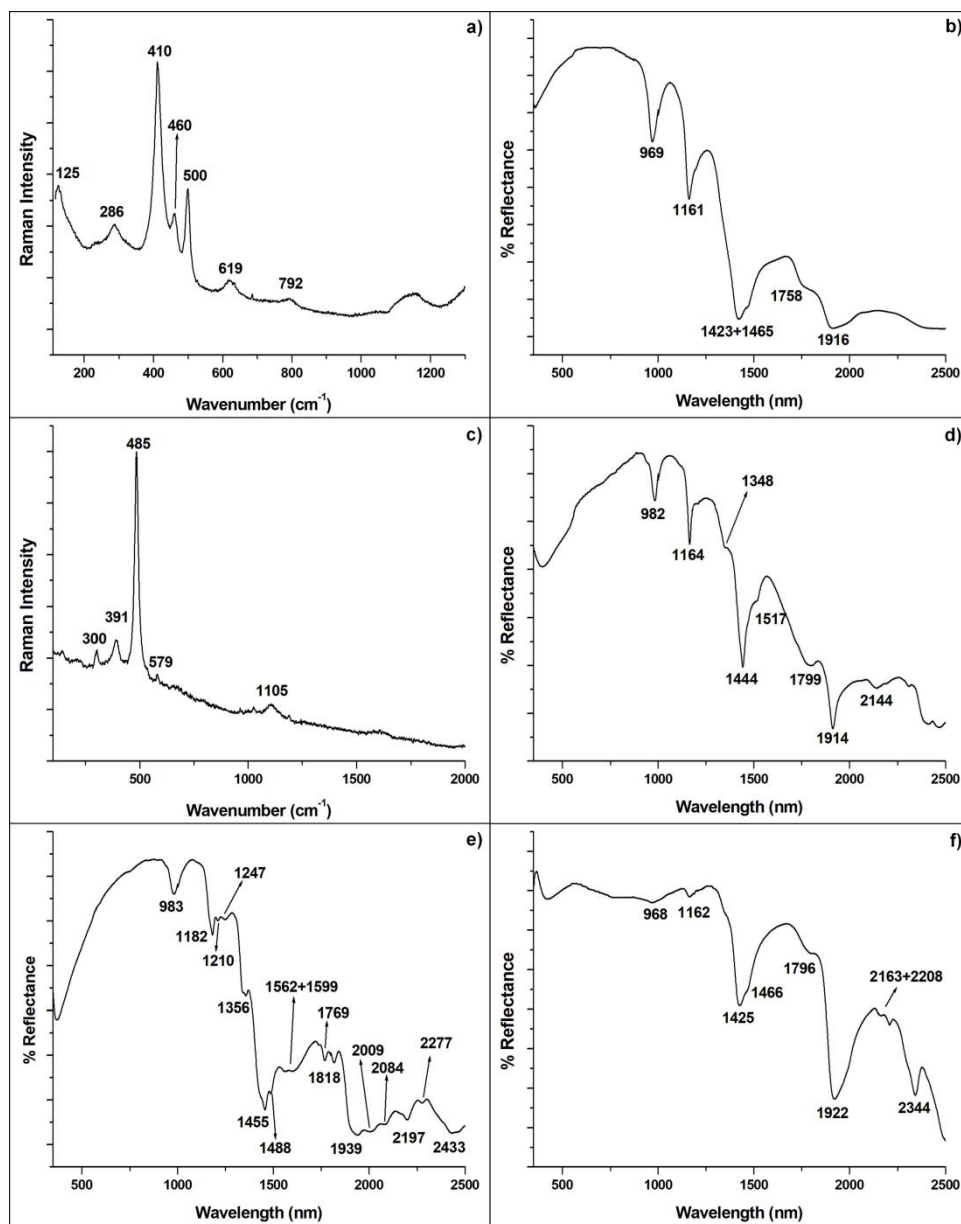

Figure 5.28. Spectra of zeolites. **a)** Raman and **b)** VNIR spectra of stilbite, **c)** Raman and **d)** VNIR spectra of analcime, **e)** VNIR spectrum of mesolite and **f)** VNIR spectrum of phillipsite-(Na)

5.4. Sulfides and sulfates

Sulfides and sulfates are other groups of high interest for Martian exploration. Indeed, sulfur-bearing materials may have played an important role in the evolution of the hydrologic history of Mars. The major amount of sulfur could originate from volcanic outgassing in the form of H_2S or SO_2, which could react with atmospheric components to form sulfates or hydrated sulfates and then fall onto the surface. During a warm and wet era, these gaseous species would have dissolved in water to form acid solutions, which were neutralized thanks to the reaction with igneous minerals. Moreover, intrusive igneous activity could also form sulfur-rich solutions [33].

Taking into account the importance of these minerals, the information related to the Raman spectroscopy is quite abundant and, therefore, almost all the sulfides and sulfates studied for the construction of this database can be found in the literature [34, 35], as is the case of diaphorite ($Pb_2Ag_3Sb_3S_8$) and linarite ($PbCu(SO_4)(OH)_2$). However, in the case of VNIR spectroscopy, the literature related with sulfides and sulfates is not as wide as that of Raman. This is the case of gersdorffite (NiAsS), gudmundite (FeSbS), serpierite ($Ca(Cu,Zn)_4(SO_4)_2(OH)_6 \cdot 3H_2O$) and langite ($Cu_4(SO_4)(OH)_6 \cdot 2H_2O$).

Diaphorite (Figure 5.4.a) has Raman bands at 171 (m) and 306 (s) cm^{-1} and it is formed in hydrothermal veins with other sulfides formed at medium temperatures [36]. Linarite (Figure 5.4.b) occurs as a secondary mineral in the oxidized parts of deposits originally containing lead and copper sulfides [37]. It has Raman bands at 113 (w), 367 (w), 438 (m), 513 (w), 633 (w) and 967 (s) cm^{-1}.

In the case of the VNIR spectra, gersdorffite (Figure 5.4.c), which is formed as an alteration of nickel sulfides and occurs in close spatial association with chalcopyrite [38], is characterized by VNIR bands at 397, 484, 622, a broad band with the centre at 1068, 1986, 2162, and 2335 nm. The bands of gudmundite (Figure 5.4.d) appear at 737, 1037, 1396, 1499, 1911, 2001, 2115, 2316 and 2389 nm and it is the antimony equivalent of arsenopyrite, occurring as a common mineral constituent in polymetallic ores [39].

Finally, the sulfates serpierite and langite are shown. Serpierite (Figure 5.4.e) is a secondary mineral in the oxidized zone of hydrothermal Cu-Zn bearing deposits [36] and has VNIR bands at 684, 802, 1432, 1918, 2305 and 2354 nm. Langite (Figure 5.4.f) has its bands at 719, 899, 1430, 1051, 2128, 2218, 2263, 2336, 2455 and 2482 nm and, along with other copper minerals, indicates later deposition in an arid saline environment [40].
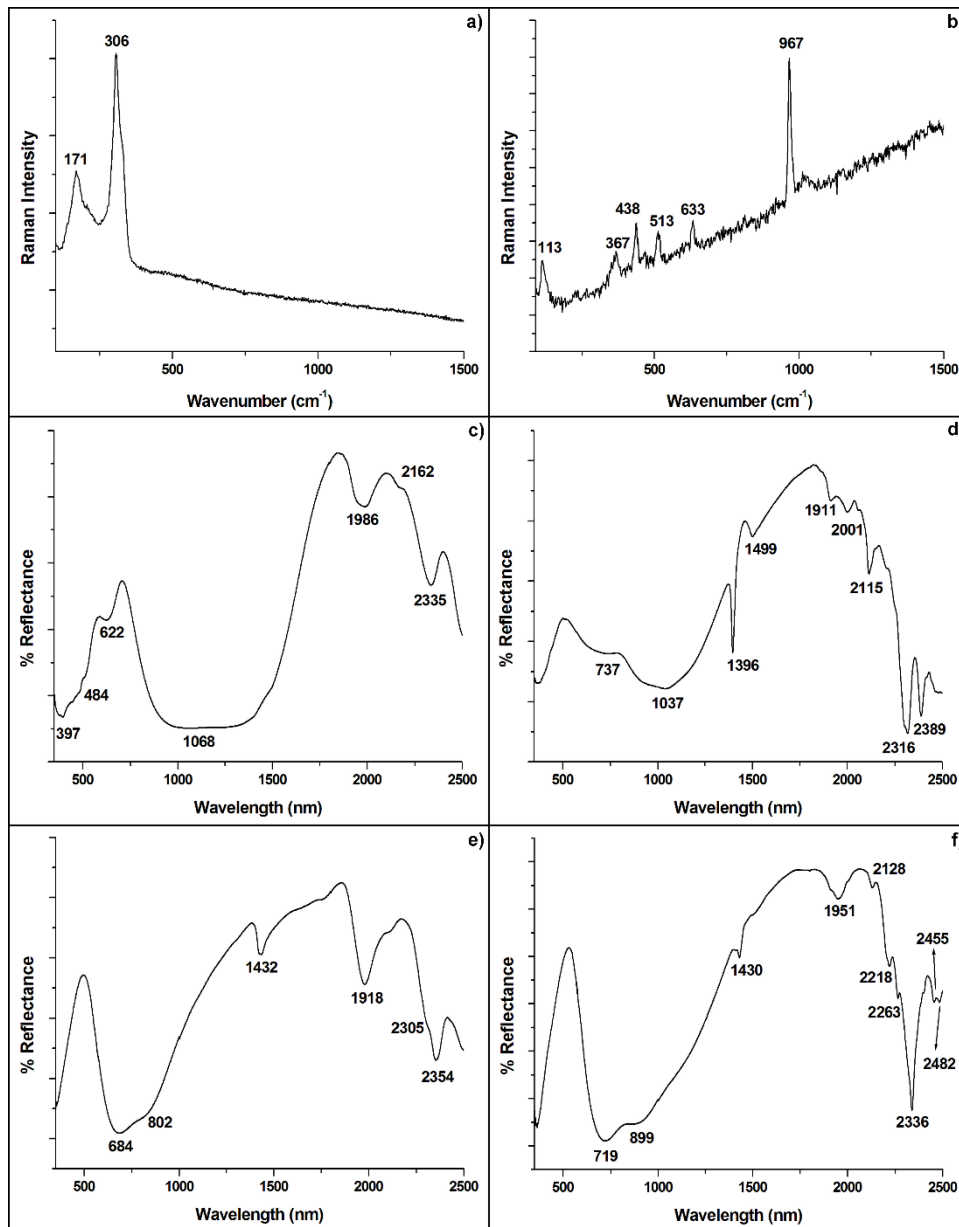
Figure 5.4. Spectra of sulfides and sulfates. **a)** Raman spectrum of diaphorite, **b)** Raman spectrum of linarite, **c)** VNIR spectrum of gersdorffite, **d)** VNIR spectrum of gudmundite, **e)** VNIR spectrum of serpierite, **f)** VNIR spectrum of langite

5.5. Carbonates

As has been mentioned before (*Introduction* section), this type of minerals are very important for the understanding of the relation that exists between the presence of water and carbon and the possible existence of life. This relation is based in the carbon cycle that could happen on Earth. The few outcrops of Mg-rich carbonates detected on Mars, occur in association with geological units exposed to acidic paleoenvironments, which on Earth relate the carbon cycle with the presence of life. Therefore, it can be assumed that the presence or absence of microbial forms of life should have affected the distribution of those carbonate compounds on Mars [41].

As in the case of sulfates, carbonates have been very widely studied using Raman spectroscopy [42, 43] instruments, existing in the literature all the carbonates measured for this database. Nevertheless, the studies of these minerals by VNIR are only limited to the most common ones. Some spectra of minerals not reported in the literature are: barytocalcite ($BaCa(CO_3)_2$), bismutite ($Bi_2(CO_3)O_2$), spherocobaltite ($CoCO_3$) and stichtite ($Mg_6Cr_2^{3+}(OH)_{16}(CO_3) \cdot 4H_2O$).

Barytocalcite (Figure 5.5.a) is an uncommon accessory mineral in metallic veins, formed by reaction of hydrothermal fluids [36]. It has VNIR bands at 375, 1451, 1933, 1989 and a triplet at 2296, 2336, 2379 nm.

In Figure 5.5.b the VNIR spectrum of bismutite is shown. It has bands at 379, 1443, 1725, 1942, 2273, 2305 and 2345 nm. This mineral is a common alteration product of other bismuth-bearing minerals in hydrothermal deposits [36].

Spherocobaltite (Figure 5.5.c) with VNIR bands at 543, 758, 1456, 1877, 1931, 1993, 2157, and a doublet at 2292 and 2339 nm, occurs as a crystal filling void spaces in rocks and as microscopic inclusions [44].

Finally, stichtite (Figure 5.5.d), which is a rare hydrated carbonate-hydroxide that occurs exclusively in Cr-rich serpentinites of ophiolites or greenstone belts [45], has its characteristic bands at 437, 569, 648, 950, 1284, 1360, 1391, 1976, 2133, 2271 and 2325 nm.
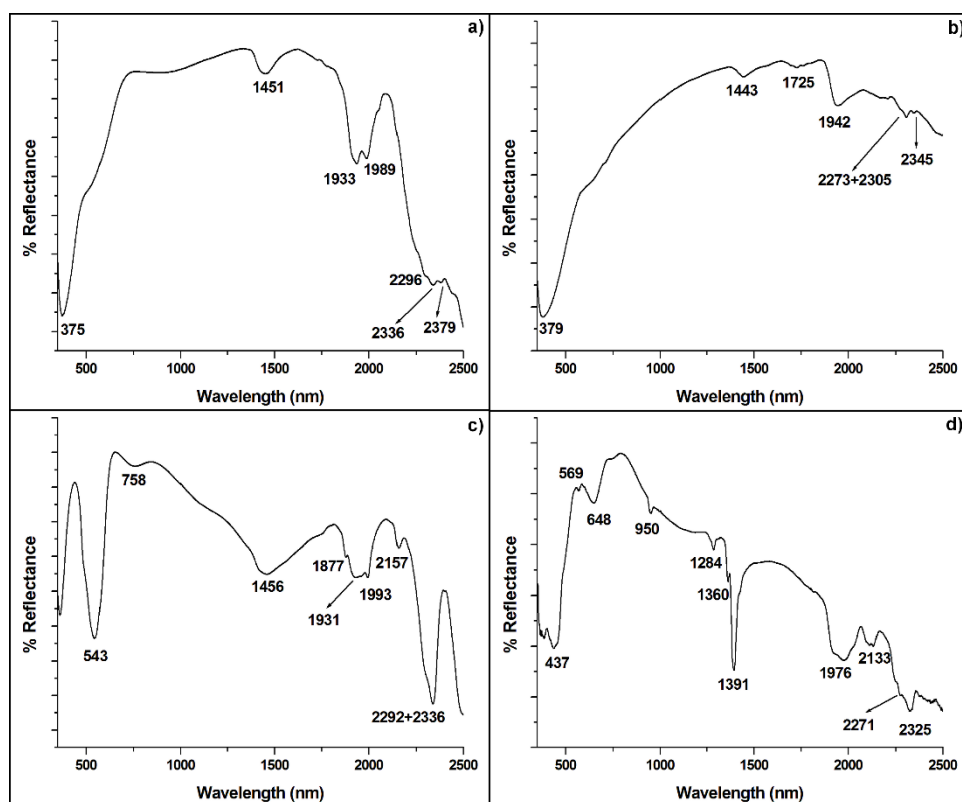

Figure 5.29. VNIR spectra of carbonates. **a)** Barytocalcite, **b)** bismutite, **c)** spherocobaltite and **d)** stichtite

5.6. Oxides

Following the VNIR spectral reflectance observations of Mars performed during the early missions, the presence of ferric iron was demonstrated, and due to the shape of the spectra curve observed in the Martian spectra, the most probable minerals in which this iron is present was confirmed to be oxides [46]. Therefore, it can be argued that, the most common oxides in the Martian surface are those of iron and are some of the principal components of the regolith. This type of minerals, which are also very common on Earth, are reported in many literature references, and their Raman and VNIR spectroscopic characteristics are well known [47, 48]. In Figure 5.6 the Raman and VNIR spectra of hematite (Fe_2O_3) and goethite (α-FeOOH) can be observed. Hematite has Raman bands at 228 (m), 246 (vw), 293 (s), 413 (m), 499 (vw), 615 (w) and 1326 (bb) cm^{-1} (Figure 5.5.a). Goethite (Figure 5.5.c) Raman bands are 161 (vw), 201 (w), 220 (vw), 240 (w), 295 (m), 382 (vs), 413 (sh, shoulder), 478 (w), 546 (m) and 685 (vw) cm^{-1}.

In the case of the VNIR spectra (Figure 5.5.b and 5.5.d), the bands that evidence the presence of these oxides are those that are related with iron, at 478 and 855 nm for hematite, and at 477, 645 and 907 nm for goethite.
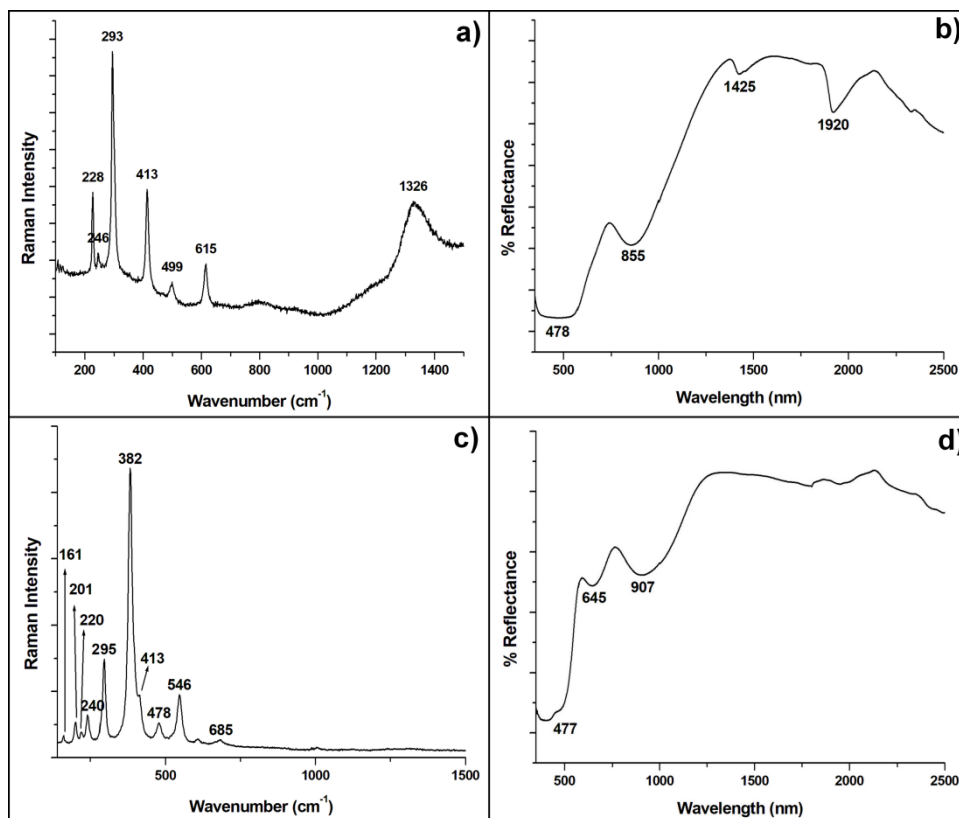

Figure 5.30. Spectra of oxides. **a)** Raman spectrum of hematite, **b)** VNIR spectrum of hematite, **c)** Raman spectrum of goethite and **d)** VNIR spectrum of goethite

5.7. Conclusions

The building of a database is an involved process but very necessary when complex samples are being studied, Martian samples in this case. Although some minerals of the

database have been already reported to be present on Mars, many others have not. Therefore, in this sense, this database plays an important role for the future interpretation of the upcoming data and possible new discoveries. Moreover, the use of the analytical techniques that will be included on board the rovers of future planetary missions to Mars will make the IMPAT-Database an important reference for those studies..

This work can help not only in the interpretation of the experimental spectroscopic data that will come from the planetary missions, but also in the study of terrestrial Martian analogues and in the analysis of meteorites, and, in general, in the study of geological samples and minerals.

5.8.   Bibliography

1. Lafuente B., Downs R. T., Yang H., Stone N. The power of databases: the RRUFF project. In: *Highlights in mineralogical crystallography.* Ed. T. Armbruster, R. M. Danisi. *W. De Gruyter,* Berlin. **2015,** pp. 1-30.

2. Wang A., Han J., Guo L., Yu J., Zeng P. Database of standard Raman spectra of minerals and related inorganic crystals. *Appl. Spectrosc.,* **1994,** 48, 959-968.

3. Cloutis E. A., Mann P., Izawa M. R. M., Applin D. M., Samson C., Kruzelecky R., Glotch T. D., Mertzman S. A., Mertzman K. R., Haltigin T. W., Fry C. The Canadian space agency planetary analogue materials suite. *Planet. Space Sci.,* **2015,** 119, 155-172.

4. Clark R. N., Swayze A. R., Wise G., Livo, E., Hoefen T., Kokaly R., Sutley S. J. *USGS digital spectral library splib06a: U.S. Geological Survey, Digital Data Series 231.* http://speclab.cr.usgs.gov/spectral.lib06 (last update 2020/01/21).

5. Instituto Geológico y Minero de España http://www.igme.es/ (last update 2020/07/23).

6. Torre-Fdez I., Aramendia J., Gómez-Nubla L., Castro K., Madariaga J. M. Geochemical study of the Northwest Africa 6148 Martian meteorite and its terrestrial weathering processes. *J. Raman Spectrosc.,* **2017,** 48, 1536-1543.

7. Orofino V., Blanco A., D'Elia M., Fonti S., Giuri M. Spectroscopic analysis of particulate samples of altered olivine for planetological studies. *Mem. S. A. It. Suppl.,* **2011,** 16, 113-118.

8. Freeman J. J., Wang A., Kuebler K. E., Jolliff B. L., Haskin L. A. Characterization of natural feldspars by Raman spectroscopy for future planetary exploration. *Can. Mineral.,* **2008,** 46, 1477-1500.

9. Adams J. B., Goullaud L. H. Plagioclase feldspars: Visible and near infrared diffuse reflectance spectra as applied to remote sensing. *Proc. Lunar Planet. Sci. Conf.,* **1978,** 3, 2901-2909.

10. Huang E., Chen C. H., Huang T., Lin E. H., Xu J. A. Raman spectroscopic characteristics of Mg-Fe-Ca pyroxenes. *Am. Mineral.,* **2000,** 85, 473-479.

11. Cloutis E. A. Pyroxene reflectance spectra: Minor absorption bands and effects of elemental substitutions. *J. Geophys. Res.,* **2002,** 107, 6-1; 6-12.

12. Altheide T. S., Chevrier V. F., Dobrea E. N. Mineralogical characterization of acid weathered phyllosilicates with implications for secondary Martian deposits. *Geochim. Cosmochim. Acta,* **2010,** 74, 6232-6248.

13. Craig P. I., Ming D. W., Rampe E. B. Sulfate formation from acid-weathered phyllosilicates: Implications for the aqueous history of Mars. *Eight International Conference on Mars,* **2014,** abst. 1323.

14. Baldridge A. M., Hook S. J., Crowley J. K., Marion G. M., Kargel J. S., Michalski J. L., Thomson B. J., de Souza Filho C. R., Bridges N. T., Brown A. J. Contemporaneous deposition of phyllosilicates and sulfates: Using Australian acidic saline lake deposits to describe geochemical variability on Mars. *Geophys. Res. Lett.,* **2009,** 36, L19201, 1-6.

15. Bibring J. P., Langevin Y., Mustard J. F., Poulet F., Arvidson R., Gendrin A., Gondet B., Mangold N., Pinet P., Forget F., OMEGA team. Global mineralogical and aqueous mars history derived from OMEGA/Mars express data. *Science,* **2006,** 312, 400-404.

16. Bishop J. L., Velbel M. A. Comparison of phyllosilicates observed on the surface of Mars with those found in Martian meteorites. *80th Annual Meeting of the Meteoritical Society.* **2017,** abst. 6115.

17. Barre P., Fernández-Ugalde O., Virto I., Velde B., Chenu C. Impact of phyllosilicate mineralogy on organic carbon stabilization in soils: incomplete knowledge and exciting prospects. *Geoderma,* **2014,** 235, 382-395.

18. Craig P., Chevrier V., Sayyed M. R. G., Islam R. Spectral analysis of Deccan intrabasaltic bole beds: Implications for the formation and alteration of phyllosilicates on Mars. *Planet. Space Sci.,* **2017,** 135, 55-63.

19. Bishop J. L., Baker L. L., Fairén A. G., Gross C., Velbel M. A., Rampe E. B., Michalski J. R. Unraveling the diversity of early aqueous environments and climate on Mars through the phyllosilicate record. *LPSC 48,* **2017,** abst. 1804.

20. Tischendorf G., Forster H. J., Gottesmann B., Rieder M. True and brittle micas: composition and solid-solution series. *Mineral. Mag.,* **2007,** 71, 285-320.

21. Kodera P., Murphy P. J., Rankin A. H. Retrograde mineral reactions in saline fluid inclusions: The transformation ferropyrosmalite clinopyroxene. *Am. Mineral.,* **2003,** 88, 151-158.

22. Frost R., Xi Y. Raman spectroscopic study of the minerals apophyllite-(KF) $(KCa_4Si_8O_{20}F\cdot8H_2O)$ and apophyllite-(KOH) $(KCa_4Si_8O_{20}(F,OH)\cdot8H_2O)$. *J. Mol. Struct.,* **2012,** 1028, 200-207.

23. Mer'kov A. N., Bussen I. V., Goyko Ye. A., Kul'chitskaya Ye. A., Men'shikov Yu. P., Nedorezova A. P. Raite and zorite, new minerals from the Lovozero Tundra. *Int. Geol. Rev.,* **1973,** 15-9, 1087-1094.

24. Ruiz-Galende P., Torre-Fdez I., Aramendia J., Gómez-Nubla L., Castro K., Arana G., Fdez-Ortiz de Vallejuelo S., Maguregui M., Medina J., Baonza V. G., Rull F., Madariaga

J. M. New Raman-visible near-infrared database of inorganic and mineralogical planetary and terrestrial compounds and its implications for Mars: Phyllosilicates. *J. Raman Spectrosc.,* **2019,** 1-11.

25. Tokano T., Bish D. L. Hydration state and abundance of zeolites on Mars and the water cycle. *J. Geophys. Res.,* **2005,** 110, .

26. Çelik-Karakaya M., Karakaya N., Yavuz F. Geology and conditions of formation of the zeolite-bearing deposits Southeast of Ankara (Central Turkey). *Clays Clay Miner.,* **2015,** 63, 85-109.

27. Cloutis E. A., Asher P. M., Mertzman S. A. Spectral reflectance properties of zeolites and remote sensing implications. *J. Geophys. Res. Planet.,* **2002,** 107 (E9), 5067, 1-19.

28. Ruff S. Spectral evidence for zeolite in the dust on Mars. *Icarus,* **2004,** 168, 131-143.

29. Liou J. G. Stilbite-laumontite equilibrium. *Contrib. Mineral. Petr.,* **1971,** 31, 171-177.

30. English P. M. Formation of analcime and moganite at Lake Lewis, central Australia: significance of groundwater evolution in diagenesis. *Sediment. Geol.* **2001,** 143, 219-244.

31. Weisenberger T., Selbekk R. S. Multi-stage zeolite facies mineralization in the Hvalfjördur area, Iceland. *Int. J. Earth Sci.,* **2009,** 98, 985-999.

32. Glaccum R., Boström K. (Na, K)-phillipsite: Its stability conditions and geochemical role in the deep sea. *Mar. Geol.* **1976,** 21, 47-58.

33. Wang A., Freeman J. J., Jolliff B. L., Chou I. M. Sulfates on Mars: A systematic Raman spectroscopic study of hydration states of magnesium sulfates. *Geochim. Cosmochim. Acta,* **2006,** 70, 6118-6135.

34. Košek F., Culka A., Drahota P., Jehlička J. Applying portable Raman spectrometers for field discrimination of sulfates: Training for successful extraterrestrial detection: Raman spectrometers for field discrimination of sulfates. *J. Raman Spectrosc.,* **2017,** 48, 1085-1093.

35. Sasaki K. Distinction of jarosite group compounds by Raman spectroscopy. *Canad. Mineral.,* **1998,** 36 (5), 1225-1235.

36. Anthony J. W., Bideaux R. A., Bladh K. W., Nichols M. C. *Handbook of Mineralogy, Mineralogical Society of America, Chantilly, USA.* http://www.handbookofmineralogy.org/ (last update 2020/01/21).

37. Bloise A., Dattola L., Allegretta I., Terzano R., Miriello D. Linarite and connellite dataset from Calabria region (Southern Italy): First evidence. *Data in Brief,* **2019,** 27, 104597, 1-8.

38. Baensch A. PhD thesis. *The mineralogy of the massive sulphides in the high grade Silver Swan Massive Nickel Sulphide Deposit. With an emphasis on the distribution of arsenic and cobalt mineralisation.* Western Australian School of Mines Curtin University, Kalgoorlie, Australia, **2000.**

39. Seetharam R. Gudmundite from base metal sulphide deposit of Askot, Pithoragarh District, (U. P.). *J. Geol. Soc. India,* **1981,** 22, 5, 216-219.

40. El-Baz F. The geology of Egypt. *Leiden E. J. BRILL,* The Netherlands. **1984**.

41. Fernández-Remolar D. C., Sánchez-Román M., Amils R. The case of the lacking carbonates and the emergence of early life on Mars. *Sustainability,* **2010,** 2, 2541-2554.

42. Edwards H. G. M., Villar S. E. J., Jehlička J., Munshi T. FT–Raman spectroscopic study of calcium-rich and magnesium-rich carbonate minerals. *Spectrochim. Acta A Mol. Biomol. Spectrosc.* **2005,** 61, 2273-2280.

43. Dufresne W. J. B., Rufledt C. J., Marshall C. P. Raman spectroscopy of the eight natural carbonate minerals of calcite structure. *J. Raman Spectrosc.,* **2018,** 49, 1999-2007.

44. Barton I. F., Yang H., Barton M. D. The mineralogy, geochemistry, and metallurgy of cobalt in the rhombohedral carbonates. *Canad. Mineral.,* **2014,** 52, 653-669.

45. Ashwal L. D., Cairncross B. Mineralogy and origin of stichtite in chromite-bearing serpentinites. *Contrib. Mineral Petr.,* **1997,** 127, 75-86.

46. Bell III J. F., McCord T. B., Owensby P. D. Observational evidence of crystalline iron oxides on Mars. *J. Geophys. Res.,* **1990,** 95, 14447-14461.

47. Hanesch M. Raman spectroscopy of iron oxides and (oxy)hydroxides at low laser power and possible applications in environmental magnetic studies. *Geophys. J. Int.,* **2009,** 177, 941-948.

48. Horgan B. H. N., Cloutis E. A., Mann P., Bell J. F. Near-infrared spectra of ferrous mineral mixtures and methods for their identification in planetary surface spectra. *Icarus.* **2014,** 234, 132-154.

CHAPTER 6:

MEÑAKOZ (BARRIKA)

In this chapter, the geochemical characterization of the Meñakoz outcrop is described. The techniques used were those detailed in the *Experimental Procedure* section including those that will be employed in the Martian missions, in order to provide a comparison in the interpretation of the results with those that will be obtained on Mars. The results obtained in Meñakoz supported the proposal of this emplacement as a Martian analogue. Its volcanic origin and the highly weathered materials observed make this outcrop a good example since it is one of the scenarios expected on the Martian surface [1].

According to the obtained results (see below), it should be noted that there were no mineralogical or chemical differences between the two groups of samples taken during the sampling procedure. This implies that the weathering processes they suffered were similar.

The first step in the characterization was the elemental analyses using the energy dispersive X-Ray fluorescence spectroscopy (EDXRF) in mapping mode. In the following figures (Figure 6.1 and 6.2), some examples of the obtained elemental mappings are shown, representing all the analysed samples, which have similar elemental composition with different distribution of the elements. Utilisingthis type of analysis, it was possible to establish relations among the elements and, therefore, in some cases they could serve

as a guide to interpret the results of subsequent molecular analyses. As was stated by Namieśnik [2], minor elements are below 1 % w/w concentration and major ones are above 1 % w/w. Most of the detected elements were in minor concentration and those that gave the most valuable information for the molecular analyses were in major concentration. As the most concentrated elements, these last ones were the most common ones and were found to be present in all of the analysed samples.

In the example shown in Figure 6.1 the major elements were calcium, silicon and iron. Titanium, magnesium and manganese were in minor concentration and zirconium, rubidium, zinc and nickel were the trace elements. Calcium, which was the most concentrated element, was distributed along the entire sample surface except in the green areas. The most probable mineral for this element would be calcite ($CaCO_3$, confirmed by XRD and Raman spectroscopy). In the green areas, silicon, iron and titanium were the most concentrated elements. The presence of silicon and iron could means that in these areas the existence of silicates is more probable. Moreover, oxides of these elements, such as quartz or hematite, were also very common (see below). In the case of titanium, the most probable mineral associated with this element would be TiO_2 (most probably in anatase form) as can be seen in the Raman spectra (see below). Finally, magnesium and manganese were more or less homogeneously distributed through the entire surface. The presence of magnesium, which was common in the analysed samples, could be related with the presence of some silicates, such as chlorites, which are also detected using other techniques (Raman and VNIR spectroscopies). Manganese was expected to be in the form of oxides. Trace elements were represented by zirconium, rubidium, zinc and nickel. They were found in almost all the samples but always in low concentrations and, therefore, they would not be linked to the minerals identified by other spectroscopies.
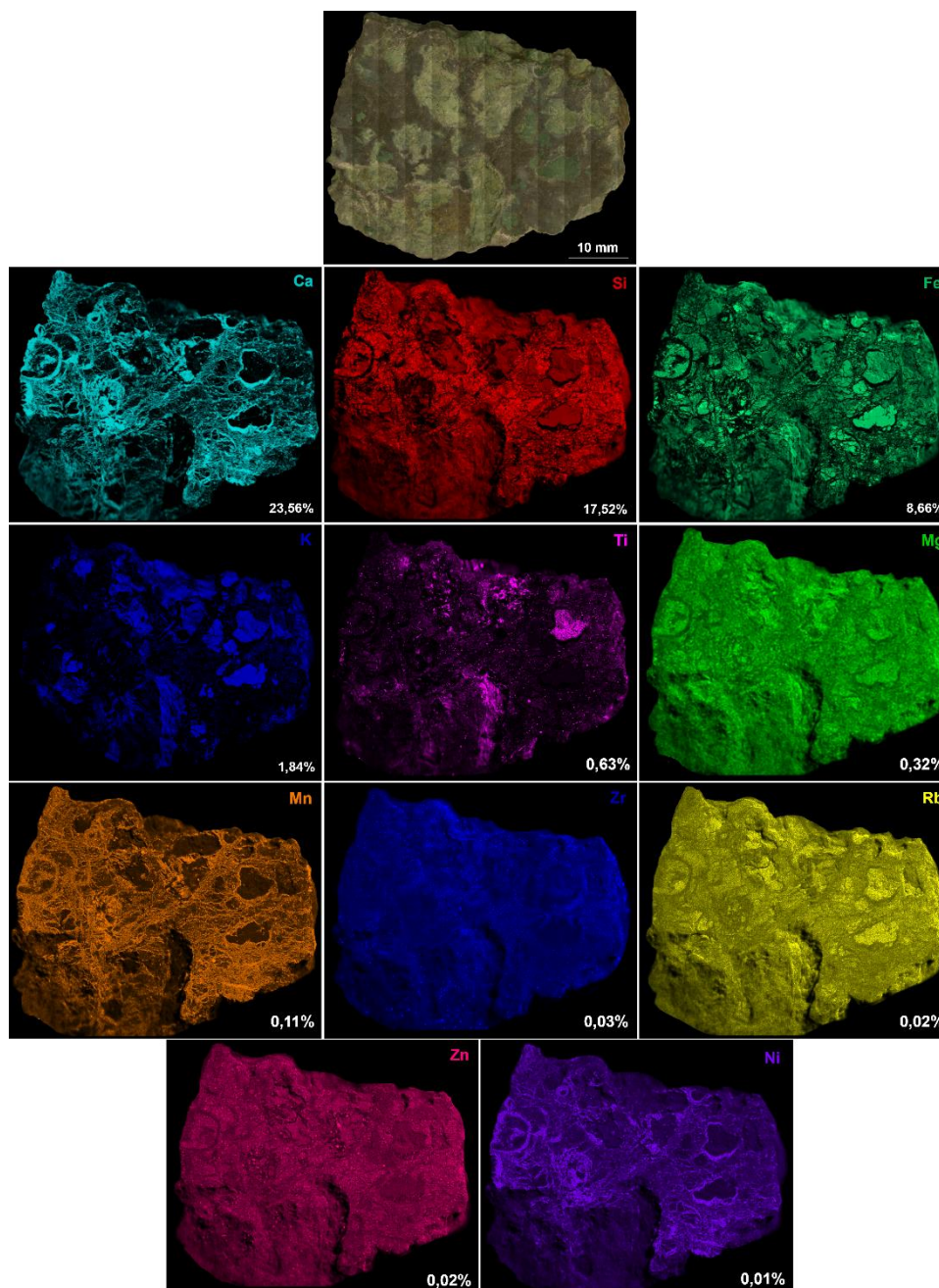
Figure 6.1. EDXRF mapping with the elemental distribution in a sample collected in the cliff of the Meñakoz outcrop

In Figure 6.2, another analysis of a Meñakoz sample is shown. In this case, apart from Ca, Si and Fe, aluminium was also a major element and could be related with the presence of aluminosilicates. Other major elements would be explained in the same way as for the previous example.

In this case, the presence of phosphorous (trace element) related with calcium suggests the presence of apatite ($Ca_5(PO_4)_3(F,Cl,OH)$), which was detected by Raman spectroscopy in some spectra thanks to the presence of its principal band (964 cm^{-1}). The low concentration observed here and the low intensity of the band observed by Raman analysis leads to the conclusion that the quantity of apatite was also low.

The minor elements were magnesium, manganese, potassium and sulfur. Magnesium, as in the previous case, was distributed through the entire surface and was associated with the presence of silicates, most probably with chlorites ($(Mg,Al,Fe)_6(Al,Si)_4O_{10}(OH)_8$), which were also identified using the other analytical techniques. Manganese, which also appeared in the previous sample, was distributed in the same way as calcium, but it was expected to be present in the form of oxides. For its part, potassium was related with aluminium and iron, suggesting that it formed part of the structure of aluminosilicates. The presence of sulfur was limited to specific (and small) areas and, as the Raman analyses showed, pyrite (FeS_2) would be the most probable compound in which this element be found. Elements such as cobalt, chromium, nickel, copper, zinc and rubidium, which were in trace concentration, are common in this type of sample. However, as in the previous example, due to their low concentration, minerals with these elements were not expected to be detected using other techniques.
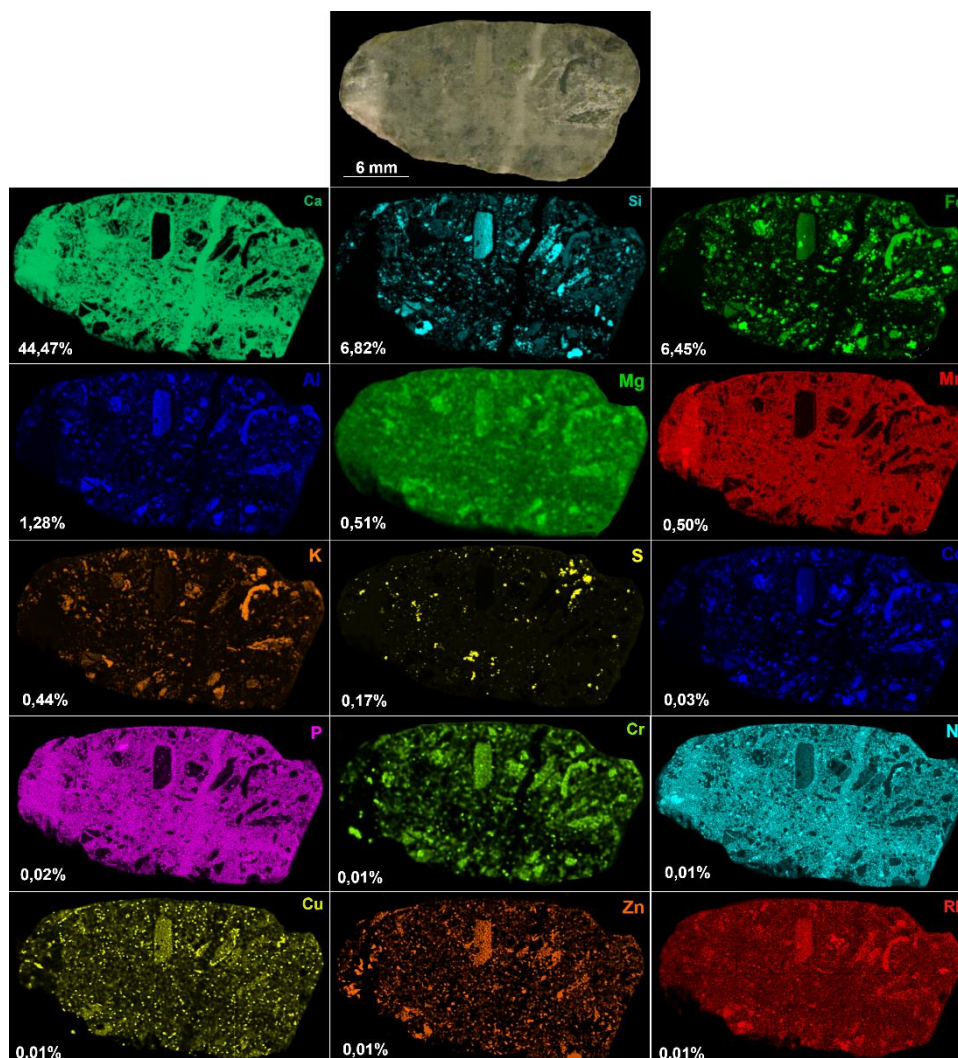

Figure 6.231. EDXRF mapping with the elemental distribution in a sample collected in the areas close to the sea in the Meñakoz outcrop

Regarding the molecular analyses, X-Ray diffraction measurements were also performed. All of the diffractograms had a considerable background elevation due to the contribution of the amorphous phases.

The minerals detected most frequently were quartz (SiO_2) and calcite ($CaCO_3$), which were present in all the measured samples and that is in agreement with the elemental results, which gave high concentrations of calcium and silicon. Other carbonates such as siderite ($FeCO_3$) and oxides such as anatase (TiO_2) or birnessite ($(Na,Ca,K)_{0.6}(Mn^{4+},Mn^{3+})_2O_4 \cdot 1.5H_2O$) were identified in some samples and their presence is consistent with the identified elemental compositions as well.

On the other hand, the presence of silicates was highly recurrent. Diffraction peaks related with feldspars (plagioclases) and phyllosilicates (kaolinites, micas and chlorites) were detected. The different minerals that form part of each group have the same or very similar diffraction peaks and, therefore, it was not possible to confirm which specific mineral was present in the sample. Some of the minerals given by the software for the XRD data treatment were albite ($NaAlSi_3O_8$), clinochlore ($Mg_5Al(Si_3Al)O_{10}(OH)_8$), celadonite ($K(Mg,Fe^{2+})(Fe^{3+},Al)Si_4O_{10}(OH)_2$), illite ($(K,H_3O)(Al,Mg,Fe)_2(Si,Al)_4O_{10}[(OH)_2,(H_2O)]$) and muscovite ($KAl_2(AlSi_3O_{10})(OH)_2$).

In order to complete and specify the information provided by XRD, Raman and VNIR spectroscopies were used. According to the results, most of the groups identified by XRD could be also identified by these techniques, thus, it was possible to determine the exact mineral phases that were present in the sample.

The presence of albite, which is a Na-feldspar (plagioclase, $NaAlSi_3O_8$, Figure 6.4.a) was detected using Raman spectroscopy. As can be seen in the figure, its main Raman bands are located at 287 (weak, w), 412 (w), 478 (medium, m), 508 (strong, s), 762 (w) and 813 (w) cm^{-1}. These shifts correspond to a high disordered albite as is reported by Freeman et al. [3].

Feldspars are the most abundant minerals in the igneous rocks, and they define its evolution better than any other group of minerals. Therefore, it can be stated that this mineral is the original one from which the following phyllosilicates arise [4]. Concretely, plagioclases occur at high and low temperatures being those of high temperature formation significantly less stable than the lower ones. Moreover, they are relatively easily influenced by water and weathering generating compounds such as kaolinite (which could be identified by VNIR spectroscopy) [5]. Taking into account the Bowen's reactions series [6] (Figure 6.3), the original basaltic rock should be enriched with calcium plagioclases. The contact of these rocks with the sea water (due to the antique submarine volcanic character of the emplacement and its current location next to the sea), which has a high concentration of sodium, the low temperature of this water compared with that of the emerged lava, and the presence of CO_2, result in Na-rich volcanic rocks being formed. This process is known as albitization [6].
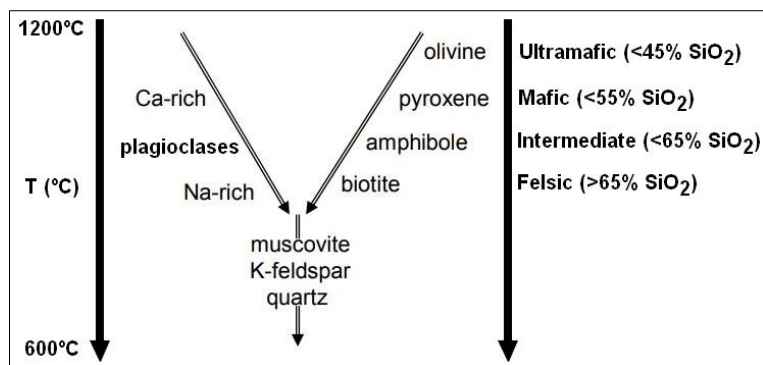
Figure 6.3. Bowen's reactions series (Image adapted from Gammons et al. [7])

Edwards et al. [8] and Wang et al. [9] report finding this type of silicates in some Martian meteorites, which are indicators of shock and thermal history of Mars. Milam et al. [10] studied TES (Thermal Emission Spectrometer) spectra and identified plagioclases as the dominant minerals in the Martian crust, with labradorite $((Ca,Na)(Si,Al)_4O_8$, An $(anorthite)_{50-70})$ and bytownite $((Ca,Na)(Al(Al,Si)Si_2O_8)$, $An_{70-90})$ as the main components of the observed plagioclases. This fact is comparable to the most common plagioclases in terrestrial volcanic rocks, reinforcing that the formation of albite is an Earth weathering process, which could also have happened on Mars if saline water existed.

Phyllosilicates were widely present in the measured samples. These minerals are of high importance for the geological knowledge of Mars, as they require the presence of water for their formation. Therefore, the existence of this type of minerals in the Martian surface implies the presence of water during its history and it could mean that Mars could be considered as a potential habitable planet (see section *Phyllosilicates* in *Chapter 1* and *5*).

The first example of phyllosilicates is kaolinite $(Al_2Si_2O_5(OH)_4$, see Figure 6.4.b), which was found in the samples by VNIR spectroscopy thanks to a doublet at 1399 and 1413 nm (due to the overtone of the OH group), another one at 2162 and 2207 nm, and a triplet with bands at 2323, 2358 and 2386 nm [11]. Bands related to the presence of iron could also be observed. The Fe^{2+}-Fe^{3+} charge transfer band appears at 745 nm, and Fe^{2+} crystal-field transition bands appear at 986 and 1158 nm with a possible additional contribution from Fe^{3+} ligand-field transitions to the first one [12]. The position of these iron bands depends on the crystal field energy of the mineral [13]. Even though the kaolinite does not have iron in its structure, this element is present in the bulk of the samples and, for that reason, its transition bands could be identified. A doublet at 1919 and 1959 nm is attributed to the combination bands of water, which in this case is due to the environmental humidity.

Kaolinite forms part of the kaolinite-serpentine group and it is typical of three main environments (weathering profiles, hydrothermal alterations, sedimentary rocks), and feldspars (such as the albite found in the analysed samples) are the most common parent minerals from which they develop. The physical and chemical conditions under

which the kaolin minerals form are relatively low pressures and relatively low temperatures [14].

This phyllosilicate was first observed on Mars by the OMEGA instrument in a small region of the southern highlands, whereas CRISM observed kaolinite in Nili Fosae and Mawrth Vallis [15, 16].
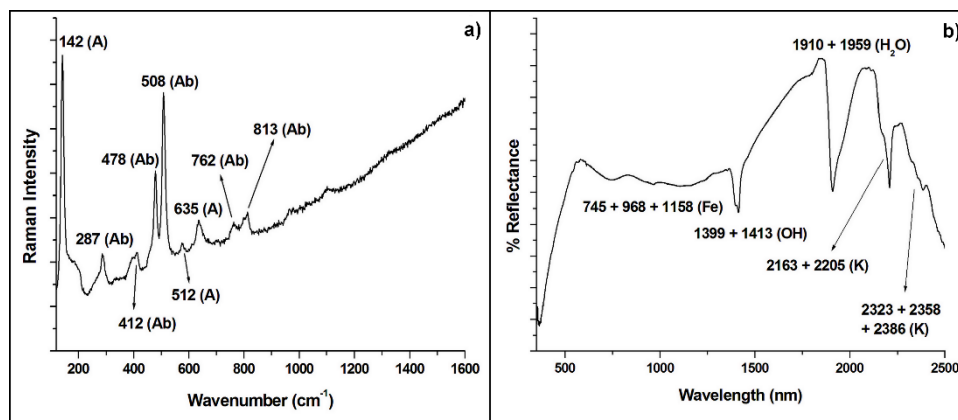

Figure 6.432. a) Raman spectrum of albite (Ab) together with some bands of anatase (A) and **b)** VNIR spectrum of kaolinite (K)

Another example from the phyllosilicates group is celadonite $(K(Mg,Fe^{2+})(Fe^{3+},Al)(Si_4O_{10})(OH)_2$, Figure 6.5), which was identified together with glauconite $((K,Na)(Fe^{3+},Al,Mg)_2(Si,Al)_4O_{10}(OH)_2)$ using Raman spectroscopy. In Figure 6.4.a, bands at 179 (s), 274 (m), 392 (w), 548 (s) and 701 (very strong, vs) cm^{-1} are observed and they are consistent with the presence of celadonite. In addition, bands at 317 (very weak, vw), 455 (m) and 597 (s) cm^{-1} would be consistent with the presence of glauconite.

As can be seen in Figure 6.5.b celadonite was also detected by VNIR spectroscopy. The spectrum shows bands at 2254, 2314 and 2356 nm that correspond to the Metal-OH vibrations, and bands consistent with the ionic transitions of iron (764, 926 and 1119 nm). Moreover, the overtone due to the vibration of the OH group appears at 1413 nm as well as the combination bands of water fundamental vibrations at 1910 and 1969 nm [16].

Celadonite and glauconite have similar composition because they are Fe^{2+}-bearing micas, but their formation mechanism is different. Celadonite is commonly formed from volcanic materials in low pressure and low temperature environments, which could also occur on Mars and is therefore an important mineral for the establishment of Meñakoz as a Martian analogue. Once formed, celadonite is very stable even under high temperatures. In contrast, glauconite is formed as green sand in marine sediments and is altered to biotite-rich deposits or layers containing kaolinite, iron hydroxides and silica [17], and is less abundant than celadonite.

Even though, celadonite has not been detected on Mars, Bridges et al. [18] modelled the pottencial formation of this mineral on the Martian surface.
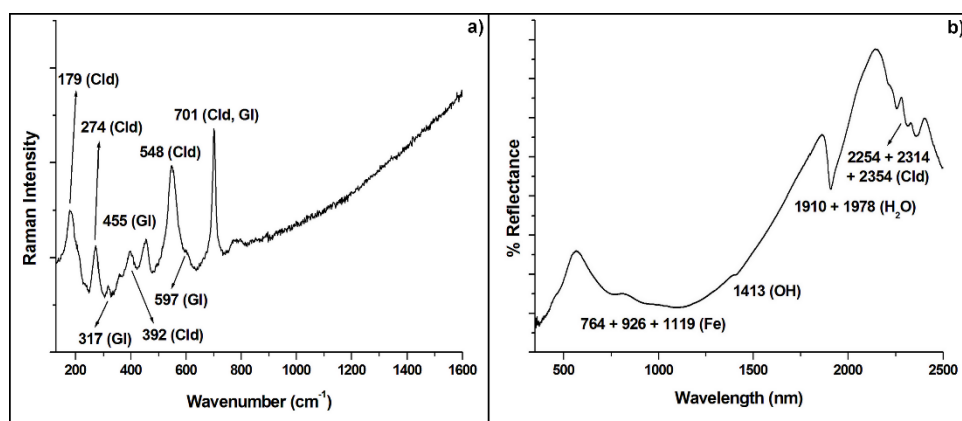
Figure 6.5. Spectra of celadonite. **a)** Raman spectrum together with glauconite (Gl) and **b)** VNIR spectrum

In Figure 6.6.a, VNIR bands corresponding to different minerals are shown. The band recorded at 2209 nm could belong to illite $((K,H_3O)(Al,Mg,Fe)_2(Si,Al)_4O_{10}[(OH)_2,(H_2O)])$ or muscovite $(KAl_2(Si_3Al)O_{10}(OH)_2)$, while the band at 2253 nm could be consistent with the presence of epidote $(Ca_2Fe^{3+}Al_2(Si_2O_7)(SiO_4)O(OH))$ or chlorite $((Mg,Al,Fe)_6(Al,Si)_4O_{10}(OH)_8)$. Finally, the band at 2351 nm is a band present in the four compounds mentioned [19]. Besides, the bands consistent with the presence of iron (which forms part of these silicate structures) at 741 nm (Fe^{2+}-Fe^{3+} charge transfer), 922 nm (Fe^{2+} and/or Fe^{3+} transitions) and 1109 nm (Fe^{2+} transitions) nm, the vibrations due to the overtone of OH group (1412 nm) and the combination bands of H_2O (1907 and 1973 nm) can also be seen in this case.

Chlorites were also identified by Raman spectroscopy (Figure 6.6.b), thus, the doubt that arose during VNIR analysis was solved. In this spectrum, features related to Fe^{2+}-rich (Chamosite) and Mg-rich (Clinochlore) chlorites could be identified. This fact suggests that the chlorite found is a mixture of both of them (Fe^{2+}/Mg-chlorite). These bands are 194 (s) and 288 (vw) cm^{-1} for the chamosite, and 359 (w), 549 (s) and 679 (vs) cm^{-1} for the clinochlore.

Chamosite and clinochlore are two members of the chlorite sub-group and have the same molecular formula but with different proportions of iron and magnesium. They are mainly formed from low grade metamorphic rocks, and as a product of the alteration of Fe and Mg bearing minerals [20]. The first one is typically diagenetic (low temperature) and the second one is metamorphic (high temperature) [21]. These minerals were found on Mars in Nili Fossae by CRISM aboard MRO [16, 22] and are interpreted to be products of low grade thermal metamorphism of hydrothermal interaction, along diagenesis, suggesting that past aqueous alteration of the subsurface crust occurred at elevated temperatures [23]. The finding of these phyllosilicates on Mars and Meñakoz reinforces the proposal of Meñakoz as a Martian analogue.

Illite is a mica and is formed by the decomposition of other micas and feldspars, which are predominant in marine clays [22]. This type of compounds has been found on the surface of Mars by CRISM in Nili Fossae [16].

Muscovite, which is another type of mica, replaces illite within higher metasedimentary rocks and is abundant in metamorphic rocks [22, 24]. It is the most common mica and appears under a wide variety of geological conditions [25] and, as illite, it has also been found on Mars in Nili Fossae by CRISM [16].

Taking into account the results of the elemental analyses and the absence of any of these minerals in the Raman spectra, the most probable phase in the samples would be illite since it has iron in its structure.

The last phyllosilicate found was montmorillonite ($(Na,Ca)_{0.33}(Al,Mg)_2(Si_4O_{10})(OH)_2 \cdot nH_2O$, see Figure 6.6.c) and it was identified through the VNIR band at 2207 nm. Moreover, in the bands related to OH (1414 nm) and H_2O (1938 nm), there is a shoulder to the right of both bands (1492 and 1989 nm respectively) that is a characteristic feature of the presence of montmorillonite [26]. In the same spectrum the presence of gibbsite ($Al(OH)_3$), with a band at 2267 nm, is also observed [11]. Once again, bands consistent with the presence of Fe^{3+} transitions can be seen (435 and 905 nm) due to the presence of iron in the bulk of the samples.

Montmorillonite is an Al-smectite and it is formed by the alteration of igneous rocks rich in Ca and Mg [22] (like those found in Meñakoz). Poulet et al. [27] reported the presence of montmorillonite according to the data collected by OMEGA in the western part of Mawrth Vallis, near Oxia Planum. On the other hand, gibbsite is considered an ultimate end product [28] of weathering and is usually present in old weathered soils. However, it has not been reported to be present on Martian surface yet, thus, the results obtained with the Meñakoz samples could help in the future identification of this mineral on Mars.
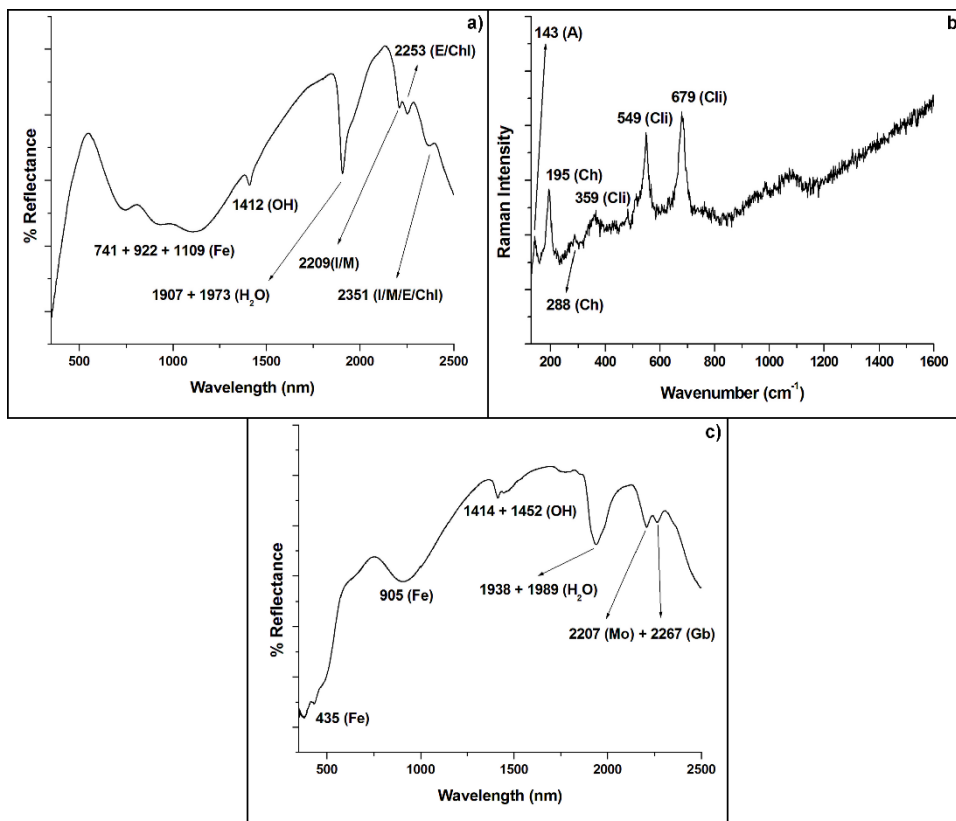
Figure 6.633. Spectra of phyllosilicates. **a)** Mixture of phyllosilicates: illite (I), muscovite (M), epidote (E) and chlorite (Chl), **b)** Raman spectrum of chlorite with bands consistent with the presence of chamosite (Ch) and clinochlore (Clin) and **c)** VNIR spectrum of montmorillonite (Mo) together with gibbsite (Gb)

Sulfur bearing compounds could also be identified. Pyrrhotite (Fe_7S_8, Figure 6.7.a) was detected due to its Raman bands at 336 (m) and 369 (s) cm^{-1}, and pyrite (FeS_2, Figure 6.7.b) with bands at 340 (m), 377 (s) and 425 (vw) cm^{-1}. Moreover, a band at 323 (m) cm^{-1} is due to the presence of marcasite, another polymorph of iron disulfide that could coexist with pyrite [29].

Pyrite is formed under various conditions and in different geological contexts and depositional environments (marine and continental). It can be found in hydrothermal veins in igneous rocks and as diagenetic replacement in sedimentary rocks [30] being considered as the latest stage of crystallization. An increase in sulfur activity due to the concentration of H_2S on magma fractionation may lead to the destabilization of pyrrhotite and the production of pyrite. Another point of view is that pyrrhotite becomes unstable with cooling basaltic magma due to an increase in oxidation state [31].

Some studies suggest that the presence of sulfates such as jarosite (see below) on the Martian surface is the result of past weathering of pyrrhotite and pyrite. Zolotov et al. [32] hypothesized that regional heating in the Meridiani Planum area caused a release of sulfide-rich hydrothermal waters, leading to the formation of pyrite deposits whose oxidation allowed the formation of sulfates. Moreover, the OMEGA/Mars Express visible–near infrared hyperspectral imager identified hydrated sulfates in Valles Marineris [33] and its presence has been recently suggested in Oxia Planum [34].

By means of VNIR spectroscopy jarosite ($KFe_3^{3+}(SO_4)_2(OH)_6$, Figure 6.7.c) was identified. In the spectrum, bands at 1850 and 2266 nm are attributed to the presence of this sulfate, and there are some others consistent with the presence of illite, which are 2209 nm in the doublet feature due to the Al-OH bond, and the doublet at 1413 and 1472 nm related to the OH vibrations, that is also assigned to this phyllosilicate. The broader band at ~1900 nm due to the combination bands of water was also detected. The bands observed at 430 and 980 nm were assigned to iron transitions that form part of the structure of both compounds but the shape of the bands observed in the spectrum is characteristic of the presence of jarosite [12].

Jarosite is a ferric sulfate known as a secondary mineral formed under acidic conditions and in sulfate-rich environments. This acid conditions result from the oxidation of pyrite, which may be due to bacterial action or through air-oxidation [35]. The Opportunity Rover detected it for the first time on Mars in Meridiani Planum. Orbital observations of jarosite have also been reported in Mawrth Vallis [36]. The association of the presence of jarosite with the presence of water makes this finding relevant to the potential habitability of Mars.
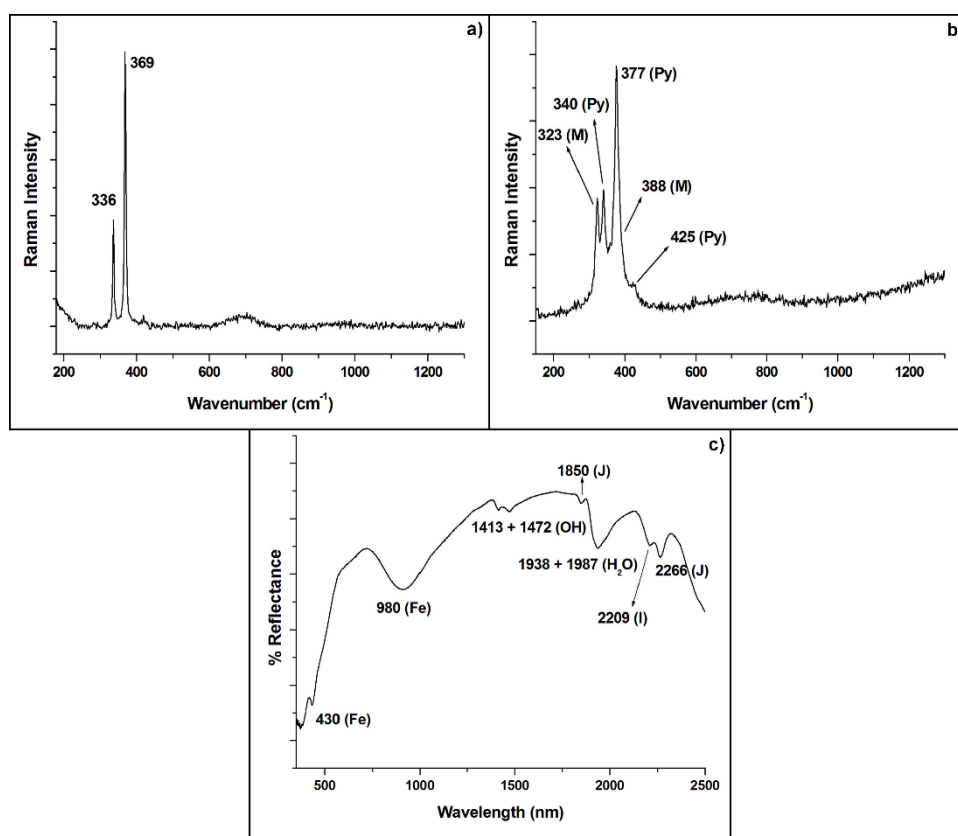

Figure 6.7. Raman spectra of **a)** pyrrhotite and **b)** pyrite (Py) together with marcasite (M), **c)** VNIR spectrum of jarosite (J) together with illite (I)

Other compounds such as oxides were identified. On the one hand, the main polymorphs of titanium dioxide (TiO_2) could be identified by Raman spectroscopy, anatase (Figure 6.8.a) with its Raman bands at 143 (vs), 198 (vw), 397 (w), 514 (w) and 637 (m) cm^{-1}, brookite (Figure 6.7.b) whose bands are 154 (s), 214 (vw), 248 (w), 284

(vw), 322 (m), 366 (w), 410 (vw), 501 (vw), 543 (vw) and 640 (w) cm^{-1}, and rutile (Figure 6.8.c) with bands at 442 (m) and 610 (s) cm^{-1}.
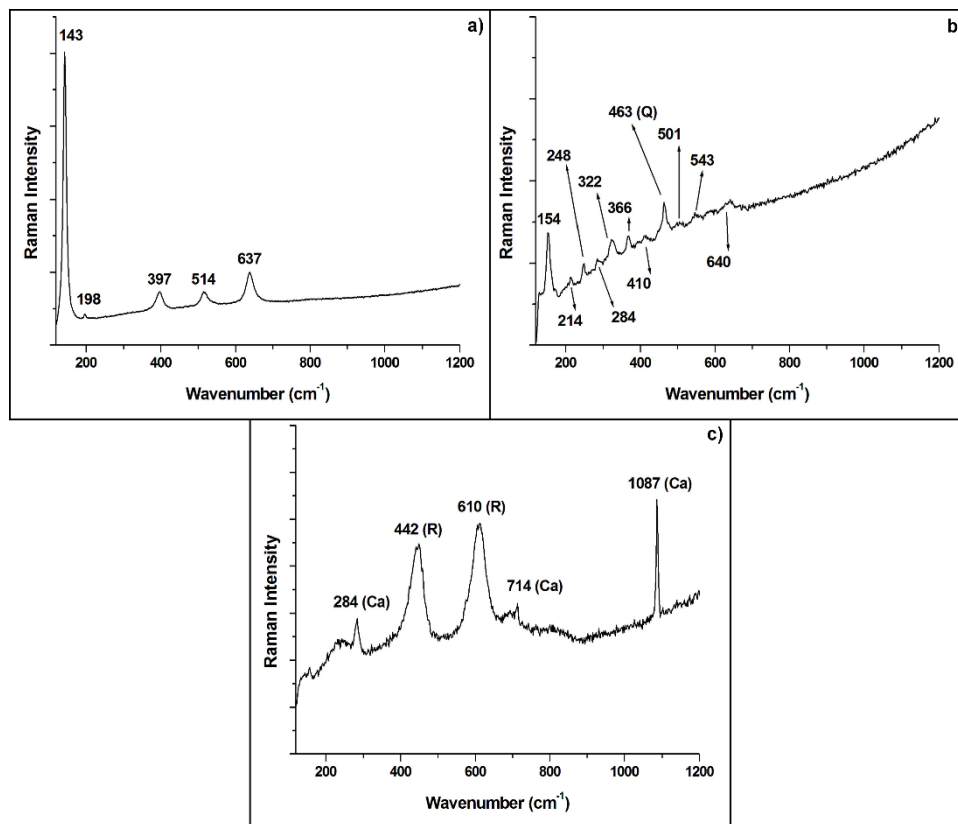

Figure 6.8. Raman spectra of titanium dioxides: **a)** anatase, **b)** brookite together with quartz (Q) and **c)** rutile (R) together with calcite (Ca)

Anatase and brookite are the low temperature polymorphs. Anatase could arise as an alteration product of titanium rich minerals and its formation suggests, again, a hydrothermal origin [37]. Brookite has the lowest stability and due to this fact it is a rare natural TiO_2 form, whose formation mechanism is unclear. It may be formed by hydrothermal conditions but also during the cooling of the lava [38]. Rutile is the high pressure and high temperature polymorph that may occur during the eruption of the volcano when the pressure and the temperature are high enough for its formation, and another formation mechanism is by hydrothermal alteration (like brookite) [39]. The differences related to the temperature or pressure for the formation of the different polymorphs could provide clues to establish different formation environments and, thus, to understand the environmental and geological past of Martian rocks. The presence of rutile indicates that there was an episode where the temperature and pressure were high, probably during the eruption of the volcano. The later rapid cooling of the lava flow due to the contact with water (the Meñakoz outcrop was a submarine volcano in origin), could explain the existence of this polymorph in the samples nowadays. The other polymorphs (brookite and anatase) arise from alteration processes indicating their higher abundance and later formation [40]. On Mars, they were identified in Gale Crater as trace minerals [41].

On the other hand, iron oxides were also detected. Goethite (α-FeOOH, Figure 6.9.a), with Raman bands at 243 (m), 299 (m), 393 (s), 480 (m) and 549 (w) cm^{-1}, was identified together with hematite (Fe_2O_3, Figure 6.9.b) thanks to the Raman bands at 222 (m), 241 (w), 295 (m), 407 (s), 496 (w), 603 (m), 657 (m) and 1308 (vs) cm^{-1}. This hematite spectrum has a band (657 cm^{-1}) that is normally a forbidden band for Raman transitions. This band represents an incomplete symmetry of hematite due to stress defects or impurities [42].

Goethite is the most stable iron oxide at ambient temperature, and therefore, the first one to form [43]. It arises from weathering of natural iron-containing minerals such as lepidocrocite [44] or silicates, like in this case (which are very common on the surface of Mars). Hematite occurs in surface outcrops of volcanic and sedimentary rocks and it is attributed to modern weathering of ferrous-rich minerals [45]. These oxides were reported to be present on Mars by Klingelhöfer et al. [46] in Columbia Hills in Gusev Crater thanks to the Mars-Exploration-Rovers (MER) Spirit.
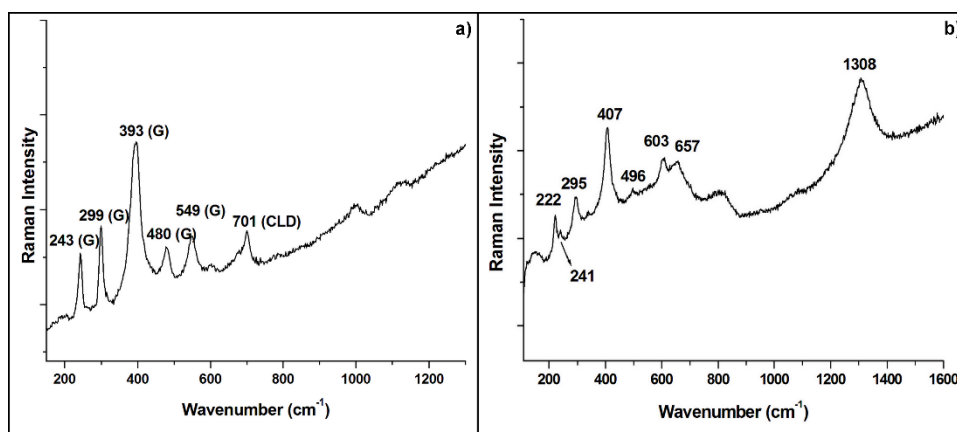

Figure 6.9. Raman spectra of iron oxides: **a)** geothite (G) together with celadonite (Cld) and **b)** hematite

Finally, manganese oxides and quartz (SiO_2) were identified using Raman spectroscopy. The presence of manganese oxides (Figure 6.10.a) is confirmed by the prsence of the bands at 278 (vw), 396 (w), 487 (m), 571 (s) and 615 (s) cm^{-1}. Most of Mn oxides are amorphous and this is the reason of the relative broad bands observed. Moreover, they are highly reactive mineral phases that play important roles in elemental biogeochemical cycles being some of the strongest oxidants naturally found in the environment [47]. In this case, the most probable oxide is lithiophorite ($LiAl_2(Mn_2^{4+},Mn^{3+})O_6(OH)_6$) as reported by Bernardini et al. [48]. In the Kimberley region of Gale Crater (Mars), Curiosity rover observed high Mn abundances in fracture filling-materials, providing unique indicators of water-rich environments and their redox states [49].

In the case of quartz (Figure 6.10.b), the Raman bands are located at 201 (m), 263 (w), 354 (w), 463 (vs), 802 (vw) and 1158 (vw) cm^{-1}. Quartz is the low temperature and low pressure stable polymorph of SiO_2 [50]. Moreover, taking into account the Bowen's series [6] (Figure 6.3), this oxide is the last product of weathering processes. On Mars, the Antoniadi Crater region is the only location identified from orbital data to exhibit spectral

signatures consistent with the presence of quartz, found in impact craters and in fractured terrains [51].
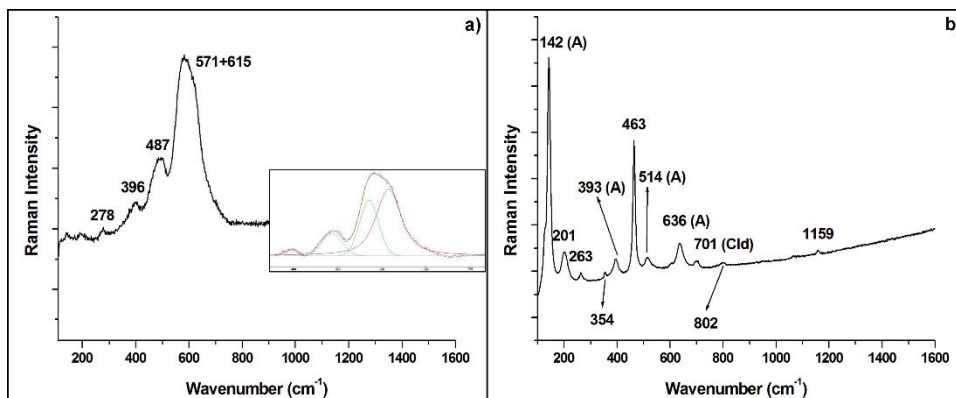

Figure 6.10. Raman spectrum of **a)** lithiophorite with the decomposition of the broad band, and **b)** quartz together with anatase (A) and celadonite (Cld)

Calcite ($CaCO_3$, Figure 6.11.a), with its main Raman bands at 156 (w), 281 (m), 712 (w) and 1086 (vs) cm^{-1}, was found in white areas. VNIR spectroscopy bands (Figure 6.11.b) consistent with the presence of calcite are located at 1876, 1993, 2163 nm, and a broad band composed of two bands at 2293 and 2338 nm [52]. Moreover, a band at 1115 nm can be observed due to the crystal field transition of Fe^{2+}-Fe^{3+}, which is present in the bulk of the sample. Finally, bands at 1414 nm consistent with the overtone of the OH, and 1917 nm due to the combination band of H_2O, are present because of the environmental humidity.

Calcite could be formed by the combination of calcium with carbonates found in older limestone by two different mechanisms: chemical precipitation, after dissolution of older calcium carbonates in water (the most probable one in this study), or, shock wave reaction, due to natural of artificial impacts [53]. It appeared always in form of veins and vesicles reinforcing that its formation is by chemical precipitation and that it is a secondary mineral phase from the primary basaltic minerals. Calcite, among other carbonates, confirmed to be present on Mars thanks to the instruments on the Phoenix Lander [54]. Carbonates play an important role in determining the history of Mars because they provide trace for the presence of liquid water available in a CO_2 atmosphere [55].
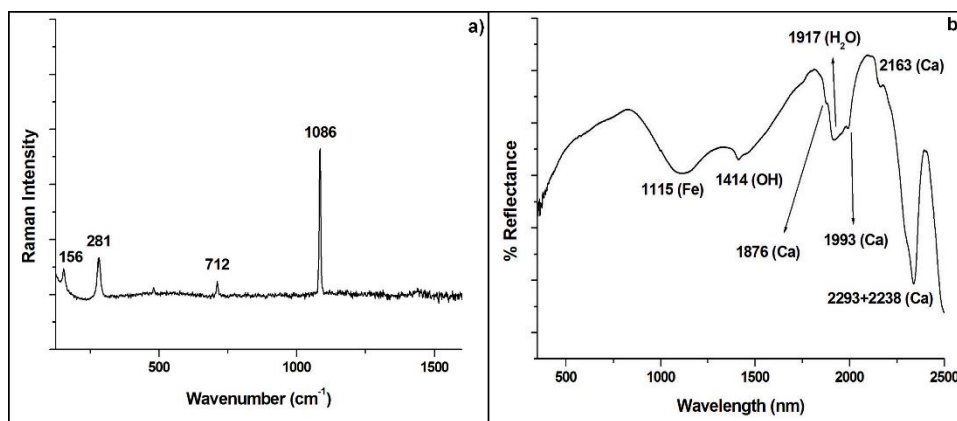
Figure 6.11. a) Raman spectrum and **b)** VNIR spectrum of calcite

6.1. Conclusions

The results presented in this chapter confirm that silicates are the most common compounds found in the Meñakoz samples.

The elemental techniques such as EDXRF, are a good starting point for the comprehensive characterization of the samples. As the mapping mode shows the distribution of the elements in the samples, the analyses performed by non-destructive molecular techniques (Raman and VNIR) are easier. Moreover, the semi-quantitative information could help with discerning between minerals with different cations, as happened with illite and muscovite in this chapter.

As demonstrated, molecular techniques complement each other since there are minerals that were only found by means of one of the employed techniques and some others that were identified by all of them. This fact, in the case of Raman and VNIR spectroscopies, is relevant because it means that both techniques are necessary to achieve a complete characterization of those kind of samples. Consequently, the selection of them for the Martian missions is important decision in order to ensure the complete characterization of Martian mineralogy.

According to the identified silicates, it could be possible to differentiate between the original phases, such as feldspars, and the weathered ones, such as phyllosilicates. These are the most important ones because, as has been explained previously, their presence provides evidence for the existence of water, and for that reason, they could be considered as a signature of possible habitability. This fact can help in the comprehension of the silicate formation mechanisms on the Martian surface and it could be concluded that their presence provides evidence for the existence of liquid water at some point in Mars' history. Besides, some of them are formed due to the weathering processes of basaltic rocks, which are characteristics of volcanic zones like Mars and Meñakoz. Moreover, sulfides are also very important minerals because they can help in the comprehension of the formation mechanisms of sulfates, which provide further evidence for the presence of water since they need it for their formation.

Apart from the minerals that are present on Mars, there are some compounds that were found in Meñakoz, that have not yet been reported to be present on Mars. Due to this fact, Meñakoz could help in future discoveries regarding these minerals and its formation mechanisms. In addition, the environmental conditions in both emplacements could have been similar, and therefore, the processes suffered by the detected minerals should be similar. All these facts reinforce the proposal of Meñakoz as a Martian analogue site.

6.2. Bibliography

1. Ruiz-Galende P., Torre-Fdez I., Aramendia J., Gómez-Nubla L., Castro K., Arana G., Madariaga J. M. Study of a terrestrial Martian analogue: Geochemical characterization of the Meñakoz outcrops (Biscay, Spain). *J. Raman Spectrosc.,* **2019,** 1-10.

2. Namieśnik J. Trace Analysis — Challenges and Problems. *Crit. Rev. Anal. Chem.,* **2002,** 32, 271-300.

3. Freeman J. J., Wang A., Kuebler K. E., Jolliff B. L., Haskin L. A. Characterization of natural feldspars by Raman spectroscopy for future planetary exploration. *Can. Mineral.,* **2008,** 46, 1477-1500.

4. Brown W. L., Parsons I. Feldspars in igneous rocks. In: *Feldspars and their reactions.* Ed. Parsons I. *Springer,* Dordrecht. **1994,** pp. 449-499.

5. Haldar S. K., Tišljar J. Chapter 2 - Basic mineralogy. In: *Introduction to mineralogy and petrology.* Eds. Haldar S. K., Tišljar J. *Elsevier,* Oxford. **2014,** pp. 39-79.

6. Haldar S. K., Tišljar J. Chapter 4 - Igneous rocks. In: *Introduction to mineralogy and petrology.* Eds. Haldar S. K., Tišljar J. *Elsevier,* Oxford. **2014,** pp. 93-120.

7. Gammons C., Harris L., Castro J., Cott P., Hanna B. Creating lakes from open pit mines: processes and considerations, with emphasis on northern environments. Canadian Technical Report of Fisheries and Aquatic Sciences. *Can. Tech. Rep. Fish. Aquat. Sci. 2826,* Canada. **2009**.

8. Edwards H. G. M., Farwell D. W., Grady M. M., Wynn-Williams D. D., Wright I. P. Comparative Raman microscopy of a Martian meteorite and Antarctic lithic analogues. *Planet. Space Sci.,* **1999,** 47, 353-362.

9. Wang A., Kuebler K. E., Jolliff B. L., Haskin L. A. Mineralogy of a Martian meteorite as determined by Raman spectroscopy. *J. Raman Spectrosc.,* **2004,** 35, 504-514.

10. Milam K. A., McSween H. Y., Jr., Moersch J., Christensen P. R. Distribution and variation of plagioclase compositions on Mars. *J. Geophys. Res. Planet.,* **2010,** 115, E09004, 1-15.

11. de Oliveira J. F., Brossard M., Corazza E. J., Marchão R. L., de Fátima Guimarães M. Visible and near Infrared spectra of ferralsols according to their structural features. *J. Near Infrared Spectrosc.,* **2016,** 24, 243-254.

12. Cloutis E. A., Craig M. A., Kruzelecky R. V., Jamroz W. R., Scott A., Hawthorne F. C., Mertzman S. A. Spectral reflectance properties of minerals exposed to simulated Mars surface conditions. *Icarus,* **2008,** 195, 140-168.

13. Leone N., Mercurio M., Grilli E., Leone A. P., Langella A., Buondonno A. Potential of vis-NIR reflectance spectroscopy for the mineralogical characterization of synthetic gleys: a preliminary investigation. *Period. di Mineral.,* **2011,** 80, 433-453.

14. Ruiz Cruz M. D. Genesis and evolution of the kaolin-group minerals during the diagenesis and the beginning of metamorphism. *Seminarios SEM,* **2007,** 3, 41-52.

15. Ehlmann B. L., Mustard J. F., Swayze G. A., Clark R. N., Bishop J. L., Poulet F., Des Marais D. J., Roach L. H., Milliken R. E., Wray J. J., Barnouin-Jha O., Murchie S. L. Identification of hydrated silicate minerals on Mars using MRO-CRISM: Geologic context near Nili Fossae and implications for aqueous alteration. *J. Geophys. Res. Planet.,* **2009,** 114, E00D08, 1-33.

16. Mustard J. F., Murchie S. L., Pelkey S. M., Ehlmann B. L., Milliken R. E., Grant J. A., Bibring J. P., Poulet F., Bishop J., Dobrea E. N., Roach L., Seelos F., Arvidson R. E., Wiseman S., Green R., Hash C., Humm D., Malaret E., McGovern J. A., Seelos K., Clancy T., Clark R., Des Marais D., Izenberg N., Knudson A., Langevin Y., Martin T., McGuire P., Morris R., Robinson M., Roush T., Smith M., Swayze G., Taylor H., Titus T., Wolff M. Hydrated silicate minerals on mars observed by the Mars reconnaissance orbiter CRISM instrument. *Nature,* **2008,** 454, 305-309.

17. Bishop J. L., Lane M. D., Dyar M. D., Brown A. J. Reflectance and emission spectroscopy study of four groups of phyllosilicates: smectites, kaolinite-serpentines, chlorites and micas. *Clay Miner.,* **2008,** 43, 35-54.

18. Bridges J. C., Schwenzer S. P., Leveille R., Westall F., Wiens R. C., Mangold N., Bristow T., Edwards P., Berger G. Diagenesis and clay mineral formation at Gale Crater, Mars. *J. Geophys. Res. Planet.,* **2015,** 120, 1-19.

19. Kerr A., Rafuse H., Sparkes G., Hinchey J., Sandeman H. Visible/Infrared spectroscopy as a research tool in economic geology: background and pilot studies from New Fouland and Labrador. *Current Research,* **2011,** Report 11-1, 145-166.

20. Bishop J. L., Englert P. A. J., Patel S., Tirsch D., Roy A. J., Koeberl C., Boettger U., Hanke F., Jaumann R. Mineralogical analyses of surface sediments in the Antarctic Dry Valleys: coordinated analyses of Raman spectra, reflectance spectra and elemental abundances. *Phil. Trans. R. Soc. A,* **2014,** 372, 20140198, 1-26.

21. Huggett J. M. Clay Minerals. In: *Encyclopedia of Geology. Elsevier,* London. **2015,** pp. 358-365.

22. Churchman G. J., Lowe, D. J. Alteration, formation and occurrence of minerals in soils. In: *Handbook of soil science. 2nd edition.* Ed. Huang P. M., Li Y., Sumner M.E. *CRC Press,* Boca Raton, FL. **2012,** pp. 20.1.

23. Viviano-Beck C. E., Moersch J. E., McSween H. Y. Implications for early hydrothermal environments on Mars through the spectral evidence for carbonation and chloritization reactions in the Nili Fossae region. *J. Geophys. Res. Planet.,* **2013,** 118, 1858-1872.

24. Hunziker J. C., Frey M., Clauer N., Dallmeyer R. D., Friedrichsen H., Flehmig W., Hochstrasser K., Roggwiler P., Schwander H. The evolution of illite to muscovite - Mineralogical and isotopic data from the Glarus Alps, Switzerland. *Contrib. Mineral. Petrol.,* **1986,** 92, 157-180.

25. Oneil J. R., Taylor H. P. Oxygen isotope equilibrium between muscovite and water. *J. Geophys. Res.,* **1969,** 74, 6012-6022.

26. Viviano-Beck C. E., Seelos F. P., Murchie S. L., Kahn E. G., Seelos K. D., Taylor H. W., Taylor K., Ehlmann B. L., Wisemann S. M., Mustard J. F., Morgan M. F. Revised CRISM spectral parameters and summary products based on the currently detected mineral diversity on Mars. *J. Geophys. Res. Planet.,* **2014,** 119, 1403-1431.

27. Poulet F., Bibring J. P., Mustard J. F., Gendrin A., Mangold N., Langevin Y., Arvidson R. E., Gondet B., Gomez C., Omega Team. Phyllosilicates on Mars and implications for early Martian climate. *Nature,* **2005,** 438, 623-627.

28. Watanabe T., Funakawa S., Kosaki T. Distribution and formation conditions of gibbsite in the upland soils of humid Asia: Japan, Thailand and Indonesia. *19th World Congress of Soil Science,* **2010,** 17-20.

29. White S. N. Laser Raman spectroscopy as a technique for identification of seafloor hydrothermal and cold seep minerals. *Chem. Geol.,* **2009,** 259, 240-252.

30. Cavalazzi B., Agangi A., Barbieri R., Franchi F., Gasparotto G. The formation of low-temperature sedimentary pyrite and its relationship with biologically-induced processes. *Geol. Ore Deposits,* **2014,** 56, 395-408.

31. Hall A. J. Pyrite-pyrrhotine redox reactions in nature. *Mineral. Mag.,* **1986,** 50, 223-229.

32. Zolotov M. Y., Shock E. L. Formation of jarosite-bearing deposits through aqueous oxidation of pyrite at Meridiani Planum, Mars. *Geophys. Res. Lett.,* **2005,** 32, L21203, 1-5.

33. Gendrin A., Mangold N., Bibring J. P., Langevin Y., Gondet B., Poulet F., Bonello G., Quantin C., Mustard J. F, Arvidson R., LeMouélic S. Sulfates in Martian layered terrains: the OMEGA/Mars Express view. *Science,* **2005,** 307, 1587-1591.

34. Reyes K. I. PhD thesis. *Análisis geológico de la región Oxia Planum en Marte, sitio principal de aterrizaje de la Misión ExoMars 2020.* Universidad Nacional Autónima de México, México, **2016.**

35. Klingelhöfer G., Morris R. V., Bernhardt B., Schröder C., Rodionov D. S., de Souza P. A., Yen A., Gellert R., Evlanov E. N., Zubkov B., Foh J., Bonnes U., Kankeleit E., Gütlich P., Ming D. W., Renz F., Wdowiak T., Squyres S. W., Arvidson R. E. Jarosite and hematite at Meridiani Planum from Opportunity's Mössbauer spectrometer. *Science,* **2004,** 306, 1740-1745.

36. Kaplan H. H., Milliken R. E., Fernandez-Remolar D., Amils R., Robertson K., Knoll A. H. Orbital evidence for clay and acidic sulfate assemblages on Mars based on mineralogical analogs from Río Tinto, Spain. *Icarus,* **2016,** 275, 45-64.

37. Papoulis D., Tsolis-Katagas P., Kalampounias A. G., Tsikouras B. Progressive formation of halloysite from the hydrothermal alteration of biotite and the formation mechanisms of anatase in altered volcanic rocks from Limnos Island, Northeast Aegean Sea, Greece. *Clays Clay Miner.,* **2009,** 57, 566-577.

38. Bakardjieva S., Stengl V., Szatmary L., Subrt J., Lukac J., Murafa N., Niznansky D., Cizek K., Jirkovsky J., Petrova N. Transformation of brookite-type TiO_2 nanocrystals to rutile: correlation between microstructure and photoactivity. *J. Mater. Chem.,* **2006,** 16, 1709-1716.

39. Meinhold G. Rutile and its applications in earth sciences. *Earth Sci. Rev.* **2010,** 102, 1-28.

40. Ruiz-Galende P., Torre-Fdez I., Aramendia J., Gómez-Nubla L., Castro K., Arana G., Madariaga J.M. Formation of titanium oxide (TiO_2) polymorphs in an emerged submarine volcano environment: Implications for Mars. *EPSC.* **2018,** abst. 988.

41. Rampe E. B., Ming D. W., Blake D. F., Bristow T. F., Chipera S. J., Grotzinger J. P., Morris R. V., Morrison S. M., Vaniman D. T., Yen A. S., Achilles C. N., Craig P. I., Des Marais D. J., Downs R. T., Farmer J. D., Fendrich K. V., Gellert R., Hazen R. M., Kah L. C., Morookian J. M., Peretyazhko T. S., Sarrazin P., Treiman A. H., Berger J. A., Eigenbrode J., Fairén A. G., Forni O., Gupta S., Hurowitz J. A., Lanza N. L., Schmidt M. E., Siebach K., Sutter B., Thompson L. M. Mineralogy of an ancient lacustrine mudstone succession from the Murray formation, Gale crater, Mars. *Earth Planet. Sci. Lett.* **2017,** 471, 172-185.

42. Kilias S., Chatzitheodoridis E., Lyon I. Molecular, chemical and morphological evidence for hematite biogenicity at the Quaternary Cape Vani Mn-(Ba-Fe) deposit, Milos, Greece. *B. Geol. Soc. Greece,* **2013,** 47 (2), 834-842.

43. Cornell R. M., Schwertmann U. The iron oxides. Structure, properties, reactions, occurrences and uses. *WILEY-VCH,* Germany. **2003.**

44. Nagano T., Mitamura H., Nakayama S., Nakashima S. Formation of goethite and hematite from neodymium-containing ferrihydrite suspensions. *Clays Clay Miner.,* **1999,** 47, 748-754.

45. Kato Y., Suzuki K., Nakamura K., Hickman A., Nedachi M., Kusakabe M., Bevacqua D. C., Ohmoto H. Hematite formation by oxygenated groundwater more than 2.76 billion years ago. *Earth Planet. Sci. Lett.,* **2009,** 278, 40-49.

46. Klingelhöfer G., DeGrave E., Morris R. V., Van Alboom A., de Resende V. G., De Souza P. A., Rodionov D., Schröder C., Ming D. W., Yen A. Mössbauer spectroscopy on Mars: goethite in the Columbia Hills at Gusev crater. *Hyperfine Interact.,* **2005,** 166, 549-554.

47. Tebo B., Bargar J., Clement B., Dick G., Murray K., Parker D., Verity R., Webb S. Biogenic manganese oxides: Properties and mechanisms of formation. *Annu. Rev. Earth Planet. Sci.,* **2004,** 32, 287-328.

48. Bernardini S., Bellatreccia F., Municchia A. C., Della Ventura G., Sodo A. Raman spectra of natural manganese oxides. *J. Raman Spectrosc.,* **2019,** 50, 873-888.

49. Lanza N. L., Wiens R. C., Arvidson R. E., Clark B. C., Fischer W. W., Gellert R., Grotzinger J. P., Hurowitz J. A., McLennan S. M., Morris R. V., Rice M. S., Bell J. F. I., Berger J. A., Blaney D. L., Bridges N. T., Calef F. I., Campbell J. L., Clegg S. M., Cousin A., Edgett K. S., Fabre C., Fisk M. R., Forni O., Frydenvang J., Hardy K. R., Hardgrove C., Johnson J. R., Lasue J., Le Mouelic S., Malin M. C., Mangold N., Martín-Torres J., Maurice S., McBride M. J., Ming D. W., Newsom H. E., Ollila A. M., Sautter V., Schroder S., Thompson L. M., Treiman A. H., VanBommel S., Vaniman D. T., Zorzano M. Oxidation of manganese in an ancient aquifer, Kimberley formation, Gale crater, Mars. *Geophys. Res. Lett.,* **2016,** 43, 7398-7407.

50. Gómez-Nubla L., Aramendia J., Fdez-Ortiz de Vallejuelo S., Alonso-Olazabal A., Castro K., Cruz Zuluaga M., Angel Ortega L., Murelaga X., Manuel Madariaga J. Multispectroscopic methodology to study Libyan desert glass and its formation conditions. *Anal. Bioanal. Chem.,* **2017,** 409, 3597-3610.

51. Smith M. R., Bandfield J. L. Geology of quartz and hydrated silica-bearing deposits near Antoniadi Crater, Mars. *J. Geophys. Res. Planet.,* **2012,** 117, E06007, 1-24.

52. Fox N., Parbhakar-Fox A., Moltzen J., Feig S., Goemann K., Huntington J. Applications of hyperspectral mineralogy for geoenvironmental characterisation. *Minerals Eng,* **2017,** 107, 63-77.

53. Miura Y. Formation of calcium-carbonates by natural and artificial shock wave impacts: new type formation of carbonates. *LPSC 38.* **2007,** abst. 1277.

54. Boynton W. V., Ming D. W., Kounaves S. P., Young S. M. M., Arvidson R. E., Hecht M. H., Hoffman J., Niles P. B., Hamara D. K., Quinn R. C., Smith P. H., Sutter B., Catling D. C., Morris R. V. Evidence for Calcium Carbonate at the Mars Phoenix Landing Site. *Science,* **2009,** 325, 61-64.

55. Bandfield J. L., Glotch T. D., Christensen P. R. Spectroscopic identification of carbonate minerals in the Martian dust. *Science,* **2003,** 301, 1084-1087.

CHAPTER 7:

ARMINTZA (LEMOIZ)

As in the previous chapter, the geochemical characterization of the Armintza outcrop, proposed as a Martian analogue site, will be described here. This emplacement shows the dichotomy between sedimentary and volcanic rocks (both in the same area), also observed in some areas of Mars. The differences observed in the two types of rocks and the possible interaction between them could help in the understanding of the chemical reactions and weathering mechanisms for the future study of Mars.

In this case, two different rock groups were analysed (see *Chapter 4*) and some differences in the mineralogical composition were observed and are described in this chapter.

In order to determine the elemental composition of the analysed samples, EDXRF was used. Elemental mappings together with semi-quantitative results of some of the samples are shown in Figures 7.1 and 7.2. The first one corresponds to a sample collected in the volcanic area of the emplacement. The second was obtained from the sedimentary area.

The limits in concentrations were the same as those described in the previous chapter (<1% w/w minor elements and >1% w/w major elements) [1]. As in the case of the

Meñakoz samples, the most concentrated elements were in general, Si, Fe and Al (and in some cases Ca).

Figure 7.1 shows that calcium was the most concentrated element and it was supposed to be in the form of carbonates. However, its distribution was only related with phosphorous, which could lead to think that apatite ($Ca_5(PO_4)_3(F,Cl,OH)$) could be present, as in the case of Meñakoz. Silicon and aluminium were intimately related and homogenously distributed. These elements were also correlated with magnesium and potassium in some areas, suggests the presence of silicates (kaolinite ($Al_2Si_2O_5(OH)_4$) and chlorites ($(Mg,Al,Fe)_6(Al,Si)_4O_{10}(OH)_8$), respectively). Iron was also homogeneously distributed and it exhibited higher concentrations in specific areas (iron hot spots). It could form part of the silicates or could be in form of oxides. Sodium was distributed throughout the entire surface with some hot spots and it was related with the presence of feldspars (see below). The rest of the elements were detected in specific areas. Titanium and manganese were expected to be in the form of oxides and sulfur in form of sulfides or sulfates.
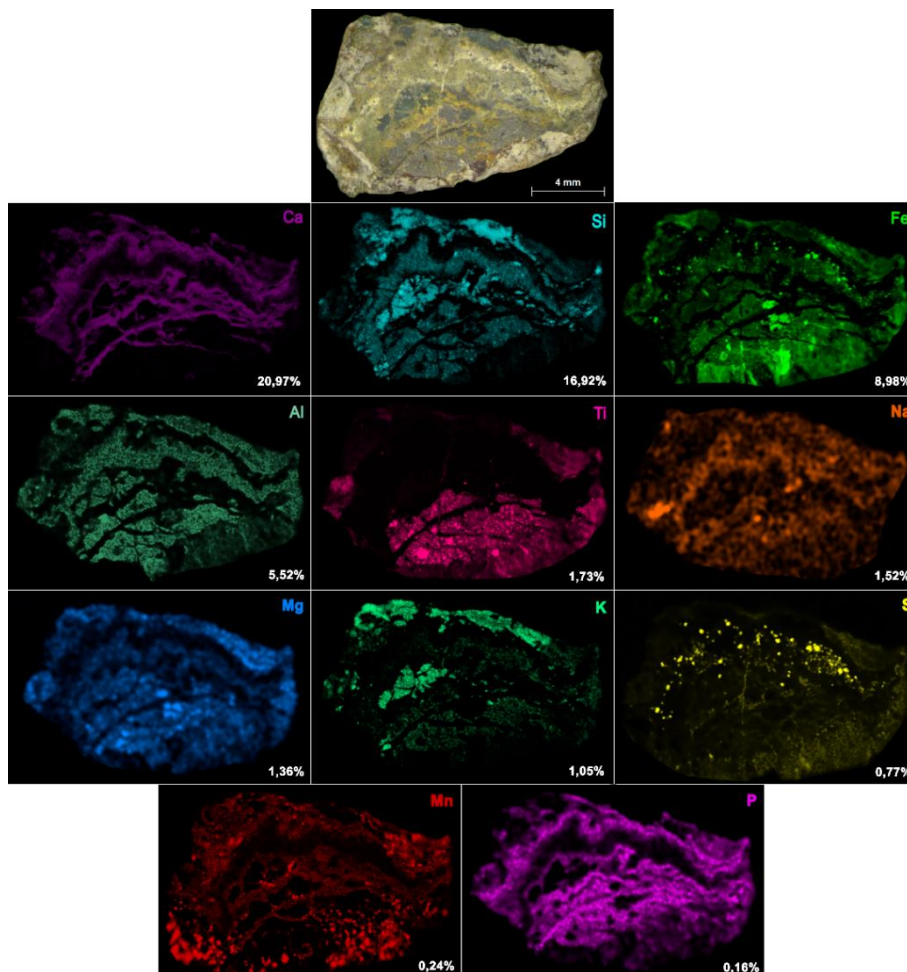
Figure 7.1. EDXRF mapping with the elemental distribution in a sample from the volcanic area in the Armintza outcrop

In Figure 7.2 it is clear that more elements were detected and their distribution was a little bit different. In this case calcium was not a major element. It was associated again with the presence of carbonates but, taking into account the Raman results (see below), it makes sense that its proportion in this type of samples were lower. Moreover, in this case, the distribution of almost all the elements was more or less homogeneous. Si, Al, K, Na and Mg were supposed to be related with the presence of silicates. Iron was not directly related with silicon and aluminium, which leads to the conclusion that the most probable form for this element in this example were in oxide minerals. Titanium and manganese were distributed along the entire surface in localized areas, and they were associated with the presence of oxides. Strontium was a common element in the analysed rocks and in most of the cases appeared related with Ca, as it were an impurity of the calcium carbonate. The rest of the elements, such as Zn, Cr and Ni, were in very low concentration and therefore it was not expected to find minerals with them in their structure.
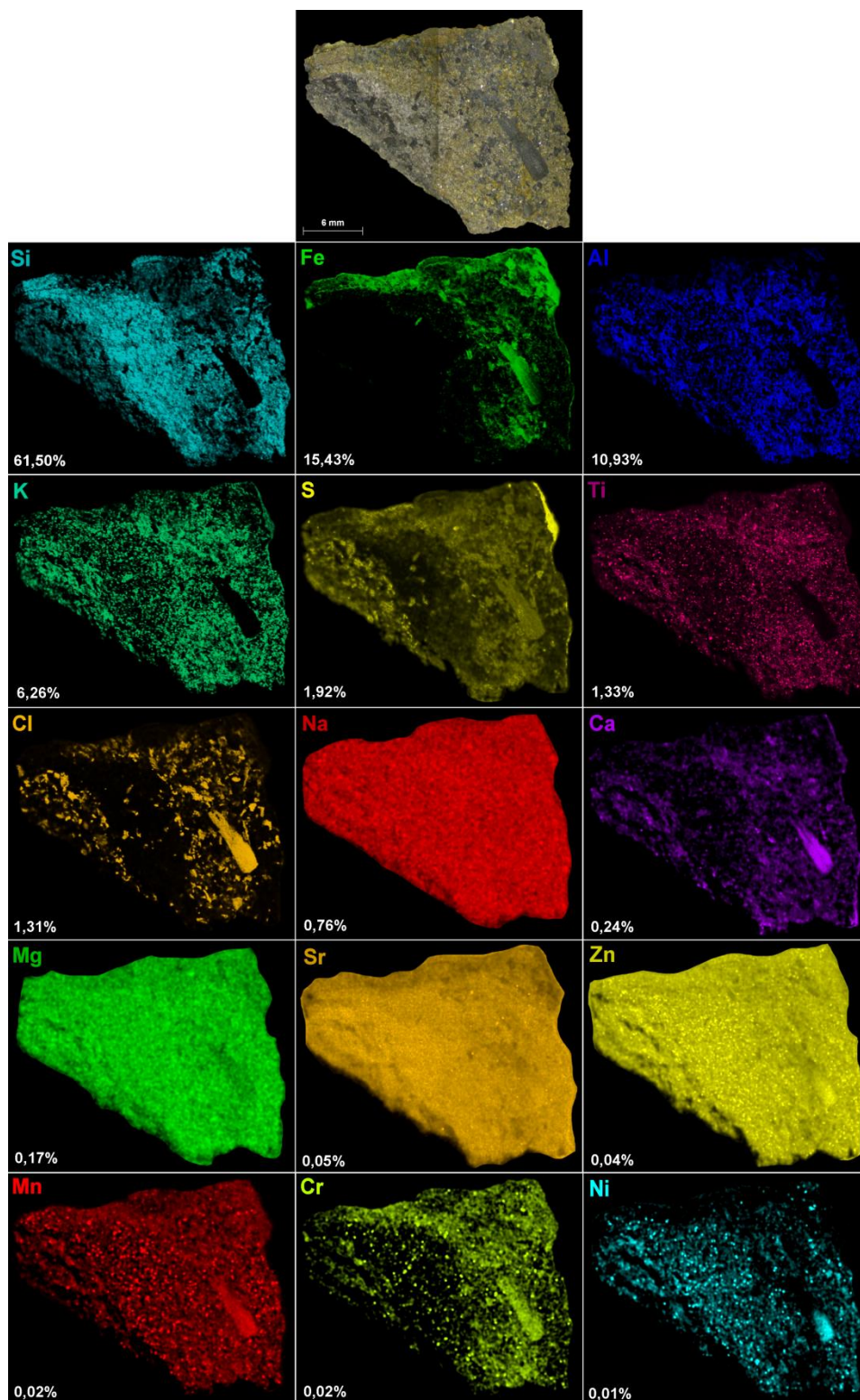
Figure 7.2. EDXRF mapping with the elemental distribution in a sample from the sedimentary area in the Armintza outcrop

According to the XRD analyses, the most abundant compounds were calcite ($CaCO_3$), quartz (SiO_2) and phyllosilicates (plagioclases, chlorites and micas). Detailed analysis of the last group suggests the specific presence of anorthite ($CaAl_2Si_2O_8$), clinochlore ($Mg_5Al(Si_3Al)O_{10}(OH)_8$) and muscovite ($KAl_2(AlSi_3O_{10})(OH)_2$) respectively. Moreover, in

some of the samples the presence of carbonates such as dolomite ($CaMg(CO_3)_2$), ankerite ($CaFe^{2+}(CO_3)_2$) and siderite ($FeCO_3$) could also be confirmed. Pyrite (Fe_2S) and iron oxides such as hematite (Fe_2O_3) and goethite (α-$FeOOH$) were also identified in the analysed samples. All these results are in agreement with the elemental analyses, as the described minerals contain the elements with the highest concentrations according to the EDXRF analyses.

Raman and VNIR measurements were able to determine the specific phyllosilicates that were present in the samples, and therefore, complete (and complement) the information obtained by XRD measurements.

In the area of the pillow lavas, silicates were the most expected minerals as was the case of Meñakoz. The first example is the plagioclase albite ($NaAlSi_3O_8$), which was identified by means of Raman spectroscopy (Figure 7.3.a) and whose bands are located at 290 (vw), 480 (w) and 508 (m) cm^{-1}. Taking into account that by means of XRD the identified plagioclase was anorthite (that of calcium), the albitization process described by Haldar [2] can be observed. Comparing with Mars, and specificaly with Oxia Plamun, since it is the selected landing site of the next ESA's mission, this type of minerals could be present in the western part of the mentioned area. The volcanic origin of the plagioclases is comparable to the Amazonian volcanic deposits observed there [3]. In this spectrum (Figure 7.3.a), a band at 964 cm^{-1} was observed and would be consistent with the presence of apatite ($Ca_5(PO_4)_3$), as suggested by EDXRF analysis. This band was weak, and it means that the concentration of this mineral is low, which was supported by the low concentration of phosphorous observed in the elemental analyses.

Phyllosilicates, which were also detected in Meñakoz, represent a very important group of minerals for the study of Martian history, since as has been explained before, they require the presence of water for their formation. Some of them, such as kaolinite and dickite (both with the $Al_2Si_2O_5(OH)_4$ chemical formula) were identified by means of VNIR, as can be seen in Figure 7.3.b and c. The spectra exhibit two characteristic doublets, one at 1399 and 1414 nm for kaolinite due to the OH overtone (1383 and 1414 nm for the dickite), and the other one at 2161 and 2205 nm in the case of kaolinite, and at 2179 and 2205 nm in the case of dickite, which are due to the vibration of the Al-OH overtone. Moreover, in the case of dickite, three bands can be observed at 2305, 2353 and 2383 nm, which are also characteristic of these minerals.

Kaolinite and dickite are two polymorphs from the kaolinite-serpentine group [4]. The difference between these two polymorphs is the crystallization system, being triclinic for the kaolinite and monoclinic for the dickite. This last mineral is thought to be of hydrothermal origin and it seems that temperature is not the only factor controlling its formation [5]. Comparing with Oxia Planum, these types of minerals might be present in the east part of Oxia Planum since Al-rich phyllosilicates are thought to be present there [6]. These minerals have been identified, among others, in Nili Fossae on Mars as reported by Ehlmann et al. [7].
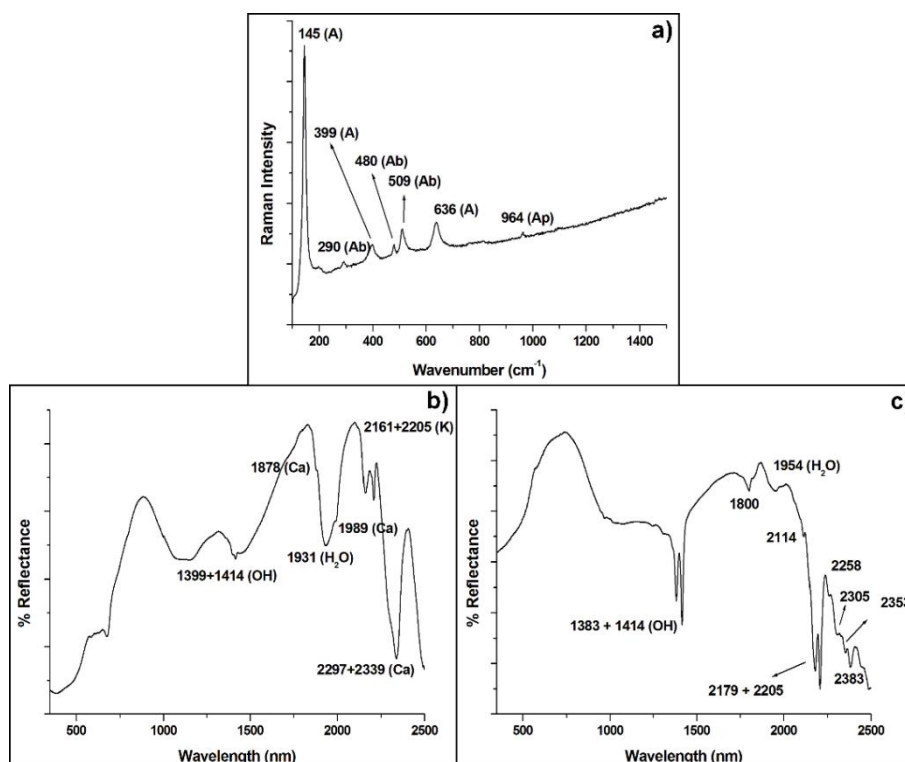
Figure 7.3. a) Raman spectrum of albite (Ab) together with anatase (A) and apatite (Ap), and VNIR spectra of **b)** kaolinite (K) together with calcite (Ca) and **c)** dickite

In addition, some micas and chlorites were identified in the samples from the volcanic area (pillow lavas) by Raman and VNIR spectroscopies. They were illite $((K,H_3O)(Al,Mg,Fe)_2(Si,Al)_4O_{10})$, muscovite $(KAl_2(AlSi_3O_{10})(OH)_2)$, chamosite $(Fe_5Al(Si_3Al)O_{10}(OH)_8)$ and clinochlore $(Mg_5Al(Si_3Al)O_{10}(OH)_8)$, whose spectra are shown in Figure 7.4.

In the VNIR spectrum (Figure 7.4.a), bands corresponding to the OH overtone (1411 nm) and the combination bands of the water (a doublet at 1912 and 1961 nm) can be observed. Furthermore, bands consistent with the presence of different clay minerals were detected. The band at 2209 nm could be due to the presence of illite or muscovite. The one at 2258 nm is a characteristic band of chlorites (chamosite or clinochlore). Finally, the band at 2349 nm could belong to all of them. In Figure 7.4.b, Raman bands of different chlorites were observed at 192 (w) cm^{-1} for the chamosite and bands at 543 (m) and 676 (s) cm^{-1}are due to clinochlore. Finally in Figure 7.4.c, the spectrum of muscovite can be observed with its Raman bands at 191 (m), 264 (s), 369 and 406 (w) and 705 (s) cm^{-1}. These Raman spectra indicate that the bands that could belong to illite or muscovite in the VNIR spectrum actually belong to the latter.

These minerals are very important in the context of Martian exploration for two reasons; they are among the most abundant compounds found on Mars, as orbiters and meteorite studies suggest, and they need the presence of water for their formation. This fact is key to demonstrating the potential habitability of Mars, which is one of the main objectives of the upcoming missions to Mars.
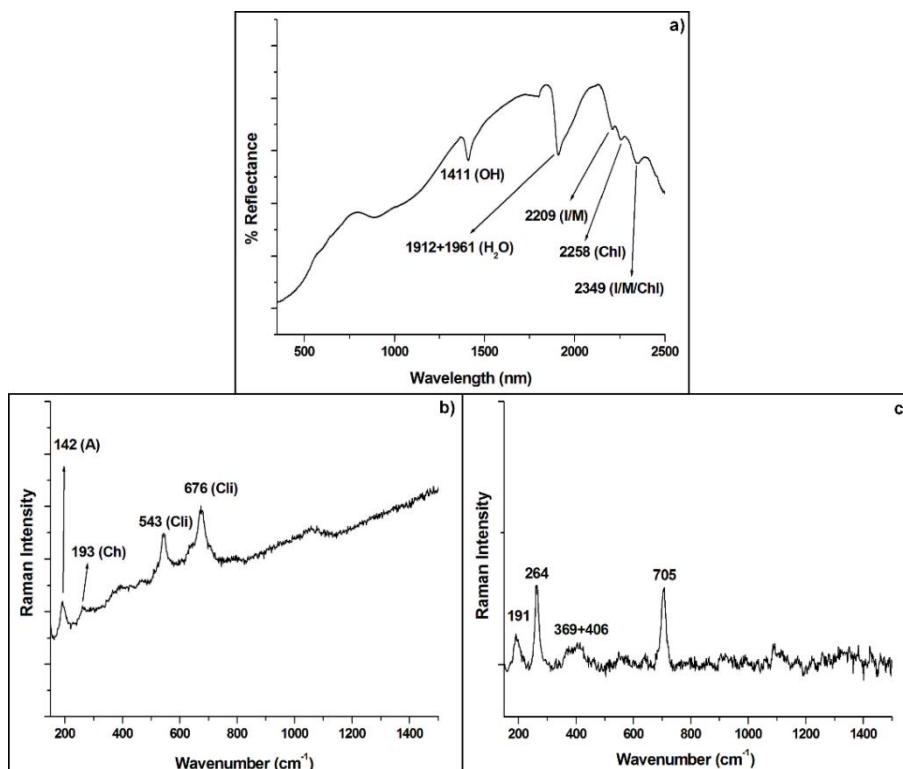
Figure 7.4. a) VNIR spectrum with bands consistent with the presence of illite (I), muscovite (M) and chlorites (Chl), Raman spectra of **b)** chamosite (Ch) and clinochlore (Cli) together with anatase (A) and **c)** muscovite

Apart from silicates, other minerals were identified in the volcanic samples. Carbonates (Figure 7.5) were detected by Raman and VNIR spectroscopies and appeared in the form of veins and bubbles in the volcanic samples (as in Meñakoz). However, calcite and ankerite were also found in the samples from the sedimentary area but in a lower concentrations.

The most abundant carbonates were dolomite ($CaMg(CO_3)_2$) and calcite ($CaCO_3$). It was also possible to identify aragonite, which is a polymorph of calcite. Dolomite Raman bands (Figure 7.5.a) appear at 174 (w), 294 (m), 723 (vw) and 1095 (vs) cm^{-1}, calcite bands (Figure 7.5.b) at 157 (vw), 283 (w) and 1089 (vs) cm^{-1}, and those of aragonite (Figure 7.5.c) appear at 154 (m), 208 (w), 705 (w) and 1085 (s) with two doublets, one at 1202 (w) and 1235 (w) and another one at 1304 (m) and 1329 (m) cm^{-1}. Besides, ankerite ($CaFe^{2+}(CO_3)_2$, Figure 7.5.d) was identified by VNIR spectroscopy, together with calcite, as can be seen in the spectrum in Figure 7.5.b. A doublet at 1040 and 1309 nm that forms a very wide band related with the presence of iron in the structure of this mineral, characterizes the spectrum of ankerite. The combination band of the water appears at 1940 nm and the doublet of the carbonate group at 2283 and 2327 nm.
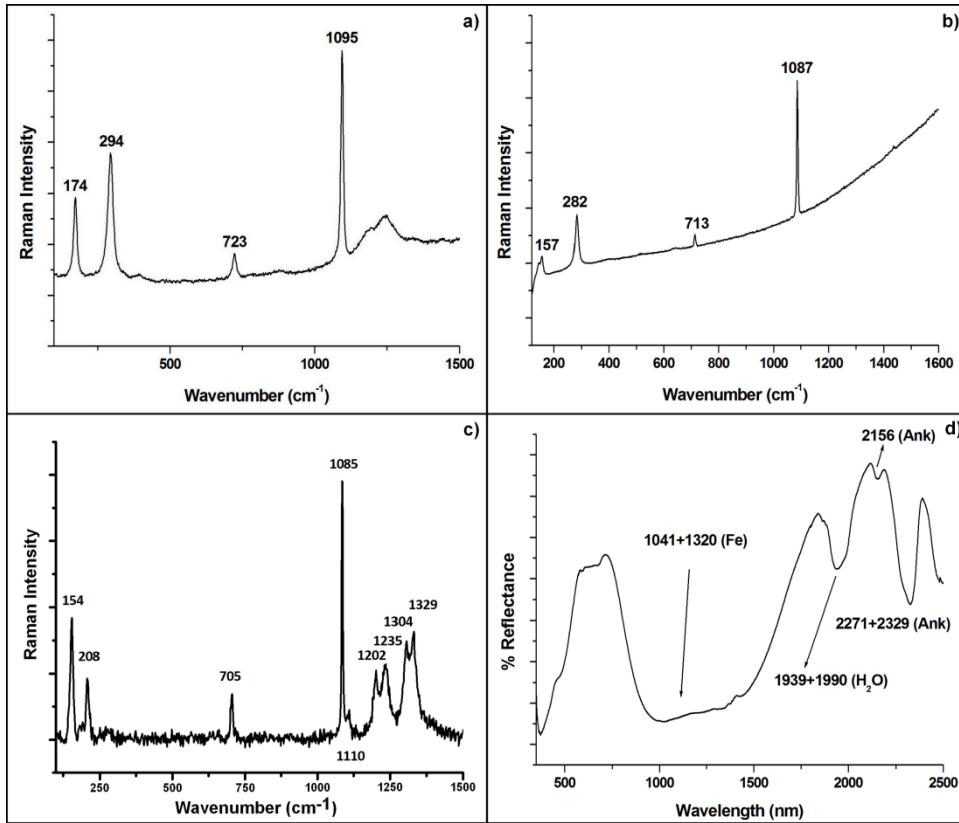
Figure 7.5. Raman spectra of **a)** dolomite, **b)** calcite, **c)** aragonite and **d)** VNIR spectrum of ankerite

As these minerals can have different possible origins, their presence in the samples from volcanic areas as well as in the sedimentary ones, is unsurprising. The origin of these compounds may be the same as was identified for Meñakoz as they appear in similar disposition (veins and bubbles). Regarding these minerals, some visual similarities were observed between the Armintza outcrop and the Martian surface. In Figure 7.6, two images from Armintza (top) and Mars (bottom) are shown and the same structure can be observed in both. Knowing that in Armintza those veins are made of carbonates (calcite among all), it could be suggested that these features observed on Mars could also contain carbonates.

Figure 7.6. Comparative image of veins observed in Armintza (top) and Mars (bottom)

Pyrite (FeS_2) is also a signature of the igneous past of the studied location. The Raman bands (Figure 7.7.a) of this sulfide are located at 343 (m) and 379 (s) cm^{-1} and, as can be seen in the figure, sometimes it appears together with marcasite (band at 324 cm^{-1}), which is a polymorph of the pyrite.

In addition, some sulfates were identified using Raman spectroscopy such as jarosite ($Fe_6(SO_4)_4(OH)_{12}$) and barite ($BaSO_4$). Jarosite Raman bands (Figure 7.7.b) are located at 139 (m), 224 (s), 297 (w), 361 (vw), 439 (s), 453 (w), 566 (w), 623 (m), 1009 (s), 1106 (s) and 1154 (w) cm^{-1}. Barite has Raman bands at 147 (w), 462 (m) and 988 (s) cm^{-1} (Figure 7.7.c).

As in the case of carbonates, pyrite was identified in both volcanic and sedimentary areas of Armintza, and therefore, this mineral could have had different formation mechanisms in each environment.

The sulfate compounds were only identified in the samples collected from the pillow lavas, which would be consistent with the hydrothermal processes, or the oxidation of the sulfides such as pyrite. However, ferric sulfates like jarosite were also detected in the sedimentary rocks of Armintza, as occurs in Río Tinto [8]. Other sulfates could originate from evaporation of standing bodies of water, and they could be formed at depths in the

presence of sulfur-rich fluids in hydrothermal contexts [9]. In igneous rocks, two mechanisms are possible; oxidation of primary sulfide in silicate magma (the most probable way due to the volcanic origin of the location), and hydrolysis of SO_2 gas in aqueous fluids [10].
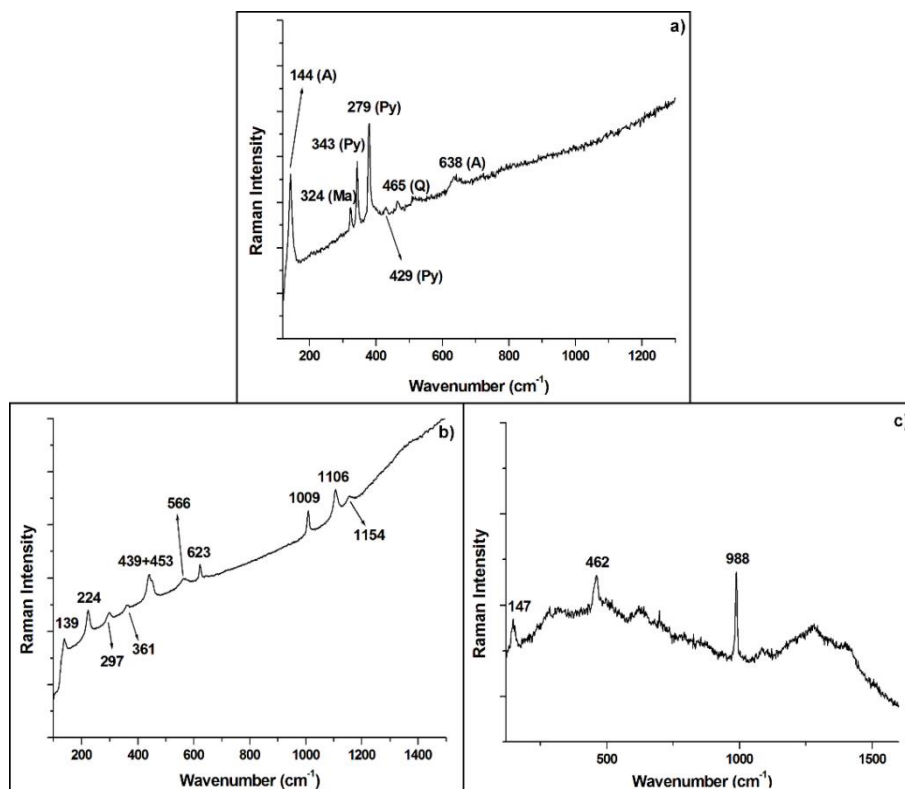

Figure 7.7. Raman spectra of **a)** pyrite (Py) tgether with marcasite (Ma), anatase (A) and quartz (Q), **b)** jarosite and **c)** barite

Oxides were also identified by means of Raman spectroscopy, such as titanium oxides (anatase, rutile and brookite) and iron oxides (hematite and goethite).

Anatase Raman bands are located at 145 (s), 396 (w), 513 (w) and 637 (w) cm^{-1}, those of rutile at 449 (m) and 609 (m) cm^{-1} and the bands of brookite at 153 (s), 214 (vw), 247 (w), 286 (vw), 324 (w), 367 (w), 414 (vw), 501 (vw), 548 (w) and 638 (w) cm^{-1}. The Raman bands of the iron oxides are located at 296 (m) and 392 (m) cm^{-1} for the goethite (α-FeOOH), and 222 (m), 286 (s), 406 (m) and 609 (w) cm^{-1} for the hematite (Fe_2O_3).

Anatase was found both in volcanic and sedimentary samples, since it is the most stable one. However, rutile was only found in volcanic samples and brookite only in the sedimentary samples. This fact supports the origin conclussions of the different polymorphs that was explained in Chapter 6 [11]. The iron oxides were found in both volcanic and sedimentary areas of the Armintza samples. The observed spectra were the same as in the Meñakoz outcrop.

7.1. Conclusions

The study of the mineralogy of sedimentary and volcanic rocks is of high importance for the exploration of Mars. For instance, Oxia Planum and its dichotomy of early Hesperian sedimentary deposits and Amazonian volcanic rocks make the knowledge about similar types of terrestrial rocks interesting and relevant to the next planetary missions like ExoMars 2022.

Using wide range spectroscopic techniques, the mineralogical characterization of the samples obtained from the Armintza outcrop was performed. Minerals like feldspars and phyllosilicates are readily identified by means of the mentioned techniques and it is very relevant for the Martian analyses since they are compounds that need the presence of water for their formation. This is also the case of carbonates and sulfates. In these cases, it was possible to discern between, for example, calcite and dolomite, being this fact important for the knowledge of the Martian surface. Carbonates have become minerals of high interest for Martian exploration (see *Chapter 1* and *5*) and Armintza is the only studied emplacement in this PhD work where other carbonates apart from calcite could be identified.

The identification of weathering products (such as iron oxides) may help to establish the conditions and the processes that could have happened on Mars.

In this sense, Armintza seems to be a promising Martian analogue since it has the same dichotomy observed in Oxia Planum, and the identified minerals are consistent with those expected on this region of Mars. With this study, the most probable origin of the minerals found could be established and, therefore, it confirms the suitability of Armintza as a Martian analogue, and particularly for Oxia Planum.

7.2. Bibliography

1. Namieśnik J. Trace Analysis — Challenges and Problems. *Crit. Rev. Anal. Chem.,* **2002,** 32, 271-300.

2. Haldar S. K., Tišljar J. Chapter 4 - Igneous rocks. In: *Introduction to mineralogy and petrology.* Eds. Haldar S. K., Tišljar J. *Elsevier,* Oxford. **2014,** pp. 93-120.

3. Pajola M., Rossato S., Baratti E., Pozzobon R., Quantin C., Carter J., Thollot P. Boulder abundances and size-frequency distributions on Oxia Planum-Mars: Scientific implications for the 2020 ESA ExoMars rover. *Icarus,* **2017,** 296, 73-90.

4. Zotov A., Mukhamet-Galeev A., Schott J. An experimental study of kaolinite and dickite relative stability at 150-300 ºC and the thermodynamic properties of dickite. *Am. Mineral.,* **1998,** 83, 516-524.

5. Chen P. Y., Wang M. K., Yang D. S. Mineralogy of dickite and nacrite from northern Taiwan. *Clays Clay Miner.,* **2001,** 49, 586-595.

6. Vago J. L., Westall F., Coates A. J., Jaumann R., Korablev O., Ciarletti V., Mitrofanov I., Josset J. L., De Sanctis M. C., Bibring J. P., Rull F., Goesmann F., Steininger H.,

Goetz W., Brinckerhoff W., Szopa C., Raulin F., Westall F., Edwards H. G. M., Whyte L. G., Fairen A. G., Bridges J., Hauber E., Ori G. G., Werner S., Loizeau D., Kuzmin R. O., Williams R. M. E., Flahaut J., Forget F., Rodionov D., Svedhem H., Sefton-Nash E., Kminek G., Lorenzoni L., Joudrier L., Mikhailov V., Zashchirinskiy A., Alexashkin S., Calantropio F., Merlo A., Poulakis P., Witasse O., Bayle O., Bayon S., Meierhenrich U., Carter J., García-Ruiz J. M., Baglioni P., Haldemann A., Ball A. J., Debus A., Lindner R., Haessig F., Monteiro D., Trautner R., Voland C., Rebeyre P., Goulty D., Didot F., Durrant S., Zekri E., Koschny D., Toni A., Visentin G., Zwick M., van Winnendael M., Azkarate M., Carreau C., Pasteur Instrument Teams, Landing Site Selection Working, ExoMars Project Team. Habitability on early Mars and the search for biosignatures with the ExoMars rover. *Astrobiology,* **2017,** 17, 471-510.

7. Ehlmann B. L., Mustard J. F., Swayze G. A., Clark R. N., Bishop J. L., Poulet F., Des Marais D. J., Roach L. H., Milliken R. E., Wray J. J., Barnouin-Jha O., Murchie S. L. Identification of hydrated silicate minerals on Mars using MRO-CRISM: Geologic context near Nili Fossae and implications for aqueous alteration. *J. Geophys. Res. Planet.,* **2009,** 114, E00D08, 1-33.

8. Fernández-Remolar D. C., Morris R. V., Gruener J. E., Amils R., Knoll A. H. The Río Tinto basin, Spain: Mineralogy, sedimentary geobiology, and implications for interpretation of outcrop rocks at Meridiani Planum, Mars. *Earth Planet. Sci. Lett.,* **2005,** 240, 149-167.

9. Gendrin A., Mangold N., Bibring J. P., Langevin Y., Gondet B., Poulet F., Bonello G., Quantin C., Mustard J., Arvidson R., LeMouélic S. Sulfates in Martian layered terrains: the OMEGA/Mars Express view. *Science,* **2005,** 307, 1587-1591.

10. Hattori K., Cameron E. M. Archean magmatic sulfate. *Nature,* **1986,** 319, 45-47.

11. Ruiz-Galende P., Torre-Fdez I., Aramendia J., Gómez-Nubla L., Castro K., Arana G., Madariaga J.M. Formation of titanium oxide (TiO_2) polymorphs in an emerged submarine volcano environment: Implications for Mars. *EPSC.* **2018,** abst. 988.

CHAPTER 8: ENEKURI (ERANDIO) and FRUIZ (URIBE-BUTROE)

In this chapter, the geochemical characterization of two other emplacements located in the Basque Cantabrian Basin is presented: Enekuri and Fruiz. However, in this case, these outcrops are not in contact with the sea-water nowadays. In fact, they are in the inland part of the basin and belong to the Iberian and European plate respectively. In the case of Enekuri, it is the only analysed outcrop in this PhD work that belongs to the Iberian plate.

Since the environment in which these outcrops are located differs from that of the previous emplacements (Meñakoz and Armintza), it was supposed that the weathering processes observed would be different, and therefore, the mineralogical composition might be also different. Moreover, some differences were expected between Enekuri and Fruiz due to the different plate in which they are located and the different geological formation of the outcrop (pillow lava and columnar disjunction respectively).

Elemental characterization was peformed using EDXRF. In Figures 8.1 and 8.2 for Enekuri, and Figures 8.3 and 8.4 for Fruiz, the elemental composition of some of the analysed samples from these emplacements is shown.

In general terms, the composition of all the analysed samples was similar. The elements under 1% w/w were considered minor elements and those that were over 1 % w/w were the major elements[1] and the most interesting ones for the molecular characterization. As in the previous cases, the most concentrated elements were in general, Ca, Si, Fe, Al and Mg, which is in concordance with the molecular characterization as will be described below.

In Figure 8.1, one example of the Enekuri samples is shown. As can be seen, Si, Al and K were the most homogeneously distributed elements, which leads to think in the presence of silicates as the most common minerals. Ca, Mn and Sr were the elements found in the white areas. Calcium was supposed to be in the form of carbonate and manganese in the form of oxides. In the case of Sr, it appeared as an impurity of the calcium carbonate and for that reason they were closely related in all the analysed samples. Fe, Al, Mg, Ti, V and Co were detected in the same regions of a specific area of the sample. Thanks to the Raman analyses (see below) chlorites and oxides were identified in those areas. Sulfur was found in very localised points and, as in the other emplacements, is related to the presence of sulfides or sulfates.
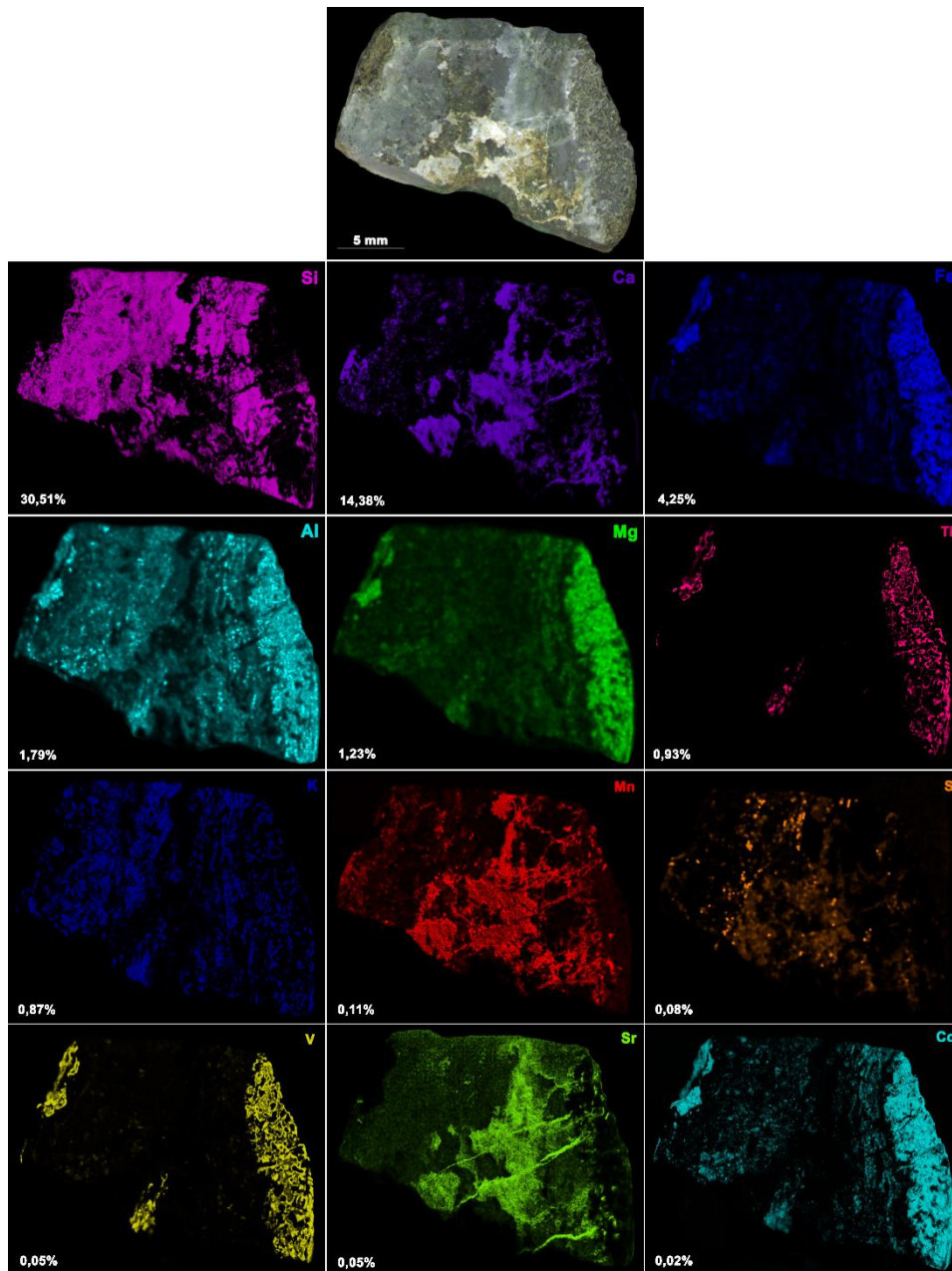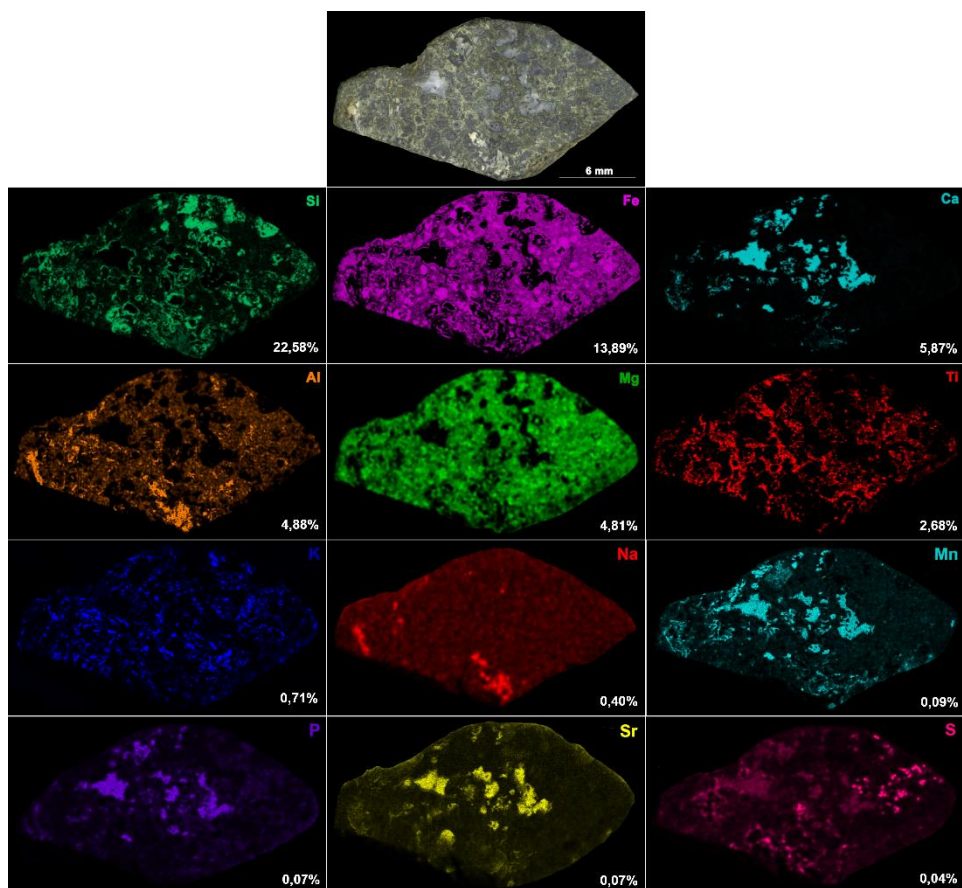
Figure 8.1. EDXRF mapping with the elemental distribution in one sample from the Enekuri outcrop

In Figure 8.2 another example of the analysed samples from Enekuri can be seen. The elements distribution was more or less the same as in the previous example. The only difference was the presence of sodium, which was related to aluminium, probably due to the presence of some silicates, and the presence of phosphorous, which was in the same areas as calcium, and it could be due to the presence of apatite $(Ca_5(PO_4)_3(F,Cl,OH))$ in very low concentrations.

Figure 8.2. EDXRF mapping with the elemental distribution in one sample from the Enekuri outcrop

In Figure 8.3 one example of the Fruiz samples is shown. A homogeneous distribution can be seen in almost all the displayed elements. Si, Al, Fe, Ca, Mg and Na were the most concentrated ones. All of them were supposed to be related to the presence of silicates or carbonates. The minor and trace elements were explained as in the previous cases, except in the case of chromium, which was also identified in Meñakoz. It appeared in very localized areas. However, taking into account its minor concentration, it was not possible to detect any mineral with this element by the other techniques.
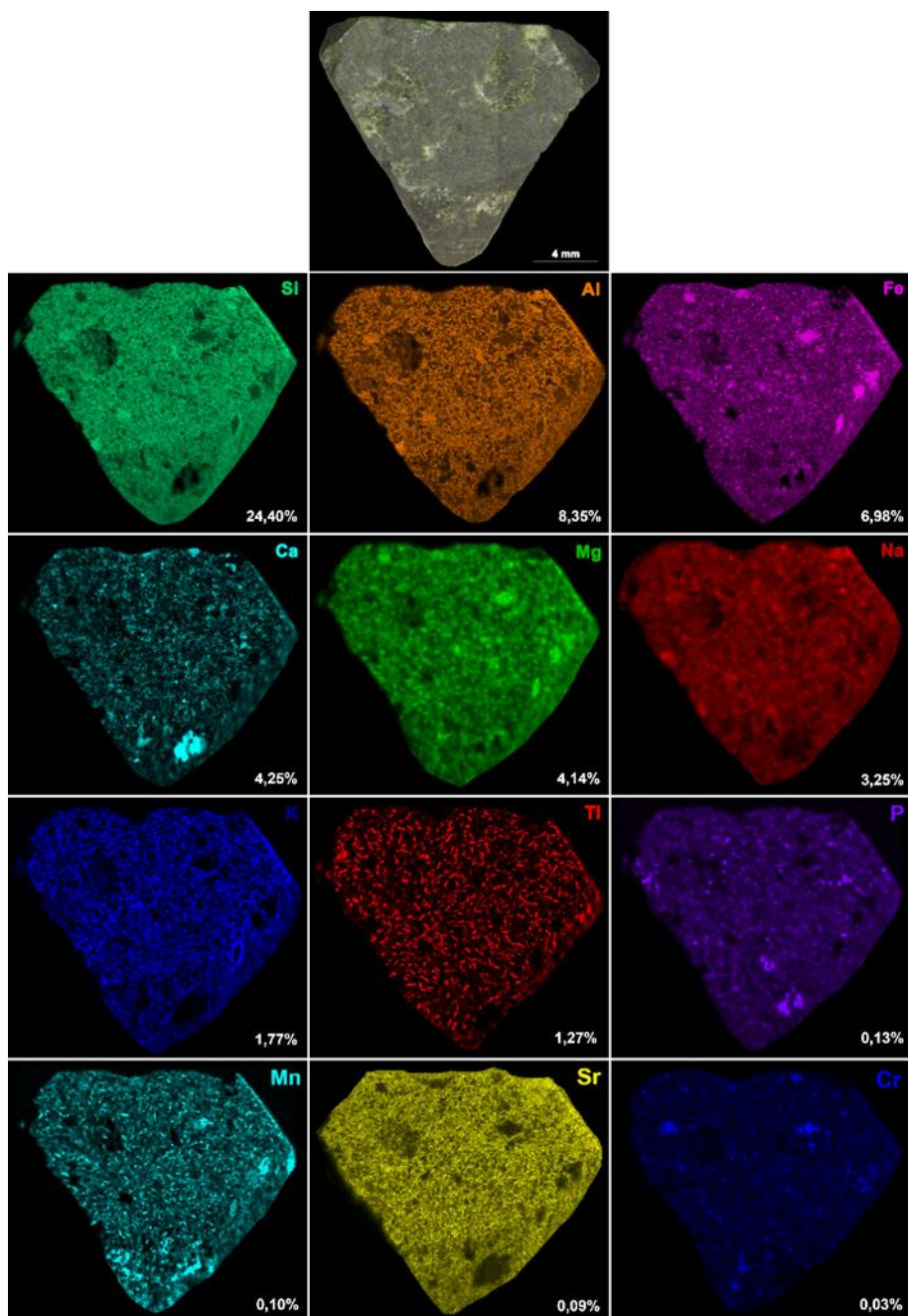
Figure 8.3. EDXRF mapping with the elemental distribution in one sample from the Fruiz outcrop

In the following example (Figure 8.4), the result was very similar to that observed in the previous one and the elements were homogeneously distributed. However, in this case, calcium appeared in most localized areas as well as sulfur, which did not appear in Figure 8.3, and it was also located as hot spots in specific areas. As in the previous cases, these elements were likely related with the presence of carbonates and sulfides/sulfates respectively.
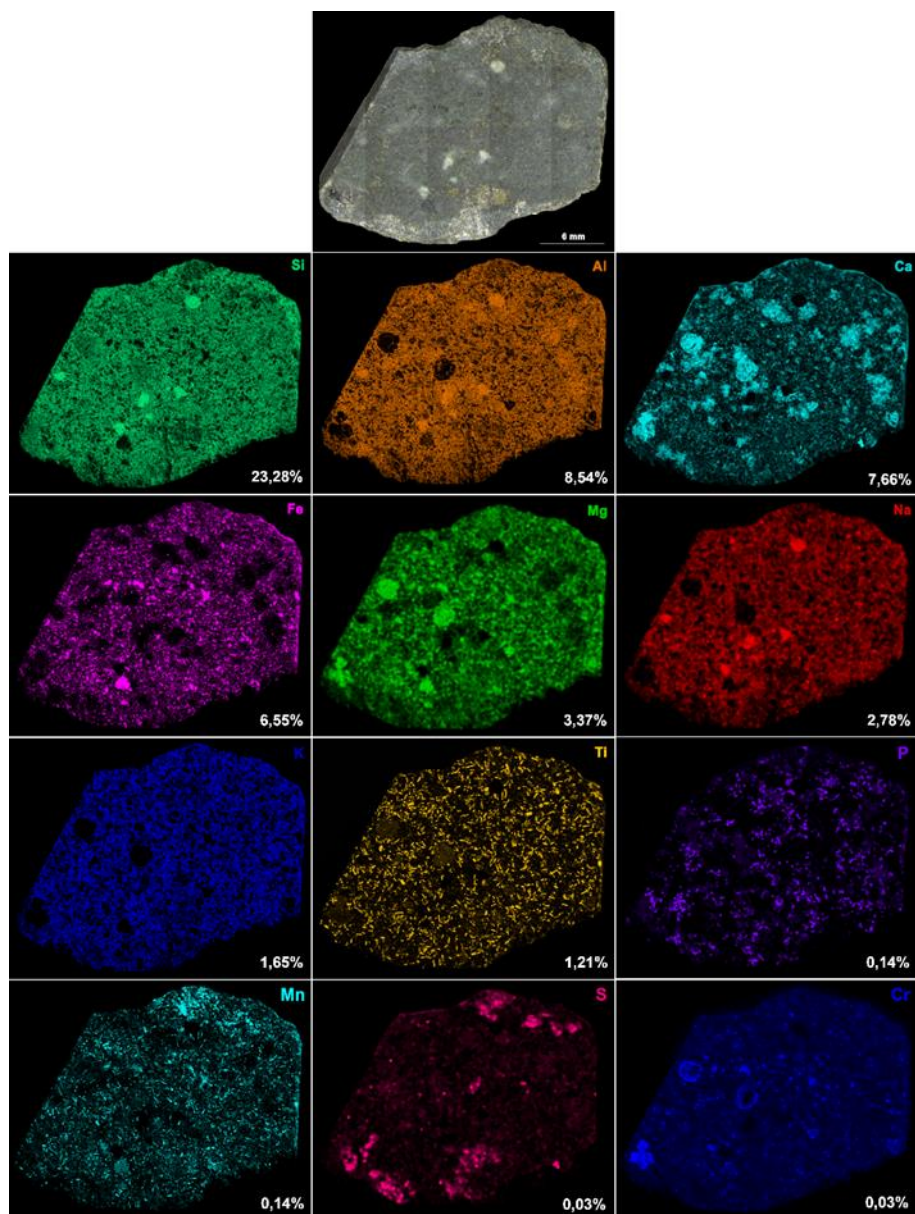
Figure 8.4. EDXRF mapping with the elemental distribution in one sample from the Fruiz outcrop

As in the other emplacements, the molecular characterization began with XRD analyses.

In Enekuri the most found minerals were quartz and calcite (present in all the measured samples). Other oxides such as anatase, and carbonates, such as dolomite and ankerite, were detected in lower proportions.

Regarding the silicates, the most recurrent ones were micas and plagioclases and the results suggested clinochlore ($Mg_5Al(Si_3Al)O_{10}(OH)_8$) and anorthite ($CaAl_2Si_2O_8$), respectively. In some samples, peaks related with the presence of sanidine (($(K,Na)(Si,Al)_4O_8$), muscovite ($KAl_2(AlSi_3O_{10})(OH)_2$), laumontite ($CaAl_2Si_4O_{12}·4H_2O$), and wairakite ($CaAl_2Si_4O_{12}·2H_2O$) were found. The latest two belong to the group of the zeolites, which are commonly related to hydrothermal processes that could have occured in this emplacement. Zeolites, also observed on Mars by TES [2] and CRISM [3], easily incorporate a large amount of volatiles, therefore, their existence on Mars could have

important implications for the explanation of the geological history [4], because they could be an important sink for a variety of Martian volatiles. The identification of these compounds is in agreement with the elemental information obtained by EDXRF for most of the elements.

According to the XRD analyses for Fruiz samples, albite ($NaAlSi_3O_8$), clinochlore, diopside ($CaMgSi_2O_6$) and sanidine were the minerals found in all the samples but in very low concentrations. In addition, in some of the samples quartz was also identified.

In order to complete the molecular characterization and since they are the techniques implemented in the Martian missions, Raman and VNIR spectroscopies were performed.

As in Meñakoz and Armintza, the Na-feldspar, albite ($NaAlSi_3O_8$), was identified thanks to its Raman bands at 293 (w), 480 (s) and 510 (s) cm^{-1} (Figure 8.5.a), both in Enekuri and Fruiz. Taking into account the study made by Freeman et al. [5] these Raman bands correspond to a low ordered albite. This finding leads to conclusion that the same submarine volcanic is the origin of all the analysed outcrops.

Moreover, minerals of the pyroxene group could be identified for the first time in the considered and studied emplacements in this work. Concretely, clinopyroxenes such as diopside ($CaMgSi_2O_6$, Figure 8.5.b) were identified thanks to its Raman bands at 326 (m), 360 (w), 392 (m), 666 (s), 860 (w), 1008 (s) and 1158 (w) cm^{-1}. This spectrum is very similar to that of the augite (($Ca,Mg,Fe)_2(Si, Al)_2O_6$), and therefore, it is difficult to differentiate between them. They are rock-forming ferromagnesian silicates that occur as stable phases in almost every type of igneous rocks. They belong to the inosilicate minerals and, depending on the crystallization system, they are divided into orthopyroxenes and clinopyroxenes [6]. Moreover, in nature, pyroxenes are often mixtures, which make the differentiation between them even more difficult. Geochemically, the augite series is the most important and its members are the most important constituents of igneous rocks [7]. Pyroxenes on Mars are present along its entire surface. For example, Bandfield et al. [8] demonstrated their presence in Syrtus Major and Achilles et al. [9] demonstrate the existence of this type of minerals in Gale Crater.

Titanite ($CaTiSiO_5$) is a nesosilicate identified by Raman spectroscopy with its bands: 165 (w), 258 (m), 314 and 340 (m), 429 (w), 471 (m), 510 (w), 550 (w), 613 (s), 863 (w) and 914 (w) cm^{-1} (Figure 8.5.c). Natural titanite occurs in igneous and metamorphic rocks and the incorporation of trace elements such as U, Th or rare earth elements is very common [10]. It is an example of an accessory mineral, which could provide insight into the trace-element composition of the rock and, therefore, it helps to address questions about the formation of silicic plutonic and volcanic rocks and how they are related [11]. Titanite is not reported to be present on Mars, but on Earth evidences for microbial alteration in subaqueous volcanic rocks have been reported, where titanite is one of the phases that help in the preservation of bioalteration textures generated by that microbial alteration [12].
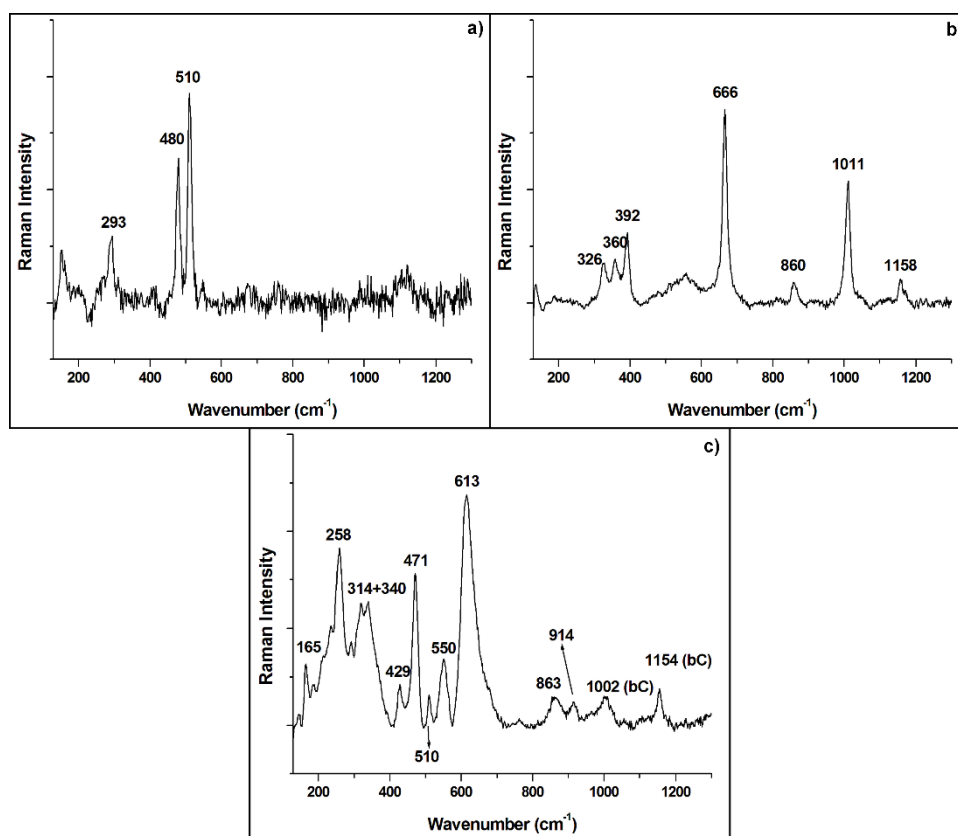
Figure 8.5. Raman spectra of **a)** albite, **b)** diopside and **c)** titanite together with β-carotenes (bC) found in Enekuri and Fruiz samples

In this emplacement, among the most found weathering products there were chlorites ($(Fe,Mg)_5Al(Si_3Al)O_{10}(OH)_6$), concretely, chamosite (Fe-rich chlorite) and clinochlore (Mg-rich chlorite), as was the case in Meñakoz and Armintza. The Raman bands related to the presence of chamosite are 193 (m) and 366 (w) cm^{-1}, and those related to clinochlore are 547 (s) and 679 (s) cm^{-1} (Figure 8.6.a). Chlorites were also identified by means of VNIR (Figure 8.6.b and c). Chamosite was found in samples from Enekuri thanks to the bands at 2253 and 2340 nm, which are due to the vibrations of Fe-OH and Mg-OH respectively. Besides, the bands related with the presence of iron can be observed at 743, 926 and 1119 nm. In some chamosite spectra (the example of Figure 8.6.b), a weak band at 2205 nm can be observed. This band is due to the Al-OH vibration and suggests the presence of the denominated white micas, such as muscovite or celadonite, which are alteration minerals formed by hydrothermal processes [13]. On the other hand, the spectrum of clinochlore was identified in Fruiz samples (Figure 8.6.c) thanks to the bands of the Fe-OH (2295 nm) and Mg-OH (2356 nm) vibrations, which differ slightly from those of chamosite. This group of phyllosilicates comes from the weathering of feldspars (albite) or from pyroxenes (diopside), and they are alteration products of Fe- and Mg- bearing minerals. They are common minerals in rocks that have experienced hydrothermal processes [14], as it could have happened here in the moment of the volcano eruption.
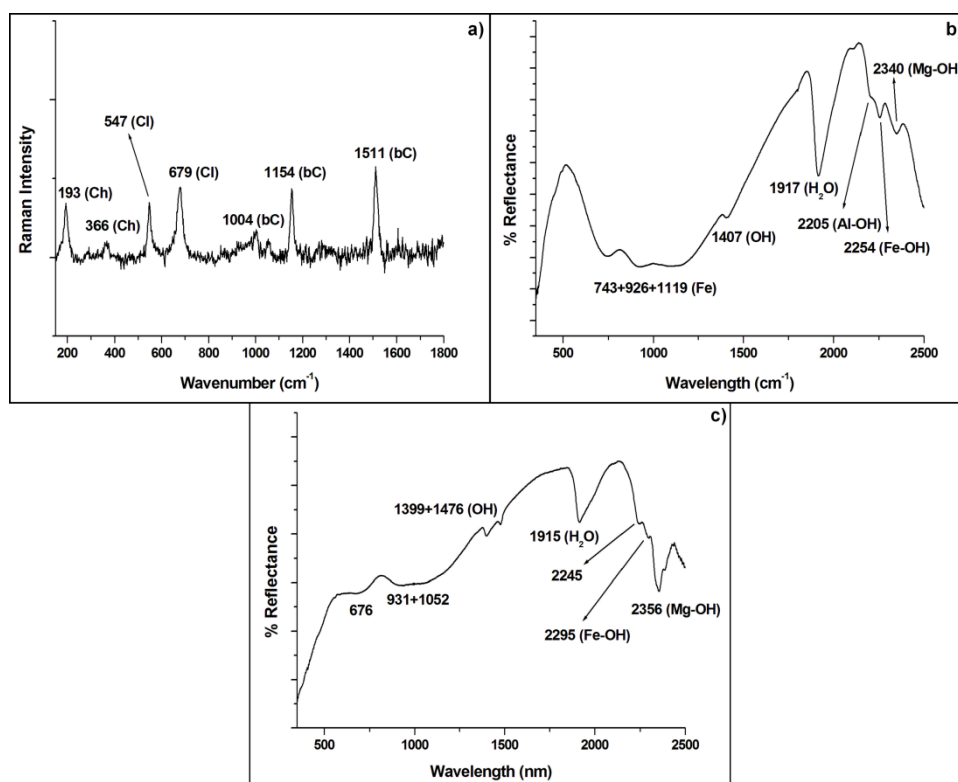
Figure 8.6. a) Raman spectrum of chamosite (Ch) and clinochlore (Cl) together with beta-carotenes (bC) and **b)** VNIR spectrum of chamosite and **c)** VNIR spectrum of clinochlore

In Enekuri, prehnite was found by means of Raman spectroscopy (Figure 8.7.a) and analcime by means of VNIR spectroscopy (Figure 8.7.b). Prehnite $(Ca_2Al(Si_3Al)O_{10}(OH)_2)$ is a metamorphic inosilicate hydrothermally formed in basic igneous rocks [15]. Its Raman bands appear at 389 (w) and 521 (s) cm^{-1}. Analcime $(NaAlSi_2O_6 \cdot H_2O)$ is a zeolite generally formed by reactions between saline solutions and volcanic glass [16]. It has VNIR bands at 965, 1158, a doublet at 1421 and 1465 due to the OH vibrations, 1801, 1908 (H_2O combination band), 2117 and 2207 nm. This finding completes the information provided by XRD, where some other zeolites were identified. The zeolites detected by XRD technique were those of calcium, however, as Barth-Wischling et al. [17] stated, Na-rich zeolites could be formed from Ca-rich ones during their last alteration states when the concentration of Na, the alkalinity and the temperature are the proper ones. The formation of analcime can be due to alteration processes; in a close system by reaction of concentrated alkaline saline solutions (sea-water) at low temperatures, or in an open system by reaction with dilute sodium solutions at elevated temperatures [17]. On Mars, both minerals are present in Nili Fossae and they were identified by CRISM [3]. The presence of prehnite and zeolites (like analcime) in and around the impact crater of the Nilli Fossae area are indicators of low grade metamorphic or aqueous hydrothermal alteration [3].
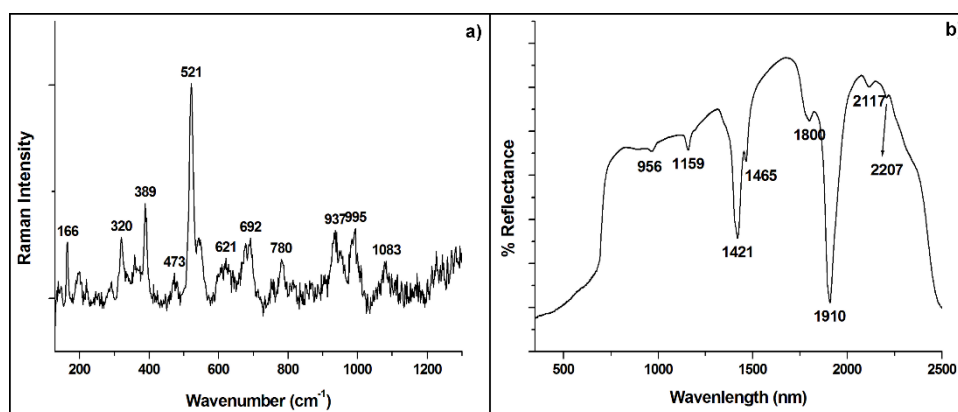
Figure 8.7. a) Raman spectrum of prehnite and **b)** VNIR spectrum of analcime

In Fruiz, some oxides could be identified. In Figure 8.8.a, a broad Raman band that was decomposed into several bands can be seen. These bands are 499, 577, 612 and 654 cm^{-1}, and are consistent with the presence of manganese oxides. Most of Mn oxides are amorphous and this is the reason why a broad band is observed. As has been explained in *Chapter 6* these minerals are very reactive and therefore are very important for biogeochemical processes due to their high oxidizing capacity [18]. Another oxide found in Fruiz is magnesioferrite ($MgFe_2O_4$). It is a spinel, which arise from the second stage of oxidation of olivine, probably present in the original matter from the submarine volcano. This process consists of a first oxidation of the olivine to ferriolivine and a second one in which the magnesioferrite is formed as a final product [19]. It was identified by the VNIR spectroscopy (Figure 8.8.b) and the bands related to this mineral are located at 701 and 1034 nm, which are attributed to the Fe^{3+} intra-atomic transitions [20]. In the same Figure, a band consistent with the presence of chamosite can be seen although the number of times that chamosite was detected was much fewer than those observed related to the presence of clinochlore (the other chlorite found). There is no reference confirming the presence of magnesioferrite on Mars, but Zhang et al. [21] found this mineral thanks to high resolution TEM analyses in the Martian meteorite NWA 7755.
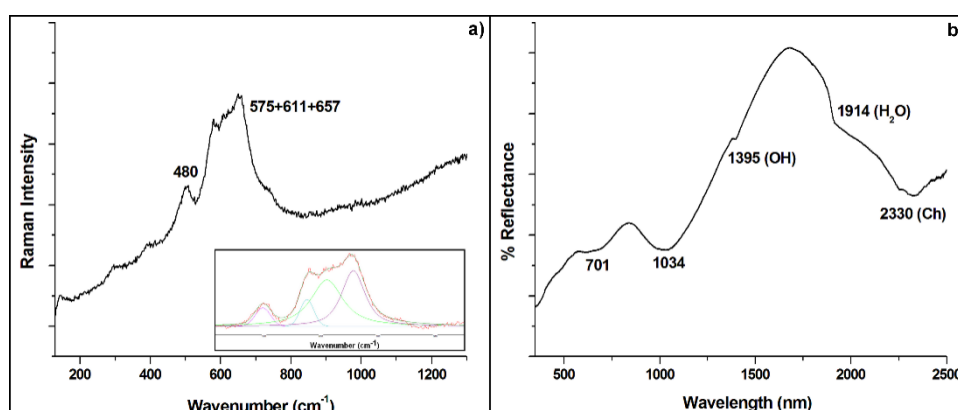

Figure 8.8. a) Raman spectrum of manganese oxide and **b)** VNIR spectrum of magnesioferrite together with bands related with the presence of chamosite

Quartz (SiO_2) and calcite ($CaCO_3$, Figure 8.9) were also detected during the Raman and VNIR spectroscopic analyses. Quartz was found in all the samples from both emplacements throughout the surfaces. In the case of calcite, it was localized in vesicles in the Enekuri samples, as in the case of Meñakoz and Armintza, which evidenced the secondary formation of this mineral and, therefore, the same geological formation, the pillow lavas. However, in the Fruiz samples this carbonate was not found in vesicles, which could be due to the different type of outcrop, a columnar disjunction in this case.
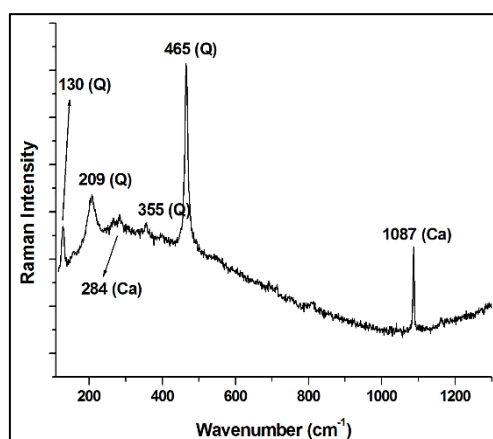
Figure 8.9. Raman spectrum of quartz (Q) together with calcite (Ca)

8.1.   Conclusions

The statement made at the beginning of this chapter in which it was affirmed that the weathering processes that have occurred in these emplacements should be different to those observed in Meñakoz or Armintza, has been confirmed with the obtained results. The only compounds in common with these latest emplacements were albite and chlorites. Albite could be formed in aqueous conditions (albitization process) since the geological formations observed in these emplacements have a submarine origin. For their part, chlorites appear as hydrothermal products, which is in agreement with the mentioned formations.

However, the lack of contact with sea-water nowadays led us to conclude that the environmental transformation of these minerals had to be different since the compounds observed in the samples from Enekuri and Fruiz outcrops are different from those observed in Meñakoz or in Armintza. The existence of pyroxenes in the analysed samples in this chapter could lead to the conclusion that the weathering process did not progress as much as in the emplacements in contact with the sea-water. This could be also the case of the titanite, which has magmatic origin and has commonly been reported to be altered to anatase [22], among other oxides whose presence was not as evident as in Meñakoz (or Armintza). Moreover, due to the existence of titanite, both Enekuri and Fruiz, could be considered good examples for the studies of biological activity and the possible implication with Mars.

The presence of chlorites indicates that the first steps of the weathering process should be similar to those observed in the previous studied emplacements. Moreover, the hydrothermal origin of these minerals is consistent with the submarine volcanic origin of the analysed areas.

However, there are also differences observed between Enekuri and Fruiz, which could be related with the geological feature observed (pillow lavas and columnar disjunction) or with the different plates in which they are present (Iberian and European respectively). In Enekuri, prehnite and analcime, and in Fruiz, manganese oxides and magnesioferrite are supposed to be minerals that arose in the first steps of the weathering process because, if not, they would have been observed in the Meñakoz and Armintza outcrops too.

8.2. Bibliography

1. Namieśnik J. Trace Analysis — Challenges and Problems. *Crit. Rev. Anal. Chem.,* **2002,** 32, 271-300.

2. Ruff S. Spectral evidence for zeolite in the dust on Mars. *Icarus,* **2004,** 168, 131-143.

3. Bishop J. L., Michalski J. R. Carter J. Chapter 14 - Remote detection of clay minerals. In: *Infrared and Raman spectroscopies of clay minerals.* Eds. Gates W. P., Kloprogge J. T., Madejová J., Bergaya F. *Elsevier,* **2017,** pp. 482-514.

4. Cloutis E. A., Asher P. M., Mertzman S. A. Spectral reflectance properties of zeolites and remote sensing implications. *J. Geophys. Res. Planet.,* **2002,** 107 (E9), 5067, 1-19.

5. Freeman J. J., Wang A., Kuebler K. E., Jolliff B. L., Haskin L. A. Characterization of natural feldspars by Raman spectroscopy for future planetary exploration. *Can. Mineral.,* **2008,** 46, 1477-1500.

6. Buchs D. M., Howie R. A. Pyroxenes. In: *Reference module in Earth systems and environmental sciences. Elsevier,* **2016,** pp. 1-4.

7. Huang P. M., Wang M. K. MIinerals, Primary. In: *Encyclopedia of soils in the environment.* Ed. Hillel D. *Elsevier,* Oxford. **2005,** pp. 500-510.

8. Bandfield J. L. Global mineral distributions on Mars. *J. Geophys. Res. Planet.,* **2002,** 107 (E6), 5042, 1-7.

9. Achilles C. N., Downs R. T., Ming D. W., Rampe E. B., Morris R. V., Treiman A. H., Morrison S. M., Blake D. F., Vaniman D. T., Ewing R. C., Chipera S. J., Yen A. S., Bristow T. F., Ehlmann B. L., Gellert R., Hazen R. M., Fendrich K. V., Craig P. I., Grotzinger J. P., Des Marais D. J., Farmer J. D., Sarrazin P. C., Morookian J. M. Mineralogy of an active eolian sediment from the Namib dune, Gale crater, Mars. *J. Geophys. Res. Planets,* **2017,** 122, 2344-2361.

10. Zhang M., Salje E. K. H., Redfern S. A. T., Bismayer U., Groat L. A. Intermediate structures in radiation damaged titanite ($CaTiSiO_5$): a Raman spectroscopic study. *J. Phys. Condens. Mat.,* **2013,** 25,115402, 1-12.

11. Ackerson M. PhD thesis. *Trace element partitioning between titanite and groundmass in silicic volcanic systems.* University of North Carolina, Chapel Hill, **2011.**

12. Banerjee N., Bridge N., Izawa M., Anderson L., Bebout G., Flemming R. Glassy subaqueous lavas as a habitat for life on Earth, Mars, and elsewhere? *LPSC 40,* **2009,** abst 1331.

13. Wang R., Cudahy T., Laukamp C., Walshe J. L., Bath A., Mei Y., Young C., Roache T. J., Jenkins A., Roberts M., Barker A., Laird J. White mica as a hyperspectral tool in exploration for the sunrise Dam and Kanowna Belle Gold Deposits, Western Australia. *Econ. Geol.,* **2017,** 112, 1153-1176.

14. Beaufort D., Rigault C., Billon S., Billault V., Inoue A., Inoué S., Patrier P. Chlorite and chloritization processes through mixed-layer mineral series in low-temperature geological systems - a review. *Clay Miner.,* **2015,** 50, 497-523.

15. Michailidis K., Kassolifournaraki A., Ericsson T., Filippidis A., Godelitsas A. Prehnite formation and metamorphic relations in the metagabbros of the Oreokastro ophiolite suite, Macedonia, Greece. *Gff,* **1995,** 117, 15-21.

16. English P. M. Formation of analcime and moganite at Lake Lewis, central Australia: significance of groundwater evolution in diagenesis. *Sediment. Geol.,* **2001,** 143, 219-244.

17. Barth-Wirsching U., Klammer D., Kovic-Kralj P. The formation of analcime from laumontite in the Smrekovec volcanics, Northwest Slovenia - an experimental approach. *Stud. Surf. Sci. Catal.,* **1994,** 84, 299-305.

18. Tebo B., Bargar J., Clement B., Dick G., Murray K., Parker D., Verity R., Webb S. Biogenic manganese oxides: Properties and mechanisms of formation. *Annu. Rev. Earth Planet. Sci.,* **2004,** 32, 287-328.

19. Khisina N. R., Khramov D. A., Kolosov M. V., Kleschev A. A., Taylor L. A. Formation of ferriolivine and magnesioferrite from Mg-Fe-olivine - Reactions and kinetics of oxidation. *Phys. Chem. Miner.,* **1995,** 22, 241-250.

20. Pailhé N., Wattiaux A., Gaudon M., Demourgues A. Correlation between structural features and vis-NIR spectra of α-Fe2O3 hematite and AFe2O4 spinel oxides (A=Mg, Zn). *J. Solid State Chem.,* **2008,** 181, 1040-1047.

21. Zhang A., Wang S., Tomioka N., Lu X., Ding Z., Ma C., Wang P., Chen J., Xu S., Gu L., Bai Y., Li Y., Sakamoto N., Wang R. An example of high-T, high-symmetry crystallization: Spherical (Mg, Fe)-oxides formed by particle attachment in the shocked martian meteorite Northwest Africa 7755. *Am. Mineral.,* **2019,** 104, 150-157.

22. Morad S., El-Ghali M. A. K., Caja M. A., Al-Ramadan K., Mansurbeg H. Hydrothermal alteration of magmatic titanite: Evidence from proterozoic granitic rocks, southeastern Sweden. *Canad. Mineral.,* **2009,** 47, 801-811.

CHAPTER 9:

ORGANIC MATERIAL

DETECTION

In the *Introduction* chapter it was mentioned that the search for evidence of past and present life on Mars is one of the top scientific priorities in the past and future planetary missions. In 1996, ESA already proposed that the finding of organic matter on Mars was one of the main priorities in order to test the possible existence of life on Mars [1]. Parnell et al. [1] in 2007 asserted that the major priority of the Martian exploration was the detection of organic matter, concretely those molecules that might be evidence of past or present life. On Mars, these molecules may have been formed abiotically, produced by possible past or present Martian life or delivered from space. For this reason, the landers and rovers sent to Mars have been carefully cleaned (Planetary protection) to avoid possible terrestrial contamination from the Earth [2]. Until today, the instruments designed for the detection of organics have only detected organic volatiles [3], as in the case of the gas chromatograph mass spectrometer on-board the Viking landers, or the SAM (sample analysis at Mars) on-board the Curiosity rover [4]. Other missions, such as Phoenix, detected compounds like perchlorates (ClO_4^-), which are used in the metabolic pathway

of some microbes and they can interfere with the detection of organic compounds. Therefore, it is unclear if Phoenix found organic compounds on Mars or not [5]. However, some studies made on Martian meteorites have demonstrated the presence of organic signatures [6-8]. For example, Madariaga et al. [9] and Torre-Fdez et al. [10] detected several Raman bands related to the presence of organic compounds in inclusions of the NWA 6148 Martian meteorite.

Taking into account that hypothetical Martian life could be similar to terrestrial life, Martian exploration has focused on four major types of organic compounds; carbohydrates, lipids, proteins (amino acids) and nucleic acids [2]. Amino acids and lipids are two of the most important molecules because they are building blocks of life. Additionally, they are chemically stable and show great persistence in the geological record. Amino acids are the building blocks of proteins in all domains of life and lipids are the major components of cell membranes and are essential for the permeability of that membrane [11].

In the next planetary missions, instruments for the detection of organic signatures (see *2022 Planetary Missions* section) will be implemented. Briefly, MOMA (ESA) consists of a combined pyrolysis gas chromatography mass spectrometer and laser desorption mass spectrometer, and SHERLOC (NASA) is a UV Raman spectrometer.

The techniques used to obtain the results shown in this chapter (described in *Analysis of organics* section) were similar to the techniques of the ExoMars 2022 rover (Rosalind Franklin) and the Mars 2020 rover (Perseverance). ToF-SIMS (Time of Flight-Secondary Ion Mass Spectrometry), linear ion trap mass spectrometry and GC-MS provided additional mass spectrometry information and are similar to MOMA instrument. Organic signals were also obtained by the Raman analyses of the samples with a 532 excitation laser at micrometric scale. Even though the wavelength of the employed laser was not the same as the one used in SHERLOC, the position of the expected signals should be the same.

Armintza, Enekuri, Meñakoz and Fruiz samples were analysed and the obtained results are summarized below. Unfortunately, the highly weathered samples from Meñakoz did not contain any organic matter above the detection limit of the techniques utilised.

Regarding the results obtained by ToF-SIMS, only the ion images of the distribution of the positive fragments are shown because the negative mode did not give any relevant information. These fragments are divided into alkanes, nitrogenated fragments and aromatic fragments. Only the last two are taken into account because alkanes do not evidence the presence of organic matter relevant for this type of studies. The scale bar observed in the distribution images corresponds to the intensity (counts) of each fragment in the mass spectrum. The image on the right corresponds to the overlay of the two other ion images.

Table 9.1 shows the ratios of the organic fragments in some samples with respect to Al^+ (m/z 27, which represents the inorganic fraction). The nitrogenated fragments (CH_4N^+

(m/z 30) $C_2H_6N^+$ (m/z 44), $C_4H_8N^+$ (m/z 70) and $C_4H_{10}N^+$ (m/z 72)) indicate the existence of amino acids. In fact, they are related to the presence of glycine, alanine, proline and valine respectively [12]. Moreover, aromatic fragments such as $C_5H_5^+$ (m/z 65), $C_6H_5^+$ (m/z 77) and $C_7H_7^+$ (m/z 91) could be observed. The ions $C_6H_5^+$ and $C_7H_7^+$ can be attributed to benzyl or aryl aromatic ions, being m/z 91 (called tropylium cation) responsible for fragment ions at m/z 65, which also confirms the aromatic nature of the compound [13].

Table 9.1. Ratios of the different fragments observed in Armintza samples

/Al$^+$ Sample	CH_4N^+	$C_2H_6N^+$	$C_4H_8N^+$	$C_4H_{10}N^+$	$C_5H_5^+$	$C_6H_5^+$	$C_7H_7^+$
Ar01_01	1.05	0.48	0.38	0.33	0.29	0.29	0.29
Ar01_02	0.61	0.41	0.37	0.67	0.67	0.48	0.48
Ar01_03	0.33	0.31	0.33	<LOD	0.19	0.10	0.08
Ar02_01	0.66	0.80	0.64	0.28	0.32	0.28	0.36
Ar02_02	0.50	0.50	0.52	0.24	0.19	0.17	0.17
Ar02_03	0.27	0.26	0.23	0.18	0.17	0.15	0.12
Ar03_01	0.54	0.54	0.46	0.23	0.61	0.54	0.46
Ar03_02	0.21	0.25	0.18	0.25	0.21	0.23	0.21
Ar03_03	0.20	0.23	0.23	0.22	0.26	0.20	0.20

As can be seen in the table 9.1, the general tendency was that the nitrogenated fragments were found in higher amounts than the aromatic ones. There were some exceptions in which the aromatic fragments were, more or less, in the same (or even in higher) proportion as the nitrogenated ones. Moreover, these ratios were <1 in most of the cases, which means that the proportion of organic matter was lower than the inorganic one, and compared with those observed in Enekuri and Fruiz (see Table 9.4 with the average values of each fragment in each emplacement), were the lowest ones. Therefore, it could be stated that there is less organic matter in Armintza than in the other emplacements.

In Figure 9.1 the ToF-SIMS distribution images of some Armintza samples are shown, being representative for all the measurements carried out with the Armintza samples. The Al$^+$ and CH_4N^+, $C_2H_6N^+$ and $C_5H_5^+$ fragments are represented in the different examples, denoting the distribution of the organic material with respect to the inorganic. Almost all the organic fragments in each sample had the same spatial distribution throughout the measurement area (see Appendix IV in Chapter 13).
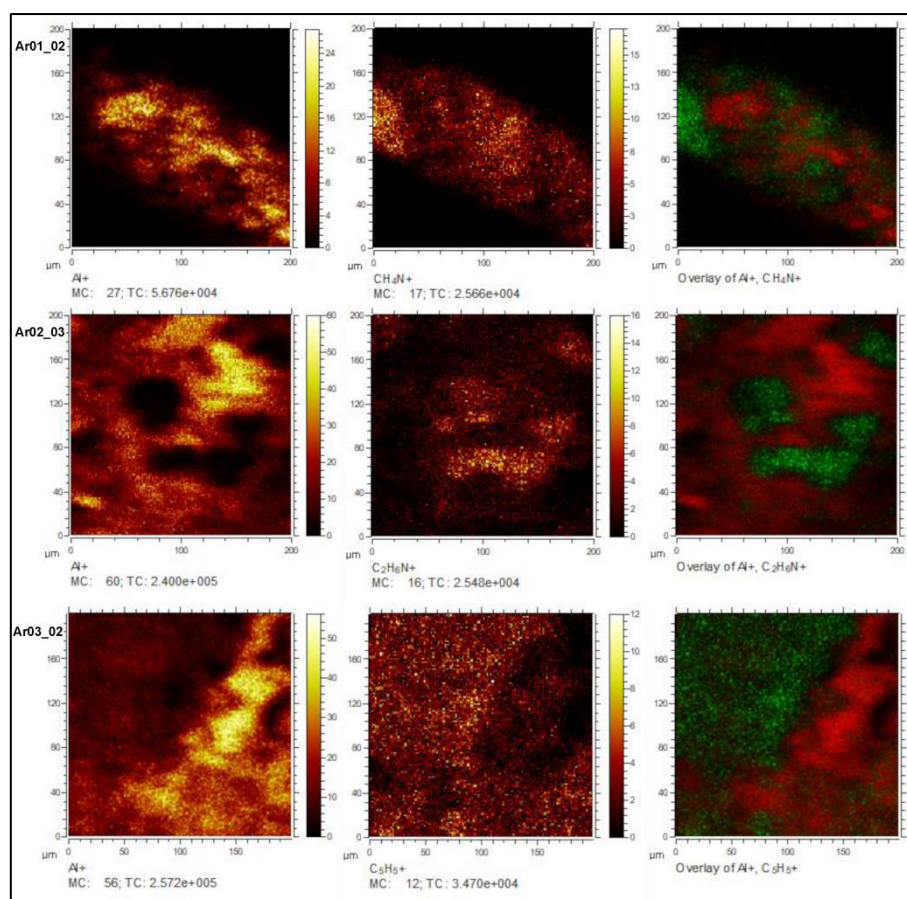
Figure 9.1. ToF-SIMS images with the signal given by Al^+ (red) and CH_4N^+, $CH_2H_6N^+$ and $C_5H_5^+$ fragments (green) in positive mode as well as the overlay between them in three different samples from Armintza

In the samples from Enekuri, the number of the measurements which gave organic signals were higher than in Armintza, and therefore, it was suggested that the quantity of organic molecules was also higher. As can be seen in the resuts from this emplacement (see *Enekuri and Fruiz* chapter), the weathering processes were not as severe as in Armintza or Meñakoz and, therefore, the detection of organic matter, if it exists, should be easier since the organics would be more accesible and they were not lost with the weathering of the rocks.

As in the case of Armintza, the nitrogenated fragments observed were CH_4N^+ (m/z 40), $C_2H_6N^+$ (m/z 44), $C_4H_8N^+$ (m/z 70) and $C_4H_{10}N^+$ (m/z 72). As Brunning et al. [12] suggest, they could be consistent with the presence of glycine, alanine, proline and valine, respectively. Aromatic fragments such as $C_5H_5^+$ (m/z 65), $C_6H_5^+$ (m/z 77) and $C_7H_7^+$ (m/z 91) were, again, detected in these samples. In addition, in this case (and as we will see in the Fruiz samples) other fragments such as $C_{10}H_8^+$ (m/z 128) and $C_{12}H_8^+$ (m/z 152) were detected in lower proportions. As stated by Ashcroft [13], these fragments arise from the fragmentation of benzyl or aryl aromatic ions. On the other hand, the fragments at m/z 128 and 152 are characteristic of PAHs (Polycyclic Aromatic Hydrocarbons) [14]. These environmental pollutants are generated mainly due to an incomplete combustion of organic material [15]. Taking into account the location of the Enekuri outcrop (close to a highway) the origin of these PAHs could be due to anthropogenic activities. However,

they could also arise due to the presence of kerogen or come from the air in the laboratory.

Regarding the ratios observed for some examples (Table 9.2), the nitrogenated fragments in Enekuri were ≥ 1 and higher than that observed for Armintza. This could indicate that there is more organic matter in the Enekuri samples compared with the Armintza samples. Aromatic fragments were in a lower proportion than the nitrogenated ones, but in higher amounts than in the previously described emplacement (Armintza outcrop).

Table 9.2. Ratios of the different fragments observed in Enekuri samples

/Al$^+$ Sample	CH$_4$N$^+$	C$_2$H$_6$N$^+$	C$_4$H$_8$N$^+$	C$_4$H$_{10}$N$^+$	C$_5$H$_5^+$	C$_6$H$_5^+$	C$_7$H$_7^+$
En01_01	1.44	1.41	1.41	1.41	0.33	0.33	0.44
En01_02	1.17	1.56	1.17	0.72	0.28	0.33	0.45
En01_03	1.00	0.82	0.23	0.29	0.35	0.47	0.47
En02_01	1.63	1.75	1.38	1.13	0.63	0.88	0.88
En02_02	1.17	1.42	1.17	1.00	0.50	0.58	0.58
En02_03	1.07	1.23	1.40	1.07	0.43	0.53	0.53
En03_01	1.62	1.85	1.77	1.15	0.54	0.73	0.65
En03_02	1.50	1.80	1.90	1.25	0.75	1.00	1.10
En03_03	1.29	0.86	0.86	0.43	0.71	0.71	0.71

In Figure 9.2 the signals of Al$^+$ compared with different organic fragments (CH$_2$H$_6$N$^+$, C$_5$H$_5^+$ and C$_{10}$H$_8^+$ respectively) are represented. These examples are also representative for all the results obtained from Enekuri samples. The distribution of most of the organic fragments was also the same.
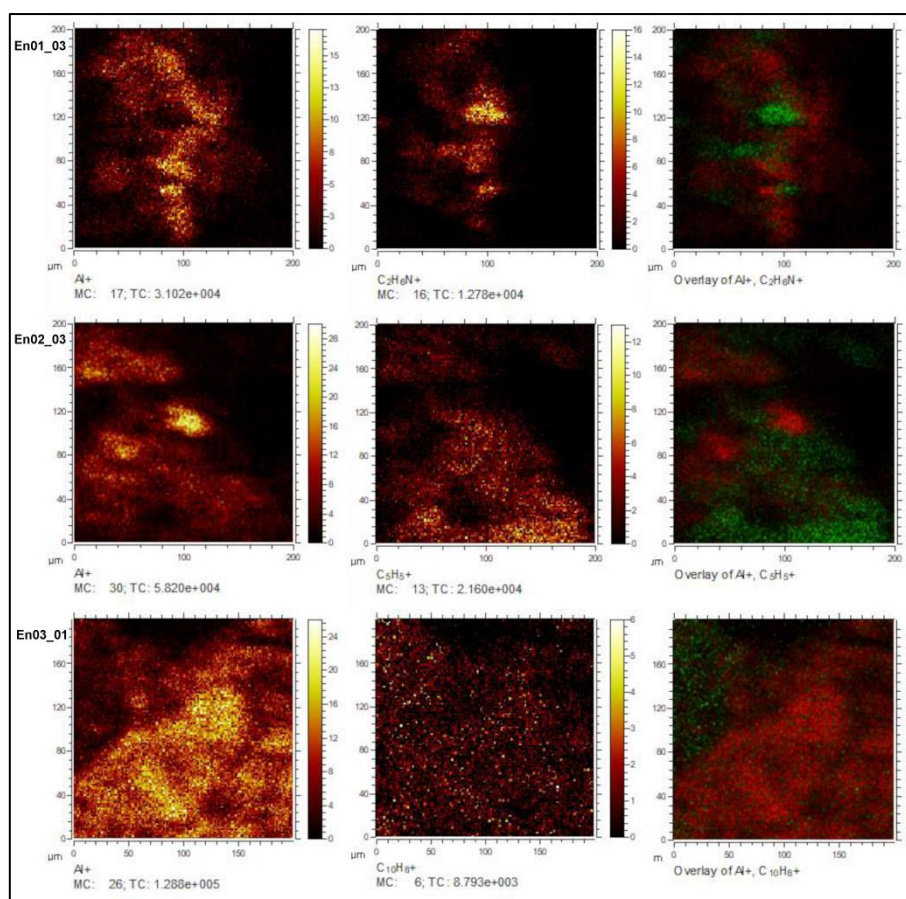
Figure 9.2. ToF-SIMS image with the signal given by Al^+ (red) and $CH_2H_6N^+$, $C_5H_5^+$ and $C_{10}H_8^+$ fragments (green) in positive mode as well as the overlay between them in three different samples from Enekuri

Finally, in Fruiz the results were almost the same as those observed for Enekuri. CH_4N^+ (m/z 40) $C_2H_6N^+$ (m/z 44), $C_4H_8N^+$ (m/z 70) and $C_4H_{10}N^+$ (m/z 72) detected fragments were due to the presence of glycine, alanine, proline and valine, respectively [12]. In the case of aromatic fragments, those in higher proportions were $C_5H_5^+$ (m/z 65), $C_6H_5^+$ (m/z 77) and $C_7H_7^+$ (m/z 91) due to the benzyl fragmentation [13], and in lower proportions $C_9H_7^+$ (m/z 115) or $C_{10}H_8^+$ (m/z 128), which could be related to the fragmentation of PAHs [14]. As in the case of Enekuri, the Fruiz outcrop is near to a highway and therefore the PAH origin could be anthropogenic [15] or come from the air in the laboratory.

As can be observed in Table 9.3, the ratios were even higher than in the previous emplacements, which could be due to the higher amount of organic matter in these samples. In the same way, the aromatic fragments were in lower amounts than the nitrogenated ones.

Table 9.3. Ratios of the different fragments observed in Fruiz samples

/Al$^+$ Sample	CH$_4$N$^+$	C$_2$H$_6$N$^+$	C$_4$H$_8$N$^+$	C$_4$H$_{10}$N$^+$	C$_5$H$_5$$^+$	C$_6$H$_5$$^+$	C$_7$H$_7$$^+$
Fr01_01	4.73	5.46	3.82	3.82	1.00	0.91	1.18
Fr01_02	2.70	3.40	2.25	1.50	0.80	0.75	0.80
Fr01_03	2.20	2.24	2.04	1.24	0.76	0.84	0.80
Fr02_01	3.87	4.60	5.47	3.27	1.27	1.47	1.47
Fr02_02	2.67	4.22	4.22	2.56	0.67	0.89	0.89
Fr02_03	1.57	2.00	1.79	1.29	0.57	0.64	0.71
Fr03_01	2.78	3.67	3.67	2.89	0.67	0.72	0.78
Fr03_02	2.25	3.25	3.75	2.38	0.63	0.75	0.50

Figure 9.3 shows examples where Al$^+$ and different organic fragments in each sample can be observed. These fragments represent the distribution of the organic material with respect to the inorganic.

Figure 9.3. ToF-SIMS image with the signal given by Al$^+$ (red) and CH$_2$H$_8$N$^+$, C$_7$H$_7$$^+$ and C$_9$H$_7$$^+$ fragments (green) in positive mode as well as the overlay between them in three different samples from Fruiz
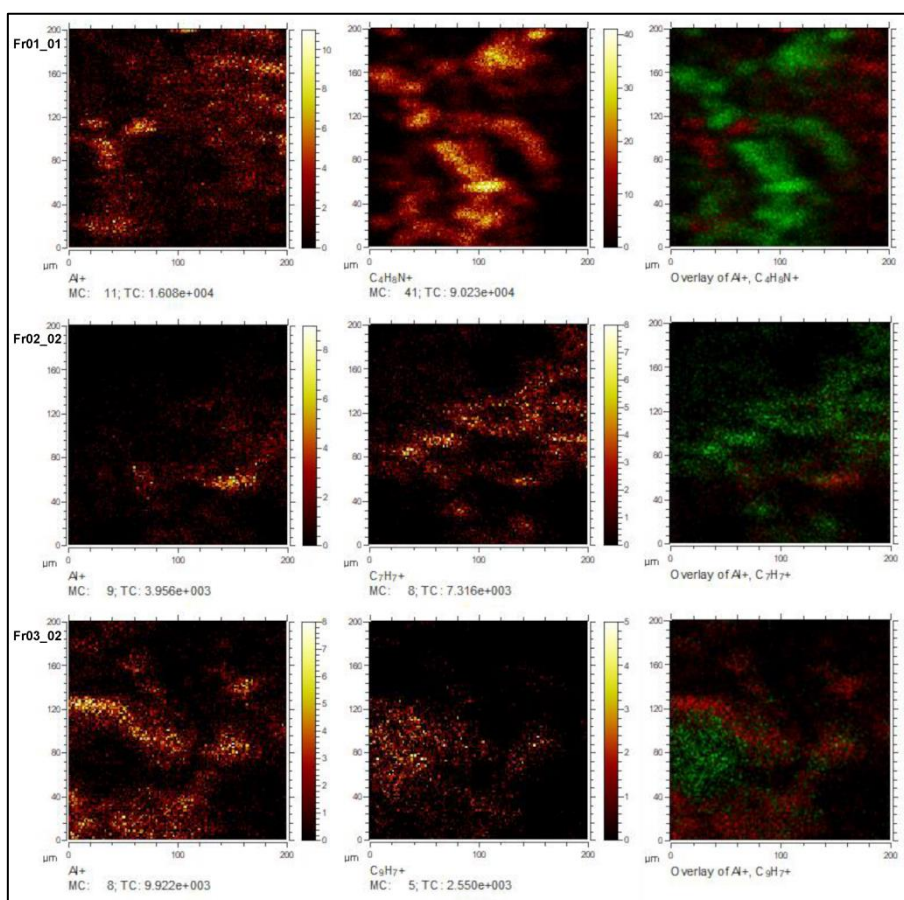
In Table 9.4 an overview of the mean value of each organic fragment in the different outcrops is shown. As has been mentioned before, Armintza is the outcrop with the lowest amounts of organic fragments and Fruiz is that with the higher proportion of them. Enekuri is between these two.

Table 9.4. Average values and standard deviation of the ratios of the organic fragments

	CH_4N^+	$C_2H_6N^+$	$C_4H_8N^+$	$C_4H_{10}N^+$	$C_5H_5^+$	$C_6H_5^+$	$C_7H_7^+$
Ar	0.49±0.27	0.42±0.18	0.37±0.15	0.30±0.16	0.32±0.19	0.27±0.15	0.26±0.14
En	1.32±0.24	1.41±0.38	1.25±0.50	0.94±0.38	0.50±0.17	0.62±0.23	0.65±0.22
Fr	2.85±1.00	3.61±1.16	3.38±1.26	2.37±0.96	0.80±0.23	0.87±0.26	0.89±0.30

Some samples from Armintza, Fruiz and Enekuri were measured with the LTQ mass spectrometer from NASA Goddard Space Flight centre. That device is a commercial replica of the MOMA instrument. Thanks to the obtained mass spectra (Figure 9.4) it was possible to observe differences among the samples from different locations and even identify organics and related clusters. It has to take into account that, in some cases, the observed differences are showed in the negative mode. However, the MOMA instrument only has positive mode, therefore, care must be taken if the spectra from Mars were compared with those obtained from the analogues. Moreover, most of the intense peaks in the positive mass spectra are likely related with minerals, most likely Ca_xO_y clusters, which can be seen by the mass difference of 56. However, they cannot be directly assigned as pure oxide clusters. Furthermore, the mass of many peaks were odd numbered, which lead to thing that these peaks might be adducts to the minerals clusters.
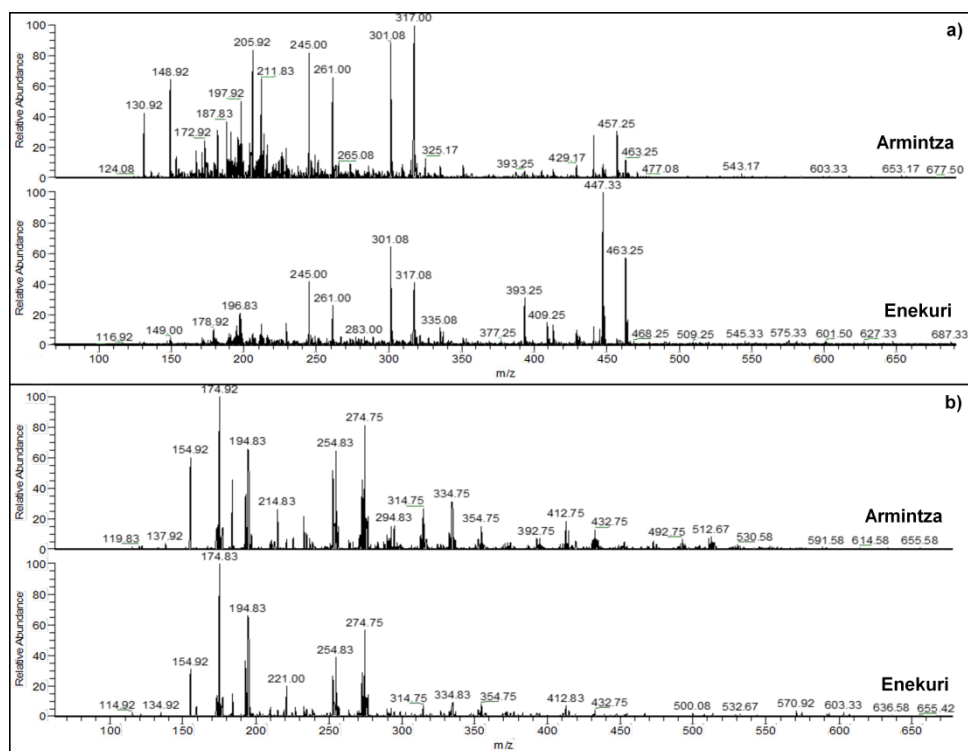
Figure 9.4. Mass spectra from the LIT in **a)** positive mode and **b)** negative mode of Armintza and Enekuri samples

Finally, the last mass technique employed was GC-MS on the samples from Enekuri and Fruiz, taking in mind that they presented the highest organic fraction (see above).

In Figure 9.5, GC-MS chromatograms as recorded at the Univiversity of Göttingen are shown. The analysed samples did not contain much extractable organic material. Total Organic Carbon (TOC) determined via elemental analyser (carbon combustion) was generally low (between 0.04−0.12 w/w%) and the soluble organic fraction was dominated by terrestrial long-chain-n-alkanes.
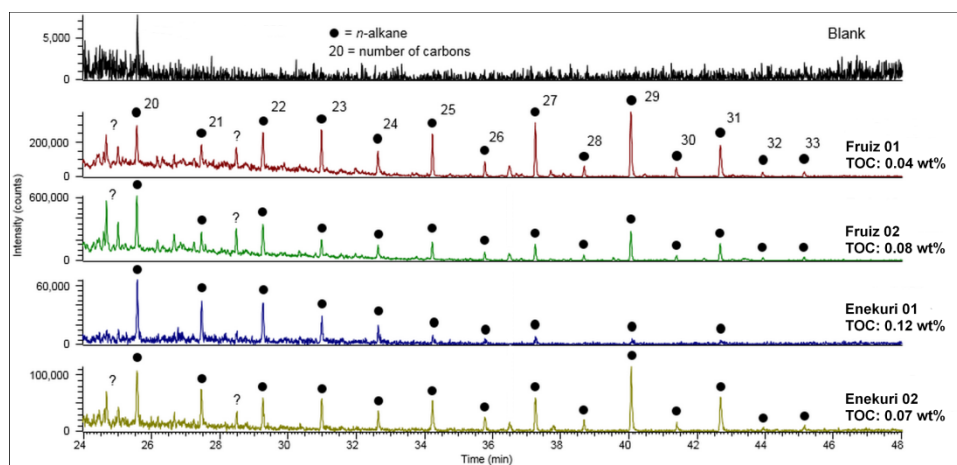
Figure 9.5. GS-MS chromatograms of soluble organics

The presence of C_{27}, C_{29} and C_{31} n-alkanes evidences the allochtonous organic matter, which is originated from higher plants (terrestrial signal). They could also be due to the presence of lichens in the sample [12]. The carbon-chain-length-preferences (odd over even) of n-alkanes in Fruiz 01, Fruiz 02 and Enekuri 02 point to a low maturity of this fraction of the organic matter. In the case of Enekuri 01, a decrease in abundance with increasing chain length of n-alkanes (except n-C_{27}, n-C_{29} and n-C_{31}) was observed. This fact suggested thermal overprint of this fraction of the organic matter. In all the samples (except in Enekuri 01) a peak at minute 36.5 was observed. This peak could be assigned to isoprenoids, which are considered as microbial signatures. Some peaks at 24.5 and 28.5 minutes of retention time were not assigned and they were present in all the samples except in Enekuri 01. Unfortunately, it was not possible to identify their origin.

It has to take into account that the extractable fraction of the organic matter in ancient rocks (from Cretaceous in this case) is usually less than 10% of the total organic matter. However, in Enekuri and Fruiz all of the organic matter seemed to belong to bitumen (extractable phase), as no kerogen could be separated after mineral dissolution and density separation. Furthermore, the extractable fraction is prone to be influenced by oil migration/contamination, i.e. may contain allochthonous compounds (as interpreted here). Molecular signatures from non-extractable macromolecular organic matter (kerogen), instead, are considered syngenetic to the host rock (kerogen is generally non-motile). The samples, however, did not contain kerogen according to the mineral dissolution.

Knowing the existence of organic fragments, all samples that contained them were analysed by Raman spectroscopy.

In the Armintza samples, the inner part of some rocks collected in the sedimentary area, kerogen (Figure 9.6) was detected. It shows its main Raman bands at 1352 (D) and 1601 (G) cm^{-1} and, as can be observed in Figure 10.6, the D band is formed by the sum of several bands located at 1161 (D4), 1265 (D5), 1354 (D1) and 1442 (D3) cm^{-1}, which could be determined by performing a Lorentzian-Gaussian decomposition of the Raman band. In samples from Enekuri and Fruiz, kerogen was not found. This result together with the results obtained by the mineral dissolution lead to think that kerogen in these samples was not present. Moreover, in the ToF-SIMS ion images from Armintza samples the best separation between inorganics and organics was observed, which could be because of the presence of this kerogen.

Kerogen represents the dispersed, insoluble, organic carbon as well as the coal and mineral oil deposits in rocks [16]. Terrestrial kerogen is commonly captured and preserved in aqueous lithologies, such as silica, carbonates or sulfates, all of which have been detected both in Armintza and on Mars. Kerogen exemplifies one possible biosignature, which could be of high relevance for the knowledge of ancient Mars [17]. The G band is related to the sp^2 bond stretching within the aromatic ring in a large graphene-like cluster. The D1 peak is usually predominant and is a sub-band present in graphitic carbon. It corresponds to the breathing mode of the sp^2 aromatic ring within a graphitic cluster and it is strongly influenced by the electronic structure of the local environment. The D4 and D5 peaks appear as broad shoulders of the D1 peak. The D4 peak is related to vibrations of $C_{aromatic}$-C_{alkyl} such as aromatic aryl-alkyl ethers, C-C in aromatic rings and C-H in aromatic rings (the most probable one in this case), or trans-polyene-like C-C and C=C stretch bonds. Vibrations associated with the D5 peak are often related to the presence of methyl groups in either saturated or unsaturated alkane chains, therefore, is uniquely related to the vibrations originated from aliphatic hydrocarbon chains [18].
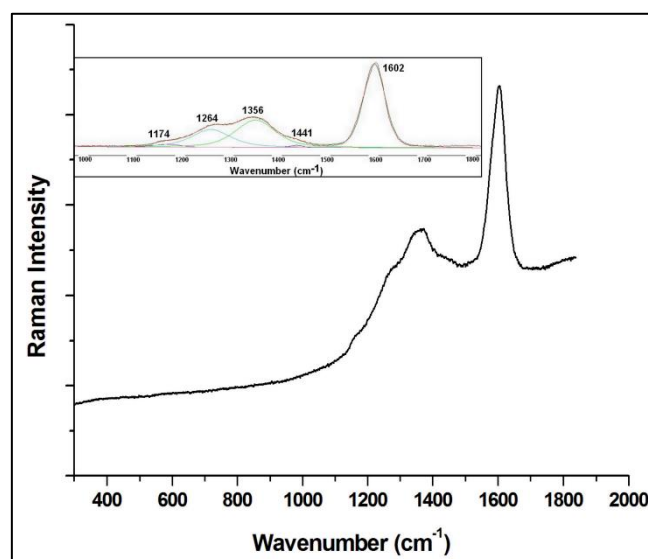
Figure 9.6. Raman spectrum of kerogen found in Armintza sedimentary samples

Thanks to the Curiosity rover, evidences of the presence of insoluble organic matter (IOM) (mass spectra with fragments characteristic of this carbonaceous compound) have been identified [19]. Nevertheless, the future missions, such NASA Mars 2020 rover, will carry Raman spectroscopy for the first time and, therefore, these results are a very interesting background for those missions.

In Figure 9.7 some examples of spectra with organic signals found on Enekuri and Fruiz samples are shown. In Figure 9.7.a, a mixture of astaxanthin and scytonemin is observed. Bands at 1005, 1153 and 1513 cm^{-1} are due to the presence of astaxanthin carotenoid and the bands at 1172, 1556, 1599, 1633 and 1715 cm^{-1} (only observed in the second spectrum) are those consistent with the presence of scytonemin. Astaxanthin is an antioxidant that appears as the principal xanthophyll containing alcohol and keto groups with twelve C=C double bonds, in highly polluted areas together with the UV screening pigment scytonemin, which is a common compound characteristic of most lichens living in extreme conditions, such as highly polluted atmospheres [20]. Since Enekuri and Fruiz outcrops are in contact with highways, the presence of this type of compound is recurrent. This fact supports the lichen origin of the long alkane's signatures as the GC-MS results suggested.

In Figure 9.7.b the bands due to the presence of carotenoids are also present (1004, 1155 and 1514 cm^{-1}). Some other bands can be observed. However, these bands are so wide that band decomposition was necessary in order to discern overlapped bands. Between 1260 and 1380 cm^{-1} stretching of the C-N bond in aromatic amines can be observed. The band that appears at 1430 cm^{-1} could be related with the bending vibration of the CH_2 groups in aliphatic molecules. In the range from 1590 and 1690 cm^{-1} many signals related with the presence of organic molecules could appear. Stretching of the C=C bond in aliphatic molecules, bending of the NH_2 and stretching of the C=N in amines are examples of the vibrations that could give bands in this region of the spectrum [21]. These bands, related with the presence of amines, would be in agreement with the ToF-SIMS analyses, where nitrogenated fragments were detected.

Taking into account that by ToF-SIMS analyses signals from aromatic compounds could also be detected, some of the bands observed in the Raman spectra can be due to the presence of this type of compounds. Many studies related to the spectroscopic characteristics of aromatic hydrocarbons are present in the literature. Bao et al. [22] defined four spectral regions of special interest in the study of aromatic hydrocarbons. In the range 1650-1550 cm^{-1} there are the ring stretching modes mixed with little contribution of the CH in-plane bending, bands between 1500 and 1350 cm^{-1} are mainly attributed to CH in-plane bending coupled to weak ring breathing, 1300-600 cm^{-1} range is related to the CH bending, and finally, the range from 1000 to 600 cm^{-1} is due to out-of-plane bends. More concretely, bands at 1025 and 1186 cm^{-1} in the Fruiz spectrum (Figure 10.7. b) can be assigned to CH in-plane vibrations and 1582, 1585 and 1602 cm^{-1} correspond to the stretching vibrations of the benzene ring [23].
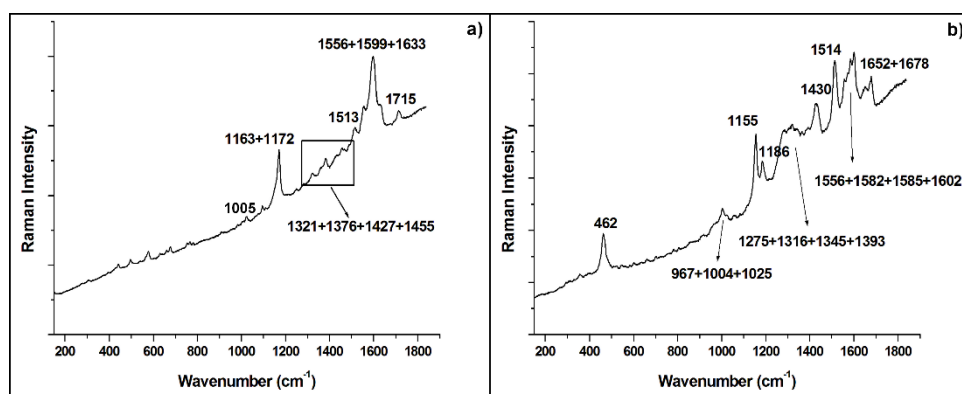
Figure 9.7. Raman spectra of **a)** astaxanthin and scytonemin in Enekuri samples and **b)** vibrations of carotenoids together with other organic functional groups in Fruiz samples

9.1   Conclusions

Considering that one of the main objectives of the Martian missions is to find signals of possible existence of life in the neighbouring planet, the existence of organic signatures in Martian analogue samples is a good starting point to improve the knowledge and interpretation of those signatures.

The information found in this work, provided by mass spectrometry, with the help of the ToF-SIMS and the GC-MS, is of high interest for the ESA's Exomars mission as MOMA is a GS-MS device. It is very important for the MOMA team to have well-characterized samples to test the instrument and to have a background provided by previous results (as with the other instruments of the rover) in order to better interpret the future data of the Exomars mission.

Even though, the interpretation of the organic signals by Raman spectroscopy could be difficult as many bond vibrations appear at very similar Raman shifts, any information about these organic signals by Raman spectroscopy plays a very important role for the detection of these kind of molecules using the SHERLOC instrument on NASA's Mars 2020 mission and the RLS instruments of the ESA's Exomars mission.

Having all this information and knowing how the signals related to these molecules are, the treatment of the upcoming results from the Mars missions would be easier if some biomarkers were present in the Martian surface.

9.2   Bibliography

1. Parnell J., Cullen D., Sims M. R., Bowden S., Cockell C. S., Court R., Ehrenfreund P., Gaubert F., Grant W., Parro V., Rohmer M., Sephton M., Stan-Lotter H., Steele A., Toporski J., Vago J. Searching for life on Mars: Selection of molecular targets for ESA's aurora ExoMars mission. *Astrobiology,* **2007,** 7, 578-604.

2. ten Kate I. L. Organic molecules on Mars. *Science,* **2018,** 360, 1068-1069.

3. Blanco Y., Gallardo-Carreno I., Ruiz-Bermejo M., Puente-Sánchez F., Cavalcante-Silva E., Quesada A., Prieto-Ballesteros O., Parro V. Critical assessment of analytical

techniques in the search for biomarkers on Mars: A mummified microbial mat from Antarctica as a best-case scenario. *Astrobiology,* **2017,** 17, 984-996.

4. Freissinet C., Glavin D. P., Mahaffy P. R., Miller K. E., Eigenbrode J. L., Summons R. E., Brunner A. E., Buch A., Szopa C., Archer Jr. P. D., Franz H. B., Atreya S. K., Brinckerhoff W. B., Cabane M., Coll P., Conrad P. G., Des Marais D. J., Dworkin J. P., Fairén A. G., François P., Grotzinger J. P., Kashyap S., ten Kate I. L., Leshin L. A., Malespin C. A., Martin M. G., Martin-Torres F., McAdam A. C., Ming D. W., Navarro-González R., Pavlov A. A., Prats B. D., Squyres S. W., Steele A., Stern J. C., Sumner D. Y., Sutter B., Zorzano M. -., the MSL S. T. Organic molecules in the Sheepbed Mudstone, Gale Crater, Mars. *J. Geophys. Res. Planets,* **2015,** 120, 495-514.

5. Darling D. S. D. The extraterrestrial encyclopedia. *First Edition Design Pub,* Florida, EEUU. **2016**.

6. Wright I. P., Grady M. M., Pillinger C. T. Organic materials in a Martian meteorite. *Nature,* **1989,** 340, 220-222.

7. Steele A., McCubbin F. M., Fries M. D. The provenance, formation, and implications of reduced carbon phases in Martian meteorites. *Meteorit. Planet. Sci.,* **2016,** 51, 2203-2225.

8. Steele A., Benning L. G., Wirth R., Siljeström S., Fries M. D., Hauri E., Conrad P. G., Rogers K., Eigenbrode J., Schreiber A., Needham A., Wang J. H., McCubbin F. M., Kilcoyne D., Rodriguez Blanco J. D. Organic synthesis on Mars by electrochemical reduction of CO_2. *Sci. Adv.,* **2018,** 4, eaat5118, .

9. Madariaga J. M., Torre-Fdez I., Ruiz-Galende P., Aramendia J., Gómez-Nubla L., Fdez-Ortiz de Vallejuelo S., Maguregui M., Castro K. , Arana G. Advanced analytical methodologies based on Raman spectroscopy to detect prebiotic and biotic molecules: Applicability in the study of the Martian nakhlite NWA 6148 meteorite. *2nd International Mars Sample return.* **2018,** abst. 6114.

10. Torre-Fdez I., Ruiz-Galende P., Aramendia J., Gómez-Nubla L., Castro K., Fdez-Ortiz de Vallejuelo S., Arana G. , Madariaga J. M. Study of organic compounds present in the NorthWest Africa 6148 Nakhlite by means of Raman spectroscopy. *EPSC.* **2018,** abst. 967.

11. Roling W. F. M., Aerts J. W., Patty C. H. L., ten Kate I. L., Ehrenfreund P., Direito S. O. L. The significance of microbe-mineral-biomarker interactions in the detection of life on Mars and beyond. *Astrobiology,* **2015,** 15, 492-507.

12. Bruuning C., Hellweg S., Dambach S., Lipinsky D., Arlinghaus H. F. Improving the interpretation of ToF-SIMS measurements on adsorbed proteins using PCA. *Surf. Interface Anal.,* **2006,** 38, 191-193.

13. Ashcroft A. E. Ionization methods in organic mass spectrometry. *The Royal Society of Chemistry,* United Kingdom. **1997**.

14. Dall' Osto M., Harrison R. Urban organic aerosols measured by single particle mass spectrometry in the megacity of London. *Atmos. Chem. Phys,* **2012,** 12, 4127-4142.

15. Abdel-Shafy H. I., Mansour M. S. M. A review on polycyclic aromatic hydrocarbons: Source, environmental impact, effect on human health and remediation. *Egypt. J. Pet.* **2016,** 25, 107-123.

16. von Bloh W. Climate Change 2: Long-Term Dynamics. In: *Encyclopedia of Ecology.* Eds. Jørgensen S. E., Fath B. D. *Academic Press,* Oxford. **2008,** pp. 592-598.

17. Shkolyar S., Eshelman E., Farmer J., Hamilton D., Daly M., Youngbull C. Detecting kerogen as a biosignature using colocated UV time-gated Raman and fluorescence spectroscopy. *Astrobiology,* **2018,** 18-2, 431-453.

18. Ferralis N., Matys E. D., Knoll A. H., Hallmann C., Summons R. E. Rapid, direct and non-destructive assessment of fossil organic matter via micro-Raman spectroscopy. *Carbon,* **2016,** 108, 440-449.

19. Eigenbrode J., Summons R., Steele A., Freissinet C., Millan M., Navarro-González R., Sutter B., Mcadam A., Franz H., Glavin D., Archer P., Mahaffy P., Conrad P., Hurowitz J., Grotzinger J., Gupta S., Ming D., Sumner D., Szopa C., Coll P. Organic matter preserved in 3-billion-year-old mudstones at Gale crater, Mars. *Science,* **2018,** 360, 1096-1101.

20. Ibarrondo I., Prieto-Taboada N., Martínez-Arkarazo I., Madariaga J. M. Resonance Raman imaging as a tool to assess the atmospheric pollution level: carotenoids in Lecanoraceae lichens as bioindicators. *Environ. Sci. Pollut. R.,* **2016,** 23, 6390-6399.

21. Larkin P. IR and Raman spectra-structure correlations: Characteristic group frequencies. In: *Infrared and Raman spectroscopy: principles and spectral interpretation. Elsevier,* USA. **2011,** pp. 73-115.

22. Bao L., Sheng P., Li J., Wu S., Cai Q., Yao S. Surface enhanced Raman spectroscopic detection of polycyclic aromatic hydrocarbons (PAHs) using a gold nanoparticles-modified alginate gel network. *Analyst,* **2012,** 137, 4010-4015.

23. Varghese H., Panicker C. Y., Mary Y. S. IR, Raman, first hyperpolarizability and computational study of 1-chloroethyl benzene. *Mat. Sci. Res. India,* **2012,** 9, 117-121.

CHAPTER 10:

DISCUSSION AND

CONCLUSIONS

As demonstrated in this PhD work, the study of Terrestrial analogues plays a very important role in the exploration of the Solar System since they serve as a tool for the proper interpretation of the results from the planetary missions. Concretely, comparing with Mars and due to the similarities observed between both planets, the geological processes that have happened on Earth, could have happened on Mars in the past or maybe are happening nowadays.

The geochemical characterization made of all the studied emplacements in the Basque-Cantabrian basin was the main objective of this thesis. This objective has been fulfilled thanks to the spectroscopic techniques employed in the analyses of the samples. These techniques, apart from being some of those implemented in the upcoming missions by ESA and NASA (ExoMars 2022 and Mars 2020, respectively) offered very good results because the provided information was complementary.

The elemental analyses made with EDXRF in mapping mode were the starting point for all. On the one hand, the distribution of the elements observed in the maps facilitated the

subsequence molecular analyses. On the other hand, the semi-quantitative information helped in the differentiation between minerals that had similar XRD, Raman or VNIR spectra. Moreover, in the preparation of the database (*Chapter 5*), this semi-quantification allowed to establish an agreement between the EDXRF values and the expected chemical composition.

Regarding the molecular analyses, the results from XRD, Raman and VNIR made possible the identification of the minerals present in the rocks and, therefore, establish the formation processes and some relations existing between them. Thanks to XRD it was possible to confirm the results obtained by EDXRF because all the minerals detected by diffraction had the elements observed with the X-Ray fluorescence spectroscopy. Nevertheless, in some cases, it was not possible to assure which minerals were present in the samples due to the problems of XRD technique identifying phases that are not well crystallized. Besides, minerals of the same subgroup (feldspars for example) gave similar diffraction peaks. Taking into account the lower sensitivity of XRD, Raman and VNIR helped in the identification of the specific minerals present in the samples. Compounds of all the major groups of minerals were found, being the most important ones those which are expected to be present on Mars. As has been seen along this PhD work, most of the minerals present in the analogue samples have already been found on Mars. However, some others, such as gibbsite or titanite, have not been reported to be present on the Martian surface yet, and the collected spectral information will be very helpful for the interpretation of the upcoming data of the next Martian missions.

The most ubiquitous minerals were silicates and, effectively, they were the most found ones according to the identified minerals. There were three silicates, concretely from the feldspars and chlorites subgroups, which were common in all the analysed emplacements. These were albite, chamosite and clinochlore.

The presence of albite suggests that the albitization process has taken place in every emplacement. As can be seen in the Bowen's reaction series, Ca-rich feldspars (identified in some cases by XRD analyses) are the first plagioclase minerals present in the igneous rocks. They, in contact with and Na-rich environment, suffer a change in the cation forming the Na-rich feldspar (albite). This process would be more evident in the case of Meñakoz and Armintza outcrops since they are nowadays in contact with sea water (Na-rich environment). In Enekuri or Fruiz, which are not in contact with sea water, it would be more difficult to explain this process. However, the presence of this Na-feldspar even in emplacements without contact with a Na-rich environment, demonstrates its contact with this type of environments (sea water) in some moment in the past, due to their submarine character.

Chamosite and clinochlore are products of hydrothermal processes, which would be consistent with the volcanic origin of the outcrops and, moreover, it is a process that could have happened on Mars. These two minerals have different formation temperatures. Clinochlore is formed at high temperature and is therefore, associated

with the moment of the eruption of the volcano. Chamosite, in contrast, is formed at lower temperature, when the lava flow contact with sea water. These minerals are also important because they belong to the phyllosilicates groups, and as has been explained before, these minerals are of high importance for Martian exploration because they require water for their formation.

Other phyllosilicates were found in Meñakoz and Armintza emplacements. Kaolinite (kaolinite-serpentine group), illite and muscovite (micas group) were present in both emplacements. These minerals arise mainly from the decomposition of feldspars like in this case albite. Only in Meñakoz, celadonite, glauconite and montmorillonite were detected. They are also weathering products which, as were not found in the Armintza outcrop (which is in a similar environment), were associated with a different formation process and conditions. Concretely, it was supposed that the process of weathering in Meñakoz has proceeded further.

In Enekuri and Fruiz, chlorites were the only phyllosilicates found. However, only in these emplacements pyroxene minerals (diopside) were identified.

Pyroxenes are characteristic of the first steps of the weathering of igneous rocks. Therefore, taking into account that phyllosilicates are later weathering products (Bowen's reaction series), the absence of this type of minerals and the presence of pyroxenes leads to the conclusion that the weathering processes in Enekuri and Fruiz are less significant that those that are taking place in Meñakoz and Armintza.

In addition, the nesosilicate titanite was detected in Enekuri and Fruiz outcrops. Its importance lies, on the one hand, in its ability to incorporate rare elements (U or Th), which could help in the establishment of its formation process, and more important, on the other hand, it is a mineral which helps in the conservation of the biological signatures. As is commented below, Enekuri and Fruiz are the emplacements where the presence of organic molecules is more evident, which could be related with the presence of titanite.

Finally, regarding the silicates group, prehnite (inosilicate) and analcime (zeolite) were detected only in the Enekuri outcrop. Prehnite is formed hydrothermally in basic igneous rocks, which is related with the submarine volcanic character of the emplacement. In the case of zeolites, a similar process to that described for the feldspars was observed. Thanks to the XRD analyses, Ca-rich zeolites were identified (laumontite and wairakite), however, by VNIR analcime (Na-rich zeolite) was detected. This fact could be explained because, when the alkalinity and the temperature are the proper ones, Ca-rich zeolites can be altered to Na-rich ones. Even though these minerals are not in high abundance either on the Earth or on Mars, they are very important for the Martian exploration due to their capability to retain water or organic molecules.

Another group of minerals important for Martian exploration are sulfides and sulfates. Like the phyllosilicates, they need the presence of water for their formation, but also, it is thought that sulfur is one of the fundamental elements to maintain liquid water in the

Martian surface. This type of minerals was found in Meñakoz and Armintza emplacements (e. g. phyrrhotite, pyrite and jarosite). Thanks to this finding, the complete process of the formation of sulfates was explained. Besides, the presence of jarosite is very interesting for the knowledge about Mars since it may be formed due to bacterial action.

Related with the detection of organic material or the signatures of the presence of life, carbonates are of high importance. Calcite appeared in all the emplacements. It is considered a secondary mineral formed by chemical precipitation. The case of Armintza is considered the most important one for the study of carbonates since it was the only outcrop where other carbonates, apart from calcite, such as dolomite, aragonite and ankerite, could be identified.

Moreover, the vein distribution observed in Armintza is very similar to that observed on Mars, and therefore, it would be possible to establish geological similarities more easily regarding to the presence of sulfates and carbonates.

Finally, many oxides were identified in all the studied outcrops. They are important and some of the most studied minerals along the history of Martian exploration since they are the major components of the regolith and therefore the most accessible part of Mars. The most ubiquitous was quartz. As can be seen in the Bowen's series reaction, it is the last product of the weathering process. This could make sense in the case of Meñakoz or Armintza, but not for Enekuri and Fruiz because, as has been seen, these last two should be in the first stages of the weathering process. However, it has to take into account that in Enekuri and Fruiz there was a lower proportion of quartz compared with Meñakoz and Armintza.

In the case of the titanium dioxide, all its polymorphs (anatase, rutile and brookite) were identified and their formation process was associated with the different stages of the lava eruption. Rutile, due to be the high pressure and temperature polymorph could be associated with the eruption of the volcano. Anatase and brookite, as arise from alteration process, could have been formed in any moment of the formation of the outcrop. Knowledge about this type of processes on Earth may help in the interpretation of Martian data or in the assumptions made about the process that have happened there.

The last type of oxides that are very important for the Mars exploration are those of manganese. Even though, it is very difficult to characterize the exact oxide that is present in the sample because they are usually amorphous, they play a very important role in the biological cycles. They are very reactive minerals and, among the oxides, with most oxidant character.

As was stated in the *Introduction*, one of the main objectives of the planetary missions to Mars is to demonstrate the potential habitability of Mars. For that purpose, it is necessary to find evidences of life (past or present) and, therefore, another of the objectives of this thesis was to increase knowledge about the organic signatures.

Thanks to the analyses performed by ToF-SIMS, LTQ and GS-MS, the presence of organics was demonstrated. Signals related with the presence of aminoacids, aromatic compounds or long-chain alkanes could be identified. Thanks to the analyses done by Raman spectroscopy, this information was supported because bands related with the presence of such organic material could be identified. Therefore, once again, the employed techniques complement each other.

Due to the importance of this type of analysis for Martian exploration and the difficulties that they face (for example their interpretation by Raman spectroscopy), the work in this field is very relevant and has to be one of the main topics in the investigation regarding Martian analogues. Thus, all the information that we have about organic molecules may help in the interpretation of the upcoming data.

In the Mars 2020 mission, one of the instruments designed for the detection of organics is SHERLOC, which is a UV Raman spectrometer. One of the next steps is to analyse the analogue samples with a Raman with this wavelength laser, since with this laser, the detection of the organic material should be easier and the future comparison with the results obtained on Mars will be more reliable. Moreover, taking into account that in MOMA (ExoMars 2022) the employed technique for the detection of organics is a GC-MS, it would be interesting to deepen the analyses of the analogue samples with this technique.

On the other hand, the necessity of geological background was evident during the development of this PhD work. For the proper characterization, and to obtain conclusions of the formation and weathering processes, it is crucial to work together with geology experts. The transdisciplinary work would be very interesting for the proposal and establishment of Earth emplacements as Martian analogues.

Moreover, it would be very useful to analyse more outcrops of this type around the Basque-Cantabrian Basin and, therefore, have a wide area with different geological processes, which could be compared with different areas of Martian surface. Seeing the way in which the planetary missions are taking place and all the knowledge necessary to interpret the results from Mars, the study of Terrestrial Martian analogues becomes essential and study more emplacements of different characteristics has to be the procedure to follow in this type of studies. Thanks to the findings made on Earth and the spectroscopic information collected, it is possible to know the composition of Mars, and, knowing the context in which the existing minerals are, establishing their origin formation and evolution.

CHAPTER 11:

BIBLIOGRAPHY

Abdel-Shafy H. I., Mansour M. S. M. A review on polycyclic aromatic hydrocarbons: Source, environmental impact, effect on human health and remediation. *Egypt. J. Pet.* **2016,** 25, 107-123.

Achilles C. N., Downs R. T., Ming D. W., Rampe E. B., Morris R. V., Treiman A. H., Morrison S. M., Blake D. F., Vaniman D. T., Ewing R. C., Chipera S. J., Yen A. S., Bristow T. F., Ehlmann B. L., Gellert R., Hazen R. M., Fendrich K. V., Craig P. I., Grotzinger J. P., Des Marais D. J., Farmer J. D., Sarrazin P. C., Morookian J. M. Mineralogy of an active eolian sediment from the Namib dune, Gale crater, Mars. *J. Geophys. Res. Planets*, **2017,** 122, 2344-2361.

Ackerson M. PhD thesis. *Trace element partitioning between titanite and groundmass in silicic volcanic systems.* University of North Carolina, Chapel Hill, **2011.**

Adams J. B., Goullaud L. H. Plagioclase feldspars: Visible and near infrared diffuse reflectance spectra as applied to remote sensing. *Proc. Lunar Planet. Sci. Conf.,* **1978,** 3, 2901-2909.

Agirrezabala L. Kinematic indicators and mineralization on the Elgoibar fault (Basque-Cantabrian Basin). *Geogaceta,* **2001,** 30, 7-10.

Ahechu I. - Flickr https://www.flickr.com/photos/128718836@N03/ (last update 2020/05/26).

Albee A., Arvidson R., Palluconi F., Thorpe T. Overview of the Mars Global Surveyor mission. *J. Geophys. Res. Planet.,* **2001,** 106, 23291-23316.

Allwood A. C., Wade L.A., Hurowitz J.A. PIXL investigation on the Mars 2020 rover: spatially-resolved fine scale elemental chemistry and the challenging search for ancient biosignatures. *AbSciCon.* **2015,** abst. 7609.

Altheide T. S., Chevrier V. F., Dobrea E. N. Mineralogical characterization of acid weathered phyllosilicates with implications for secondary Martian deposits. *Geochim. Cosmochim. Acta,* **2010,** 74, 6232-6248.

Amils R., Fernández-Remolar, D. and the Ipbsl Team. Río Tinto: a geochemical and mineralogical terrestrial analogue of Mars. *Life,* **2014,** 4, 511-34.

Anthony J. W., Bideaux R. A., Bladh K. W., Nichols M. C. *Handbook of Mineralogy, Mineralogical Society of America, Chantilly, USA.* http://www.handbookofmineralogy.org/ (last update 2020/01/21).

Aróstegui J., Zuluaga M. C., Velasco F., Ortega-Huertas M., Nieto F. Diagenesis of the central Basque-Cantabrian Basin (Iberian Peninsula) based on illite-smectite distribution. *Clay Miner.,* **1991,** 26, 535-548.

Arvidson R. E. Introduction to special section on results from the Mars Exploration Rover Spirit and Opportunity missions. *J. Geophys. Res. Planet.,* **2008,** 113, E06S01.

Ashcroft A. E. Ionization methods in organic mass spectrometry. *The Royal Society of Chemistry,* United Kingdom. **1997**.

Ashwal L. D., Cairncross B. Mineralogy and origin of stichtite in chromite-bearing serpentinites. *Contrib. Mineral Petr.,* **1997,** 127, 75-86.

Azua-Bustos A., González-Silva C., Corsini G. The hyperarid core of the Atacama Desert, an extremely dry and carbon deprived habitat of potential interest for the field of carbon science. *Front- Microbiol.,* **2017,** 8, 993, 1-6.

Badillo J. M., Orue-Etxebarria X., Rodríguez-Lázaro J. Las facies Supraurgonianas entre La Avanzada y el Puente de Rontegui (Bizkaia) son de esas Albiense Superior. *Estudios del Instituto Alavés de la Naturaleza,* **1987,** 2, 171-177.

Baensch A. PhD thesis. *The mineralogy of the massive sulphides in the high grade Silver Swan Massive Nickel Sulphide Deposit. With an emphasis on the distribution of arsenic and cobalt mineralisation.* Western Australian School of Mines Curtin University, Kalgoorlie, Australia, **2000.**

Bakardjieva S., Stengl V., Szatmary L., Subrt J., Lukac J., Murafa N., Niznansky D., Cizek K., Jirkovsky J., Petrova N. Transformation of brookite-type TiO_2 nanocrystals to rutile: correlation between microstructure and photoactivity. *J. Mater. Chem.,* **2006,** 16, 1709-1716.

Baldridge A. M., Hook S. J., Crowley J. K., Marion G. M., Kargel J. S., Michalski J. L., Thomson B. J., de Souza Filho C. R., Bridges N. T., Brown A. J. Contemporaneous deposition of phyllosilicates and sulfates: Using Australian acidic saline lake deposits to describe geochemical variability on Mars. *Geophys. Res. Lett.,* **2009,** 36, L19201, 1-6.

Bandfield J. L., Glotch T. D., Christensen P. R. Spectroscopic identification of carbonate minerals in the Martian dust. *Science,* **2003,** 301, 1084-1087.

Bandfield J. L. Global mineral distributions on Mars. *J. Geophys. Res. Planet.,* **2002,** 107 (E6), 5042, 1-7.

Bandfield J. L, Hamilton V., Christensen P. A global view of Martian surface composition from MGS-TES. *Science,* **2000,** 287, 1626-1630.

Banerdt W., Smrekar S., Lognonné P., Spohn T., Asmar S., Banfield D., Boschi L., Christensen U., Dehant V., Folkner W., Giardini D., Goetze W., Golombek M., Grott M., Hudson T., Johnson C., Kargl G., Kobayashi N., Maki J. , Hurst K. InSight: a discovery mission to explore the interior of Mars. *LPSC 44.* **2013,** abst. 1915.

Banerjee N., Bridge N., Izawa M., Anderson L., Bebout G., Flemming R. Glassy subaqueous lavas as a habitat for life on Earth, Mars, and elsewhere? *LPSC 40,* **2009,** abst 1331.

Bao L., Sheng P., Li J., Wu S., Cai Q., Yao S. Surface enhanced Raman spectroscopic detection of polycyclic aromatic hydrocarbons (PAHs) using a gold nanoparticles-modified alginate gel network. *Analyst,* **2012,** 137, 4010-4015.

Barlow N. Mars: An introduction to its interior, surface and atmosphere. *Cambridge University Press,* UK. **2008**.

Barre P., Fernández-Ugalde O., Virto I., Velde B., Chenu C. Impact of phyllosilicate mineralogy on organic carbon stabilization in soils: incomplete knowledge and exciting prospects. *Geoderma,* **2014,** 235, 382-395.

Barth-Wirsching U., Klammer D., Kovic-Kralj P. The formation of analcime from laumontite in the Smrekovec volcanics, Northwest Slovenia - an experimental approach. *Stud. Surf. Sci. Catal.,* **1994,** 84, 299-305.

Barton I. F., Yang H., Barton M. D. The mineralogy, geochemistry, and metallurgy of cobalt in the rhombohedral carbonates. *Canad. Mineral.,* **2014,** 52, 653-669.

Beaufort D., Rigault C., Billon S., Billault V., Inoue A., Inoué S., Patrier P. Chlorite and chloritization processes through mixed-layer mineral series in low-temperature geological systems - a review. *Clay Miner.,* **2015,** 50, 497-523.

Beegle L. W., Bhartia R., Carrier B., DeFlores L., Abbey W., Asher S., Burton A., Fries M., Conrad P., Clegg S., Edgett K. S., Ehlmann B., Hug W., Reid R., Kah L., Nealson K., Nelson T., Minitti M., Popp J., Langenhorst F., Sobron P., Steele A., Tarcea N., Wiens R., Williford K., Yingst R. A. The SHERLOC investigation for Mars 2020. *LPSC 48.* **2017,** abst. 2839.

Beegle L. W., Peters G. H., Mungas G. S., Bearman G. H., Smith J. A., Anderson R. C. Mojave Martian simulant: a new Martian soil simulant. *LPSC 38.* **2007,** abst. 2005.

Bell III J. F., McCord T. B., Owensby P. D. Observational evidence of crystalline iron oxides on Mars. *J. Geophys. Res.,* **1990,** 95, 14447-14461.

Bernardini S., Bellatreccia F., Municchia A. C., Della Ventura G., Sodo A. Raman spectra of natural manganese oxides. *J. Raman Spectrosc.,* **2019,** 50, 873-888.

Bibring J. P., Langevin Y., Mustard J. F., Poulet F., Arvidson R., Gendrin A., Gondet B., Mangold N., Pinet P., Forget F., OMEGA team. Global mineralogical and aqueous mars history derived from OMEGA/Mars express data. *Science,* **2006,** 312, 400-404.

Bibring J. P, Hamm V., Pilorget C., Vago J. L., MicrOmega Team. The MicrOmega investigation onboard ExoMars. *Astrobiology,* **2017,** 17 (6, 7), 621-626.

Bishop J. L., Baker L. L., Fairén A. G., Gross C., Velbel M. A., Rampe E. B., Michalski J. R. Unraveling the diversity of early aqueous environments and climate on Mars through the phyllosilicate record. *LPSC 48,* **2017,** abst. 1804.

Bishop J. L., Lane M. D., Dyar M. D., Brown A. J. Reflectance and emission spectroscopy study of four groups of phyllosilicates: smectites, kaolinite-serpentines, chlorites and micas. *Clay Miner.,* **2008,** 43, 35-54.

Bishop J. L., Michalski J. R. Carter J. Chapter 14 - Remote detection of clay minerals. In: *Infrared and Raman spectroscopies of clay minerals.* Eds. Gates W. P., Kloprogge J. T., Madejová J., Bergaya F. *Elsevier,* **2017,** pp. 482-514.

Bishop J. L., Velbel M. A. Comparison of phyllosilicates observed on the surface of Mars with those found in Martian meteorites. *80th Annual Meeting of the Meteoritical Society.* **2017,** abst. 6115.

Bishop J. L., Englert P. A. J., Patel S., Tirsch D., Roy A. J., Koeberl C., Boettger U., Hanke F., Jaumann R. Mineralogical analyses of surface sediments in the Antarctic Dry Valleys: coordinated analyses of Raman spectra, reflectance spectra and elemental abundances. *Phil. Trans. R. Soc. A,* **2014,** 372, 20140198, 1-26.

Bishop J. L., Schelble R. T., McKay C. P., Brown A. J., Perry K. A. Carbonate rocks in the Mojave Desert as an analogue for Martian carbonates. *Int. J. Astrobiol.,* **2011,** 10, 349-358.

Blanco Y., Gallardo-Carreno I., Ruiz-Bermejo M., Puente-Sánchez F., Cavalcante-Silva E., Quesada A., Prieto-Ballesteros O., Parro V. Critical assessment of analytical techniques in the search for biomarkers on Mars: A mummified microbial mat from Antarctica as a best-case scenario. *Astrobiology,* **2017,** 17, 984-996.

Bloise A., Dattola L., Allegretta I., Terzano R., Miriello D. Linarite and connellite dataset from Calabria region (Southern Italy): First evidence. *Data in Brief,* **2019,** 27, 104597, 1-8.

Board S. S., National Research Council An astrobiology strategy for the exploration of Mars. *National Academies Press,* **2007**.

Bost N., Ramboz C., Foucher F., Westall F. The Skouriotissa mine: a new terrestrial analogue for hydrated minerals formation on early Mars. *Analog Sites for Mars Missions II.* **2013,** abst. 4006.

Bost N. PhD thesis. *Geochemical and mineralogical analysis of Mars analogue materials and the creation of the International Space Analogue Rock Store (ISAR).* Université d'Orléans, France, **2012.**

Boynton W. V., Ming D. W., Kounaves S. P., Young S. M. M., Arvidson R. E., Hecht M. H., Hoffman J., Niles P. B., Hamara D. K., Quinn R. C., Smith P. H., Sutter B., Catling D. C., Morris R. V. Evidence for Calcium Carbonate at the Mars Phoenix Landing Site. *Science,* **2009,** 325, 61-64.

Bridges J. C., Hicks L.J., Treiman A.H. Chapter 5: Carbonates on Mars. In: *Volatiles in the Martian crust.* Ed. Filiberto J. and Schwenzer S.P. *Elsevier,* **2018,** pp. 89-118.

Bridges J. C., Schwenzer S. P., Leveille R., Westall F., Wiens R. C., Mangold N., Bristow T., Edwards P., Berger G. Diagenesis and clay mineral formation at Gale Crater, Mars. *J. Geophys. Res. Planet.,* **2015,** 120, 1-19.

Brown W. L., Parsons I. Feldspars in igneous rocks. In: *Feldspars and their reactions.* Ed. Parsons I. *Springer,* Dordrecht. **1994,** pp. 449-499.

Bruuning C., Hellweg S., Dambach S., Lipinsky D., Arlinghaus H. F. Improving the interpretation of ToF-SIMS measurements on adsorbed proteins using PCA. *Surf. Interface Anal.,* **2006,** 38, 191-193.

Buchs D. M., Howie R. A. Pyroxenes. In: *Reference module in Earth systems and environmental sciences. Elsevier,* **2016,** pp. 1-4.

Cannon K. M., Mustard J. F., Salvatore M. R. Alteration of immature sedimentary rocks on Earth and Mars: Recording aqueous and surface-atmosphere processes. *Earth Planet. Sci. Lett.,* **2015,** 417, 78-86.

Carr M. H. The surface of Mars. *Cambridge University Press,* Cambridge. **2007**.

Carr M. H, Head J. Geologic history of Mars. *Earth Planet. Sci. Lett.,* **2010,** 294, 185-203.

Carracedo-Sánchez M., Sarrionandia F., Juteau T. El vulcanismo submarino de edad cretácica de la Cuenca Vasco-Cantábrica. *Macla,* **2012,** 16, 260-267.

Carracedo-Sánchez M., Sarrionandia F., Juteau T., Gil-Ibarguchi J. I. Structure and organization of submarine basaltic flows: sheet flow transformation into pillow lavas in shallow submarine environments. *Int. J. Earth Sci.,* **2012,** 101, 2201-2214.

Carracedo-Sánchez M., Larrea F., Alonso A. Estructura y organización de las coladas submarinas: características de las lavas almohadilladas de edad cretácica que afloran en la Cordillera Vasco-Cantábrica. *Estudios Geológicos,* **1999,** 55, 209-222.

Carter J., Quantin C., Thollot P., Loizeau D., Ody A., Lozach L. Oxia Planum, a clay-laden landing site proposed for the ExoMars rover mission: aqueous mineralogy and alteration scenarios. *LPSC 47.* **2016,** abst. 2064.

Castañares L. M., Robles S., Vicente J. C. Distribución estratigráfica de los episodios volcánicos submarinos del Albiente-Santoniense en la Cuenca Vasca (sector Gernika-Plentzia, Bizkaia). *Geogaceta,* **1997,** 22, 43-46.

Cavalazzi B., Agangi A., Barbieri R., Franchi F., Gasparotto G. The formation of low-temperature sedimentary pyrite and its relationship with biologically-induced processes. *Geol. Ore Deposits,* **2014,** 56, 395-408.

Çelik-Karakaya M., Karakaya N., Yavuz F. Geology and conditions of formation of the zeolite-bearing deposits Southeast of Ankara (Central Turkey). *Clays Clay Miner.,* **2015,** 63, 85-109.

Chen P. Y., Wang M. K., Yang D. S. Mineralogy of dickite and nacrite from northern Taiwan. *Clays Clay Miner.,* **2001,** 49, 586-595.

Churchman G. J., Lowe, D. J. Alteration, formation and occurrence of minerals in soils. In: *Handbook of soil science. 2nd edition.* Ed. Huang P. M., Li Y., Sumner M.E. *CRC Press,* Boca Raton, FL. **2012,** pp. 20.1.

Ciarletti V., Clifford S., Plettemeier D., Le Gall A., Herve Y., Dorizon S., Quantin-Nataf C., Benedix W., Schwenzer S., Pettinelli E., Heggy E., Herique A., Berthelier J., Kofman W., Vago J. L., Hamran S., Wisdom Team. The WISDOM Radar: Unveiling the Subsurface Beneath the ExoMars Rover and Identifying the Best Locations for Drilling. *Astrobiology,* **2017,** 17 (6, 7), 565-584.

Citron R. I., Manga M., Tan E. A hybrid origin of the Martian crustal dichotomy: Degree-1 convection antipodal to a giant impact. *Earth Planet. Sci. Lett.* **2018,** 491, 58-66.

Clark R. N., Swayze A. R., Wise G., Livo E., Hoefen, T., Kokaly, R., Sutley, S. J. *USGS digital spectral library splib06a: U.S. Geological Survey, Digital Data Series 231.* http://speclab.cr.usgs.gov/spectral.lib06 (last update 2020/01/21).

Cloutis E. A., Asher P. M., Mertzman S. A. Spectral reflectance properties of zeolites and remote sensing implications. *J. Geophys. Res. Planet.,* **2002,** 107 (E9), 5067, 1-19.

Cloutis E. A., Craig M. A., Kruzelecky R. V., Jamroz W. R., Scott A., Hawthorne F. C., Mertzman S. A. Spectral reflectance properties of minerals exposed to simulated Mars surface conditions. *Icarus,* **2008,** 195, 140-168.

Cloutis E. A. Pyroxene reflectance spectra: Minor absorption bands and effects of elemental substitutions. *J. Geophys. Res.,* **2002,** 107, 6-1; 6-12.

Cloutis E. A., Mann P., Izawa M. R. M., Applin D. M., Samson C., Kruzelecky R., Glotch T. D., Mertzman S. A., Mertzman K. R., Haltigin T. W., Fry C. The Canadian space agency planetary analogue materials suite. *Planet. Space Sci.,* **2015,** 119, 155-172.

Coates A. J., Jaumann R., Griffiths A. D., Leff C. E., Schmitz N., Josset J. -., Paar G., Gunn M., Hauber E., Cousins C. R., Cross R. E., Grindrod P., Bridges J. C., Balme M., Gupta S., Crawford I. A., Irwin P., Stabbins R., Tirsch D., Vago J. L., Theodorou T., Caballo-Perucha M., Osinski G. R., PanCam Team. The PanCam instrument for the ExoMars rover. *Astrobiology,* **2017,** 17 (5, 6), 511-541.

Cornell, R. M., Schwertmann, U. The iron oxides. Structure, properties, reactions, occurrences and uses. *WILEY-VCH,* Germany. **2003**.

Craig P. I., Ming D. W., Rampe E. B. Sulfate formation from acid-weathered phyllosilicates: Implications for the aqueous history of Mars. *Eight International Conference on Mars,* **2014,** abst. 1323.

Craig P., Chevrier V., Sayyed M. R. G., Islam R. Spectral analysis of Deccan intrabasaltic bole beds: Implications for the formation and alteration of phyllosilicates on Mars. *Planet. Space Sci.,* **2017,** 135, 55-63.

Cuevas J., Garrote A., Tubía J. M. Análisis y significado de diferentes tipos de estructuras en el magmatismo del cretácico superior de la cuenca Vasco-Cantábrica (1ª Parte). *Munibe. Sociedad de Ciencias ARANZADI,* **1981,** 1-2, 1-20.

Dall' Osto M., Harrison R. Urban organic aerosols measured by single particle mass spectrometry in the megacity of London. *Atmos. Chem. Phys,* **2012,** 12, 4127-4142.

Darling D. S. D. The extraterrestrial encyclopedia. *First Edition Design Pub,* Florida, EEUU. **2016**.

de Oliveira J. F., Brossard M., Corazza E. J., Marchão R. L., de Fátima Guimarães M. Visible and near Infrared spectra of ferralsols according to their structural features. *J. Near Infrared Spectrosc.,* **2016,** 24, 243-254.

de Sanctis M. C., Altieri F., Ammannito E., Biondi D., De Angelis S., Meini M., Mondello G., Novi S., Paolinetti R., Soldani M., Mugnuolo R., Pirrotta S., Vago J. L., Ma Miss Team. Ma-MISS on ExoMars: mineralogical characterization of the Martian subsurface. *Astrobiology,* **2017,** 17 (6, 7), 612-620.

Dickinson W. W., Rosen M. R. Antarctic permafrost: An analogue for water and diagenetic minerals on Mars. *Geology,* **2003,** 31, 199-202.

Ding S., Dasgupta R., Tsuno K. Sulfur concentration of Martian basalts at sulfide saturation at high pressures and temperatures - Implications for deep sulfur cycle on Mars. *Geochim. Cosmochim. Acta,* **2014,** 131, 227-246.

Dufresne W. J. B., Rufledt C. J., Marshall C. P. Raman spectroscopy of the eight natural carbonate minerals of calcite structure. *J. Raman Spectrosc.,* **2018,** 49, 1999-2007.

Edwards H. G. M., Farwell D. W., Grady M. M., Wynn-Williams D. D., Wright I. P. Comparative Raman microscopy of a Martian meteorite and Antarctic lithic analogues. *Planet. Space Sci.,* **1999,** 47, 353-362.

Edwards H. G. M., Villar S. E. J., Jehlička J., Munshi T. FT–Raman spectroscopic study of calcium-rich and magnesium-rich carbonate minerals. *Spectrochim. Acta A Mol. Biomol. Spectrosc.* **2005,** 61, 2273-2280.

Egea-González I., Jiménez-Díaz A., Parro L. M., Mansilla F., Holmes J. A., Lewis S. R., Patel M. R., Ruiz J. Regional heat flow and subsurface temperature patterns at Elysium Planitia and Oxia Planum areas, Mars. *Icarus,* **2019,** 113379.

Ehlmann B. L., Bish D. L., Ruff S. W., Mustard J. F. Mineralogy and chemistry of altered Icelandic basalts: Application to clay mineral detection and understanding aqueous environments on Mars. *J. Geophys. Res. Planet.,* **2012,** 117, E00J16, 1-27.

Ehlmann B. L., Edwards C. S. Mineralogy of the Martian surface. *Annu. Rev. Earth Planet. Sci.,* **2014,** 42, 291-315.

Ehlmann B. L., Mustard J. F., Swayze G. A., Clark R. N., Bishop J. L., Poulet F., Des Marais D. J., Roach L. H., Milliken R. E., Wray J. J., Barnouin-Jha O., Murchie S. L. Identification of hydrated silicate minerals on Mars using MRO-CRISM: Geologic context near Nili Fossae and implications for aqueous alteration. *J. Geophys. Res. Planet.,* **2009,** 114, E00D08, 1-33.

Eigenbrode J., Summons R., Steele A., Freissinet C., Millan M., Navarro-Gonzalez R., Sutter B., Mcadam A., Franz H., Glavin D., Archer P., Mahaffy P., Conrad P., Hurowitz J., Grotzinger J., Gupta S., Ming D., Sumner D., Szopa C., Coll P. Organic matter preserved in 3-billion-year-old mudstones at Gale crater, Mars. *Science,* **2018,** 360, 1096-1101.

El-Baz F. The geology of Egypt. *Leiden E. J. BRILL,* The Netherlands. **1984**.

Ellert M. PhD thesis. *Calibration and characterization of a nin-imagin field spectroradiometer supporting imagin spectrometer validation and hyperspectral sensor modelling.* Universität Zürich, Zürich, **1998.**

El-Maarry M., Black S., Hynek B., Mchenry L. Mineralogy of fumarolic deposits from Iceland as analogs for ancient hydrothermal systems on Mars: role of temperature. *LPSC 48.* **2017,** abst. 2870.

English P. M. Formation of analcime and moganite at Lake Lewis, central Australia: significance of groundwater evolution in diagenesis. *Sediment. Geol.* **2001,** 143, 219-244.

European Space Agency. *ESA tests self-steering rover in 'Mars' desert.* http://www.esa.int/Enabling_Support/Space_Engineering_Technology/ESA_tests_self-steering_rover_in_Mars_desert (last update 2020/05/26).

European Space Agency. *ExoMars Mission 2022.* https://exploration.esa.int/web/mars/-/48088-mission-overview (last update 2020/04/27).

European Space Agency. *Mars sample return.* https://www.esa.int/Science_Exploration/Human_and_Robotic_Exploration/Exploration/Mars_sample_return (last update 2020/04/27).

European Space Agency. *Robotic exploration of Mars - Oxia Planum.* https://exploration.esa.int/web/mars/-/54724-oxia-planum (last update 2020/04/27).

Eusko Jaularitza/Gobierno Vasco *geoEuskadi, Infraestructura de Datos Espaciales de Euskadi.* https://www.geo.euskadi.eus/s69-bisorea/es/x72aGeoeuskadiWAR/index.jsp (last update 2020/07/23).

Fernández-Remolar D., Prieto-Ballesteros O., Rodríguez N., Gómez F., Amils R., Gómez-Elvira J., Stoker C. Underground habitats in the Río Tinto basin: a model for subsurface life habitats on Mars. *Astrobiology,* **2008,** 8 (5), 1023-1047.

Fernández-Remolar D. C., Morris R. V., Gruener J. E., Amils R., Knoll A. H. The Río Tinto basin, Spain: Mineralogy, sedimentary geobiology, and implications for

interpretation of outcrop rocks at Meridiani Planum, Mars. *Earth Planet. Sci. Lett.,* **2005,** 240, 149-167.

Fernández-Remolar D. C., Sánchez-Román M., Amils R. The case of the lacking carbonates and the emergence of early life on Mars. *Sustainability,* **2010,** 2, 2541-2554.

Ferralis N., Matys E. D., Knoll A. H., Hallmann C., Summons R. E. Rapid, direct and non-destructive assessment of fossil organic matter via micro-Raman spectroscopy. *Carbon,* **2016,** 108, 440-449.

Fong T., Bualat M., Deans M., Adams B., Allan M., Altobelli M., Bouyssounouse X., Cohen T., Flueckiger L., Garber J. Robotic follow-up for human exploration. **2010,** 25.

Fox N., Parbhakar-Fox A., Moltzen J., Feig S., Goemann K., Huntington J. Applications of hyperspectral mineralogy for geoenvironmental characterisation. *Minerals Eng,* **2017,** 107, 63-77.

Francis J. *10 Adventurous Things To Do In Mojave Desert, CA - TOURIST SECRETS.* https://www.touristsecrets.com/destinations/10-adventurous-things-to-do-in-mojave-desert-ca/ (last update 2020/05/26).

Freeman J. J., Wang A., Kuebler K. E., Jolliff B. L., Haskin L. A. Characterization of natural feldspars by Raman spectroscopy for future planetary exploration. *Can. Mineral.,* **2008,** 46, 1477-1500.

Freissinet C., Glavin D. P., Mahaffy P. R., Miller K. E., Eigenbrode J. L., Summons R. E., Brunner A. E., Buch A., Szopa C., Archer Jr. P. D., Franz H. B., Atreya S. K., Brinckerhoff W. B., Cabane M., Coll P., Conrad P. G., Des Marais D. J., Dworkin J. P., Fairén A. G., François P., Grotzinger J. P., Kashyap S., ten Kate I. L., Leshin L. A., Malespin C. A., Martin M. G., Martin-Torres F., McAdam A. C., Ming D. W., Navarro-González R., Pavlov A. A., Prats B. D., Squyres S. W., Steele A., Stern J. C., Sumner D. Y., Sutter B., Zorzano M. -., the MSL S. T. Organic molecules in the Sheepbed Mudstone, Gale Crater, Mars. *J. Geophys. Res. Planets,* **2015,** 120, 495-514.

Frost R., Xi Y. Raman spectroscopic study of the minerals apophyllite-(KF) ($KCa_4Si_8O_{20}F\cdot8H_2O$) and apophyllite-(KOH) ($KCa_4Si_8O_{20}(F,OH)\cdot8H_2O$). *J. Mol. Struct.,* **2012,** 1028, 200-207.

Gammons C., Harris L., Castro J., Cott P., Hanna B. Creating lakes from open pit mines: processes and considerations, with emphasis on northern environments. Canadian Technical Report of Fisheries and Aquatic Sciences. *Can. Tech. Rep. Fish. Aquat. Sci. 2826,* Canada. **2009**.

García-Florentino C., Maguregui M., Morillas H., Marcaida I., Madariaga J. M. A fast in situ non-invasive approach to classify mortars from a construction of high historical value. *Microchem. J.* **2017,** 133, 104-113.

García-Mondéjar J., Agirrezabala L., Aranburu A., Fernández-Mendiola K., Gómez-Pérez I., López-Horgue M., Rosales I. The Aptian-Albian tectonic pattern of the Basque Cantabrian Basin (Northern Spain). *Geol. J.,* **1996,** 31, 13-45.

García-Mondéjar J. G., Pujalte V. The black flysch (Upper Albian-Lower Cenomanian) in the Bay of Arminza, Vizcaya. *6th Eur. Meet. IAS,* **1985,** 307-392.

García-Mondéjar J., Carracedo-Sánchez M., Owen H. G., Fernández-Mendiola P. A. The Early Aptian volcanic episode of Gutiolo (N Spain): Expression of the Bilbao Rift Fault Zone. *Geol. J.,* **2019,** 54, 3509-3526.

Gavin P. PhD thesis. *Stability of phyllosilicates on Mars.* University of Arkansas, EEUU, **2012.**

Gendrin A., Mangold N., Bibring J., Langevin Y., Gondet B., Poulet F., Bonello G., Quantin C., Mustard J. F, Arvidson R., LeMouélic S. Sulfates in Martian layered terrains: the OMEGA/Mars Express view. *Science,* **2005,** 307, 1587-1591.

Gibson E. K., Wentworth S. J., McKay D. S. Chemical weathering and diagenesis of a cold desert soil from Wright Valley, Antarctica: An analog of Martian weathering processes. *J. Geophys. Res. Sol. Ea.,* **1983,** 88, A912-A928.

Glaccum R., Boström K. (Na, K)-phillipsite: Its stability conditions and geochemical role in the deep sea. *Mar. Geol.* **1976,** 21, 47-58.

Goesmann F., Brinckerhoff W. B., Raulin F., Goetz W., Danell R. M., Getty S. A., Siljeström S., Missbach H., Steininger H., Arevalo R. D.,Jr., Buch A., Freissinet C., Grubisic A., Meierhenrich U. J., Pinnick V. T., Stalport F., Szopa C., Vago J. L., Lindner R., Schulte M. D., Brucato J. R., Glavin D. P., Grand N., Li X., van Amerom F. H. W., Moma Science Team. The Mars Organic Molecule Analyzer (MOMA) instrument: characterization of organic material in Martian sediments. *Astrobiology,* **2017,** 17 (6, 7), 655-685.

Golden D. C., Ming D., Schwandt C., Lauer H., Socki R., Morris R., Lofgren G., McKay G. A simple inorganic process for formation of carbonates, magnetite, and sulfides in Martian meteorite ALH84001. *Am. Mineral.,* **2001,** 86, 370-375.

Golombek M., Cook R., Economou T., Folkner W., Haldemann A., Kallemeyn P., Knudsen J., Manning R., Moore H., Parker T., Rieder R., Schofield J., Smith P., Vaughan R. Overview of the Mars Pathfinder Mission and assessment of landing site predictions. *Science,* **1997,** 278, 1743-1748.

Gómez-Nubla L., Aramendia J., Fdez-Ortiz de Vallejuelo S., Alonso-Olazabal A., Castro K., Cruz Zuluaga M., Angel Ortega L., Murelaga X., Madariaga J. M. Multispectroscopic methodology to study Libyan desert glass and its formation conditions. *Anal. Bioanal. Chem.,* **2017,** 409, 3597-3610.

Grant J. A., Golombek M. P., Wilson S. A., Farley K. A., Williford K. H., Chen A. The science process for selecting the landing site for the 2020 Mars rover. *Planet. Space Sci.,* **2018,** 164, 106-126.

Grotzinger J. P., Crisp J. A., Vasavada A. R., MSL Sci Team. Curiosity's mission of exploration at Gale Crater, Mars. *Elements,* **2015,** 11, 19-26.

Haldar S. K., Tišljar J. Chapter 2 - Basic mineralogy. In: *Introduction to mineralogy and petrology.* Eds. Haldar S. K., Tišljar J. *Elsevier,* Oxford. **2014,** pp. 39-79.

Haldar S. K., Tišljar J. Chapter 4 - Igneous rocks. In: *Introduction to mineralogy and petrology.* Eds. Haldar S. K., Tišljar J. *Elsevier,* Oxford. **2014,** pp. 93-120.

Hall A. J. Pyrite-pyrrhotine redox reactions in nature. *Mineral. Mag.,* **1986,** 50, 223-229.

Hamran S., Amundsen H.E.F., Asak L., Berger T., Brovoll S., Buskenes J.I., Carter L., Damsgård L., Diaz C., Ghent R., Helleren Ø., Kohler J., Mellon M., Nunes D., Paige D., Plettemeier D., Rowe K., Russell P., Sagsveen B., Ødegaard N., Øyan M.J. The RIMFAX GPR instrument development for the Mars 2020 rover mission. *3rd International Workshop on Instrumentation for Planetary Missions.* **2016,** abst. 4031.

Hanesch M. Raman spectroscopy of iron oxides and (oxy)hydroxides at low laser power and possible applications in environmental magnetic studies. *Geophys. J. Int.,* **2009,** 177, 941-948.

Harris J. K., Cousins C. R., Gunn M., Grindrod P. M., Barnes D., Crawford I. A., Cross R. E., Coates A. J. Remote detection of past habitability at Mars-analogue hydrothermal alteration terrains using an ExoMars Panoramic Camera emulator. *Icarus,* **2015,** 252, 284-300.

Hartmann W. K., Neukum G. Cratering chronology and the evolution of Mars. *Space Sci. Rev.,* **2001,** 96, 165-194.

Hatchell D. C. Analytical Spectral Devices, Inc. (ASD) Technical Guide. 3rd Ed. **1999**.

Hattori K., Cameron E. M. Archean magmatic sulfate. *Nature,* **1986,** 319, 45-47.

Horgan B. H. N., Anderson R. B., Dromart G., Amador E. S., Rice M. S. The mineral diversity of Jezero crater: Evidence for possible lacustrine carbonates on Mars. *Icarus.* **2020,** 339, 113526.

Horgan B. H. N., Cloutis E. A., Mann P., Bell J. F. Near-infrared spectra of ferrous mineral mixtures and methods for their identification in planetary surface spectra. *Icarus.* **2014,** 234, 132-154.

Hrön R. *Mývatn in North-Iceland - Part IV - Mt. Námafjall, Krafla & Leirhnjúkur Geothermal Areas - GUIDE TO ICELAND.* https://guidetoiceland.is/connect-with-locals/regina/the-amazing-myvatn-area---part-iv (last update 2020/05/26).

Huang E., Chen C. H., Huang T., Lin E. H., Xu J. A. Raman spectroscopic characteristics of Mg-Fe-Ca pyroxenes. *Am. Mineral.,* **2000,** 85, 473-479.

Huang P. M., Wang M. K. MIinerals, Primary. In: *Encyclopedia of soils in the environment.* Ed. Hillel D. *Elsevier,* Oxford. **2005,** pp. 500-510.

Huggett J. M. Clay Minerals. In: *Encyclopedia of Geology. Elsevier,* London. **2015,** pp. 358-365.

Hughes S. S., Haberle C. W., Nawotniak S. E. K., Sehlke A., Garry W. B., Elphic R. C., Payler S. J., Stevens A. H., Cockell C. S., Brady A. L., Heldmann J. L., Lim D. S. S. Basaltic terrains in Idaho and Hawaii as planetary analogues for Mars geology and astrobiology. *Astrobiology,* **2019,** 19, 260-283.

Hunziker J. C., Frey M., Clauer N., Dallmeyer R. D., Friedrichsen H., Flehmig W., Hochstrasser K., Roggwiler P., Schwander H. The evolution of illite to muscovite -

Mineralogical and isotopic data from the Glarus Alps, Switzerland. *Contrib. Mineral. Petrol.,* **1986,** 92, 157-180.

Ibarrondo I., Prieto-Taboada N., Martínez-Arkarazo I., Madariaga J. M. Resonance Raman imaging as a tool to assess the atmospheric pollution level: carotenoids in Lecanoraceae lichens as bioindicators. *Environ. Sci. Pollut. R.,* **2016,** 23, 6390-6399.

In Memorian Ngaire Hart - Flickr https://www.flickr.com/photos/eriagn/28731154224/ (last update 2020/05/26).

Instituto Geológico y Minero de España http://www.igme.es/ (last update 2020/07/23).

Ivarsson M., Sallstedt T., Carlsson D. Morphological biosignatures in volcanic rocks - Applications for life detection on Mars. *Front. Earth Sci.,* **2019,** 7, 91-114.

Japan Aerospace Exploration Agency *Martian Moons eXploration (MMX) mission.* http://mmx.isas.jaxa.jp/en/ (last update 2020/04/27).

Yingzhuo J., Yu F., Yongliao Z. Scientific objectives and payloads of Chinese first Mars exploration. *Chinese Journal of Space Science,* **2018,** 38 (5), 650-655.

Josset J., Westall F., Hofmann B. A., Spray J., Cockell C., Kempe S., Griffiths A. D., De Sanctis M. C., Colangeli L., Koschny D., Follmi K., Verrecchia E., Diamond L., Josset M., Javaux E. J., Esposito F., Gunn M., Souchon-Leitner A. L., Bontognali T. R. R., Korablev O., Erkman S., Paar G., Ulamec S., Foucher F., Martin P., Verhaeghe A., Tanevski M., Vago J. L. The Close-Up Imager onboard the ESA ExoMars rover: objectives, description, operations, and science validation activities. *Astrobiology,* **2017,** 17 (6, 7), 595-611.

Kalli I. - Wordpress *Cyprus - Copper - Site.* https://ikallioutoforder.wordpress.com/2016/11/08/copper-cyprus-site/ (last update 2020/05/26).

Kaplan H. H., Milliken R. E., Fernandez-Remolar D., Amils R., Robertson K., Knoll A. H. Orbital evidence for clay and acidic sulfate assemblages on Mars based on mineralogical analogs from Río Tinto, Spain. *Icarus,* **2016,** 275, 45-64.

Kato Y., Suzuki K., Nakamura K., Hickman A., Nedachi M., Kusakabe M., Bevacqua D. C., Ohmoto H. Hematite formation by oxygenated groundwater more than 2.76 billion years ago. *Earth Planet. Sci. Lett.,* **2009,** 278, 40-49.

Kerr A., Rafuse H., Sparkes G., Hinchey J., Sandeman H. Visible/Infrared spectroscopy as a research tool in economic geology: background and pilot studies from New Fouland and Labrador. *Current Research,* **2011,** Report 11-1, 145-166.

Khisina N. R., Khramov D. A., Kolosov M. V., Kleschev A. A., Taylor L. A. Formation of ferriolivine and magnesioferrite from Mg-Fe-olivine - Reactions and kinetics of oxidation. *Phys. Chem. Miner.,* **1995,** 22, 241-250.

Kilias S., Chatzitheodoridis E., Lyon I. Molecular, chemical and morphological evidence for hematite biogenicity at the Quaternary Cape Vani Mn-(Ba-Fe) deposit, Milos, Greece. *B. Geol. Soc. Greece,* **2013,** 47 (2), 834-842.

Klingelhöfer G., DeGrave E., Morris R. V., Van Alboom A., de Resende V. G., De Souza P. A., Rodionov D., Schröder C., Ming D. W., Yen A. Mössbauer spectroscopy on Mars: goethite in the Columbia Hills at Gusev crater. *Hyperfine Interact.,* **2005,** 166, 549-554.

Klingelhöfer G., Morris R. V., Bernhardt B., Schröder C., Rodionov D. S., de Souza P. A., Yen A., Gellert R., Evlanov E. N., Zubkov B., Foh J., Bonnes U., Kankeleit E., Gütlich P., Ming D. W., Renz F., Wdowiak T., Squyres S. W., Arvidson R. E. Jarosite and hematite at Meridiani Planum from Opportunity's Mössbauer spectrometer. *Science,* **2004,** 306, 1740-1745.

Kodera P., Murphy P. J., Rankin A. H. Retrograde mineral reactions in saline fluid inclusions: The transformation ferropyrosmalite clinopyroxene. *Am. Mineral.,* **2003,** 88, 151-158.

Kokaly R. F., Clark R. N., Swayze G. A., Livo K. E., Hoefen T. M., Pearson N. C., Wise R. A., Benzel W. M., Lowers H. A., Driscoll R. L., Klein A. J. USGS spectral library version 7. *Data Series.* **2017,** 68.

Korablev O. I., Dobrolensky Y., Evdokimova N., Fedorova A. A., Kuzmin R. O., Mantsevich S. N., Cloutis E. A., Carter J., Poulet F., Flahaut J., Griffiths A., Gunn M., Schmitz N., Martin-Torres J., Zorzano M., Rodionov D. S., Vago J. L., Stepanov A. V., Titov A. Y., Vyazovetsky N. A., Trokhimovskiy A. Y., Sapgir A. G., Kalinnikov Y. K., Ivanov Y. S., Shapkin A. A., Ivanov A. Y. Infrared spectrometer for ExoMars: a mast-mounted instrument for the rover. *Astrobiology,* **2017,** 17 (6, 7), 542-564.

Košek F., Culka A., Drahota P., Jehlička J. Applying portable Raman spectrometers for field discrimination of sulfates: Training for successful extraterrestrial detection: Raman spectrometers for field discrimination of sulfates. *J. Raman Spectrosc.,* **2017,** 48, 1085-1093.

Labsphere (R) Technical guide. Reflectance materials and coatings. *www. labsphere. com.*

Lafuente B., Downs R. T., Yang H., Stone, N. The power of databases: the RRUFF project. In: *Highlights in mineralogical crystallography.* Ed. T. Armbruster, R. M. Danisi. *W. De Gruyter,* Berlin. **2015,** pp. 1-30.

Lalla E. A. PhD thesis. *Tenerife as Martian analogue: Multianalytic characterization (Raman, DRX, ATR-FTIR, SEM and MössBauer) of samples with planetary and artrobiological interest.* University of Valladolid, Valladolid, **2014.**

Lanza N. L., Wiens R. C., Arvidson R. E., Clark B. C., Fischer W. W., Gellert R., Grotzinger J. P., Hurowitz J. A., McLennan S. M., Morris R. V., Rice M. S., Bell,James F.,,III, Berger J. A., Blaney D. L., Bridges N. T., Calef,Fred,,III, Campbell J. L., Clegg S. M., Cousin A., Edgett K. S., Fabre C., Fisk M. R., Forni O., Frydenvang J., Hardy K. R., Hardgrove C., Johnson J. R., Lasue J., Le Mouelic S., Malin M. C., Mangold N., Martin-Torres J., Maurice S., McBride M. J., Ming D. W., Newsom H. E., Ollila A. M., Sautter V., Schroder S., Thompson L. M., Treiman A. H., VanBommel S., Vaniman D. T., Zorzano M. Oxidation of manganese in an ancient aquifer, Kimberley formation, Gale crater, Mars. *Geophys. Res. Lett.,* **2016,** 43, 7398-7407.

Larkin P. IR and Raman spectra-structure correlations: Characteristic group frequencies. In: *Infrared and Raman spectroscopy: principles and spectral interpretation. Elsevier,* USA. **2011,** pp. 73-115.

Lebreton G. - Locationscout *Námafjall Hverir - Iceland.* https://www.locationscout.net/iceland/1881-namafjall-hverir (last update 2020/05/26).

Lee P., Bunch T. E., Cabrol N., Cockell C. S., Grieve R. A. F., McKay C. P., Rice J. W. Jr., Schutt J. W., Zent A. P. Haughton-Mars 97 - I: Overview of observations at the Haughton impact crater, a unique Mars analog site in the Canadian High Arctic. *LPSC 29.* **1998,** abst. 1973.

Leman J. *What's So Special About the Atacama Desert? - LIVE SCIENCE.* https://www.livescience.com/64752-atacama-desert.html (last update 2020/05/26).

Leone N., Mercurio M., Grilli E., Leone A. P., Langella A., Buondonno A. Potential of vis-NIR reflectance spectroscopy for the mineralogical characterization of synthetic gleys: a preliminary investigation. *Period. di Mineral.,* **2011,** 80, 433-453.

Levy E. H., Solomon S. C. The science of planetary exploration. *The National Academies Press,* Washington, DC. **1979**.

Lewis J. S. Chapter 1: Introduction. In: *Physics and chemistry of the Solar System.* Ed. Lewis J. S. *Academic Press,* London. **1995,** pp. 1-4.

Lewis J. S. Chapter 3: General description of the Solar System. In: *Physics and chemistry of the Solar System.* Ed. Lewis J. S. *Academic Press,* London. **1995,** pp. 44-65.

Li X., Danell R. M., Brinckerhoff W. B., Pinnick V. T., van Amerom F., Arevalo R. D.,Jr., Getty S. A., Mahaffy P. R., Steininger H., Goesmann F. Detection of trace organics in Mars analog samples containing perchlorate by laser desorption/ionization mass spectrometry. *Astrobiology,* **2015,** 15, 104-110.

Liou J. G. Stilbite-laumontite equilibrium. *Contrib. Mineral. Petr.,* **1971,** 31, 171-177.

Liu Y., Catalano J. G. Implications for the aqueous history of southwest Melas Chasma, Mars as revealed by interbedded hydrated sulfate and Fe/Mg-smectite deposits. *Icarus,* **2016,** 271, 283-291.

López-Horgue M. A., Owen H. G., Aranburu A., Fernández-Mendiola P. A., García-Mondéjar J. Early late Albian (Cretaceous) of the central region of the Basque-Cantabrian Basin, northern Spain: biostratigraphy based on ammonites and orbitolinids. *Cretaceous Res.,* **2009,** 30, 385-400.

Lorand J., Pont S., Chevrier V., Luguet A., Zanda B., Hewins R. Petrogenesis of Martian sulfides in the Chassigny meteorite. *Am. Mineral.,* **2018,** 103, 872-885.

Madariaga J. M., Torre-Fdez I., Ruiz-Galende P., Aramendia J., Gómez-Nubla L., Fdez-Ortiz de Vallejuelo S., Maguregui M., Castro K. , Arana G. Advanced analytical methodologies based on Raman spectroscopy to detect prebiotic and biotic molecules: Applicability in the study of the Martian nakhlite NWA 6148 meteorite. *2nd International Mars Sample return.* **2018,** abst. 6114.

Martín-Chivelet J., Berástegui X., Rosales I., Vilas L., Vera J. A., Caus E., Gräfe K-U., Mas R., Puig C., Segura M., Robles S., Floquet M., Quesada S., Ruiz-Ortiz P. A., Fregenal-Martínez M. A., Salas R., Arias C., García A., Martín-Algarra A., Meléndez M.

N., Chacón B., Molina J. M., Sanz J. L., Castro J. M., García-Hernández M., Carenas B., García-Hidalgo J., Gil J., Ortega F. Cretaceous. In: *The Geology of Spain.* Ed. Gibbons W. and Moreno T. *The Geological Society,* UK. **2002,** pp. 255.

Martínez Ron A. *Expediente Río Tinto: la verdad sobre el río "extraterrestre" - VOZ PÓPULI.* https://www.vozpopuli.com/altavoz/next/Exobiologia-Astronomia-Biologia-Rio_Tinto-CAB_0_683331720.html (last update 2020/05/26).

Mehall L. K., Cisneros E., Bell III J.F., Paris K. N., Wellington D., Jenson E.H., Maki J.N., Hayes A.G., Kinch K., and the Mastcam-Z Team. Mars 2020 Mastcam-Z PDS4 data archive. *4th Planetary Data Workshop.* **2019,** abst. 2151.

Meinhold G. Rutile and its applications in earth sciences. *Earth Sci. Rev.* **2010,** 102, 1-28.

Mer'kov A. N., Bussen I. V., Goyko Ye. A., Kul'chitskaya Ye. A., Men'shikov Yu. P., Nedorezova A. P. Raite and zorite, new minerals from the Lovozero Tundra. *Int. Geol. Rev.,* **1973,** 15-9, 1087-1094.

Meschede M. The tectonic and sedimentary development of the Biscay synclinorium in Northern Spain. *Geol. Rundsch.,* **1987,** 76, 567-577.

Michael H. H, Jeffrey A. H. for the MOXIE Team. The Mars Oxygen ISRU Experiment (MOXIE) on the Mars 2020 Rover. *LPSC 46.* **2015,** abst. 2774.

Michailidis K., Kassolifournaraki A., Ericsson T., Filippidis A., Godelitsas A. Prehnite formation and metamorphic relations in the metagabbros of the Oreokastro ophiolite suite, Macedonia, Greece. *Gff,* **1995,** 117, 15-21.

Milam K. A., McSween H. Y., Jr., Moersch J., Christensen P. R. Distribution and variation of plagioclase compositions on Mars. *J. Geophys. Res. Planet.,* **2010,** 115, E09004, 1-15.

Milone E. F., Wilson W. J. F. Solar system astrophysics. Vol. 1, Background science and the inner solar system. *Springer,* New York. **2008**.

Mitrofanov I. G., Litvak M. L., Nikiforov S. Y., Jun I., Bobrovnitsky Y. I., Golovin D. V., Grebennikov A. S., Fedosov F. S., Kozyrev A. S., Lisov D. I., Malakhov A. V., Mokrousov M. I., Sanin A. B., Shvetsov V. N., Timoshenko G. N., Tomilina T. M., Tret'yakov V. I., Vostrukhin A. A. The ADRON-RM instrument onboard the ExoMars rover. *Astrobiology,* **2017,** 17 (6, 7), 585-594.

Miura Y. Formation of calcium-carbonates by natural and artificial shock wave impacts: new type formation of carbonates. *LPSC 38.* **2007,** abst. 1277.

Morad S., El-Ghali M. A. K., Caja M. A., Al-Ramadan K., Mansurbeg H. Hydrothermal alteration of magmatic titanite: Evidence from proterozoic granitic rocks, southeastern Sweden. *Canad. Mineral.,* **2009,** 47, 801-811.

Mustard J. F, Poulet F., Gendrin A., Bibring J., Langevin Y., Gondet B., Mangold N., Bellucci G., Altieri F. Olivine and pyroxene, diversity in the crust of Mars. *Science,* **2005,** 307, 1594-1597.

Mustard J. F., Murchie S. L., Pelkey S. M., Ehlmann B. L., Milliken R. E., Grant J. A., Bibring J. -., Poulet F., Bishop J., Dobrea E. N., Roach L., Seelos F., Arvidson R. E., Wiseman S., Green R., Hash C., Humm D., Malaret E., McGovern J. A., Seelos K., Clancy T., Clark R., Des Marais D., Izenberg N., Knudson A., Langevin Y., Martin T., McGuire P., Morris R., Robinson M., Roush T., Smith M., Swayze G., Taylor H., Titus T., Wolff M. Hydrated silicate minerals on mars observed by the Mars reconnaissance orbiter CRISM instrument. *Nature,* **2008,** 454, 305-309.

Nagano T., Mitamura H., Nakayama S., Nakashima S. Formation of goethite and hematite from neodymium-containing ferrihydrite suspensions. *Clays Clay Miner.,* **1999,** 47, 748-754.

Namieśnik J. Trace Analysis — Challenges and Problems. *Crit. Rev. Anal. Chem.,* **2002,** 32, 271-300.

National Aeronautics and Space Administration. *Jezero Crater, Mars 2020's landing site.* https://mars.nasa.gov/resources/22475/jezero-crater-mars-2020s-landing-site/ (last update 2020/04/27).

National Aeronautics and Space Administration. *Mars 2020 mission. Overview.* https://mars.nasa.gov/mars2020/mission/overview/ (last update 2020/01/07).

National Aeronautics and Space Administration. *The Mars Orbiter Laser Altimeter.* https://attic.gsfc.nasa.gov/mola/images.html (last update 2020/04/27).

National Aeronautics and Space Administration. *Mars sample return.* https://www.jpl.nasa.gov/missions/mars-sample-return-msr/ (last update 2020/04/27).

Niles P. B., Catling D. C., Berger G., Chassefiere E., Ehlmann B. L., Michalski J. R., Morris R., Ruff S. W., Sutter B. Geochemistry of carbonates on Mars: implications for climate history and nature of aqueous environments. *Space Sci. Rev.,* **2013,** 174, 301-328.

Ollila A. M., Wiens R. C., Maurice S., Cousin A., Anderson R., Beyssac O., Bonal L., Beck P., Clegg S., Chide B., DeFlores L., Dromart G., Fischer W., Forni O., Fouchet T., Gasnault O., Grotzinger J., Johnson J., Lasue J., Laserna J., Madariaga J. M., Madsen M., Mangold N., Nelson T., Newell R., Martinez-Frias J., McLennan S., Montmessin F., Robinson S., Sharma S., Misra A., Rull F., Venhaus D., Bernardi P., Reess J. -., Reyes-Newell A., Poulet F., Lanza N., Torre I., Aramendia J., Perez R., Cloutis E., Angel S., Mimoun D., Lorenz R., Rapin W., Meslin P. -., Frydenvang J., McConnochie T. , Bernard S. Preparing SuperCam for Jezero Crater, Mars: LIBS, Raman, VISIR, luminescence, imaging, and acoustic analyses. *Ninth International Conference on Mars.* **2019,** abst. 6352.

Oneil J. R., Taylor H. P. Oxygen isotope equilibrium between muscovite and water. *J. Geophys. Res.,* **1969,** 74, 6012-6022.

Orofino V., Blanco A., D'Elia M., Fonti S., Giuri M. Spectroscopic analysis of particulate samples of altered olivine for planetological studies. *Mem. S. A. It. Suppl.,* **2011,** 16, 113-118.

Osinski G. R., Lee P. Intra-crater sedimentary deposits at the Haughton impact structure, Devon Island, Canadian High Arctic. *Meteorit. Planet. Sci.,* **2005,** 40, 1887-1899.

Pailhé N., Wattiaux A., Gaudon M., Demourgues A. Correlation between structural features and vis-NIR spectra of α-Fe2O3 hematite and AFe2O4 spinel oxides (A=Mg, Zn). *J. Solid State Chem.,* **2008,** 181, 1040-1047.

Pajola M., Rossato S., Baratti E., Pozzobon R., Quantin C., Carter J., Thollot P. Boulder abundances and size-frequency distributions on Oxia Planum-Mars: Scientific implications for the 2020 ESA ExoMars rover. *Icarus,* **2017,** 296, 73-90.

Papike J. J., Karner J. M., Shearer C. K., Burger P. V. Silicate mineralogy of martian meteorites. *Geochim. Cosmochim. Acta.* **2009,** 73, 7443-7485.

Papoulis D., Tsolis-Katagas P., Kalampounias A. G., Tsikouras B. Progressive formation of halloysite from the hydrothermal alteration of biotite and the formation mechanisms of anatase in altered volcanic rocks from Limnos Island, Northeast Aegean Sea, Greece. *Clays Clay Miner.,* **2009,** 57, 566-577.

Parnell J., Bowden S. A., Osinski G. R., Lee P., Green P., Taylor C., Baron M. Organic geochemistry of impactites from the Haughton impact structure, Devon Island, Nunavut, Canada. *Geochim. Cosmochim. Acta,* **2007,** 71, 1800-1819.

Parnell J., Cullen D., Sims M. R., Bowden S., Cockell C. S., Court R., Ehrenfreund P., Gaubert F., Grant W., Parro V., Rohmer M., Sephton M., Stan-Lotter H., Steele A., Toporski J., Vago J. Searching for life on Mars: Selection of molecular targets for ESA's aurora ExoMars mission. *Astrobiology,* **2007,** 7, 578-604.

PMS Lab, University of Cyprus *PVROSION.* http://psm.ucy.ac.cy/pvrosion/experiments/technical-meeting-at-hellenic-copper-mines-ltd/attachment/hellinccopper5/ (last update 2020/05/26).

Poulet F., Bibring J. P., Mustard J. F., Gendrin A., Mangold N., Langevin Y., Arvidson R. E., Gondet B., Gomez C., Omega Team. Phyllosilicates on Mars and implications for early Martian climate. *Nature,* **2005,** 438, 623-627.

Poulet F., Mangold N., Loizeau D., Bibring J. -., Langevin Y., Michalski J., Gondet B. Abundance of minerals in the phyllosilicate-rich units on Mars. *Astron. Astrophys.,* **2008,** 487, L41-L44.

Rampe E. B., Ming D. W., Blake D. F., Bristow T. F., Chipera S. J., Grotzinger J. P., Morris R. V., Morrison S. M., Vaniman D. T., Yen A. S., Achilles C. N., Craig P. I., Des Marais D. J., Downs R. T., Farmer J. D., Fendrich K. V., Gellert R., Hazen R. M., Kah L. C., Morookian J. M., Peretyazhko T. S., Sarrazin P., Treiman A. H., Berger J. A., Eigenbrode J., Fairén A. G., Forni O., Gupta S., Hurowitz J. A., Lanza N. L., Schmidt M. E., Siebach K., Sutter B., Thompson L. M. Mineralogy of an ancient lacustrine mudstone succession from the Murray formation, Gale crater, Mars. *Earth Planet. Sci. Lett.* **2017,** 471, 172-185.

Reyes K. I. PhD thesis. *Análisis geológico de la región Oxia Planum en Marte, sitio principal de aterrizaje de la Misión ExoMars 2020.* Universidad Nacional Autónima de México, México, **2016.**

Robles S. Evolución geológica de la Cuenca Vasco Cantábrica. In: *Geología de la Cuenca Vasco-Cantábrica.* Eds. Bodego Aldasoro A., Mendia Aranguren M., Aranburu

Artano A., Apraiz Atutxa A. *Universidad del País Vasco/Euskal Herriko Unibertsitatea,* Leioa. **2014,** pp. 9-51.

Rodríguez-Manfredi J. A., de la Torre M., Boland J. S., Bridges N. T., Conrad P., Ferri F., Genzer M., Gómez-Gómez F., Gómez-Elvira J., Harri A-M., Kemppinnen O., Lemmon M., Martínez G., Navarro S., Newman C., Pérez-Hoyos S., Prieto O., Ramos M., Saiz-López A., Sánchez-Lavega A., Schofield J. T., Sebastian E., Smith M., Tamppari L. K. and the MEDA team. MEDA, the Environmental Dynamics Analyzer for Mars 2020. *3rd International Workshop on Instrumentation for Planetary Missions.* **2016,** abst. 4114.

Roling W. F. M., Aerts J. W., Patty C. H. L., ten Kate I. L., Ehrenfreund P., Direito S. O. L. The significance of microbe-mineral-biomarker interactions in the detection of life on Mars and beyond. *Astrobiology,* **2015,** 15, 492-507.

Ruff S. Spectral evidence for zeolite in the dust on Mars. *Icarus,* **2004,** 168, 131-143.

Ruiz Cruz M. D. Genesis and evolution of the kaolin-group minerals during the diagenesis and the beginning of metamorphism. *Seminarios SEM,* **2007,** 3, 41-52.

Ruiz-Galende P., Torre-Fdez I., Aramendia J., Gómez-Nubla L., Castro K., Arana G., Madariaga J. M. Formation of titanium oxide (TiO_2) polymorphs in an emerged submarine volcano environment: Implications for Mars. *EPSC.* **2018,** abst. 988.

Ruiz-Galende P., Torre-Fdez I., Aramendia J., Gómez-Nubla L., Castro K., Arana G., Madariaga J. M. Study of a terrestrial Martian analogue: Geochemical characterization of the Meñakoz outcrops (Biscay, Spain). *J. Raman Spectrosc.,* **2019,** 1-10.

Ruiz-Galende P., Torre-Fdez I., Aramendia J., Gómez-Nubla L., Castro K., Arana G., Fdez-Ortiz de Vallejuelo S., Maguregui M., Medina J., Baonza V. G., Rull F., Madariaga J. M. New Raman-visible near-infrared database of inorganic and mineralogical planetary and terrestrial compounds and its implications for Mars: Phyllosilicates. *J. Raman Spectrosc.,* **2019,** 1-11.

Rull F., Maurice S., Hutchinson I., Moral A., Pérez C., Díaz C., Colombo M., Belenguer T., López-Reyes G., Sansano A., Forni O., Parot Y., Striebig N., Woodward S., Howe C., Tarcea N., Rodríguez P., Seoane L., Santiago A., Rodríguez-Prieto J. A., Medina J., Gallego P., Canchal R., Santamaría P., Ramos G., Vago J. L., RLS Team. The Raman Laser Spectrometer for the ExoMars rover mission to Mars. *Astrobiology,* **2017,** 17 (6, 7), 627-654.

Salas E., Abbey W., Bhartia R., Beegle L. W. The Mojave Desert: a Martian analog site for future astrobiology themed missions. *Analogue Sites for Mars Missions: MSL and Beyond.* **2011,** abst. 161.

Salvatore M. R., Goudge T. A., Bramble M. S., Edwards C. S., Bandfield J. L., Amador E. S., Mustard J. F., Christensen P. R. Bulk mineralogy of the NE Syrtis and Jezero crater regions of Mars derived through thermal infrared spectral analyses. *Icarus,* **2018,** 301, 76-96.

Sasaki K. Distinction of jarosite group compounds by Raman spectroscopy. *Canad. Mineral.,* **1998,** 36 (5), 1225-1235.

Saxena S. K., Hrubiak R. Mapping the nebular condensates and the chemical composition of the terrestrial planets. *Earth Planet. Sci. Lett.,* **2014,** 393, 113-119.

Schmidt R., Credland J. D., Chicarro A., Moulinier P. ESA's Mars Express mission - Europe on its way to Mars. *Esa Bulletin-European Space Agency,* **1999,** 56-66.

Seelos K. D., Arvidson R. E., Jolliff B. L., Chemtob S. M., Morris R. V., Ming D. W., Swayze G. A. Silica in a Mars analog environment: Ka'u Desert, Kilauea Volcano, Hawaii. *J. Geophys. Res. Planet.,* **2010,** 115, E00D15, 1-18.

Seetharam R. Gudmundite from base metal sulphide deposit of Askot, Pithoragarh District, (U. P.). *J. Geol. Soc. India,* **1981,** 22, 5, 216-219.

Sephton M. A., Carter J. N. The chances of detecting life on Mars. *Planet. Space Sci.,* **2015,** 112, 15-22.

Shekhtman L. *With Mars methane mystery unsolved, Curiosity serves scientists a new one: oxygen.* https://www.nasa.gov/feature/goddard/2019/with-mars-methane-mystery-unsolved-curiosity-serves-scientists-a-new-one-oxygen (last update 2020/03/24).

Shkolyar S., Eshelman E., Farmer J., Hamilton D., Daly M., Youngbull C. Detecting kerogen as a biosignature using colocated UV time-gated Raman and fluorescence spectroscopy. *Astrobiology,* **2018,** 18-2, 431-453.

Shotwell R. Phoenix—the first Mars Scout mission. *Acta Atronaut.* **2005,** 57, 121-134.

Siljeström S., Parenteau M. N., Jahnke L. L., Cady S. L. A comparative ToF-SIMS and GC–MS analysis of phototrophic communities collected from an alkaline silica-depositing hot spring. *Org. Geochem.* **2017,** 109, 14-30.

Sinton W. M. On the composition of Martian surface materials. *Icarus,* **1967,** 6, 222-228.

Smith M. R., Bandfield J. L. Geology of quartz and hydrated silica-bearing deposits near Antoniadi Crater, Mars. *J. Geophys. Res. Planet.,* **2012,** 117, E06007, 1-24.

Soffen G. A. The Viking project. *J. Geophys. Res.,* **1977,** 82, 3959-3970.

Spohn T. 10.01 - Physics of terrestrial planets and moons: an introduction and overview. In: *Treatise on geophysics (Second Edition).* Ed. Schubert G. *Elsevier,* Oxford. **2015,** pp. 1-22.

Stalport F., Coll P., Cabane M., Person A., Gonzalez R. N., Raulin F., Vaulay M. J., Ausset P., McKay C. P., Szopa C., Zarnecki J. Search for past life on Mars: Physical and chemical characterization of minerals of biotic and abiotic origin: part 1 - Calcite. *Geophys. Res. Lett.,* **2005,** 32, L23205, 1-5.

Steele A., Benning L. G., Wirth R., Siljeström S., Fries M. D., Hauri E., Conrad P. G., Rogers K., Eigenbrode J., Schreiber A., Needham A., Wang J. H., McCubbin F. M., Kilcoyne D., Rodriguez Blanco J. D. Organic synthesis on Mars by electrochemical reduction of CO_2. *Sci. Adv.,* **2018,** 4, eaat5118, 1-10.

Steele A., McCubbin F. M., Fries M. D. The provenance, formation, and implications of reduced carbon phases in Martian meteorites. *Meteorit. Planet. Sci.,* **2016,** 51, 2203-2225.

Stigall A. L. *Stigall Lab - Paleobiogeography, Paleoecology, Macroevolution.* https://www.alyciastigall.org/photos/dscn1113-2/ (last update 2020/05/26).

Sutter B., Dalton J. B., Ewing S. A., Amundson R., Mckay C. P. Terrestrial analogs for interpretation of infrared spectra from the Martian surface and subsurface: Sulfate, nitrate, carbonate, and phyllosilicate-bearing Atacama Desert soils. *J. Geophys. Res. Biogeo.,* **2007,** 112, G04S10, 1-19.

Tebo B., Bargar J., Clement B., Dick G., Murray K., Parker D., Verity R., Webb S. Biogenic manganese oxides: Properties and mechanisms of formation. *Annu. Rev. Earth Planet. Sci.,* **2004,** 32, 287-328.

ten Kate I. L. Organic molecules on Mars. *Science,* **2018,** 360, 1068-1069.

Tischendorf G., Forster H. J., Gottesmann B., Rieder M. True and brittle micas: composition and solid-solution series. *Mineral. Mag.,* **2007,** 71, 285-320.

Tokano T., Bish D. L. Hydration state and abundance of zeolites on Mars and the water cycle. *J. Geophys. Res.,* **2005,** 110, .

Torre-Fdez I., Ruiz-Galende P., Aramendia J., Gómez-Nubla L., Castro K., Fdez-Ortiz de Vallejuelo S., Arana G. , Madariaga J. M. Study of organic compounds present in the NorthWest Africa 6148 Nakhlite by means of Raman spectroscopy. *EPSC.* **2018,** abst. 967.

Torre-Fdez I., Aramendia J., Gómez-Nubla L., Castro K., Madariaga J. M. Geochemical study of the Northwest Africa 6148 Martian meteorite and its terrestrial weathering processes. *J. Raman Spectrosc.,* **2017,** 48, 1536-1543.

UAE Space Agency *Emirates Mars Mission "Hope probe".* https://www.emiratesmarsmission.ae/ (last update 2020/07/23).

United States Antarctic Program-National Science Foundation *USAP Photo Library.*

https://photolibrary.usap.gov/PhotoDetails.aspx?filename=Bullpa1.jpg (last update 2020/05/26).

Vago J. L., Westall F., Coates A. J., Jaumann R., Korablev O., Ciarletti V., Mitrofanov I., Josset J., De Sanctis M. C., Bibring J., Rull F., Goesmann F., Steininger H., Goetz W., Brinckerhoff W., Szopa C., Raulin F., Westall F., Edwards H. G. M., Whyte L. G., Fairen A. G., Bibring J., Bridges J. C, Hauber E., Ori G. G., Werner S., Loizeau D., Kuzmin R. O., Williams R. M. E., Flahaut J., Forget F., Vago J. L., Rodionov D., Korablev O., Svedhem H., Sefton-Nash E., Kminek G., Lorenzoni L., Joudrier L., Mikhailov V., Zashchirinskiy A., Alexashkin S., Calantropio F., Merlo A., Poulakis P., Witasse O., Bayle O., Bayon S., Meierhenrich U., Carter J., Garcia-Ruiz J. M., Baglioni P., Haldemann A., Ball A. J., Debus A., Lindner R., Haessig F., Monteiro D., Trautner R., Voland C., Rebeyre P., Goulty D., Didot F., Durrant S., Zekri E., Koschny D., Toni A., Visentin G., Zwick M., van Winnendael M., Azkarate M., Carreau C., Pasteur Instrument Teams,

Landing Site Selection Working, ExoMars Project Team. Habitability on early Mars and the search for biosignatures with the ExoMars rover. *Astrobiology,* **2017,** 17, 471-510.

Varghese H., Panicker C. Y., Mary Y. S. IR, Raman, first hyperpolarizability and computational study of 1-chloroethyl benzene. *Mat. Sci. Res. India,* **2012,** 9, 117-121.

Viviano-Beck C. E., Moersch J. E., McSween H. Y. Implications for early hydrothermal environments on Mars through the spectral evidence for carbonation and chloritization reactions in the Nili Fossae region. *J. Geophys. Res. Planet.,* **2013,** 118, 1858-1872.

Viviano-Beck C. E., Seelos F. P., Murchie S. L., Kahn E. G., Seelos K. D., Taylor H. W., Taylor K., Ehlmann B. L., Wisemann S. M., Mustard J. F., Morgan M. F. Revised CRISM spectral parameters and summary products based on the currently detected mineral diversity on Mars. *J. Geophys. Res. Planet.,* **2014,** 119, 1403-1431.

von Bloh W. Climate Change 2: Long-Term Dynamics. In: *Encyclopedia of Ecology.* Eds. Jørgensen S. E., Fath B. D. *Academic Press,* Oxford. **2008,** pp. 592-598.

Wang A., Kuebler K., Jolliff B., Haskin L. A. Mineralogy of a Martian meteorite as determined by Raman spectroscopy. *J. Raman Spectrosc.,* **2004,** 35, 504-514.

Wang A., Freeman J. J., Jolliff B. L., Chou I. -. Sulfates on Mars: A systematic Raman spectroscopic study of hydration states of magnesium sulfates. *Geochim. Cosmochim. Acta,* **2006,** 70, 6118-6135.

Wang A., Han J., Guo L., Yu J., Zeng P. Database of standard Raman spectra of minerals and related inorganic crystals. *Appl. Spectrosc.,* **1994,** 48, 959-968.

Wang R., Cudahy T., Laukamp C., Walshe J. L., Bath A., Mei Y., Young C., Roache T. J., Jenkins A., Roberts M., Barker A., Laird J. White mica as a hyperspectral tool in exploration for the sunrise Dam and Kanowna Belle Gold Deposits, Western Australia. *Econ. Geol.,* **2017,** 112, 1153-1176.

Warren-Rhodes K. A., Lee K. C., Archer S. D. J., Cabrol N., Ng-Boyle L., Wettergreen D., Zacny K., Pointing S. B., , The NASA Life in the Atacama Project Team. Subsurface microbial habitats in an extreme desert Mars-analog environment. *Front- Microbiol.,* **2019,** 10, 69, 1-11.

Watanabe T., Funakawa S., Kosaki T. Distribution and formation conditions of gibbsite in the upland soils of humid Asia: Japan, Thailand and Indonesia. *19th World Congress of Soil Science,* **2010,** 17-20.

Wei J., Wang A., Lambert J. L., Wettergreen D., Cabrol N., Warren-Rhodes K., Zacny K. Autonomous soil analysis by the Mars Micro-beam Raman Spectrometer (MMRS) on-board a rover in the Atacama Desert: a terrestrial test for planetary exploration. *J. Raman Spectrosc.,* **2015,** 46, 810-821.

Weisenberger T., Selbekk R. S. Multi-stage zeolite facies mineralization in the Hvalfjördur area, Iceland. *Int. J. Earth Sci.,* **2009,** 98, 985-999.

Wendt L. PhD thesis. *Phyllosilicates and sulfates on Mars. Case studies from Terra Cimmeria and Valles Marineris.* Freien Universität Berlin, Berlin, **2012.**

Westall F. Early life on Earth and analogies to Mars. In: *Water on Mars and Life.* Ed. Tokano T. *Springer,* Berlin. **2005,** pp. 45-64.

White S. N. Laser Raman spectroscopy as a technique for identification of seafloor hydrothermal and cold seep minerals. *Chem. Geol.,* **2009,** 259, 240-252.

Wood J. A. Chondritic meteorites and the solar nebula. *Annu. Rev. Earth Planet. Sci.,* **1988,** 16, 53-72.

Wright I. P., Grady M. M., Pillinger C. T. Organic materials in a Martian meteorite. *Nature,* **1989,** 340, 220-222.

Zhang A., Wang S., Tomioka N., Lu X., Ding Z., Ma C., Wang P., Chen J., Xu S., Gu L., Bai Y., Li Y., Sakamoto N., Wang R. An example of high-T, high-symmetry crystallization: Spherical (Mg, Fe)-oxides formed by particle attachment in the shocked martian meteorite Northwest Africa 7755. *Am. Mineral.,* **2019,** 104, 150-157.

Zhang M., Salje E. K. H., Redfern S. A. T., Bismayer U., Groat L. A. Intermediate structures in radiation damaged titanite ($CaTiSiO_5$): a Raman spectroscopic study. *J. Phys. Condens. Mat.,* **2013,** 25,115402, 1-12.

Zolotov M. Y., Shock E. L. Formation of jarosite-bearing deposits through aqueous oxidation of pyrite at Meridiani Planum, Mars. *Geophys. Res. Lett.,* **2005,** 32, L21203, 1-5.

Zotov A., Mukhamet-Galeev A., Schott J. An experimental study of kaolinite and dickite relative stability at 150-300 ºC and the thermodynamic properties of dickite. *Am. Mineral.,* **1998,** 83, 516-524.

Zurek R. W., Smrekar S. E. An overview of the Mars Reconnaissance Orbiter (MRO) science mission. *J. Geophys. Res. Planet.,* **2007,** 112, E05S01, 1-22.

CHAPTER 12:

APPENDICES

Appendix 1: Terminological glossary and acronyms

Agpaitic mineral: mineral that is found in unusual igneous intrusive rocks that contain alkali metals and high contents of rare elements.

Brittle micas: micas which contain divalent cations in the phyllosilicate interlayer.

Chondrites: stony meteorites with ultramafic composition predominantly of Mg, Si and Fe elements, which are in form of olivine and pyroxene as major minerals.

Diagenetic mineral: mineral that has suffered low-pressure and low-temperature alteration process.

Dichotomy: division into two different parts.

Eccentric orbit: an orbit deviated from a circular path.

Lander: spacecraft designed to reach the surface of a planet and survive long enough to telemeter data back to Earth.

Lithophyte: an organism that comes from plants which grow on rocks.

Mafic material: rocks or minerals which have a high percentage of iron and magnesium.

Ophiolite: an igneous rocks consisting largely of serpentine, believed to have been formed from the submarine eruption of oceanic crustal and upper mantle material.

Orbiter: spacecraft designed to travel into the orbit of a distant planet.

Paleolacrustine: antique lake.

Pedogenic: relating to or denoting processes occurring in soil or leading to the formation of soil.

Protolith: the original, unmetamorphosed rock from which a given metamorphic rock is formed.

Regolith: region of loose unconsolidated rock and dust that sits on a layer of bedrock.

Rover: spacecraft designed to move across the solid surface of a planet and make detailed observations of the surface.

Shergottite: type of achondritic Martian meteorites made of feldspars and pyroxenes.

Theoleiitic: any of a series of igneous rocks similar in composition to basalt but having more silica and iron and less aluminium.

Trachytes: fine-grained extrusive igneous rock composed mainly of alkali feldspars.

ADRON-RM: Autonomous Detector of Radiation of Neutrons ON board rover at Mars

APXS: Alpha Proton X-Ray Spectrometer

ASPERA: Analyser of Space Plasmas and EneRgetic Atoms

BCB: Basque-Cantabrian Basin

CCD: Charge Couple Device detector

CLUPI: CLose-UP Imager

CMDM: Circum-Martian Dust Monitor

CNSA: China National Space Administration

CRISM: Compact Reconnaissance Imaging Spectrometer

DCM: DiChloroMethane

EDXRF: Energy Dispersive X-Ray Fluorescence

ESA: European Spatial Agency

FOV: Fielf Of View

FP: Fundamental Parameters

GC-MS: Gass Chromatography-Mass Spectrometry

GPR: Ground Penetrating Radar

HCP: High-Calcium Pyroxenes

HIRISE: High Resolution Imaging Science Experiment

HRSC: High Resolution Stereo Camera

IMPAT-Database: Inorganic and Mineralogical Planetary And Terrestrial compounds Database

ISEM: Infrared Spectrometer for ExoMars

ISRU: Mars In Situ Resource Utilization

JAXA: Japan Aerospace eXploration Agency

LCP: Low-Calcium Pyroxenes

LIBS: Laser Induced Breakdown Spectroscopy

LIDAR: Light Detection And Ranging

MAHLI: Mars Hand Lens Imager

Ma-MISS: Mars Multispectral Imager for Subsurface Studies

MARCI: Mars Color Imager

MaRS: Mars Radio Science

MARSIS: Mars Advanced Radar for Subsurface and Ionospheric Sounding

MAVEN: Mars Atmosphere and Volatile EvolutioN

MECA: Mars Environmental Compatibility Assessment

MEDA: Mars Environmental Dynamics Analysed

MEGANE: Mars-moon Exploration with Gamma rays and Neutrons

MER: Mars Exploration Rover

MES: Mars Express

MGS: Mars Global Surveyor

MLS: Mars Science Laboratory

MIMOS: Mössbauer spectrometer

MOC: Mars Orbiter Camera

MOLA: Mars Orbiter Laser Altimeter

MOMA: Mars Organic Molecule Analyser

MOXIE: Mars Oxygen In-Situ Resource Utilization Experiment

MRO: Mars Reconnaissance Orbiter

MSA: Mass Spectrum Analyzer

N.A.: Number of Aperture

NASA: National Aeronautics and Space Administration

OMEGA: Observatoire pour la Minéralogie l'Eau les Glaces et l'Activité

OROCHI: Optical RadiOmeter composed of Chromatic Imagers

PAH: Poly Aromatic Hydrocarbons

PanCam: Panoramic Camera

PFS: Planetary Fourier Spectrometer

PIXL: Planetary Instrument for X-ray Lithochemistry

RIMFAX: Radar Imager for Mars' subsurface eXperiment

RLS: Raman Laser Spectrometer

RMI: high resolution colour Remote Micro-Imaging

SAM: Sample Analysis at Mars

SDD: Silicon Drift Detector

SHERLOC: Scanning Habitable Environments with Raman and Luminiscence for Organics and Chemicals

SPICAM-UV: SPectrosopic Investigation of the Characteristics of the Atmosphere of Mars

TEGA: Thermal Evolved Gas Analyser

TENGOO: Telescopic Nadir imager for GeOmOrphology

TES: Thermal Emission Spectrometer

TIC: Total Inorganic Carbon

TOC: Total Organic Carbon

TOE: Total Organic Extract

ToF-SIMS: Time-of-Flight-Secondary Ion Mass Spectrometry

TRLS: Time-Resolved Luminescence Spectroscopy

VNIR: Visible and Near-Infrared Spectroscopy

WISDOM: Water Ice and Subsurface Deposit Observation On Mars

XRD: X-Ray Diffraction

Appendix II: Mineral formulation

Albite - $NaAlSi_3O_8$

Anatase/Rutile/Brookite - TiO_2

Ankerite - $CaFe^{2+}(CO_3)_2$

Anorthite - $CaAl_2Si_2O_8$

Augite - $(Ca,Mg,Fe)_2(Si, Al)_2O_6$

Apatite - $Ca_5(PO_4)_3(F,Cl,OH)$

Barite - $(BaSO_4)$

Baritocalcite - $BaCa(CO_3)_2$

Birnessite - $(Na,Ca,K)_{0.6}(Mn^{4+},Mn^{3+})_2O_4 \cdot 1.5H_2O$

Bismutite - $Bi_2(CO_3)O_2$

Bytownite - $(Ca,Na)(Al(Al,Si)Si_2O_8$

Calcite/Aragonite - $CaCO_3$

Celadonite - $K(Mg,Fe^{2+})(Fe^{3+},Al)Si_4O_{10}(OH)_2$

Chalcopyrite - $CuFeS_2$

Chamosite - $Fe_5Al(Si_3Al)O_{10}(OH)_8$

Clinochlore - $Mg_5Al(Si_3Al)O_{10}(OH)_8$

Clintonite - $Ca(Mg,Al)_3(Al_3SiO_{10})(OH)_2$

Cromodipsode - $CaMgSi_2O_6$ (with Cr impurities)

Diaphorite - $Pb_2Ag_3Sb_3S_8$

Diopside - $CaMgSi_2O_6$

Dolomite - $CaMg(CO_3)_2$

Epidote - $Ca_2Fe^{3+}Al_2(Si_2O_7)(SiO_4)O(OH)$

Fayalite - $(Fe^{2+})_2SiO_4$

Fosterite - Mg_2SiO_4

Fluoroapophyllite-K - $KCa_4(Si_8O_{20})F \cdot 8H_2O$

Gersdorffite - $NiAsS$

Gibsite - $Al(OH)_3$

Glauconite - $(K,Na)(Fe^{3+},Al,Mg)_2(Si,Al)_4O_{10}(OH)_2$

Goethite - $\alpha\text{-}FeOOH$

Gudmundite - FeSbS

Hematite - Fe_2O_3

Illite - $(K,H_3O)(Al,Mg,Fe)_2(Si,Al)_4O_{10}[(OH)_2,(H_2O)]$

Jarosite - $KFe_3^{3+}(SO_4)_2(OH)_6$

Kaolinite/Dickite - $(Al_2Si_2O_5(OH)_4$

Labradorite - $(Ca,Na)(Si,Al)_4O_8$

Langite - $Cu_4(SO_4)(OH)_6 \cdot 2H_2O$

Laumontite - $CaAl_2Si_4O_{12} \cdot 4H_2O$

Linarite - $PbCu(SO_4)(OH)_2$

Lithiophorite - $LiAl_2(Mn_2^{4+},Mn^{3+})O_6(OH)_6$

Magnesioferrite - $MgFe_2O_4$

Magnetite - $Fe^{2+}Fe^{3+}_2O_4$

Montmorillonite - $(Na,Ca)_{0.33}(Al,Mg)_2(Si_4O_{10})(OH)_2 \cdot nH_2O$

Muscovite - $KAl_2(AlSi_3O_{10})(OH)_2$

Nontronite - $Na_{0.3}Fe_2((Si,Al)_4O_{10})(OH)_2 \cdot nH_2O$

Pentlandite - $(Fe,Ni)_9S_8$

Prehnite - $Ca_2Al(Si_3Al)O_{10}(OH)_2$

Pyrite/Marcasite - FeS_2

Pyrosmalite - $Fe^{2+}_8Si_6O_{15}(OH,Cl)_{10}$

Pyrrhotite - Fe_7S_8

Quartz - SiO_2

Raite - $Na_4Mn^{2+}_3Ti_{0.25}Si_8O_{20}(OH)_2 \cdot 10H_2O$

Sanidine - $(K,Na)(Si,Al)_4O_8$

Serpierite - $Ca(Cu,Zn)_4(SO_4)_2(OH)_6 \cdot 3H_2O$

Siderite - $FeCO_3$

Spherocobaltite - $CoCO_3$

Stichtite - $Mg_6Cr_2^{3+}(OH)_{16}(CO_3) \cdot 4H_2O$

Titanite - $CaTiSiO_5$

Wairakite - $CaAl_2Si_4O_{12} \cdot 2H_2O$

Appendix III: List of minerals from IMPAT-Database

Arseniates:

Adamite - $Zn_2(AsO_4)OH$ - Raman/VNIR

Clinoclase - $Cu_3(AsO_4)(OH)_3$ - VNIR

Conichalcite - $CaCuAsO_4(OH)$ - Raman/VNIR

Erythrine - $Co_3(AsO_4)_2 \cdot 8H_2O$ - VNIR

Olivenite - $Cu_2(AsO_4)(OH)$ – VNIR

Borates:

Borax - $Na_2B_4O_7 \cdot 10H2O$ - VNIR

Ludwigite - $Mg_2Fe^{3+}(BO_3)O_2$ - VNIR

Carbonates:

Ammonium bicarbonate - $(NH_4)HCO_3$ - VNIR

Ankerite - $Ca(Fe^{2+},Mg)(CO_3)_2$ - VNIR

Aragonite - $CaCO_3$ - Raman

Azurite - $Cu_3(CO_3)_2(OH)_2$ - Raman/VNIR

Barytocalcite - $BaCa(CO_3)_2$ - VNIR

Bismutite - $(BiO)_2CO_3$ - VNIR

Calcite - $CaCO_3$ - Raman/VNIR

Cerussite - $PbCO_3$ - VNIR

Dolomite - $CaMg(CO_3)_2$ - Raman/VNIR

Magnesite - $MgCO_3$ - VNIR

Malachite - $Cu_2(CO_3)(OH)_2$ - VNIR

Natron - $Na_2CO_3 \cdot 10H_2O$ - VNIR

Parisite - $CaCe_2(CO_3)_3F_2$ - VNIR

Potassium carbonate - K_2CO_3 - VNIR

Rhodochrosite - $MnCO_3$ - VNIR

Rosasite - $(Cu,Zn)_2(CO_3)(OH)_2$ - VNIR

Siderite - $FeCO_3$ - Raman/VNIR

Sodium bicarbonate - $NaHCO_3$ - VNIR

Sodium carbonate monohydrate - $Na_2CO_3 \cdot H_2O$ - VNIR

Spherocobaltite - $CoCO_3$ - VNIR

Stitchtite - $Mg_6Cr^{3+}_2(OH)_{16}(CO_3) \cdot 4H_2O$ - VNIR

Strontium carbonate - $SrCO_3$ - VNIR

Chlorides:

Aluminium chloride - $AlCl_3$ - VNIR

Atakamite - $Cu_2(OH)_3Cl$ - VNIR

Boleite - $KPb_{26}Ag_9Cu_{24}(OH)_{48}Cl_{62}$ - VNIR

Calcium chloride - $CaCl_2$ - VNIR

Calcium chloride dihydrate - $CaCl_2 \cdot 2H_2O$ - VNIR

Halite - $NaCl$ - VNIR

Cyclosilicates:

Beryl - $Be_3Al_2(Si_6O_{18})$ - Raman/VNIR

Cordierite - $(Mg,Fe)_2Al_3(AlSi_5O_{18})$ - VNIR

Dioptase - $CuSiO_3 \cdot H_2O$ - VNIR

Elbaite (Rubellite) - $Na(Li_{1.5}Al_{1.5})Al_6(Si_6O_{18})(BO_3)_3(OH)_3(OH)$ - VNIR

Ilimaussite-(Ce) - $(Na,K)_{7-8}(Ba,K)_{10}Ce_5(Nb,Ti)_6(Si_3O_9)_4(Si_9O_{18})O_6(O,OH)_{24}$ - Raman

Steenstrupine-(Ce) - $Na_{14}Mn^{2+}_2(Fe^{3+},Mn^{3+})_2Ce_6(Zr,Th)(Si_6O_{18})_2(PO_4)_6(HPO_4)(OH)_2 \cdot 2H_2O$ - Raman

Verdelite - $Na(LiAl)_3Al_6(BO_3)_3Si_6O_{18}(OH)_4$ - Raman/VNIR

Fluorides:

Chiolite - $Na_5Al_3F_{14}$ - VNIR

Fluorite - CaF_2 - Raman/VNIR

Inosilicates:

Aegirine - $NaFe^{3+}(Si_2O_6)$ - Raman

Actinolite - $Ca_2Mg_{2.5-4.5}Fe_{0.5-2.5}(Si_8O_{22})(OH)_2$ - VNIR

Astrophyllite - $K_2NaFe2+_7Ti_2Si_8O_{28}(OH)_4F$ - Raman/VNIR

Babingtonite - $Ca_2(Fe,Mn)FeSi_5O_{14}(OH)$ - Raman

Bavenite - $Ca_4Be_2Al_2Si_9O_{26}(OH)_2$ - Raman

Chkalovite - $Na_2BeSi_2O_6$ - Raman

Diopside - $CaMgSi_2O_6$ - Raman/VNIR

Edenite - $NaCa_2Mg_5(AlSi_7O_{22})(OH)_2$ - Raman

Enstatite (Ferrosilite) - $(Mg,Fe^{2+})_2(SiO_3)_3$ - Raman

Fassaite - $(Ca,Na)(Mg,Fe^{2+},Al,Fe^{3+},Ti)(Si,Al)_2O_6$ - Raman

Hedenbergite - $CaFe^{2+}Si_2O_6$ - Raman

Hillebrandite - $Ca_2(SiO_3)(OH)_2$ - Raman

Jadeite - $Na(Al,Fe^{3+})Si_2O_6$ - Raman

Pectolite - $NaCa_2Si_3O_8(OH)$ - Raman

Prehnite - $Ca_2Al_2Si_3O_{10}(OH)_2$ - Raman

Pyrope - $Mg_3Al_2(SiO_4)_3$ - Raman

Rhodonite - $(Mn^{2+})SiO_3$ - Raman/VNIR

Richterite - $Na(Na,Ca)Mg_5(Si_8O_{22})(OH)_2$ - Raman/VNIR

Riebeckite - $Na_2(Fe2^+_3Fe^{3+}_2)Si_8O_{22}(OH)_2$ - VNIR

Serandite - $NaMn^{2+}_2Si_3O_8(OH)$ - Raman

Sorensenite - $Na_4SnBe_2Si_6O_{16}(OH)_4$ - Raman

Spodumen (Hiddenita) - $LiAlSi_2O_6$ - Raman

Spodumen (Kunzita) - $LiAlSi_2O_6$ - Raman

Stokesite - $CaSn(Si_3O_9)\cdot2H_2O$ - Raman

Tremolite - $Ca_2Mg_5(Si_8O_{22})(OH)_2$ - Raman

Nesosilicates:

Andalusite - Al_2SiO_5 - Raman

Chloritoid - $(Fe^{2+},Mg,Mn^{2+})Al_2(SiO_4)O(OH)_2$ - VNIR

Datolite - $Ca(HBSiO_5)$ - VNIR

Dumortierite - $Al_7BO_3(SiO_4)_3O_3$ - VNIR

Fayalite - $Fe^{2+}_2SiO_4$ - Raman

Fosterite - Mg_2SiO_4 - Raman

Olivine - $(Fe,Mg,Mn,Ni)_2SiO_4$ - Raman/VNIR

Spurrite - $Ca_5(SiO_4)_2(CO_3)$ - VNIR

Titanite - $CaTiSiO_5$ - VNIR

Zircon - $Zr(SiO_4)$ - VNIR

Nitrates:

Alumunium nitrate - $Al(NO_3)_3 \cdot 9H_2O$ - VNIR

Ammonium nitrate - $NH4(NO_3)_3$ - VNIR

Calcium nitrate - $Ca(NO_3)_2 \cdot 4H_2O$ - VNIR

Magnesium nitrate - $Mg(NO_3)_2$ - VNIR

Niter - KNO_3 - VNIR

Nitratine - $NaNO_3$ - VNIR

Strontium nitrate - $Sr(NO_3)_2$ - VNIR

Oxides and hydroxides:

Baria - BaO - VNIR

Brucite - $Mg(OH)_2$ - VNIR

Goethite - α-$FeO(OH)$ - Raman/VNIR

Hematite - Fe_2O_3 - Raman/VNIR

Magnesia - MgO - VNIR

Perovskite - $CaTiO_3$ – VNIR

Rutile - TiO_2 - VNIR

Spinel - $MgAl_2O_4$ - VNIR

Phosphates:

Apatite - $Ca_5(PO_4)_3(F,OH)$ - VNIR

Barbosalite - $Fe^{2+}Fe^{3+}_2(PO_4)_2(OH)_2$ - VNIR

Fairfieldite - $Ca_2(Mn^{2+},Fe^{2+})(PO_4)_2 \cdot 2H_2O$ - VNIR

Monazite-(Ce) - $Ce(PO_4)$ - VNIR

Parsonsite - $Pb_2(UO_2)(PO_4)_2$ - VNIR

Pyromorphite - $Pb_5(PO_4)_3Cl$ - VNIR

Turquoise - $Cu(Al,Fe^{3+})_6(PO_4)_4(OH)_8 \cdot 4H_2O$ - VNIR

Variscite - $AlPO_4 \cdot 2H_2O$ - VNIR

Vivianite - $Fe^{2+}_3(PO_4)_2 \cdot 8H_2O$ - VNIR

Phyllosilicates:

Alophane - $Al_2O_3(SiO_2)_{1.3-2} \cdot 2.5\text{-}3H_2O$ - VNIR

Aluminoceladonite - $K(Mg,Fe^{2+})Al(Si_4O_{10})(OH)_2$ - VNIR

Antigorite - $Mg_3(Si_2O_5)(OH)_4$ - Raman/VNIR

Appendices

Biotite - $K(Mg, Fe)_3AlSi_3O_{10}(OH,F)_2$ - VNIR

Cavansite - $Ca(VO)Si_4O_{10} \cdot 4H_2O$ - Raman/VNIR

Celadonite - $K(Mg,Fe^{2+})Fe^{3+}(Si_4O_{10})(OH)_2$ - VNIR

Chapmanite - $Fe^{3+}_2Sb^{3+}(Si_2O_5)O_3(OH)$ - Raman/VNIR

Chrysocolla - $(Cu,Al)_4H_4(OH)_8Si_4O_{10} \cdot nH_2O$ - Raman/VNIR

Chrysotile - $Mg_3(Si_2O_5)(OH)_4$ - VNIR

Clinochlore - $Mg_5Al(AlSi_3O_{10})(OH)_8$ - Raman/VNIR

Clintonite - $Ca(Mg,Al)_3(Al_3SiO_{10})(OH)_2$ - Raman/VNIR

Fluoroapofillite-(K) - $KCa_4Si_8O_{20}F \cdot 8H_2O$ - Raman/VNIR

Glauconite - $(K,Na)(Mg,Fe^{2+},Fe^{3+})(Fe^{3+},Al)(Si,Al)_4O_{10}(OH)_2$ - VNIR

Greenalite - $(Fe^{2+},Fe^{3+})_{2-3}Si_2O_5(OH)_4$ - VNIR

Gyrolite - $NaCa_{16}Si_{23}AlO_{60}(OH)_8 \cdot 14H_2O$ - Raman/VNIR

Halloysite - $Al_2(Si_2O_5)(OH)_4$ - VNIR

Hisingerite - $Fe^{3+}_2(Si_2O_5)(OH)_4 \cdot 2H_2O$ - Raman/VNIR

Hydroxyapofillite-(K) - $KCa_4(Si_8O_{20})OH \cdot 8H_2O$ - Raman/VNIR

Inesite - $Ca_2(Mn,Fe)_7Si_{10}O_{28}(OH)_2 \cdot 5H_2O$ - Raman/VNIR

Kaolinite - $Al_2(Si_2O_5)(OH)_4$ - VNIR

Kenyaite - $Na_2Si_{14}O_{29} \cdot 11H_2O$ - VNIR

Lepidolite - $K(Li, Al)_3(Si,Al)_4O_{10}(F,OH)_2$ - Raman/VNIR

Margarite - $CaAl_2(Al_2Si_2O_{10})(OH)_2$ - Raman/VNIR

Montmorillonite - $(Na,Ca)_{0.33}(Al,Mg)_2(Si_4O_{10})(OH)_2 \cdot nH_2O$ - VNIR

Muscovite - $KAl_2(AlSi_3O_{10})(OH)_2$ - Raman/VNIR

Nacrite - $Al_2(Si_2O_5)(OH)_4$ - VNIR

Naujakasite - $(Na,K)_6(Fe^{2+},Mn^{2+},Ca)(Al,Fe)_4Si_8O_{26}$ – VNIR

Neptunite - $Na_2KLiFe^{2+}_2Ti_2Si_8O_{24}$ - Raman/VNIR

Nimite - $(Ni,Mg,Al)_6(Si,Al)_4O_{10}(OH)_8$ - VNIR

Nontronite - $Na_{0.3}Fe_2(Si,Al)_4O_{10}(OH)_2 \cdot nH_2O$ - VNIR

Okenite - $Ca_{10}Si_{18}O_{46} \cdot 18H_2O$ - VNIR

Palygorskite - $(Mg,Al)_5(Si,Al)_8O_{20}(OH)_2 \cdot 8H2O$ - VNIR

Paragonite - $NaAl_2(AlSi_3O_{10})(OH)_2$ - Raman/VNIR

Parsettensite - $(K,Na,Ca)_{7.5}(Mn,Mg)_{49}Si_{72}O_{168}(OH)_{50} \cdot nH_2O$ - Raman/VNIR

Petalite - $LiAl(Si_4O_{10})$ - VNIR

Phlogopite - $KMg_3(AlSi_3O_{10})(OH)_2$ - Raman/VNIR

Pyrophyllite - $Al_2Si_4O_{10}(OH)_2$ - Raman/VNIR

Pyrosmalite - $(Mn^{2+}, Fe^{2+})_8Si_6O_{15}(OH,Cl)_{10}$ - Raman/VNIR

Raite - $Na_4Mn^{2+}_3Ti_{0.25}Si_8O_{20}(OH)_2·10H_2O$ - Raman/VNIR

Roscoelite - $K(V^{3+},Al)_2(AlSi_3O_{10})(OH)_2$ - VNIR

Sanbornite - $Ba_2(Si_4O_{10})$ - Raman

Searlesite - $NaB(Si_2O_5)(OH)_2$ - VNIR

Sepiolite - $Mg_4(Si_6O_{15})(OH)_2 · 6H_2O$ - Raman/VNIR

Sturtite - $Fe^{3+}(Mn^{2+},Ca,Mg)Si_4O_{10}(OH)_3·10H_2O$ - Raman/VNIR

Talc - $Mg_3Si_4O_{10}(OH)_2$ - Raman/VNIR

Ussingite - $Na_2AlSi_3O_8OH$ - Raman/VNIR

Vermiculite - $Mg_{0.7}(Mg,Fe,Al)_6(Si,Al)_8O_{20}(OH)_4·8H2O$ - VNIR

Yakhontovite - $(Ca,Na)_{0.5}(Cu,Fe,Mg)_2(Si_4O_{10})(OH)_2·3H_2O$ - Raman/VNIR

Sorosilicates:

Axinite - $Ca_2Fe^{2+}Al_2BSi_4O_{15}OH$ - VNIR

Epidote - $Ca_2Fe^{3+}Al_2(Si_2O_7)(SiO_4)O(OH)$ - Raman/VNIR

Vesuvianite - $Ca_{10}(Mg,Fe)_2Al_4(SiO_4)_5(Si_2O_7)_2(OH,F)_4$ - Raman/VNIR

Sulfides and sulfates:

Arcanite - K_2SO_4 - VNIR

Arsenopyrite - $FeAsS$ - VNIR

Barite - $BaSO_4$ - Raman/VNIR

Bassanite - $CaSO_4·0.5H_2O$ - VNIR

Boothite - $CuSO_4·7H_2O$ - VNIR

Brochantite - $Cu_4(SO_4)(OH)_6$ - Raman/VNIR

Caledonite - $Pb_5Cu_2(SO_4)_3(CO_3)(OH)_6$ - Raman/VNIR

Celestine - $SrSO_4$ - Raman/VNIR

Chalcopyrite - $CuFeS_2$ - Raman

Diaphorite - $Pb_2Ag_3Sb_3S_8$ - Raman

Freieslebenite - $AgPbSbS_3$ - Raman

Gersdorffite - $NiAsS$ - VNIR

Glauberite - $Na_2Ca(SO_4)_2$ - VNIR

Gudmundite - $FeSbS$ - VNIR

Gypsum - $CaSO_4 \cdot 2H_2O$ - Raman/VNIR

Jarosite - $KFe^{3+}_3(SO_4)_2(OH)_6$ - VNIR

Kiserite - $MgSO_4 \cdot H_2O$ - VNIR

Langite - $Cu_4(SO_4)(OH)_6 \cdot 2H_2O$ - VNIR

Linarite - $PbCu(SO_4)(OH)_2$ - Raman/VNIR

Magnesium sulfate - $MgSO_4$ - VNIR

Morenosite - $NiSO_4 \cdot 7H_2O$ - VNIR

Pyrite - Fe_2S - Raman

Serpierite - $Ca(Cu,Zn)_4(SO_4)_2(OH)_6 \cdot 3H2O$ - VNIR

Thenardite - Na_2SO_4 - VNIR

Tectosilicates:

Adularia - $K(AlSi_3O_8)$ - Raman/VNIR

Afghanite - $(Na,K)_{22}Ca_{10}(Si_{24}Al_{24}O_{96})(SO_4)_6Cl_6$ - VNIR

Albite - $Na(AlSi_3O_8)$ - VNIR

Analcime - $Na(AlSi_2O_6) \cdot H_2O$ - Raman/VNIR

Barrerite - $(Na,K,Ca_{0.5})_2(Al_2Si_7O_{18}) \cdot 7H_2O$ - VNIR

Chabazite - $(Ca,K_2,Na_2)_2(Al_2Si_4O_{12})_2 \cdot 12H_2O$ - VNIR

Gmelinite - $Na_4(Si_8Al_4O_{24}) \cdot 11H_2O$ - VNIR

Gonnardite - $(Na,Ca)_2(Si,Al)_5O_{10} \cdot 3H_2O$ - VNIR

Harmotome - $(Ba_{0.5},Ca_{0.5},K,Na)_5(Al_5Si_{11}O_{32}) \cdot 12H_2O$ - VNIR

Helvita - $Be_3Mn^{2+}_4(SiO_4)_3S$ - VNIR

Heulandite - $(Na,K)(Ba,Ca,Sr)_4(Si_{27}Al_9)O_{72} \cdot 24H_2O$ - Raman/VNIR

Kaliophilite - $KAlSiO_4$ - Raman/VNIR

Lazurite - $Na_3Ca(Si_3Al_3)O_{12}(SO_4,S,S_2,S_3,Cl,OH)$ - Raman/VNIR

Leucite - $K(AlSi_2O_6)$ - VNIR

Liottite - $(Na,K)_{16}Ca_8(Al_6Si_6O_{24})_3(SO_4)_5Cl_4$ - VNIR

Mesolite - $Na_2Ca_2Si_9Al_6O_{30} \cdot 8H_2O$ - VNIR

Microcline - $K(AlSi_3O_8)$ - VNIR

Natrolite - $Na_2Al_2Si_3O_{10} \cdot 2H_2O$ - VNIR

Phillipsite-(K) - $(K,Na,Ca_{0.5},Ba_{0.5})_{4-7}(Al_{4-7}Si_{12-9}O_{32})\cdot 12H_2O$ - VNIR

Phillipsite-(Na) - $(Na,K,Ca_{0.5},Ba_{0.5})_{4-7}(Al_{4-7}Si_{12-9}O_{32})\cdot 12H_2O$ - VNIR

Pollucite - $(Cs,Na)_2(Al_2Si_4O_{12})\cdot 2H_2O$ - VNIR

Sodalite - $Na_8(Al_6Si_6O_{24})Cl_2$ - Raman/VNIR

Stellerite - $Ca_4(Si_{28}Al_8)O_{72}\cdot 28H_2O$ - VNIR

Stilbite - $NaCa_4(Al_9Si_{27}O_{72}) \cdot nH_2O$ - Raman/VNIR

Thomsonite - $NaCa_2(Al_5Si_5O_{20})\cdot 6H_2O$ - VNIR

Appendix IV: ToF-SIMS distribution images
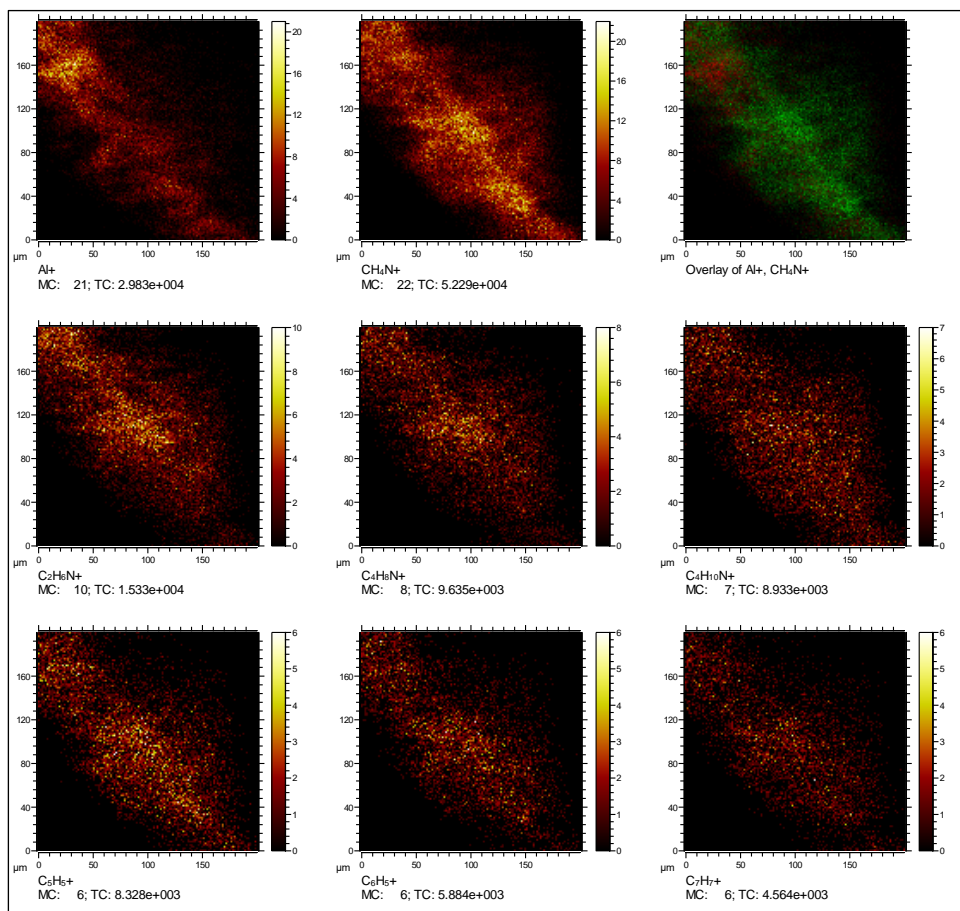
Figure A.IV.1.a) ToF-SIMS distribution images of all the fragments observed in the sample Ar01_01 (Armintza)
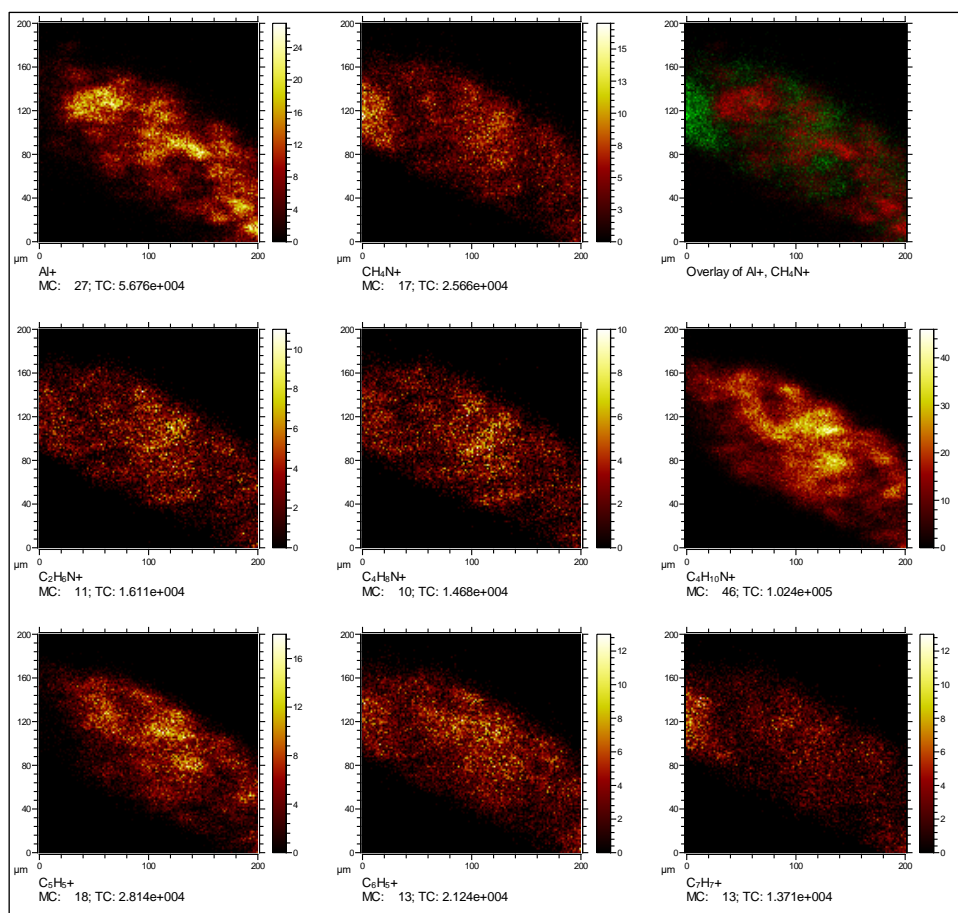
Figure A.IV.1.b) ToF-SIMS distribution images of all the fragments observed in the sample Ar01_02 (Armintza)
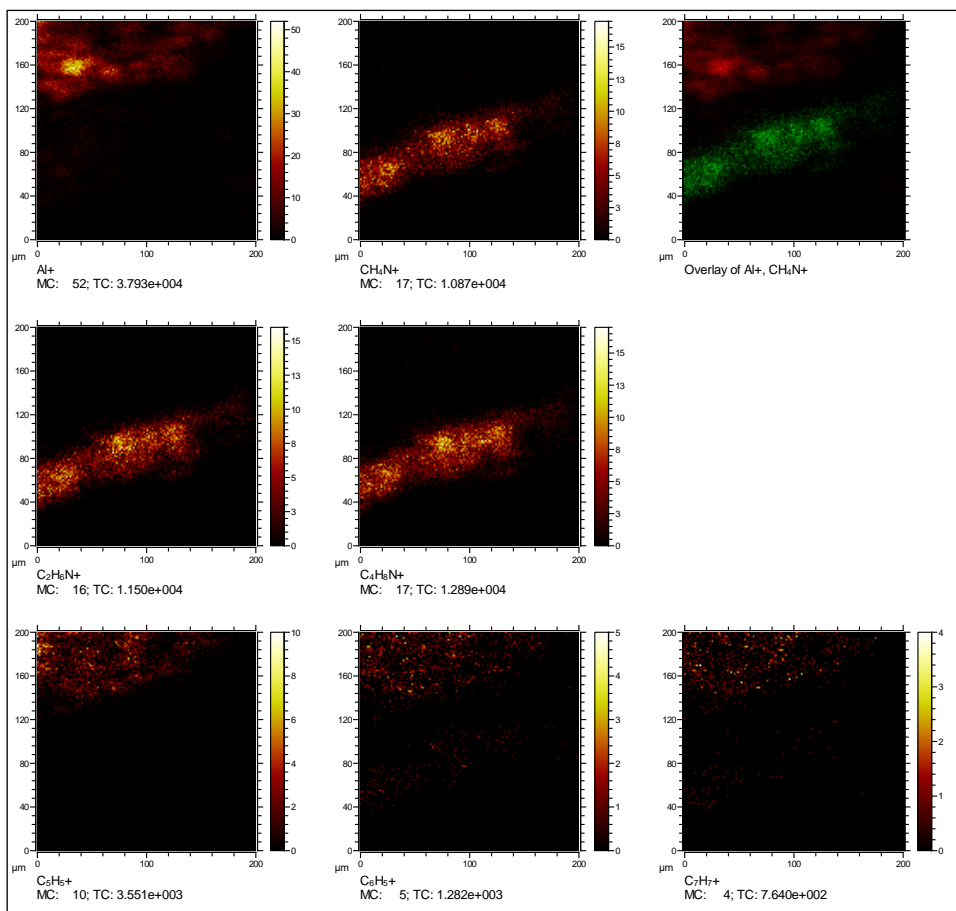
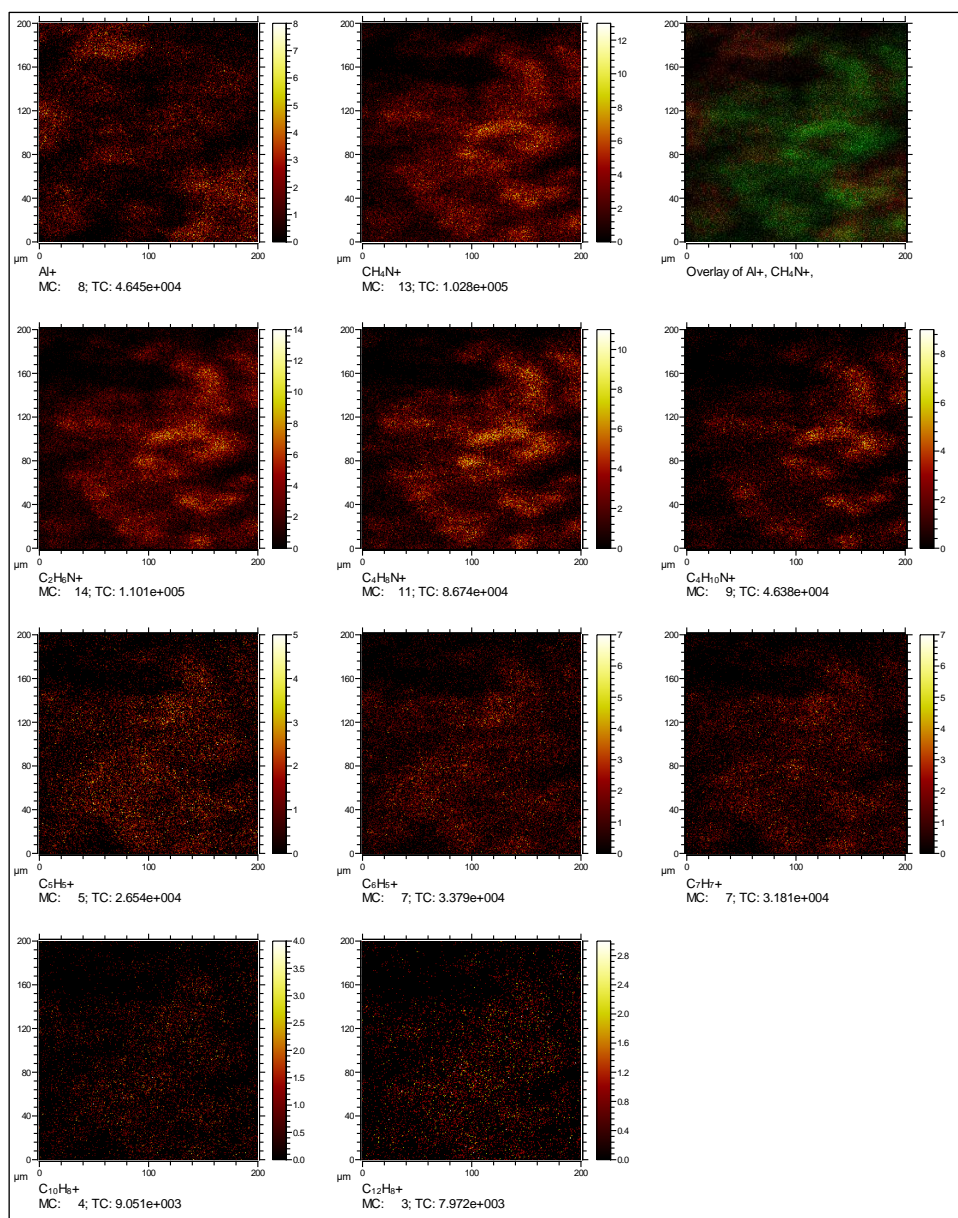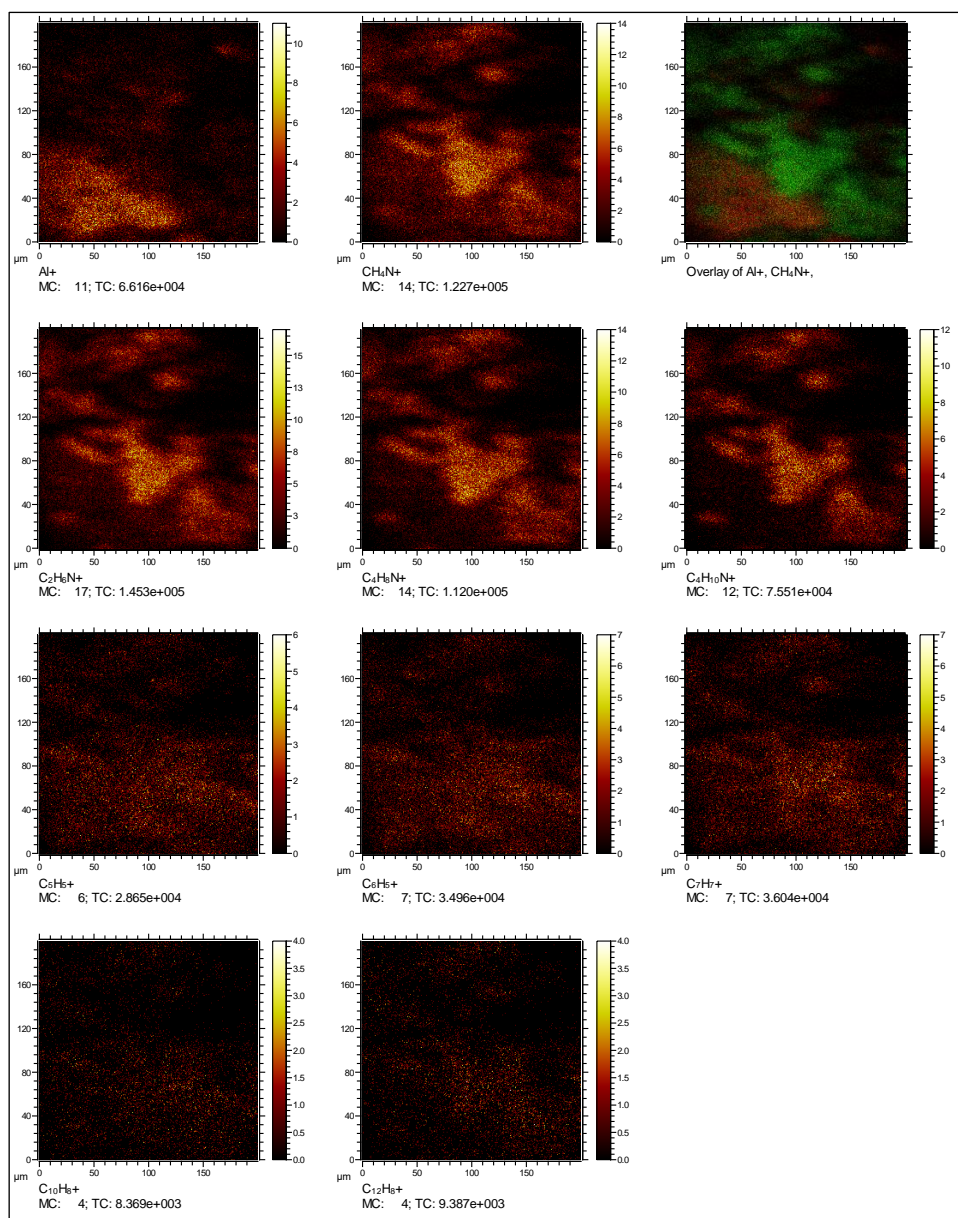**Figure A.IV.1.c)** ToF-SIMS distribution images of all the fragments observed in the sample Ar01_03 (Armintza)
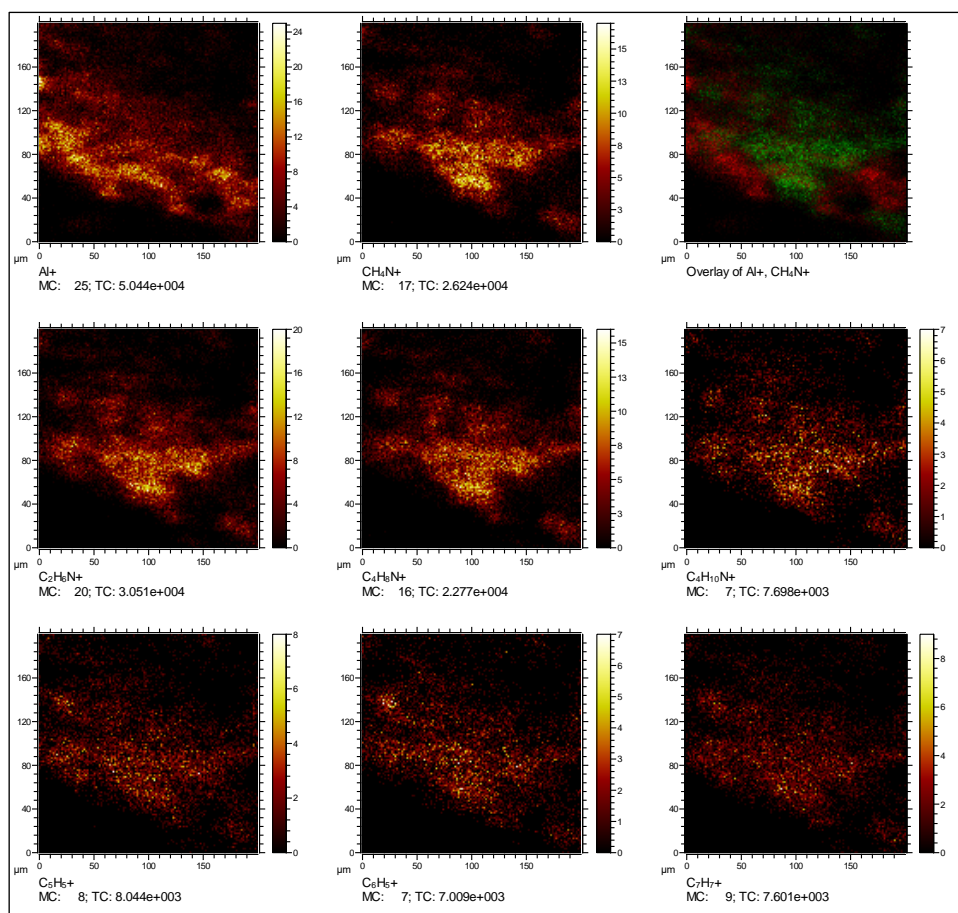
Figure A.IV.2.a) ToF-SIMS distribution images of all the fragments observed in the sample Ar02_01 (Armintza)
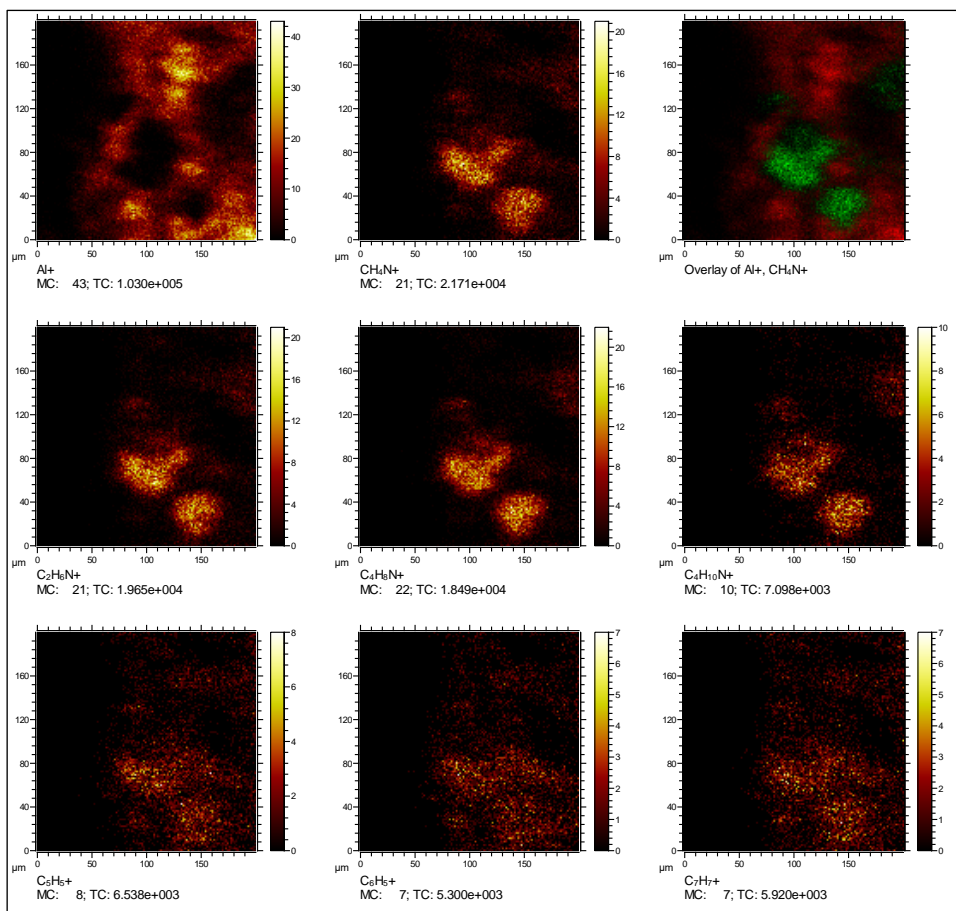
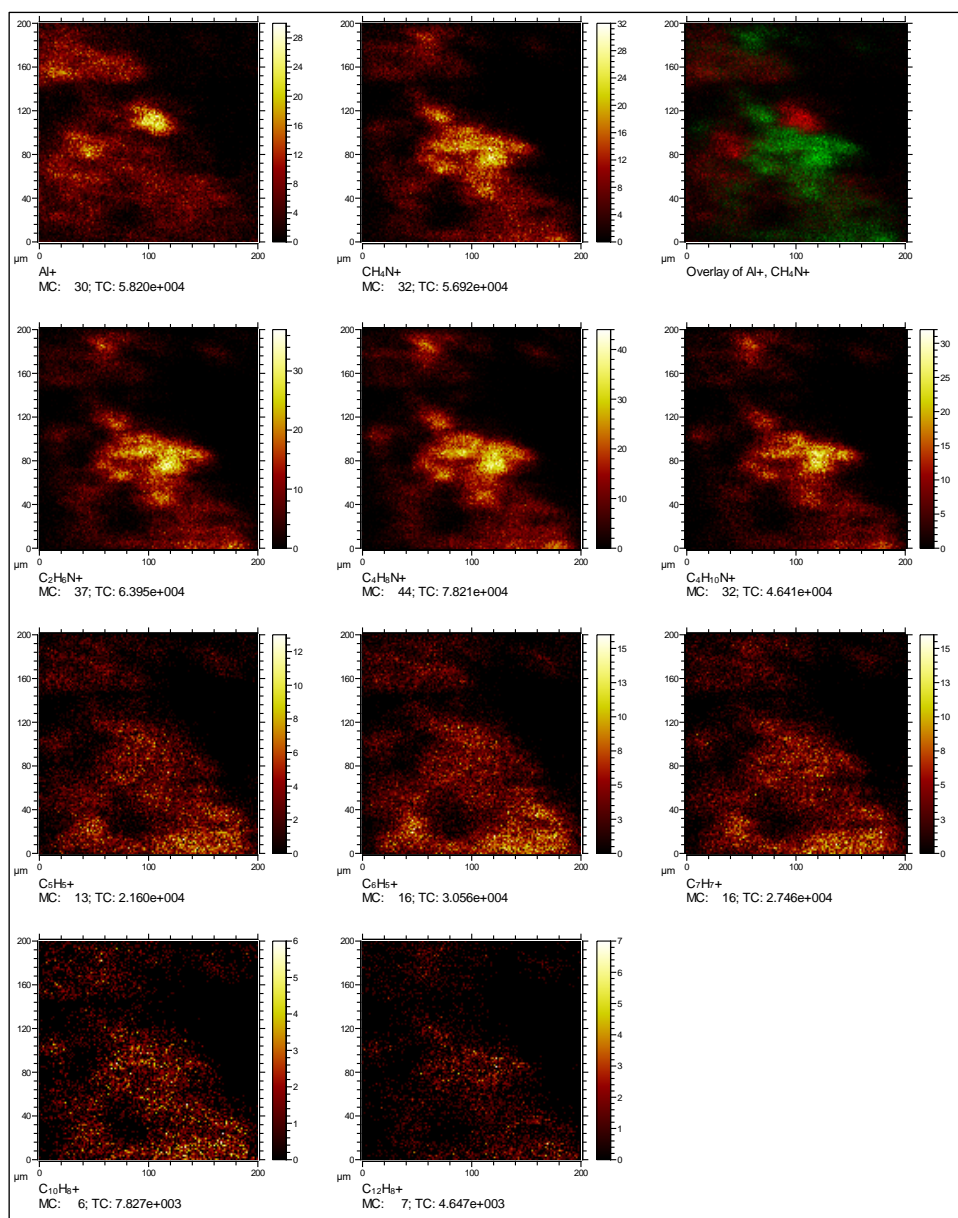**Figure A.IV.2.b)** ToF-SIMS distribution images of all the fragments observed in the sample Ar02_02 (Armintza)
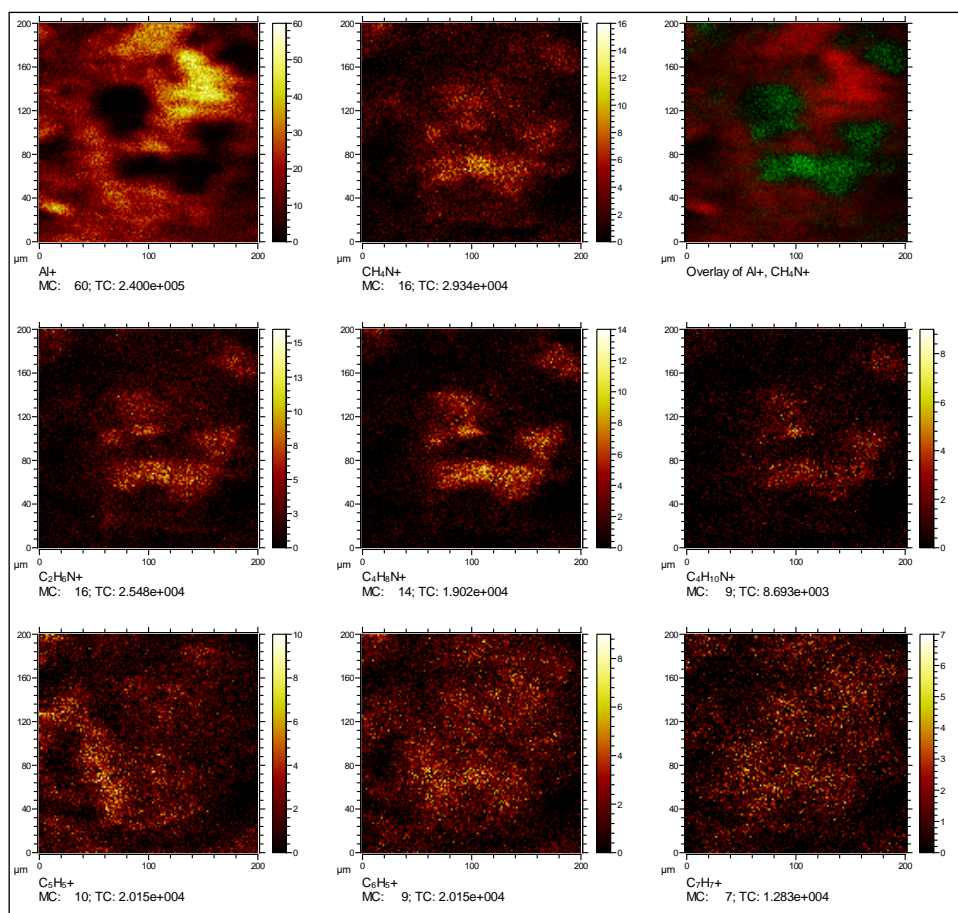
Figure A.IV.2.c) ToF-SIMS distribution images of all the fragments observed in the sample Ar02_03 (Armintza)
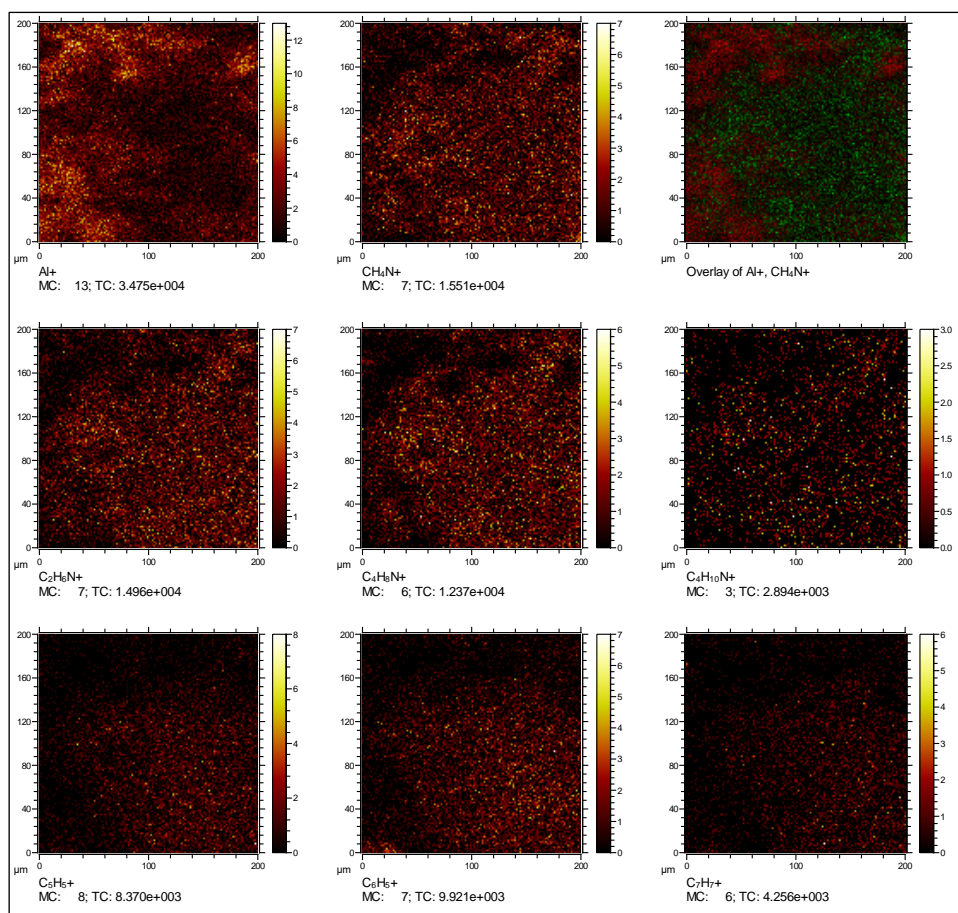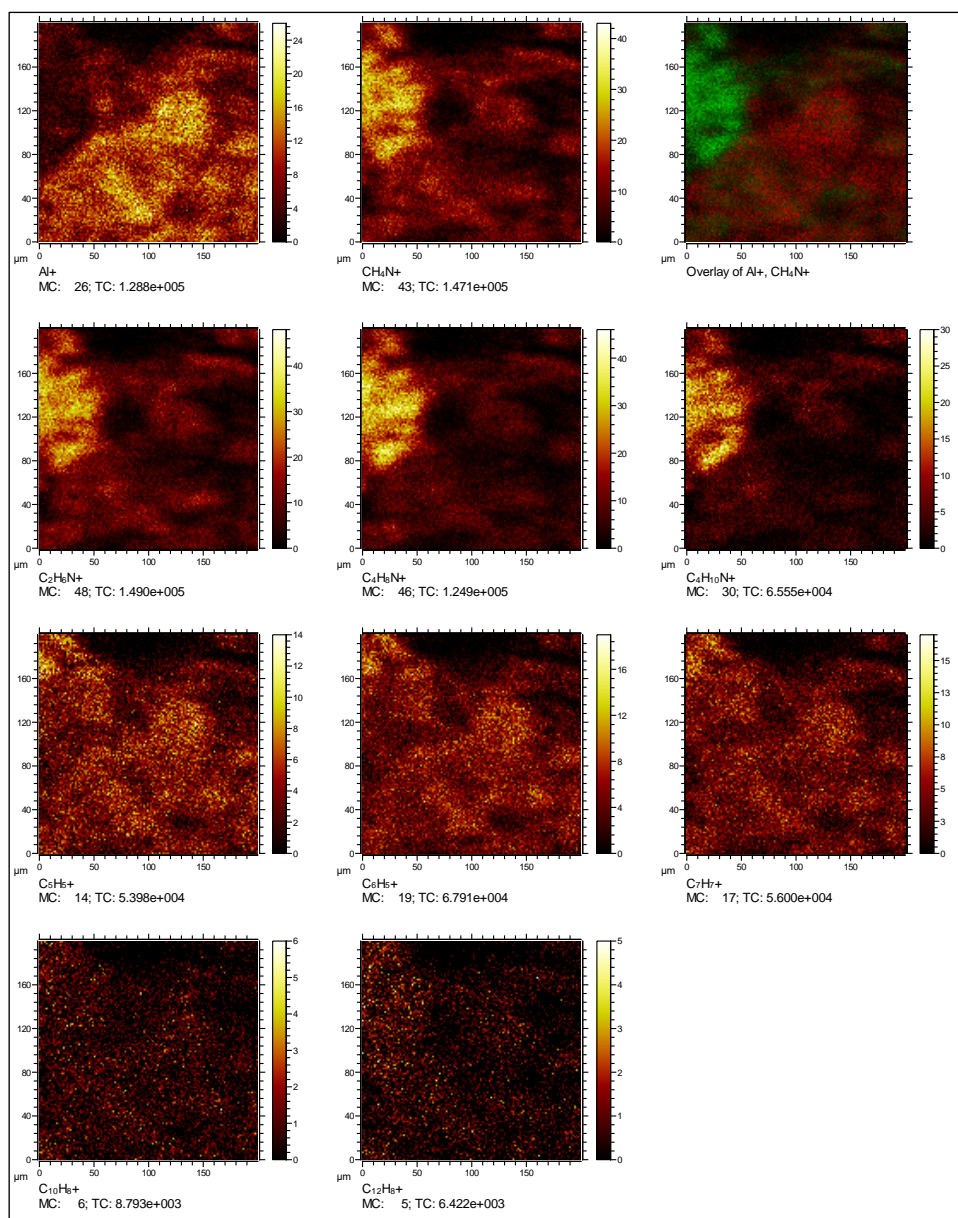
Figure A.IV.3.a) ToF-SIMS distribution images of all the fragments observed in the sample Ar03_01 (Armintza)
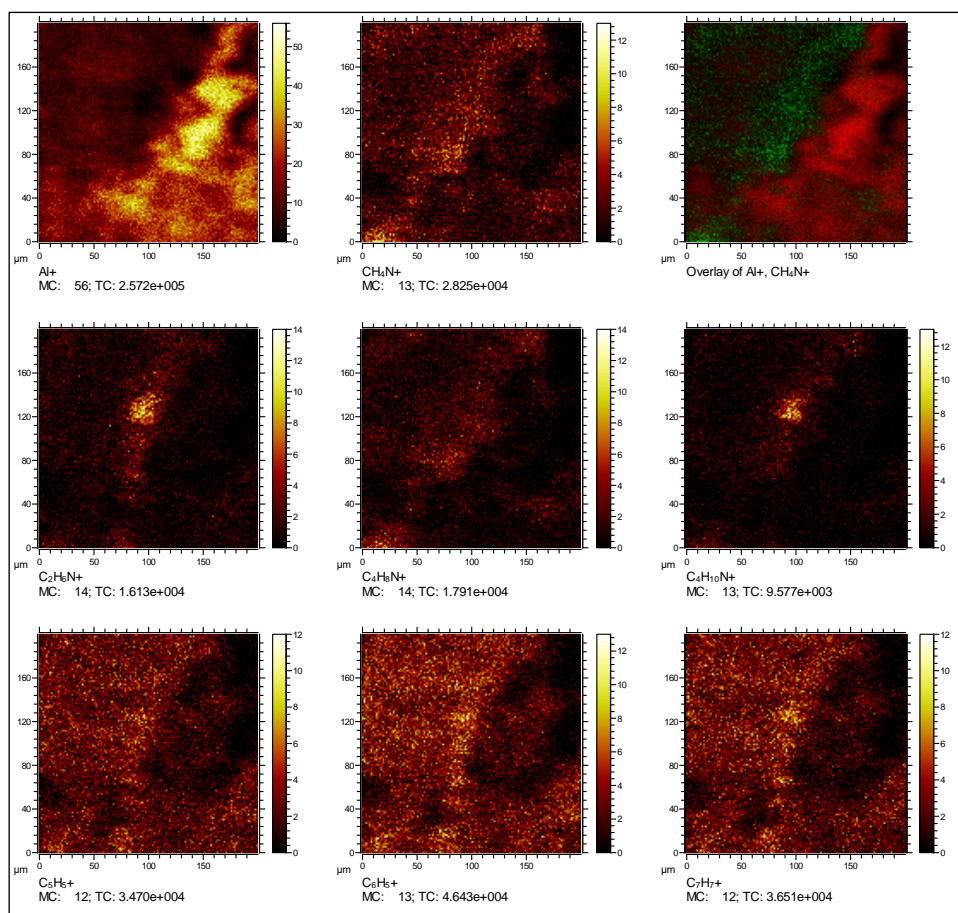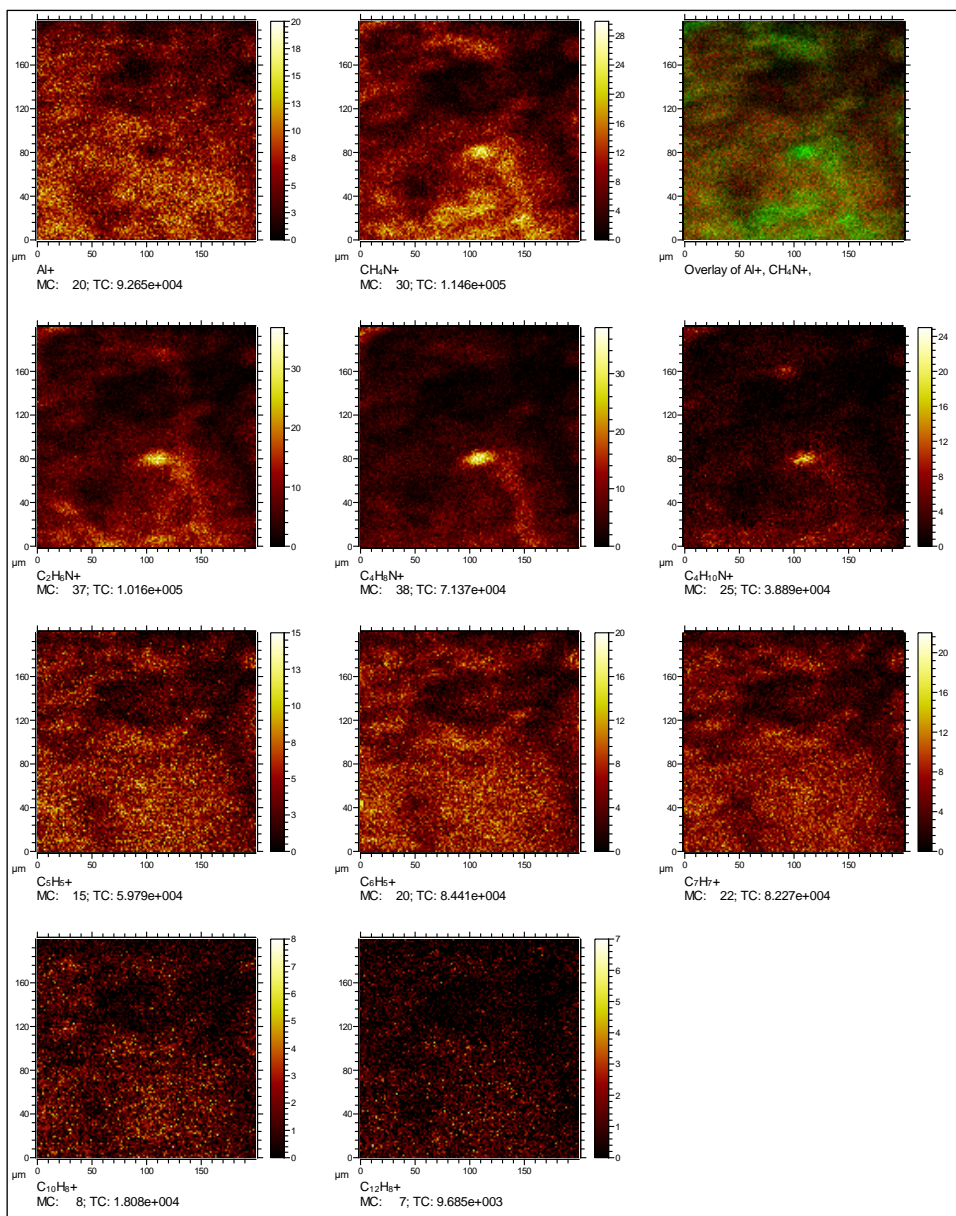
Figure A.IV.3.b) ToF-SIMS distribution images of all the fragments observed in the sample Ar03_02 (Armintza)
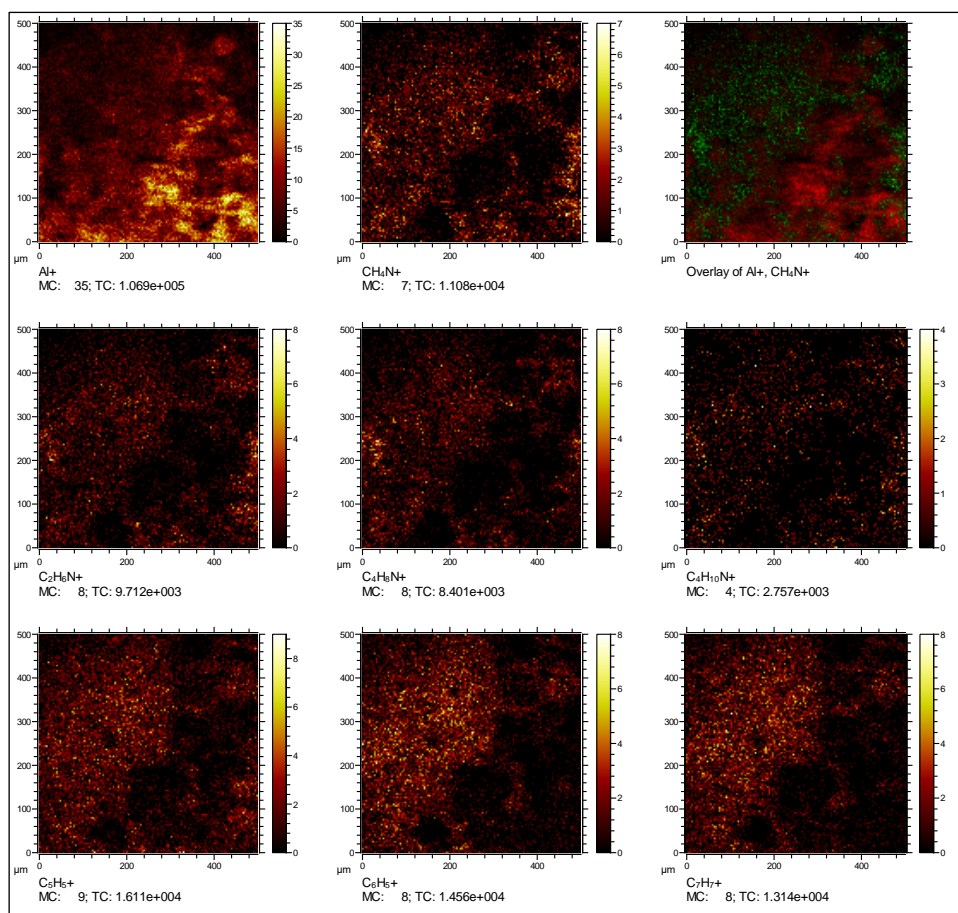
Figure A.IV.3.c) ToF-SIMS distribution images of all the fragments observed in the sample Ar03_03 (Armintza)
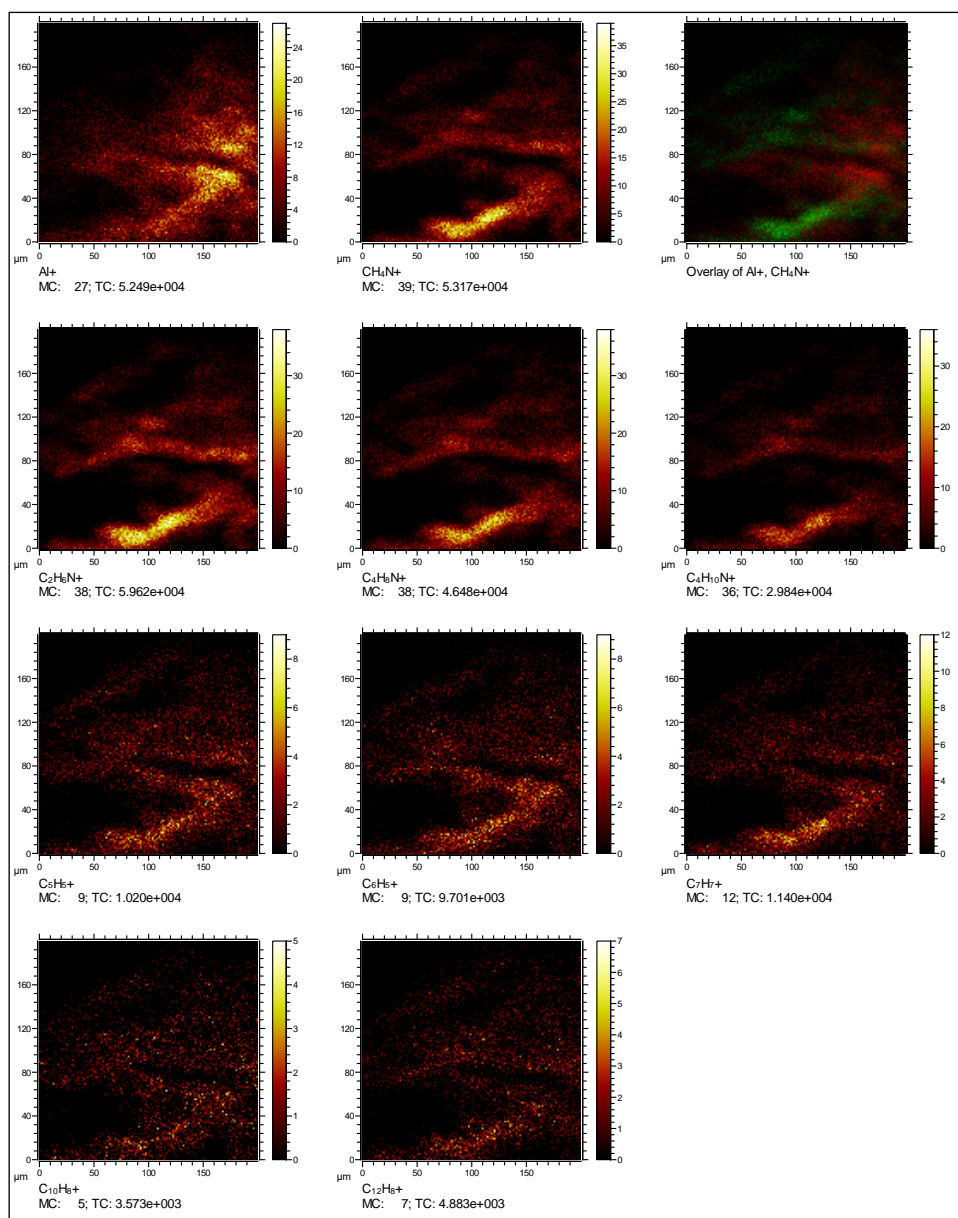
Figure A.IV.4.a) ToF-SIMS distribution images of all the fragments observed in the sample En01_01 (Enekuri)
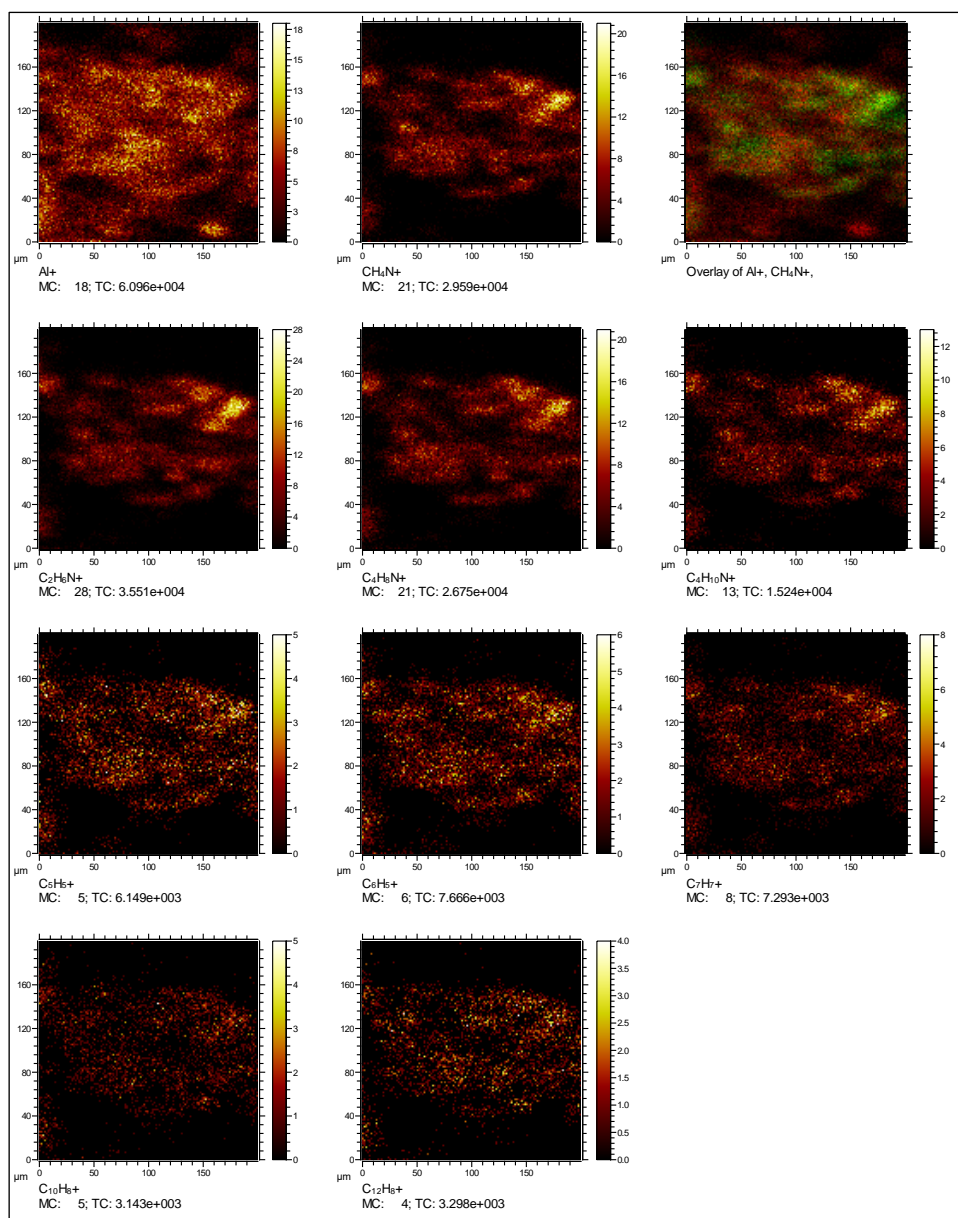
Figure A.IV.4.b) ToF-SIMS distribution images of all the fragments observed in the sample En01_02 (Enekuri)
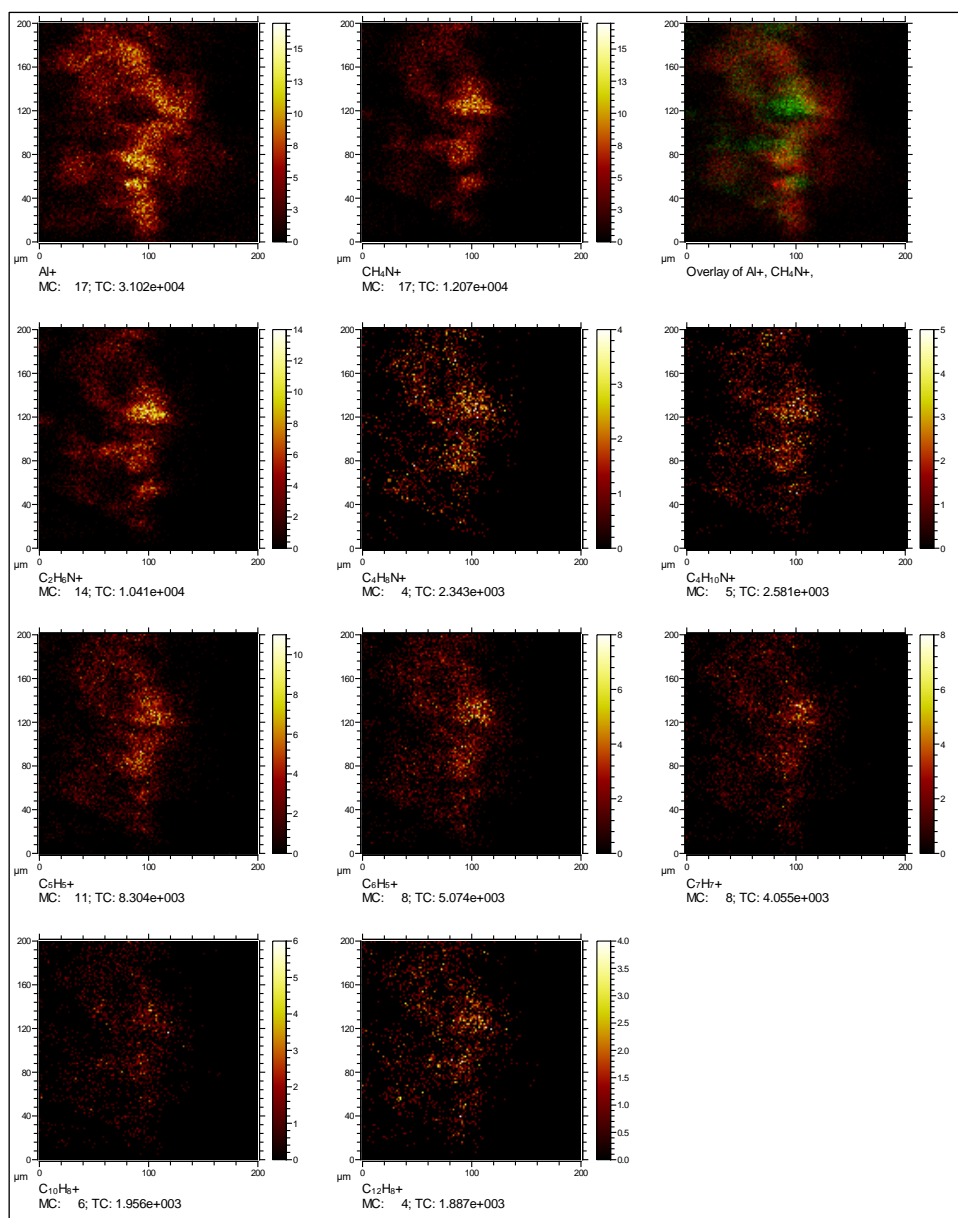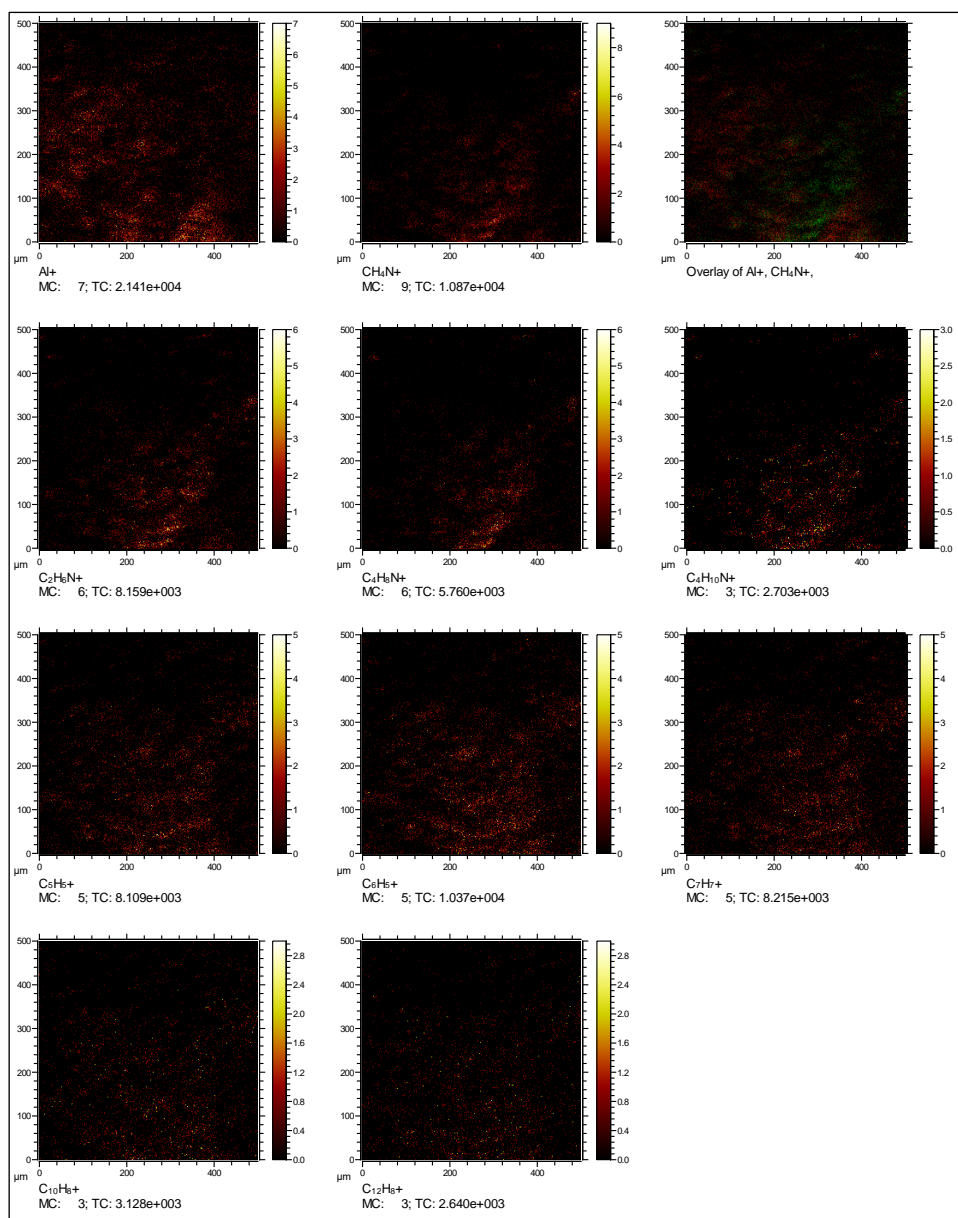
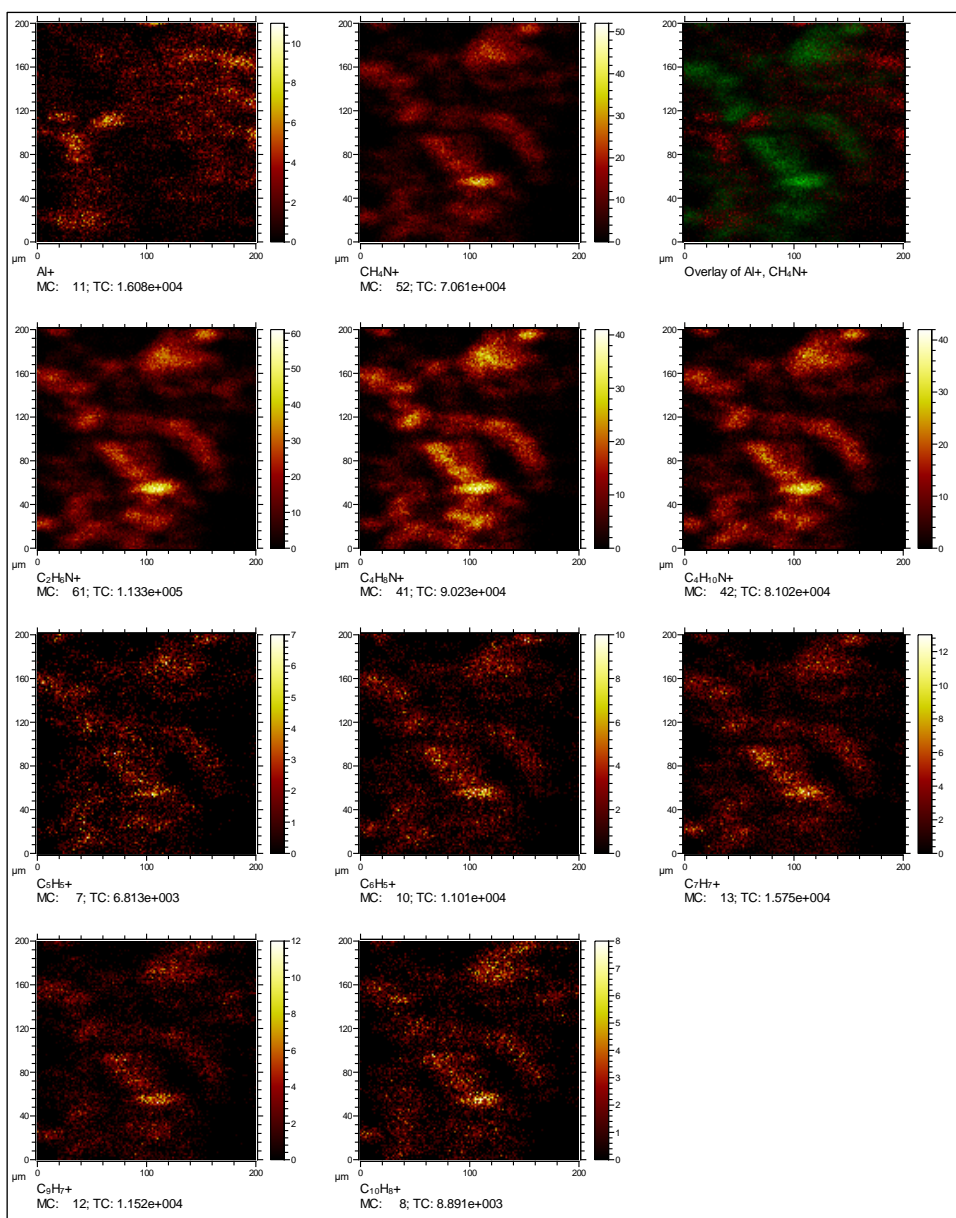**Figure A.IV.4.c)** ToF-SIMS distribution images of all the fragments observed in the sample En01_03 (Enekuri)

Figure A.IV.5.a) ToF-SIMS distribution images of all the fragments observed in the sample En02_01 (Enekuri)

Figure A.IV.5.b) ToF-SIMS distribution images of all the fragments observed in the sample En02_02 (Enekuri)

Figure A.IV.5.c) ToF-SIMS distribution images of all the fragments observed in the sample En02_03 (Enekuri)

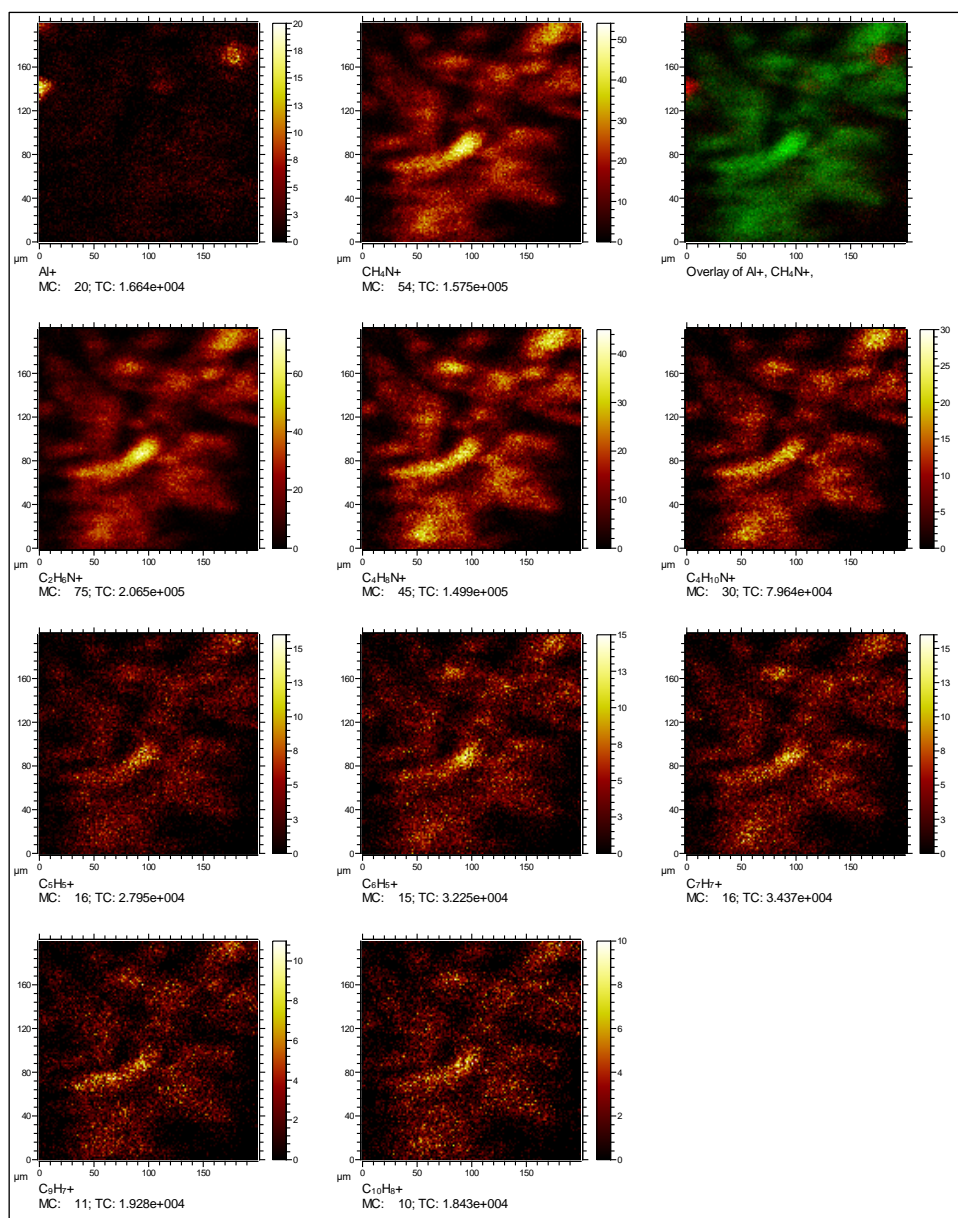**Figure A.IV.6.a)** ToF-SIMS distribution images of all the fragments observed in the sample En03_01 (Enekuri)

Figure A.IV.6.b) ToF-SIMS distribution images of all the fragments observed in the sample En03_02 (Enekuri)

Figure A.IV.6.c) ToF-SIMS distribution images of all the fragments observed in the sample En03_03 (Enekuri)

Figure A.IV.7.a) ToF-SIMS distribution images of all the fragments observed in the sample Fr01_01 (Fruiz)

Figure A.IV.7.b) ToF-SIMS distribution images of all the fragments observed in the sample Fr01_02 (Fruiz)
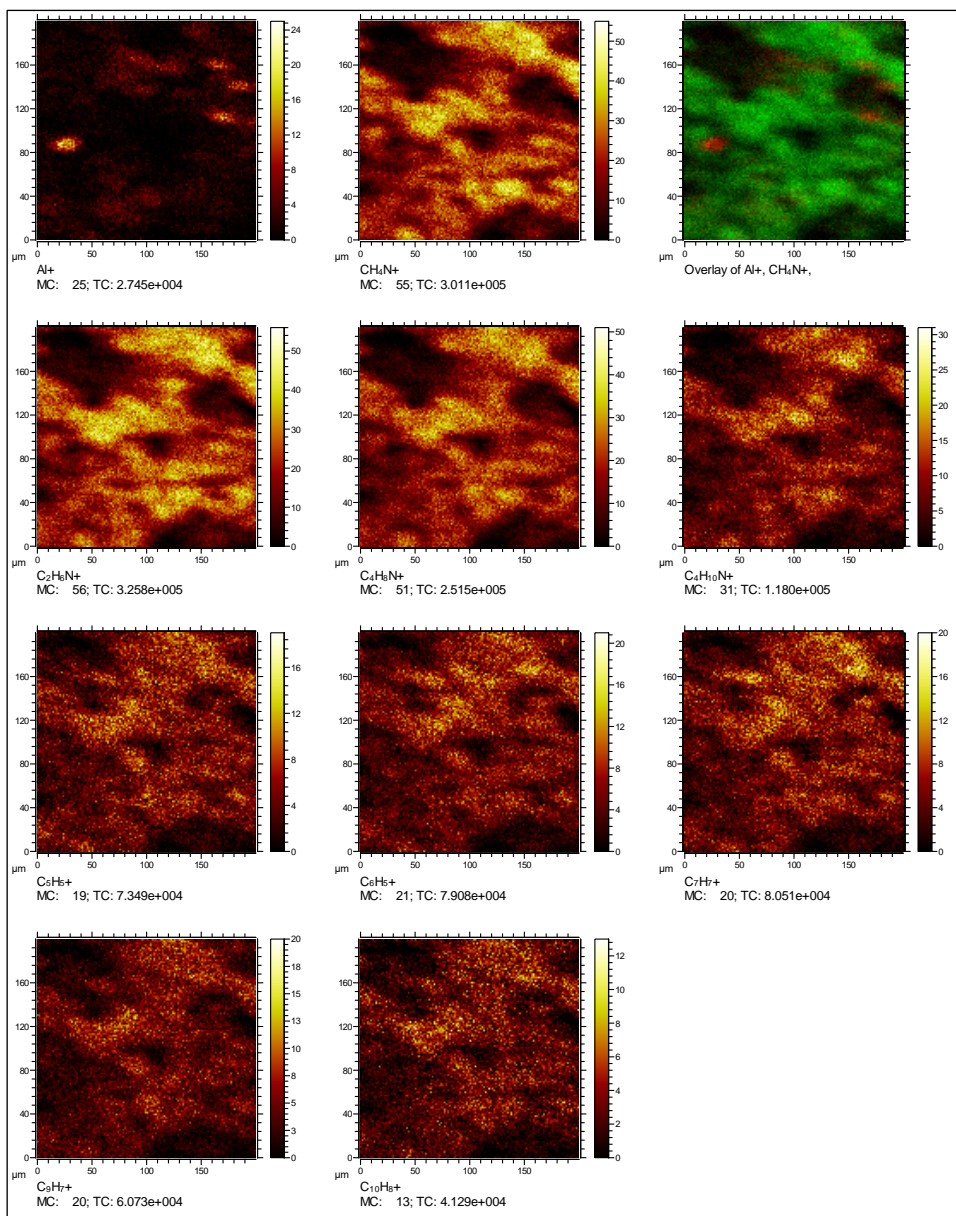
Figure A.IV.7.c) ToF-SIMS distribution images of all the fragments observed in the sample Fr01_03 (Fruiz)
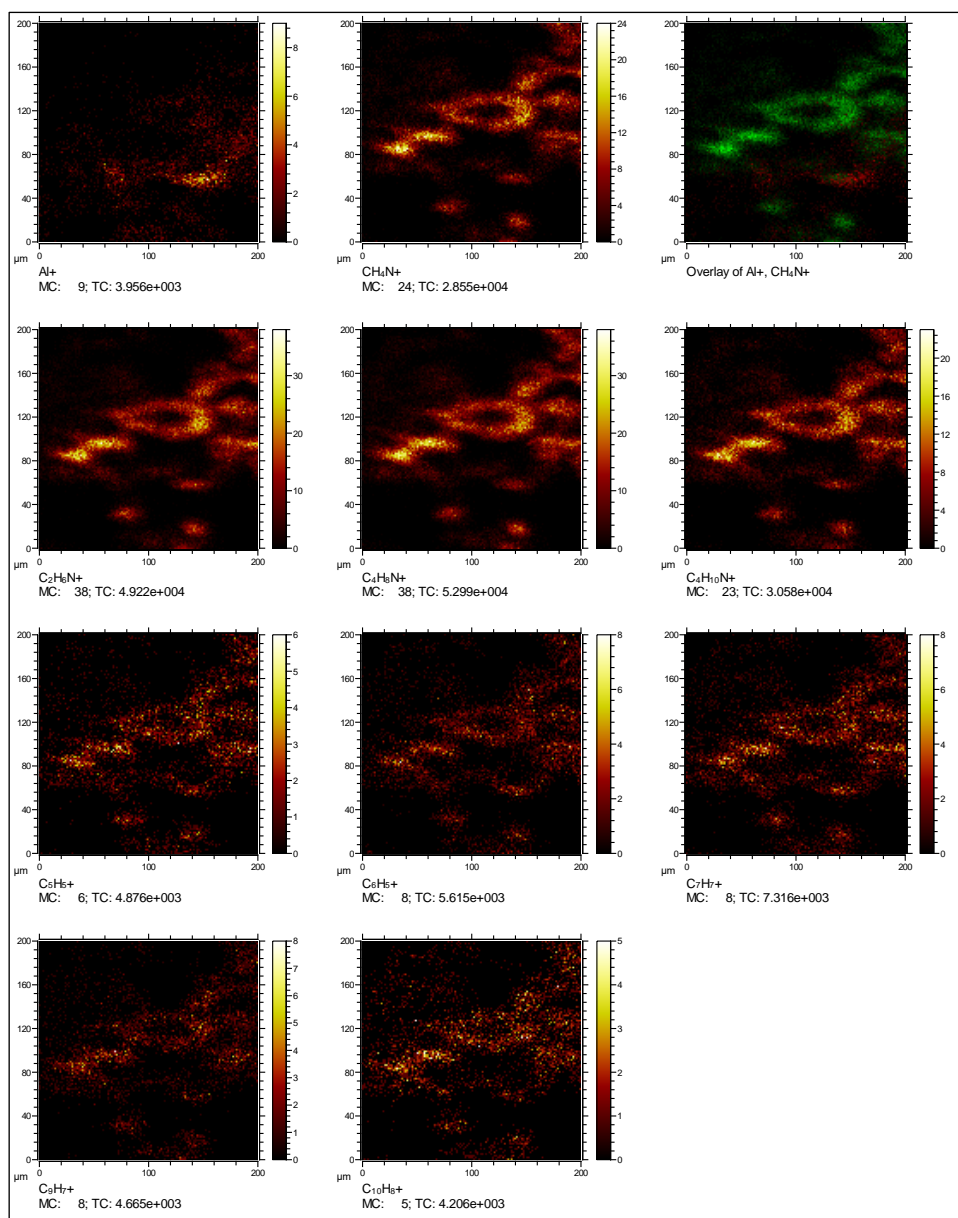
Figure A.IV.8.a) ToF-SIMS distribution images of all the fragments observed in the sample Fr02_01 (Fruiz)
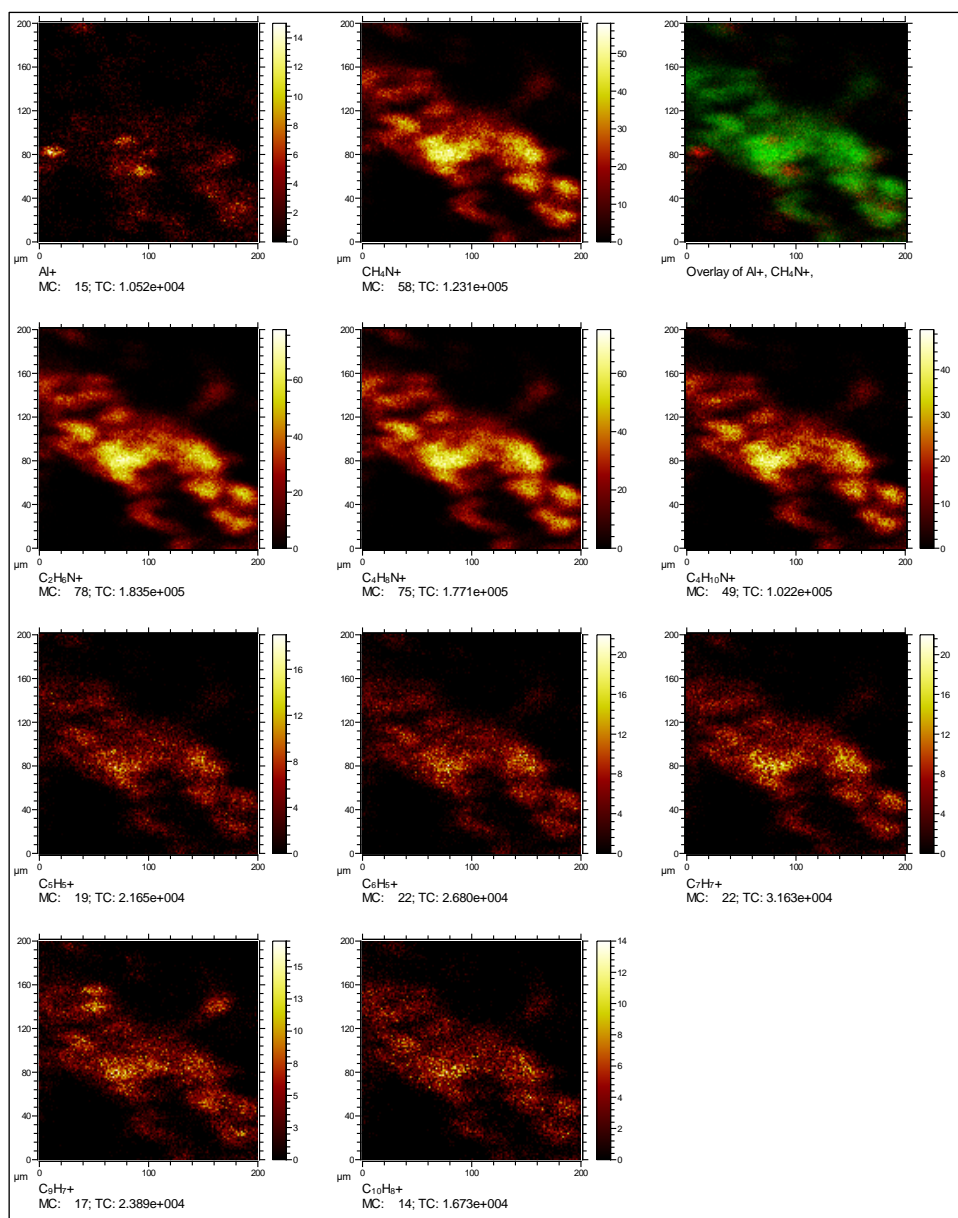
Figure A.IV.8.b) ToF-SIMS distribution images of all the fragments observed in the sample Fr02_02 (Fruiz)
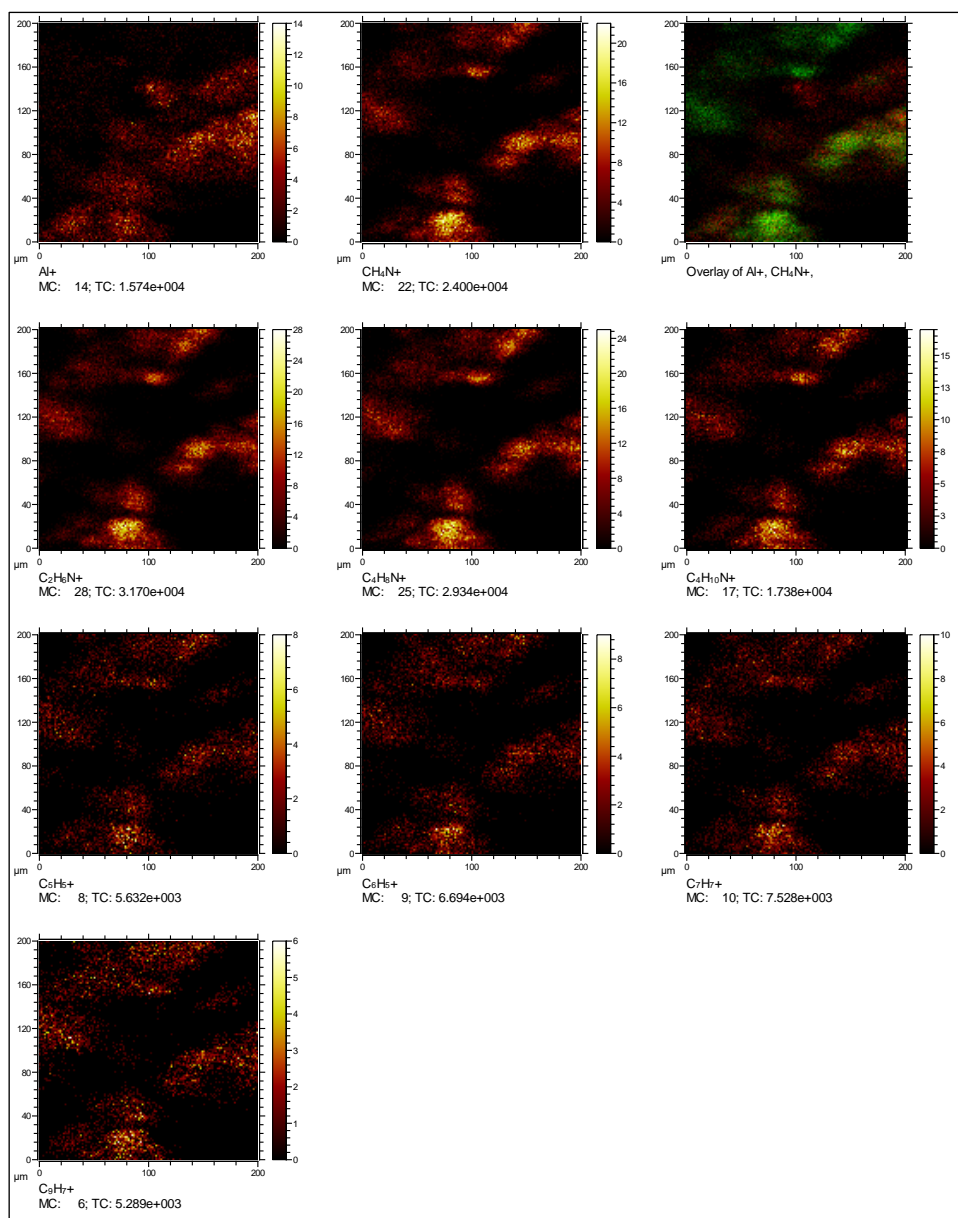
Figure A.IV.8.c) ToF-SIMS distribution images of all the fragments observed in the sample Fr02_03 (Fruiz)
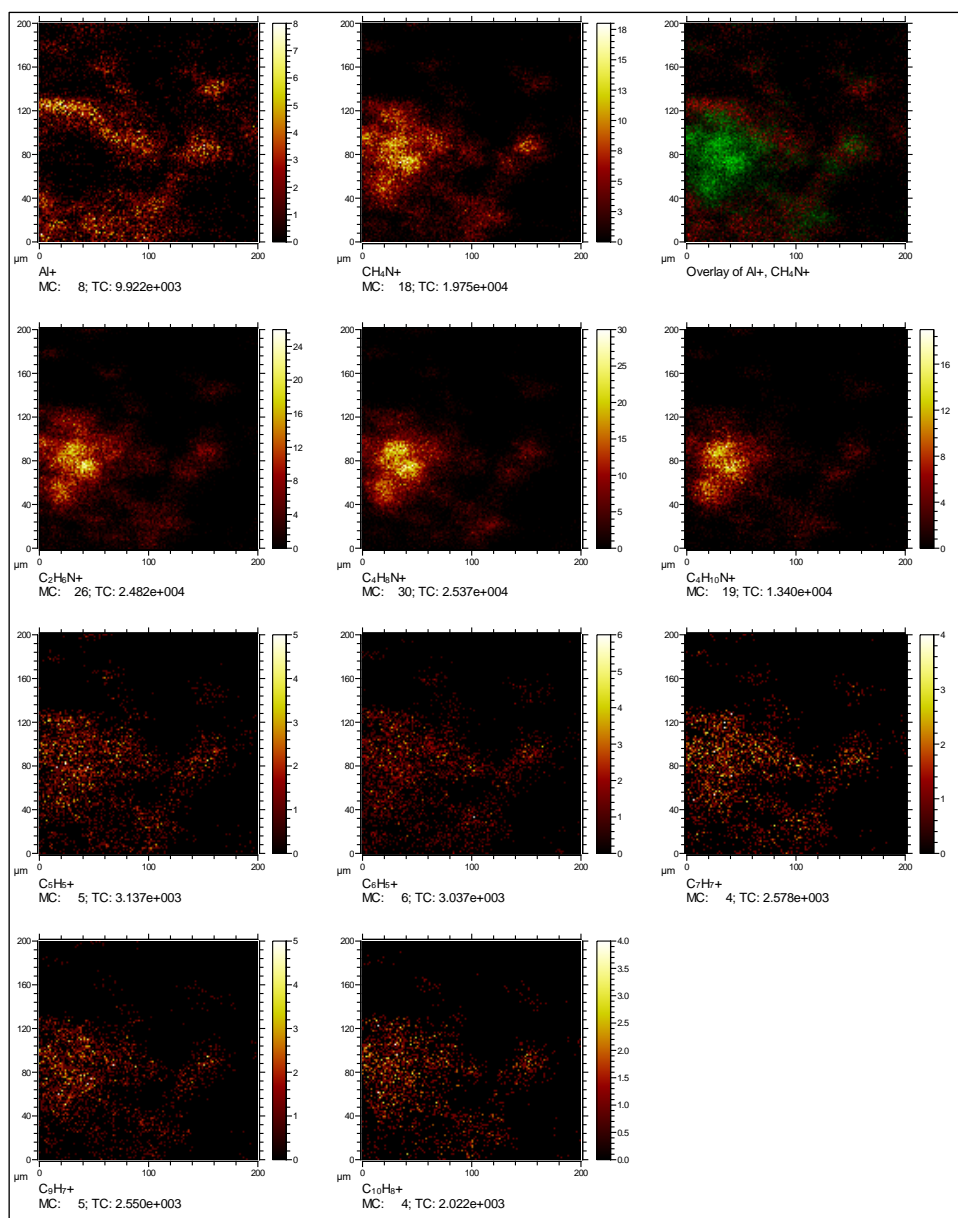
Figure A.IV.9.a) ToF-SIMS distribution images of all the fragments observed in the sample Fr03_01 (Fruiz)
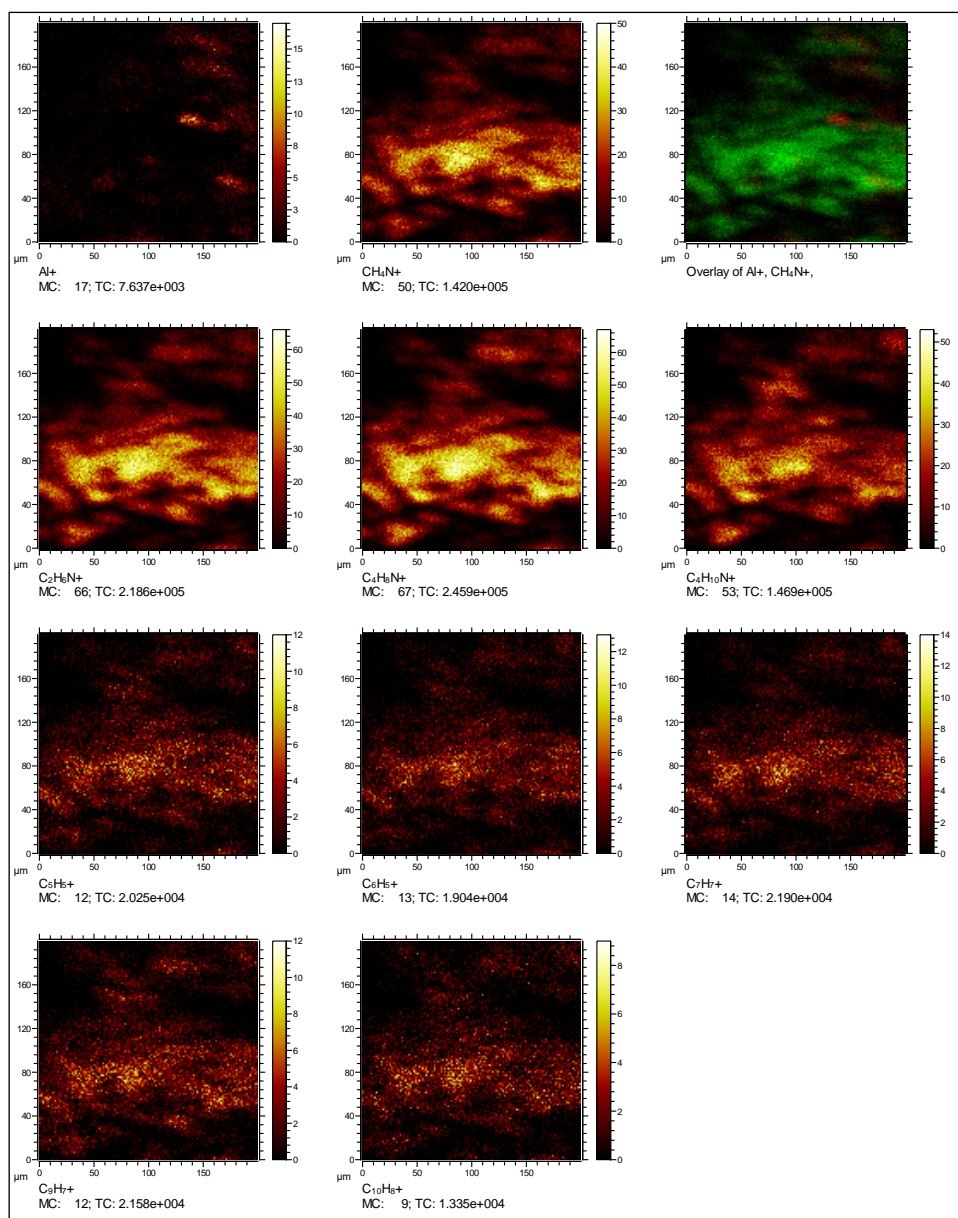
Figure A.IV.9.b) ToF-SIMS distribution images of all the fragments observed in the sample Fr03_02 (Fruiz)

Appendix V: Scientific publications

- **Scientific articles in research journals:**

- **Ruiz-Galende P.**, Fernández G., Torre-Fdez I., Aramendia J., Gómez-Nubla L., García-Florentino C., Castro K., Arana G., Madariaga J. M. Characterization of sedimentary and volcanic rocks in Armintza outcrop (Biscay, Spain) and its implication for Oxia Planum (Mars) exploration. *Spectrochim.Acta A Mol.Biomol.Spectrosc.,* **2020,** Under Review.

- **Ruiz-Galende P.**, Torre-Fdez I., Aramendia J., Gómez-Nubla L., Castro K., Arana G., Fdez-Ortiz de Vallejuelo S., Maguregui M., Medina J., Baonza V. G., Rull F., Madariaga J. M. New Raman-visible near-infrared database of inorganic and mineralogical planetary and terrestrial compounds and its implications for Mars: Phyllosilicates. *J. Raman Spectrosc.,* **2019,** https://doi.org/10.1002/jrs.5677.

- **Ruiz-Galende P.**, Torre-Fdez I., Aramendia J., Gómez-Nubla L., Castro K., Arana G., Madariaga J. M. Study of a terrestrial Martian analogue: Geochemical characterization of the Meñakoz outcrops (Biscay, Spain). *J. Raman Spectrosc.,* **2019,** https://doi.org/10.1002/jrs.5565.

- **Contributions to national and international conferences:**

- **Ruiz-Galende P.**, Siljeström S., Li X., Torre-Fdez I., Castro K., Arana G., Madariaga J. M. Characterization of organic molecules in Martian analogue samples: Implications for Mars exploration. *Goldschmidt.* **2019.**

- Huidobro J., Torre-Fdez I., García-Florentino C., **Ruiz-Galende P.**, Aramendia J., J. M. Madariaga. Terrestrial weathering of Ilmenite and Olivine in the Northwest Africa 11273 Lunar Meteorite. *Goldschmidt.* **2019.**

- García-Florentino C., Gómez-Nubla L., Torre-Fdez I., **Ruiz-Galende P.**, Aramendia J., Madariaga J. M. Transformation in the Gypsum-Syngenite-Polyhalite system to describe their formation on Mars. *Goldschmidt.* **2019.**

- **Ruiz-Galende P.**, Siljeström S., Torre-Fdez I., Castro K., Arana G., Madariaga J. M. Spectroscopic analysis of organic molecules in Martian analogue samples. 9th International Conference on Mars. **2019,** abst. 6182.

- García-Florentino C., Huidobro J., Gómez-Nubla L., Torre-Fdez I., **Ruiz-Galende P.**, Aramendia J., Castro K., Arana G., Madariaga J. M. Raman spectroscopy to detect alterations in volcanic mineral phases due to shock and environmental impacts. 9th International Conference on Mars. **2019,** abst. 6269.

-Castro K., **Ruiz-Galende P.**, Torre- Fdez I., Huidobro J., García-Florentino C., Gómez-Nubla L., Aramendia J., Fdez-Ortiz de Vallejuelo S., Maguregui M., Arana G., Madariaga J. M. Raman microspectroscopy to detect high temperature and high pressure minerals in meteorites: clues about their formation. *VI Reunión CPESS.* **2019.**

- Madariaga J. M., **Ruiz-Galende P.**, Torre- Fdez I., Huidobro J., García-Florentino C., Gómez-Nubla L., Aramendia J., Fdez-Ortiz de Vallejuelo S., Maguregui M., Castro K., Arana G. Raman microspectroscopy coupled to SEM/EDS to detect and identify organic matter in Impact Glasses, Meteorites and Terrestrial Analogs. *VI Reunión CPESS.* **2019.**

- Arana G., **Ruiz-Galende P.**, Torre- Fdez I., Gómez-Nubla L., Aramendia J., Fdez-Ortiz de Vallejuelo S., Maguregui M., Castro K., Madariaga J. M. Geochemical characterization by Raman and vis-NIR Spectroscopies of a terrestial Martian analogue: the submarine volcano of Meñakoz (Biscay, Spain). *VI Reunión CPESS.* **2019.**

- Torre-Fdez I., **Ruiz-Galende P.**, Aramendia J., Gómez-Nubla L., Castro K., Arana G., Madariaga J. M. New quantitative model to determine fayalite-forsterite content in olivine minerals by Raman spectroscopy. *LPSC 50.* **2019,** abst. 2486.

- Huidobro J., Aramendia J., **Ruiz-Galende P.**, Torre-Fdez I., Madariaga J. M. Raman spectroscopy on the new NorthWest Africa 11273 lunar meteorite to understand the initial impact and the final terrestrial weathering. *LPSC 50.* **2019,** abst. 2476.

- **Ruiz-Galende, P.**, Torre-Fdez, I., Aramendia, J., Gómez-Nubla, L., Castro, K., Arana, G., Madariaga, J.M. Formation of titanium oxide (TiO_2) polymorphs in an emerged submarine volcano environment: Implications for Mars. *EPSC.* **2018,** abst. 988.

- Torre-Fdez I., **Ruiz-Galende P.**, Aramendia J., Gómez-Nubla L., Castro K., Fdez-Ortiz de Vallejuelo S., Arana G. , Madariaga J. M. Study of organic compounds present in the

NorthWest Africa 6148 Nakhlite by means of Raman spectroscopy. *EPSC.* **2018,** abst. 967.

- Gómez-Nubla L., Aramendia J., Torre-Fdez I., **Ruiz-Galende P.**, Fdez-Ortiz de Vallejuelo S., Madariaga J. M. Identification of kerogen by SCA device in material produced by the impact of an extraterrestrial body on Earth. *EPSC.* **2018,** abst. 957.

- **Ruiz-Galende P.**, Torre-Fdez I., Aramendia J., Gómez-Nubla L., Fdez-Ortiz de Vallejuelo S., Medina J., Castro K., Maguregui M., Arana G., García Baonza V., Rull F., Madariaga J. M. New Raman-NIR Database of Inorganic and Mineralogical Planetary and Terrestrial compounds (IMPAT-Dat): Phyllosilicates. *GeoRaman XIII*, **2018.**

- **Ruiz-Galende P.**, Torre-Fdez I., Aramendia J., Gómez-Nubla L., Castro K., Arana G., Madariaga J. M. The Meñakoz outcrops (Biscay, Spain): a possible terrestrial Martian analogue. *GeoRaman XIII,* **2018.**

- Torre-Fdez I., **Ruiz-Galende P.**, Aramendia J., Gómez-Nubla L., Fdez-Ortiz de Vallejuelo S., Castro K., Arana G., García Baonza V., Medina J., Rull F., Madariaga J. M. Discrimination between original calcite and calcite from terrestrial weathering in NWA 6148 Martian meteorite by Raman spectroscopy. *GeoRaman XIII,* **2018.**

- Madariaga J. M., Torre-Fdez I., **Ruiz-Galende P.**, Aramendia J., Gómez-Nubla L., Fdez-Ortiz de Vallejuelo S., Maguregui M., Castro K. , Arana G. Advanced analytical methodologies based on Raman spectroscopy to detect prebiotic and biotic molecules: Applicability in the study of the Martian nakhlite NWA 6148 meteorite. *2nd International Mars Sample return.* **2018,** abst. 6114.

- **Ruiz-Galende P.**, Torre-Fdez I., Aramendia J., Gómez-Nubla L., Fdez-Ortiz de Vallejuelo S., Castro K., Arana G., Madariaga J. M. Geochemical characterization of a terrestrial Martian analogue: the submarine volcano of Meñakoz (Biscay, Spain). *LPSC 49.* 2018, abst. 2842.

- Torre-Fdez I., **Ruiz-Galende P.**, Aramendia J., Gómez-Nubla L., Fdez-Ortiz de Vallejuelo S., Castro K., Arana G., Madariaga J. M. In-depth study of the calcite present in the Martian Nakhlite NorthWest Africa 6148 meteorite. *LPSC 49.* 2018, abst. 2160.

- Torre-Fdez I., **Ruiz-Galende P.**, Aramendia J., Gómez-Nubla L., Fdez-Ortiz de Vallejuelo S., Medina J., Castro K., Maguregui M., Arana G., García Baonza V., Rull F., Madariaga J. M. The relevance of the creation of a Raman and NIR spectroscopic database for the upcoming mars missions. *LPSC 49.* 2018, abst. 2943.

- **Ruiz-Galende P.**, Torre-Fdez I., Gómez-Nubla L., Fdez-Ortiz de Vallejuelo S., García Baonza V., Medina J., Rull F., Madariaga J. M. Raman spectroscopic analysis of the bulk and weathered mineral phases of a potential submarine volcano Mars analogue. *XXXVI Biennial Meeting of the RSSC.* 2017.

- Torre-Fdez I., **Ruiz-Galende P.**, Castro K., Gómez-Nubla L., Aramendia J., Maguregui M., García Baonza V., Medina J., Rull F., Madariaga J. M. Novel calibration functions to quantify forsterite and fayalite in olivine minerals by Raman spectroscopy. *XXXVI Biennial Meeting of the RSSC.* 2017.